UNIVERSITY OF Southampton

University of Southampton Research Repository
ePrints Soton

Copyright © and Moral Rights for this thesis are retained by the author and/or other copyright owners. A copy can be downloaded for personal non-commercial research or study, without prior permission or charge. This thesis cannot be reproduced or quoted extensively from without first obtaining permission in writing from the copyright holder/s. The content must not be changed in any way or sold commercially in any format or medium without the formal permission of the copyright holders.

When referring to this work, full bibliographic details including the author, title, awarding institution and date of the thesis must be given e.g.

AUTHOR (year of submission) "Full thesis title", University of Southampton, name of the University School or Department, PhD Thesis, pagination

http://eprints.soton.ac.uk

·MASTER COPY

UNIVERSITY OF SOUTHAMPTON

Electrical Conduction in Single Crystal Magnesium Oxide

Thesis submitted for the degree of
Doctor of Philosophy by M. Potter

(January 1977)

UNIVERSITY OF SOUTHAMPTON

ABSTRACT

FACULTY OF SCIENCE

ELECTRONICS

Doctor of Philosophy

ELECTRICAL CONDUCTION IN SINGLE-CRYSTAL MAGNESIUM OXIDE

by Michael Potter

The object of this investigation was to identify the electrical conduction mechanisms in single crystal magnesium oxide.

The conductivity of nominally pure, chromium-doped and iron-doped samples was measured in the temperature range 200°C to 1100°C using a three-terminal measurement system, the construction of which is described.

By comparison of the measured conductivity values with those calculated for various mechanisms, it was concluded that the most likely mechanism is that of magnesium ion motion. The conductivity of the chromium-doped samples was found to decay towards that of the purer samples over a period of a few weeks, and the conductivity below 600°C was found to depend on the cooling rate of the sample. Neither of these phenomena has been reported before. They were explained by considering the effect of chromium and ferric/ferrous ions, respectively, on the magnesium ion mobility.

The non-ohmic behaviour of the samples, the slow current decays observed after a change of applied voltage, and electron spin resonance measurements are also discussed.

ACKNOWLEDGEMENTS

I would like to express my gratitude to Dr. D. R. Lamb for his help and encouragement throughout this work. I should also like to thank Mr. K. McMinn for many useful technical discussions and Dr. F. H. Mullins for his critical reading of the manuscript.

The financial support of the Control and Instrumentation Division of U.K.A.E.A. Winfrith and the assistance of the Plessey Radar Research Centre, Havant are also gratefully acknowledged.

Finally I should like to thank my wife, for her constant encouragement, and Lorraine Pearce, for typing the final draft.

CONTENTS

LIST OF FIGURES

LIST OF TABLES

LIST OF SYMBOLS

A	a constant
a	contact area (m^2)
a,b,c	parameters of fitting function (in Appendix 3)
C	a constant
C_{Fe}	iron content
D	diffusion coefficient (m^2s^{-1})
D_{Mg}	diffusion coefficient of Mg^{++} ions (m^2s^{-1})
D_o	pre-exponential factor in diffusion expression (m^2s^{-1})
E	an E.M.F. (V)
E_a	energy at acceptor level (eV)
E_c	energy at the conduction band edge (eV)
E_d	energy at donor level(eV)
E_f	energy at Fermi level (eV)
E_g	energy band gap (eV)
E_v	energy at valence band edge (eV)
F	fitting function } in Appendix 3
F_o	residual } in Appendix 3
f	Mg^{++} vacancy concentration (mole. fraction)
G	conductance (S)
h	Planck's constant ($6.625 . 10^{-34}$ Js)
I	a current (A)
I_b	current flowing in the bulk material (A)
I_{b_1}	current flowing in the bulk material (A)
I_{b_2}	current flowing in the bulk material (A)
I_g	current flowing in the gas (A)
I_{g_1}	current flowing in the gas (A)
I_{g_2}	current flowing in the gas (A)
I_l	current flowing through leakage resistances (A)

I_s	current flowing on surface (A)
I_o	parameter of decay formula (A)
I_∞	parameter of decay formula (A)
j	summing index
k	Boltzmann's constant ($1.380 \cdot 10^{-23} JK^{-1} = 8.617 \cdot 10^{-5} eV K^{-1}$)
l	a length (m)
M	rest mass of electron ($9.108 \cdot 10^{-31} kg$)
Me_1	a metal
Me_2	a metal
Me_1O	a metal oxide
Me_2O	a metal oxide
m	parameter of decay formula
m_e	effective mass of electron in conduction band (kg)
m_h	effective mass of hole in valence band (kg)
N_a	concentration of acceptor levels (m^{-3})
N_c	pre-exponential factor in expression for electron concentration (m^{-3})
N_d	concentration of donor levels (m^{-3})
N_v	pre-exponential factor in expression for hole concentration (m^{-3})
n, n_j	carrier concentration (m^{-3})
n_e	concentration of electrons in the conduction band (m^{-3})
n_h	concentration of holes in the valence band (m^{-3})
n_i	intrinsic electronic carrier concentration (m^{-3})
n_{Mg}	Mg^{++} ion concentration (m^{-3})
P'_{O_2}	oxygen partial pressure
P''_{O_2}	oxygen partial pressure
Q	general activation energy (eV)
Q'	general activation energy (eV)

Q_m	energy of motion of Mg^{++} ion (eV)
Q_s	energy of formation of Schottky defect (eV)
q	modulus of electronic charge ($+1.602 . 10^{-19}C$)
R_b	bulk resistance (Ω)
R_l	leakage resistance (Ω)
R_s	surface resistance (Ω)
R'_s	parallel combination of R_s and R_l (Ω)
T	absolute temperature (K)
T_o	a constant (K)
t	time (s)
t_e	electronic transport number
t_i	ionic transport number
t_j	general transport number
U	$\exp(-(E_c-E_f)/kT)$
V	$\exp(-(E_c-E_d)/kT)$

in Appendix 2

V	a voltage (V)
V_1	a voltage (V)
V_2	a voltage (V)
Q	atomic weight of impurity ion
(x,y)	data point
z, z_j	charge of current carrier in units of q
μ, μ_j	carrier mobility ($m^2V^{-1}s^{-1}$)
σ	conductivity (Sm^{-1})
σ_b	bulk conductivity (Sm^{-1})
σ_e	conductivity due to electronic motion (Sm^{-1})
σ_i	conductivity due to ionic motion (Sm^{-1})
σ_j	conductivity due to mechanism j (Sm^{-1})
σ_o, σ_o'	pre-exponential factor in expression for conductivity (Sm^{-1})
τ	parameter of decay formula (s)

1. INTRODUCTION

Magnesium oxide (magnesia, periclase, MgO) is the most refractory of the alkaline earth oxides, its melting point being 2852°C and its boiling point approximately 3600°C. Pure single crystal material is colourless and the powder is white. The presence of impurities causes colouration; for example iron-doped crystals are a yellowish brown, manganese-doped pink, and chromium-doped green.

Single crystals are normally manufactured by packing a large mass of magnesia powder around carbon electrodes and striking an arc between them (1). The powder melts in the arc and then solidifies to form single crystals of varying size and purity. Due to the high melting point of the material, methods of purification, such as zone refining, are not possible with the crystals, although both the "cloudiness" due to small voids, and the dislocation density may be reduced by annealing at 1800°C to 2000°C in high vacuum. This lack of purity, of even the best crystals available, was not always noted by some early workers and this led to phenomena caused by defects in the sample being attributed to intrinsic behaviour. (the term "defect" will be taken to include any deviation from the perfect crystal, e.g. vacancies, interstitials, impurity atoms, dislocations, etc.).

The magnesia lattice is a divalent analogue of the sodium chloride lattice, i.e. there are two interpenetrating face-centred cubic sub-lattices of Mg^{++} and O^{--} ions, each ion being surrounded by six ions of the other type (see Fig. 1). The bonding between the ions is mainly ionic although some evidence of covalent behaviour has been reported (2).

An important use of magnesia is as an insulator in mineral-insulated cables. Such cables are manufactured by first making a short fat coaxial cable and then drawing it through a series of dies to reduce the diameter and increase the length. The magnesia is subject to considerable mechanical working and is reduced to a powder by the drawing process.

Magnesia is used as the insulator, despite the fact that it is hygroscopic, because it is ductile in the freshly cleaved state, and thus flows as the cable is drawn through the dies. The use of a less ductile material would lead to the fracture of the cable sheath during manufacture.

The work described in this thesis was undertaken as the initial stage of an investigation into the electrical conductivity of magnesia with a view to forming the basis for further study of the factors limiting the leakage resistance of these cables. As was stated above, the magnesia insulation is in a powdered form, having a high surface area to volume ratio, and so the cable leakage resistance will be determined to a large extent by the electrical surface conductivity of the material. The characterisation of powder or polycrystalline samples is complicated by several factors which are not present in single crystal material (grain size, porosity, etc.) and so it was decided that work would start with the study of the bulk conductivity of the structurally simpler single crystal. The study included investigation of several properties of the single crystal material and is described in this thesis.

After a brief review of the published conductivity results it was clear that the conduction mechanisms were not well understood and so a much wider literature survey was undertaken. The purpose of this survey was not only to find published conductivity results but also to find results of other measurements which would be useful in understanding the structure, both electronic and ionic, of magnesia. The results of this survey, in a slightly extended and revised form, are presented in section 2.

As a result of this survey it was decided to study three types of material: nominally pure, chromium-doped and iron-doped. These two dopants were chosen for two reasons: first, they are the main constituents of stainless steel, a material commonly used for the conductors in mineral-

insulated cables; and second, the results in the literature suggested that trivalent ions (e.g. Cr^{+++}, Fe^{+++}), and especially ions of variable valence (e.g. Fe^{++}, Fe^{+++}), might significantly effect the conductivity. A measurement rig was then designed and built; a description of the apparatus is given in section 3.

The conductivity of nominally pure, chromium-doped, and iron-doped samples was measured and these measurements are discussed in section 4. It was found that the conductivity of chromium-doped samples was initially higher than that of purer samples, but that it tended to decay towards that of the purer material, over a period of a few weeks. It was also found that the conductivity below about 600°C was dependent on the cooling rate of the sample. Neither of these phenomena has been reported before.

Other measurements were also made on the samples: in particular their non-ohmic behaviour and the current decays found after a change of applied voltage were studied. These measurements are discussed in section 5.

As an aid to the identification of the conduction mechanisms present in magnesia the values of conductivity expected from many different conduction mechanisms were calculated. The calculated values, discussed in section 6, were compared with measured conductivity values, both those of this investigation, and other published results.

The most likely conduction mechanism was found to be that of magnesium ion motion. Both the decay of the conductivity of chromium-doped samples, and the dependence of the conductivity below 600°C on the cooling rate were explained by considering the effect of Cr^{+++} and Fe^{+++} ions on the magnesium ion mobility. This is discussed in section 7.

Section 8 presents some suggestions and recommendations for further work in this field, and the conclusions are summarised in section 9.

2. LITERATURE SURVEY

The literature covered in this survey is considered in seven sub-sections; each sub-section deals with the published results of measurements of different properties of magnesia.

2.1 Conductivity Measurements

2.2 Thermoelectric E.M.F. Measurements

2.3 Transport Number Measurements

2.4 Electron Spin Resonance Measurements

2.5 Diffusion Measurements

2.6 Optical Measurements

2.7 Other Measurements

2.8 Review Articles

As there is a considerable amount of literature surveyed here it has not been possible to comment at length on every paper. Short comments are made in this section where they are relevant. Papers of special relevance are dealt with in greater detail in following sections.

2.1 Conductivity Measurements

The results of many measurements of the conductivity of magnesia have been published, both on single crystal (3 - 12) and polycrystalline (8 - 10, 13 - 25) samples. The results which fall into the temperature region of interest in this thesis are plotted on Fig. 2 (single crystal) and Fig. 3 (polycrystalline). As can be seen, at the higher temperatures the results obtained on single crystal samples are similar to those obtained on polycrystalline samples; at lower temperatures there is more variation and this is discussed in section 7.5. There are however quite large differences between the results of different workers; these differences are somewhat larger for the polycrystalline samples than for the single crystals.

When one examines the published experimental details the reasons for the differences begin to become apparent. There is

considerable variation in the experimental techniques used by different workers. The ambient atmospheres used include air, vacuum, nitrogen, oxygen, etc.; both DC and AC techniques have been used; electrode materials include platinum, gold, carbon, silver, molybdenum, tungsten, etc.; the electrical systems used include 2, 3 and 4 terminal measurements (see Appendix 1). Also the samples have often been of unknown purity; this is especially true of some of the earlier measurements on polycrystalline samples. When one also considers that the polycrystalline samples will have variations of grain size and porosity and that the cooling rates used by different workers were almost certainly different, it is perhaps not surprising that there is such a large spread in the results. (Such variation of reported results is not unique to magnesia, a similar situation exists for alumina, see Ref. 26).

Almost all the single crystal measurements were made on nominally pure samples. Yamaka et al (4) heated their samples in oxygen and magnesium vapour; the increase of conductivity observed after heating in magnesium vapour may have been due to increased surface conduction as a 2-terminal measurement system was used. Mitoff (6) measured nominally pure and lithium-doped samples and found small differences of conductivity; again it is possible that the observed difference was due to surface conduction. Choi et al (11) found that additions of nickel increased the conductivity; again a 2-terminal system was used.

Several workers have measured the conductivity of doped polycrystalline samples. Generally it has been found that the conductivity is increased by the addition of impurities, but there are again variations between the results of different workers. The results of conductivity measurements of doped polycrystalline samples are shown in Table 1. This representation gives only limited information; for fuller details the original papers should be consulted. Budnikov et al (21) found an empirical relation between the conductivity σ, the iron content C_{Fe}, and the temperature T:

$$\sigma = A.C_{Fe}^{(T_o/T - 1)} \exp(-Q/kT)$$

Where A, Q and T_o are constants and k is Boltzmann's constant. T_o is found to be approximately equal to the melting point of magnesia. They also correlated a "knee" in their conductivity results with a change of valence of iron impurities in magnesia. The behaviour of iron in magnesia will be discussed in greater detail later.

Several authors have proposed mechanisms to explain the conductivity of magnesia. These are tabulated in Table 2. As can be seen, all the earlier theories assumed that the conductivity was electronic. The later theories take into account measurements which showed the presence of ionic mechanisms. It should be noted that a great variety of theories is presented by the different authors.

2.2 Thermoelectric E.M.F. Measurements

There have been four published results of thermoelectric E.M.F. (T.E.M.F.), or Seebeck effect, measurements on magnesia (4, 12, 14, 20). Although this technique seems at first sight to offer a very simple method of determining the sign of the charge carriers, it is inherently a 2-terminal measurement technique and as such is subject to errors due to surface and gas conduction. This is reflected in the variation of the published results; three investigations lead to the conclusion that the carriers are negatively charged, and one (14) to the conclusion that they are positively charged.

2.3 Transport Number Measurements

Several workers have attempted to measure the fractions of the conductivity due to ionic and electronic mechanisms respectively. There are three techniques which have been used: the electrolytic cell method, the electrode weight loss/gain method, and the method which involves detecting the growth of crystal faces as current is passed. The electrolytic cell measurements can be further sub-divided

into those where the sample is put between two atmospheres of different oxygen partial pressure (6, 27, 28) and those where the sample is placed between two pellets of mixed materials, often metals and their oxides (29 - 32). There has only been one published result each of the electrode weight technique (33) and the crystal face movement technique (34).

The results have been very varied; there seems to be some agreement of a maximum of ionic conductivity around 1100°C, but there are considerable differences between the actual values found by different workers. Alcock et al (32) review the published results up to 1971. These transport number measurements will be considered more fully in section 7.

2.4 Electron Spin Resonance (E.S.R.) Measurements

E.S.R. techniques provide a very sensitive method of investigating the behaviour of certain defects in solids; very small concentrations of defects may be examined. It is possible to determine the relative positions of impurities, vacancies, etc. by examining the symmetry of the fields set up in their vicinity. Reference 35 contains a short introduction to the technique.

The author has found several papers describing E.S.R. measurements (36 - 49) on magnesia. Many of these papers describe the behaviour of iron and chromium in the lattice (36, 38 - 41, 43, 45, 48). It has been possible to examine the state of these impurities after irradiation (X rays, U.V., visible, etc.) and after various heat treatments. Some understanding of the interaction between the different impurities and other defects in the lattice has been gained. Hansler et al (40) combined thermoluminescence measurements with E.S.R. results and drew up a partial energy band picture (see Fig. 6 e). The effect of irradiation and heat treatments on vacancies has also been studied (37, 44), and the behaviour of lithium (46) and hydroxyl (47, 49) complexes in the lattice has also been examined.

E.S.R. measurements do not give direct proof of any conduction mechanisms, but they do aid the understanding of processes occurring in the lattice, especially the behaviour of variable valence impurity ions (e.g. Fe^{++}, Fe^{+++}), and are thus of great help when considering the conductivity results predicted by different theoretical models. The results of many of the above papers will be used in sections 6 and 7.

2.5 Diffusion Measurements

There have been several studies of diffusion in magnesia, including self-diffusion measurements of magnesium (50 - 52) and oxygen (53 - 57), and impurity diffusion of several foreign cations (58 - 71). The published results are shown in Figs. 4 and 5. All these measurements have been made in the temperature range 900 to 2350°C. Work at lower temperatures is not usually possible due to the very small diffusion coefficients obtained at such temperatures. This leads to excessively long diffusion times and thus precludes the use of radio-active tracers with relatively short half-lives, the only method of measuring diffusion rates in most cases.

Harding et al (51, 52) have studied the diffusion of magnesium up to 2350°C. They have identified the intrinsic, extrinsic and impurity precipitation regions of their results. These results are very interesting and will be referred to later in sections 6 and 7. The diffusion coefficient of oxygen has been found to be much lower than that of magnesium; this is to be expected from a consideration of the size of the ions (see Fig. 1). The results of Oishi et al (53) were said to represent extrinsic diffusion, those of Narayan et al (57), measured by studying the growth rate of dislocation loops, were said to represent intrinsic diffusion. Several workers have reported that oxygen diffuses much more rapidly along grain boundaries than it does through the bulk (54 - 56).

Diffusion measurements of aluminium (70), barium (65), beryllium (63), cadmium (69), calcium (64), chromium (61, 67), cobalt (58, 59), iron (58, 60, 61, 66), manganese (61), nickel (58, 59, 66, 68) and zinc (62) in single crystal magnesia have been published. These measurements will be considered further in section 6.5 when the magnitude of impurity ion conductivity is estimated. Zaplatynsky (71) measured the interdiffusion of magnesia/nickel oxide and magnesia/cobalt oxide solid solutions and reported that the diffusion of these cations was not enhanced by the presence of grain boundaries. This result contrasts with the reported results for oxygen diffusion and suggests that there may be differences between the diffusion processes of anions and those of cations in magnesia.

2.6 Optical Measurements

Correctly interpreted optical measurements can yield valuable information about the electronic structure of magnesia. The width of the energy band gap and the positions of the isolated energy levels within it can be estimated, and information deduced about the density and mobility of electronic carriers. There are several different types of optical measurements which are all considered in this section - luminescence, absorption, photo-electric emission, photo-conductivity, reflectivity, etc. These measurements can all yield useful information, but often the interpretation is not as straightforward as it at first seems (for example see the comments of Peria (72) on the measurements of Weber (73) and Day (74)).

The total of different absorption, reflection and photo-conductivity bands reported by the various workers is very large, much greater than fifty. It is not the purpose of this survey to review in detail the optical properties of magnesia, but only to select information which is relevant to the electrical conductivity, and so most of these results will not be discussed in any detail. The more relevant papers will be discussed below, and in the later sections.

Several workers have measured the luminescence of magnesia after irradiation (75 - 81). Polycrystalline, single crystal, and powder samples have been used and the exciting radiation has varied from ultra violet (U.V.) light to X-rays. The effects of various heat treatments, including heating the samples in oxygen and magnesium vapours, have been investigated, as have the spectra caused by the addition of impurities.

Saksena et al (79, 80) deduced a band structure from their measurements (see Fig. 6a) but this structure is generally considered to be unlikely, mainly due to the small energy band gap of 5.9eV.

There have been several investigations of the optical absorbance spectrum of magnesia (72, 73, 75, 78, 82 - 87). Again the effects of various heat and irradiation - treatments, including U.V., X-rays, γ-rays and neutron irradiation, have been studied. Clarke (82) studied the effects of neutron irradiation and found many induced absorption bands. He found that Schottky, rather than Frenkel, defects predominate, and that impurities are less effective as electronic traps than are other lattice defects. He also drew up a band diagram as shown in Fig. 6b. The work by Glass and Searle (85 - 87) examines the absorption spectra of samples quenched from different temperatures. By identifying the absorption bands with different impurity complexes the behaviour of the impurity ions as a function of temperature was determined. This is a relatively uncommon example of optical measurements giving information about ionic, rather than electronic, structure. Soshea et al (84) also measured absorption spectra, and deduced an energy band picture assuming the presence of iron and chromium impurities, see Fig. 6c.

Peria (72) combined absorption and photo-conductivity measurements in a series of experiments designed to overcome the difficulties experienced by other workers whose results he showed to be ambiguous. He found photo-conductivity bands at 5.05eV, where the carriers are electrons, and at 4.0eV

where the carriers are holes. Using a combination of his measurements and those of Soshea et al (84) he drew up a band picture as shown in Fig. 6d. Other photo-conductivity measurements have been made by Day (74) and Eisenstein (81).

The reflectivity of magnesia has also been studied (83, 88 - 92). The group of papers (89 - 92) by Walker and co-workers describes a series of reflectivity measurements and theoretical predictions; the point which is of most interest is that the energy band gap is found to be 7.775 ± 0.01eV.

Stevenson (93, 94) performed thermo-and photo-electric emission results and drew up an energy band picture as shown in Fig. 6f.

Yamaka et al (95) used photo-induced carriers for Hall-effect measurements; they found that the carriers were holes with mobilities of about 1 to 2.10^{-4} $m^2V^{-1}s^{-1}$.

2.7 Other Measurements

The group of four papers (96 - 99) by Pomerantz and co-workers discusses the formation of charge carriers by relativistic electron bombardment. From the shape of the induced current pulse information about the mobility and lifetime of the carriers can be found. The work discussed in each paper is a refinement of earlier work, and ultimately acoustic mode, optical mode, and ionised impurity scattering mechanisms were included in the interpretation of the results. The last paper of the series (99) includes thermally stimulated emission measurements and the presence of four traps, as shown in Fig. 6g, is deduced. The values of mobility found varied from 7.10^{-3} $m^2V^{-1}s^{-1}$ at $200^{\circ}K$ to 10^{-3} $m^2V^{-1}s^{-1}$ at $500^{\circ}K$. These results will be considered further in section 6.

Soft X-ray absorption measurements have been made by several workers (100 - 102). The band diagrams deduced from these measurements are shown in Fig. 6h&i.

By recording the energy losses of an electron beam passing through a thin magnesia foil, Watanabe (103) concluded that the energy band gap was 11.4eV. This technique has only a low resolution and Roessler et al (90) stated that he had probably not observed fundamental absorption, but other interband transitions.

Harkins et al, using a technique of studying the increase of catalytic activity of magnesia as a function of the wavelength of irradiating light, drew up a band picture, taking an energy band gap of 10.4eV after Soshea et al (84). This is shown in Fig. 6j. They also stated that oxygen vacancies are the most common surface defect while magnesium vacancies are the most common bulk defect. These observations are consistent with the observed behaviour of oxygen and impurity cations at grain boundaries, as discussed in section 2.5 above.

By studying neutron-irradiated magnesia Roux et al (105) were able to estimate the energy of formation of a cation Frenkel defect to be 6.3eV. This contrasts with the value of 4.0eV estimated for the energy of formation of a Schottky defect by Harding (106). This estimate was arrived at by considering the heats of reaction of several solid state reactions in magnesia and agrees well with the value of 3.8eV obtained by the same author from a consideration of his diffusion measurements (52). The difference between the energies of formation of the two defects is sufficient to explain the predominance of Schottky defects, as reported by several workers.

The behaviour of iron in magnesia has been the object of a number of studies (107 - 110). Of special interest in this investigation is the valence change which iron undergoes, from ferric (Fe^{+++}) to ferrous (Fe^{++}). The paper by Davidge (109) combines optical and mechanical hardness measurements to obtain useful results about the behaviour of iron in magnesia single crystals. The paper by Bhide et al (110) describes the use of the Mössbauer technique to

study the effects of various heat-treatments on iron impurities in magnesia. The results of these two papers will be referred to in sections 6 and 7.

Ghosh et al (111) published results of their studies of etching and polishing magnesia crystals; these results are of great use as a practical guide to sample preparation.

2.8 Review Articles

The papers considered in this sub-section are not, in general, specific to magnesia. The majority of them however contain at least a section on the properties of magnesia and the author feels that the inclusion of all the papers referred to below is worthwhile, if only as suggested background reading for the fields of work discussed in this thesis. By their very nature review articles are generally fairly lengthy and so it will only be possible to describe briefly the content of each paper here.

The Hughes Aircraft Company of America carried out an extensive literature survey on the properties of magnesia. The two papers by Milek (112, 113) are preliminary publications; the final report (114) reviews more than 350 documents and lists measurements of many properties of magnesia.

There have been two useful reviews of ionic conductivity (115, 116) published in the last twenty years. The former, by Lidiard, is long and detailed. Many aspects of ionic conductivity are considered and relevant work, mostly on alkali halides, up to 1957 is discussed. The latter paper, by Fuller, discusses the progress made up to 1972, again mainly considering results obtained on alkali halides. In 1966 Mitoff published a review of electrical conductivity in oxide ceramics (117). Unlike the two papers discussed immediately above, which were written by solid state physicists, this review is written using notation familiar to a physical chemist. Magnesia is discussed as an example of an extrinsic electronic conductor, using Mitoff's previously published conductivity results (5, 6).

In 1967 Lidiard (118) published a short review on point defects in solids. He stated that Schottky defects predominate over Frenkel in magnesia, and estimated the energies of formation and motion of the defects. These estimates are very close to the values later found by Harding (52, 106). The review of defects in ionic crystals by Barr and Lidiard (119) considers a wide range of measurements and theories; again most of the examples are from work on alkali halides.

A review dealing specifically with defects in the alkaline earth oxides (baria, calcia, magnesia and strontia) was published by Henderson and Wertz (120) in 1968. This paper considers many aspects of these oxides, including the optical and magnetic properties of defects, radiation damage and its annealing.

The two papers by Steele (121) and Alcock (122) are reviews of the use of electrolytic cells for the measurement of thermodynamic data. The suitability of magnesia as a solid electrolyte is considered and some limitations of the technique are discussed. These points will be discussed in section 7.

The theory of solid electrolyte/electrode interfaces is reviewed by Raleigh (123). No specific mention of magnesia is made, but results of measurements up to 1972 on many other systems are included.

Garlick published two review papers of interest, one about photo-conductivity (124), and another about luminescence (125). The introductory sections are of general interest; all the results quoted in the sections on magnesia are disussed above. The short review by Klick (126) on colour centres and luminescence also contains information of general interest.

2.9 Comments on the Literature Surveyed

The main conclusion of the original literature survey (written in 1971) was that the state of knowledge of most .

of the properties of magnesia was rather confused. The situation seems to be a little better now and some of the later review articles have been able to draw up (at least partially) consistent descriptions of some of the processes which take place in magnesia. There is, however, still no real agreement on the predominant conduction mechanism, see Table 2.

Attempts were made to analyse the published conductivity data in terms of the published values of activation energy Q, and of the "pre-exponential factor", σ_o. This analysis was only partially successful, partly due to the difficulty of obtaining accurate values of Q and σ_o from the published data, and partly due to the differing experimental conditions used by different authors. In an attempt to clarify the situation the programme of work described in the following sections was undertaken.

3. APPARATUS AND SAMPLE PREPARATION

In order to study the bulk conductivity of magnesia over a range of temperatures it was necessary to have a means of heating samples in a controlled atmosphere, and of measuring the conductance of the samples using a technique which, as far as possible, eliminated the effects of extraneous leakage conductances. This section describes the apparatus used in this investigation, including any constructional details where appropriate. The preparation of the samples, and the method of applying contacts to them, are also described.

The apparatus and techniques will be dealt with in the following sub-sections:-

3.1 The Furnace

3.2 The Work Tube

3.3 The Gas Systems

3.4 Sample Preparation

3.5 The Sputtering System

3.6 The Electrical Measurement System

3.7 Temperature Measurement

3.1 The Furnace

The initial furnace design was arrived at after discussion with Dr. A. J. Moulson of Leeds University and consultation of reference 127. It was decided that the thermal mass of the furnace should be large, to reduce the effect of room temperature variation during measurements. A long "flat zone" at the centre of the furnace, although not essential for the measurement of the samples used, was felt to be desirable as it would remove the need for precise positioning of the sample and would also ensure that the ambient gas flowing through the work tube quickly reached the same temperature as the sample, thus reducing the likelihood of any temperature gradient across the sample. These considerations, and the limited range of sizes of suitable alumina tubes available, determined the final size of the furnace.

Although it was originally intended to take measurements up to 1000°C, it was felt desirable to design the furnace to be capable of reaching about 1200°C.

Cross-sectional diagrams of the furnace are shown in Fig. 7.

The furnace design will be considered in three parts: the furnace case and the insulation; the furnace tube and heater winding; and the furnace power supply.

3.1.1 The Furnace Case and Insulation

The furnace case was constructed from mild steel sheet painted on the outside with aluminium paint. The bottom and sides were welded together and a 20mm flange was welded to the top edges of the sides. The top of the furnace was attached to this flange, with cement when it was necessary to pass forming gas over the molybdenum windings, or with ten small clamps when a Kanthal winding was used (see section 3.1.2 below). The outside dimensions of the furnace were approximately 520mm x 520mm x 900mm.

The furnace tube was placed at the centre of the furnace along the longer horizontal axis. The tube and winding were approximately 60mm in diameter and were surrounded by approximately 20mm of Morgan's Trimor Alumina Insulating Powder No. 921 (available from Morgan Refractories Ltd., Neston, Wirral, Cheshire) on all sides. Surrounding and supporting this were Morgan's MI28 firebricks, shaped and arranged so that any gaps between bricks in one layer were covered by bricks in the layer above. Initially the bricks were packed fairly loosely to allow room for expansion on heating, but it was later found possible to partially fill the cracks with brick dust, thus improving the thermal insulation a little, with no adverse effects. The furnace tube projected approximately 50mm from the furnace case at each end, and was cemented into the case with a cement which gave way fairly easily when the tube expanded on heating, otherwise the tube would have cracked. The main purpose of

this cement was to prevent the alumina powder packed around the tube from escaping.

Three pieces of small (10mm o.d.) alumina tube were let into the side of the furnace case; a long piece reaching almost to the furnace tube, through which forming gas (90% N_2, 10%H_2) was passed when a molybdenum winding was used, and two shorter (30mm) pieces which allowed the escape of the forming gas and also provided insulating leadthroughs for the lead-in wires to the winding.

3.1.2 The Furnace Tube and Heater Winding

The furnace tube was a Morgan's Purox Recrystallised Alumina tube 1m long, with inside and outside diameters of 38mm and 46mm respectively. The diameter of this tube was determined by the sizes of tubes available for the work tube.

It was decided at first to use molybdenum wire for the heater winding. This material has a very high melting point (2625°C), and so the winding would suffer no damage if the furnace were heated rapidly up to high temperatures. (With a tubular furnace of such a design, the winding can be several hundred degrees hotter than the sample when the furnace is heated rapidly). Unfortunately molybdenum oxidises rapidly in air above 500°C and it is necessary to maintain a continuous supply of forming gas near the winding to prevent such oxidation.

It was decided to design the winding such that the maximum heating power available was 2.5kW at 1200°C. The original power supply was a variable voltage transformer fed from a stabilised mains supply; the maximum output voltage was approximately 250V rms. This determined that the winding resistance was to be 25Ω at 1200°C, and thus 4Ω at room temperature. In order to have a flat zone of about 50mm a length : diameter ratio of greater than 10 is required (127) and so the winding length was set at 500mm. The first winding was thus 200 turns of 0.8mm diameter molybdenum wire (obtained from Murex Ltd., Rainham, Essex) wound uniformly

over the central 500mm of the furnace tube. This represents a winding density of 400 turns per metre.

The wire was wound by hand directly onto the tube and held in place by Morgan's Trimor Pure Alumina Cement No. 961. The ends of the winding were looped around the tube and then welded to 1.6mm diameter molybdenum lead-in wires. The cement was allowed to dry for a few days before assembly into the furnace case, and the temperature was kept below about 150°C for a further few days to allow the furnace to dry out.

On measuring the temperature profile of the furnace it was found that the flat zone (±5°C) was about 90mm at 400°C, 60mm at 700°C and 60mm at 1000°C. The hottest part of the furnace was about 60mm from the centre.

After about two weeks of use the winding went open circuit. Upon examination the wire was found to have broken at the hottest point of the furnace and to have been drawn to a neck at the point of breakage. It was thought that this was due to the molybdenum "creeping" at high temperatures and so producing a "hot spot" which quickly burnt out.

A suggested solution to this problem was to ensure that the winding was slightly loose on the furnace tube. In order to achieve this the next winding was wound over six pieces of wire laid longitudinally along the tube. These wires were pulled out after the cement had set, thus leaving the winding slightly loose on the tube. The winding was also graded, in an attempt to extend the flat zone. The grading used was:-

The first 100mm	-	600 turns per metre
the next 50mm	-	500 turns per metre
the next 50mm	-	400 turns per metre
the next 100mm	-	300 turns per metre
the next 50mm	-	400 turns per metre
the next 50mm	-	500 turns per metre
the next 100mm	-	600 turns per metre

TOTAL 240 turns

The lead-in wires were again of 1.6mm diameter molybdenum wire, but it was decided not to weld the lead-in wires to the furnace winding. The ends of the winding were deliberately left long and brought out to the power supply twisted around the lead-in wires. This eliminated a potentially troublesome weld near the hottest part of the furnace.

The newly wound furnace tube was run in slowly as before. The temperature profile was again checked and the flat zone found to be a little longer, 120mm at 400°C, 80mm at 700°C, and 80mm at 1000°C. However the temperature profile was not ideal; there were two peaks either side of the central portion and the hottest point was as much as 30° hotter than the centre. This showed that the grading used was too steep.

After about six months of use this winding too went open circuit. On examination the wire was found to have broken in a region where the wire had thinned considerably and was covered with yellow crystals. It was concluded that too much air had leaked into the furnace case and caused the molybdenum to oxidise.

It was thus decided to try Kanthal as a winding material. The lower maximum working temperature (1350°C) would necessitate care on rapid heating but the ability of the material to work up to 1350°C in air obviated the need for a continuous supply of forming gas. Again it was decided to use a graded winding, but a gentler grading than that used previously was needed for two reasons. Firstly the resistivity of Kanthal does not vary substantially with temperature, so that the power dissipated per turn is constant at different points of the winding; this is not the case when using molybdenum. Secondly it was necessary to ensure that the hottest part of the furnace was at the centre - if there were a point significantly hotter than the centre then the wire might exceed its maximum temperature when working at high

temperatures. It was decided to use 1.016mm diameter (19 S.W.G.) Kanthal A1 wire, obtained from Hall and Pickles Ltd., Ecclesfield, Sheffield. The grading used was:-

The first	100mm	-	400 turns per metre
the next	100mm	-	350 turns per metre
the next	100mm	-	300 turns per metre
the next	100mm	-	350 turns per metre
the next	100mm	-	400 turns per metre

TOTAL 180 turns

A different and easier technique was used for winding this coil. The Kanthal wire was wound tightly onto a mandrel rotating slowly on a small lathe. The mandrel was the same diameter as the furnace tube and when the tension was released the wire sprang back to form a coil about 80mm in diameter. The furnace tube was then covered with several layers of filter paper and the Kanthal coil slipped over it. The coil was then tightened turn by turn onto the tube by hand and secured in position with cement and P.V.C. tape. When the winding was complete the P.V.C. tape was removed, the tube held in two clamps, and the winding heated by passing a current through it. This first dried the cement and then burnt away the filter paper leaving the winding loose on the tube.

This winding had a resistance of about 55Ω which allowed a maximum power of about 1.2kW; the earlier windings had needed less than 1kW when running at 1200°C, and so this was sufficient. The flat zone was found to be much longer, 160mm at 400°C, 190mm at 700°C and 160mm at 1000°C, and the hottest point was approximately 20mm from the centre and only 3°C hotter at the most.

This winding lasted for about a year before it too went open circuit. There was no opportunity to investigate the reason for the failure and an identical winding was constructed which lasted until the end of the measurements made by the author.

3.1.3 The Furnace Power Supply

As was noted above, the original power supply was simply a variable voltage transformer fed from a regulated mains supply. The early measurements were made by heating the sample, then switching off the furnace power supply and monitoring the conductivity as the furnace and sample cooled. It was not possible to take measurements at a constant temperature due to electrical interference from the 50Hz mains supply.

For the later measurements, however, it was necessary to be able to hold the sample at a constant temperature for long periods while measurements were made. To this end a regulated D.C. power supply was constructed. The circuit diagram is shown in Fig. 8. In use the output voltage was set by adjusting potentiometers RV_1, RV_2, RV_3 and the voltage across the main series transistor TR_6 (monitored by meter M_1) was kept within safe limits by adjusting the output voltage of the variable voltage transformer T_1. Details of the design of such a power supply can be found in any of the standard texts on power supply design, and no further details need be given here. The power supply was capable of delivering up to 5A at output voltages up to 230 V D.C. with an output ripple of 0.2 to 5mV.

This was sufficient to heat the Kanthal-wound furnace to above 1200°C. Although there was no temperature control circuitry used and the ability of the system to maintain a constant sample temperature depended solely on the stability of output voltage of the power supply and the thermal mass of the furnace, it was found that the sample temperature could be kept within a few degrees for periods of several days. This was sufficient for the measurements of this investigation.

3.2 The Work Tube

3.2.1 General Description

A cross-sectional diagram of the work tube is shown in

Fig. 9. All the tubes A, B, C, D and E were of Morgan's Purox recrystallised alumina, supplied cut to length by Morgan's Refractories Ltd. The end pieces F_1 and F_2 were made from stainless steel, as were the two springs S_1 and S_2. The cross-piece G and the two tailpieces T_1 and T_2 were standard vacuum fittings (obtained from Edwards High Vacuum, Crawley, West Sussex) modified where necessary to fit an insulating lead-through and tube E. All the joints at the points marked X ··· X were gastight seals made with standard Edwards fittings and "Viton" "O" ring seals. The ambient gas supply entered through the cross-piece via a P.T.F.E. insulator.

The sample, a disc 21mm in diameter, was held at the centre of the worktube A by tubes B and C which were held in position by endpieces F_1 and F_2 resting on springs S_1 and S_2. These springs in turn rested on the tailpieces T_1 and T_2. When the worktube was fully assembled the sample was held firmly between tubes B and C by the pressure exerted by springs S_1 and S_2.

Electrical contact was made to the centre of the sample by a small piece of platinum foil at the end of tube D; this was welded to a platinum wire which passed inside tube D, through a short length of alumina insulator H and some P.T.F.E. tubing to the Edwards lead-through in the tail-piece T_2. Tube D was fractionally shorter than tube C and a phosphor bronze spring washer was placed between end piece F_1 and tube C - this exerted a gentle pressure on the centre contact suffient for good electrical contact at the sample. Pieces of platinum gauze wrapped around the ends of tubes B and C gave electrical contacts to the back of the sample and the guard ring respectively. These pieces of gauze were spot-welded to platinum wires which ran along the outsides of the tubes to another two pieces of gauze wrapped around the other ends of the tubes. Thus contact was made to the guard ring via end piece F_2, spring S_2 and tailpiece T_2. Contact to the back of the sample was made either via end piece F_1, spring S_1 and

tailpiece T_1 or, as was found to be more convenient, to the platinum thermocouple wire welded to the gauze near the sample. The thermocouple wires passed along tube E, one through a length of alumina insulator, and were spot-welded to the platinum gauze within 2mm of the sample.

In order to obtain a gas flow which left no trapped pockets of gas, several 1mm diameter holes were drilled in tubes B and D. These holes were drilled using a high speed drill at A.E.E. Winfrith after attempts to use a high power CO_2 laser at the University had failed. The main gas flow path was via the cross-piece G, along tube D, back along tube C, down the inside of tube A, back along tube B and finally out through tube E, the end of which was positioned close to the back of the sample in order to prevent the formation of a "dead spot" near the sample.

In use the work tube rested on three 4.8mm diameter alumina rods placed inside the furnace tube - these rods supported the work tube along most of its length and reduced any possible contamination from the furnace tube. The work tube was 200mm longer than the furnace tube, 280mm longer than the furnace case and 700mm longer than the heater winding, so all the springs, end pieces and other fittings were well away from the hot zone. Only the sample, platinum, platinum/rhodium and alumina were in the hottest parts of the furnace.

3.2.2 Cleaning

Before the initial assembly tubes A, B, C, D and E were scrubbed with a slurry of alumina powder and water, cleaned in Aqua Regia and rinsed in acetone. However some marks on the tubes due to handling, and also the printing on the tubes, were found to be impossible to remove. After an initial heating trial to 300°C (without a sample) the tubes near the centre of the furnace were found to be covered in a brown film. This film was found to burn off at red heat in a bunsen flame and so the work tube assembly was heated to red heat while air was being drawn through it. On

dismantling the work tube it was found to be completely clean for the central 500mm although there was an accumulation of the brown film at the ends of the heated region. It was considered that this was satisfactory and the tubes were used in this condition. No evidence of a similar brown film forming on the samples was noted during the measurements.

3.2.3 Assembly

The most convenient order of assembling the work tube and sample into the furnace will now be described.

The whole work tube assembly, apart from the sample, tubes B and E, endpiece F_1, and spring S_1 and tailpiece T_1, was assembled on the bench, ensuring that the alumina insulator H was correctly positioned. This assembly was then slid carefully into the furnace tube. The sample was pushed along tube A with an alumina rod and manoeuvred upright into approximately the correct position, against tubes C and D. A small torch was found to be useful in performing this operation. The rest of the assembly was then carefully slid into tube A and the 'O' ring coupling fixing tightened into place.

3.3 The Gas Supply Systems

Two separate gas supply systems were necessary, the forming gas supply for the furnace when a molybdenum winding was being used and the system which supplied dry argon and oxygen as ambient atmospheres for the sample during measurements. The first of these was very simple, the second more complex.

3.3.1 The Forming Gas Supply

As was stated above, the molybdenum wire first used for the heater windings oxidised in air above about 500°C. It was thus necessary to maintain a reducing atmosphere around the winding, and it was decided to use forming gas (90% N_2-10% H_2) for this purpose. When the furnace was constructed,

an alumina tube, 10mm in diameter, was let into the case. The tube passed from the alumina powder which surrounded the furnace tube, through the insulation and projected about 100mm outside the furnace case (see Fig. 7). The tube was connected to a cylinder of forming gas via a piece of rubber tubing and a regulator. No metering was used and a low flow of gas was maintained throughout the course of the measurements. In view of the failure of the winding due to oxidation, it would appear that a more efficient method of protecting the winding would be necessary if it were desired to use a molybdenum heater winding.

3.3.2 The Sample Ambient Gas Supply

A schematic diagram of this gas supply system is shown in Fig. 10. Apart from the glass tubes in the flow meters, the Millipore filter element and the P.T.F.E. insulator, the whole system was metal to avoid possible contamination from plastic and rubber piping. The lines from the gas cylinders to the flow meters, from the flow meters to the 'U'-tube and from the filter to the cross-piece on the work tube were all flexible stainless steel tubing. The 'U'-tube was made from rigid stainless steel tubing.

To remove any flux remaining in the tubing after the demountable joints had been brazed to the ends of the tubes, the whole system was steam cleaned for several hours and then thoroughly dried before use. The 'U'-tube was similarly cleaned and filled with type 5A molecular sieve to ensure that the gases entering the work tube were dry. This molecular sieve was regenerated or replaced every two or three gas cylinders. The Millipore filter prevented any particles of the molecular sieve being carried over into the work tube.

In this investigation only argon and oxygen ambients were used. It was possible to switch from one gas to the other, but the transition period was fairly long due to the fairly long lengths of piping used and also to the release of gas adsorbed on the molecular sieve.

The maximum gas flow rate that the flowmeters were capable of reading was 10 litres per minute. It was noted that a higher flow rate cooled the sample and altered the conductivity measurements to a degree consistent with the observed change of temperature. The flow rate was thus generally kept within the range 0.5 to 1 litres per minute, after any initial flushing of the furnace; this is equivalent to changing the atmosphere in the work tube once every 15 to 30 seconds.

3.4 Sample Preparation

The samples used in this investigation were all cleaved from the (100) plane of magnesia single crystals grown by Spicer's Ltd., of Winchcomb, Gloucestershire. The crystals were kept in a desiccator until needed. The nominally pure and chromium-doped samples were prepared by Mr. R. Simmonds of A.E.R.E. Harwell, and the iron-doped samples by G.E.C. Hirst Research Laboratories, Wembley. All the samples were discs 21mm in diameter, and the thicknesses ranged from 0.5mm to 2mm.

The faces of the samples as received were flat enough for there to be no need for grinding or lapping, although it was decided to chemically etch the surface in order to remove any contamination or damaged surface material. The samples were etched in boiling orthophosphoric acid for a few minutes (111), stirring continuously to prevent the sample sticking to the glass dish. The samples were then removed from the acid with C.T.F.E. tweezers, allowed to cool, rinsed in acetone and cleaned in two rinses of acetone in an ultrasonic cleaning bath. The samples were kept under vacuum until needed for sputtering, and after this point were handled only with tweezers.

3.5 The Sputtering System

The system used to sputter the platinum contacts onto the samples is shown schematically in Fig. 11. The whole system was mounted inside a Birvac TE12 LHR-4 vacuum set.

The upper and lower plates were of aluminium and were held in position by nuts on the threaded rods. The H.T. lead was made from stranded copper wire insulated from the stainless steel braiding by P.T.F.E. tubing. Connection to the H.T. supply outside the vacuum chamber was made via a vacuum lead-through. The target, a piece of aluminium 40mm square wrapped in platinum foil, was connected to the H.T. lead via a short length of threaded rod and two screws, see Fig. 11b. The target was insulated from the upper plate by two ceramic insulators and held in position by the insulators and the natural springiness of the braiding.

In use the object to be metallised was placed on the lower plate directly below the target and the bell jar was evacuated to about 10^{-4} torr. The bell jar was then flushed with argon and re-evacuated; this procedure was repeated three times.

Then the baffle valve and gas inlet valve were adjusted until the pressure inside the bell jar was about 10^{-2} torr. The target was then raised to a potential of -1kV to -1.5kV when a discharge struck between the target and the lower plate. No discharge formed between the target and the upper plate as the spacing was less than the length of Crooke's dark space.

The current flowing was monitored and it was found that a current of eight to ten milliamperes was optimum. If the current was significantly higher then the apparatus became very hot and the insulation broke down, most commonly at, or close to, the ceramic insulators near the target. If the current was much lower the sputtering operation took correspondingly longer. The most convenient method of adjusting the current was to change the pressure in the bell jar by balancing the gas flow with the baffle valve and the gas inlet valve. It was found that a suitable film could be sputtered in about 30 minutes with a current of 8mA.

When sputtering a sample, it was important that no platinum should be deposited on the edges of the sample. To prevent

this occurring a shield was made. This shield consisted of a piece of brass 70mm square and 4mm thick with a stepped hole through the centre. A cross-sectional diagram of the shield is shown in Fig. 12.

In use the shield was placed over the sample and rested on it, covering the edges. This prevented any platinum from reaching the edges of the sample during sputtering.

Because it was required to apply contacts over the whole of the back of the sample, only the shield described above was necessary when sputtering the back face. The contact arrangement on the front face of the sample was more complicated - a centre contact surrounded by a guard ring. Two methods of forming such a pattern were tried. The first was to cover the whole face of the sample with platinum and then selectively etch away the unwanted annulus of platinum. This technique proved to be unsuccessful. By using photomechanical methods, as used in the fabrication of microelectronics, it was possible to define the contact areas with photoresist, but the only suitable etchant was Aqua Regia, and it was found that the platinum tended to lift away from the complete face of the sample.

The second method was to use an in-contact mask during sputtering, to prevent platinum from being deposited on the area between the centre contact and the guard ring. Such a mask was made. It consisted of a stainless steel "washer", about 1mm thick with inside and outside diameters of 10mm and 12mm respectively. This method of forming the required contact pattern was successful, but in order to obtain a well defined edge to the platinum contacts it was necessary to grind down the face of the mask so that it was flat and made good contact with the sample.

3.6 The Electrical Measurement System

3.6.1 General Description

The electrical circuit of the system used for conductivity

measurements is shown in Fig. 13. The connections at the sample were described in section 3.2.1, and the theory of the three terminal measurement method is presented in Appendix 1.

The platinum wire connecting to the back of the sample was taken, via a small connector box, to the voltage source. For the initial measurements a Farnell E350 stabilised voltage supply was used. It was suspected that some of the noise problems encountered during measurements were due to mains ripple and other mains-borne noise at the output of this supply and so it was replaced with a bank of 60V batteries. By using these batteries it was possible to obtain voltages of over 500V in steps of approximately 15V. The majority of measurements were made using the batteries.

The meter used for monitoring the current flow was a Keithley 610C Electrometer in the "fast" mode. In this mode the electrometer amplifier is connected in a virtual earth configuration and thus the voltage drop across the meter is very small. This is exactly what is required for three terminal measurements, see Appendix 1. The input voltage drop of the 610C is always less than 100μV at any current range from 3.10^{-1}A to 10^{-14}A F.S.D.

Some early measurements were made using a Vibron 33C electrometer and B33-2 converter. This instrument has a similar "fast" mode of use, but the input voltage is only reduced to one twentieth of the voltage drop across the sampling resistor. This usually leads to a considerable voltage difference between the guard ring and the centre contact, and so this is not a fully guarded system. A few measurements were taken by "backing off" the guard ring voltage to the same potential as the centre contact, using a separate voltage source. This method was found to be very inconvenient and did not allow the unattended recording of measurements on an X-t chart recorder.

Many of the later measurements involved recording the variation of the current with time. These results were recorded on a Telsec chart recorder. The chart speed could be varied between 10mm per second and 10mm per hour. Extra resistor-capacitor damping circuits were used when the currents being measured were very noisy.

It will be noted here that the arrangement of the sample and alumina tubes in the work tube enabled true volume guarded measurements to be made. The tubes B and C (see Fig. 5) which held the edges of the sample did not make perfectly gastight joints, but the platinum gauze and the sputtered platinum guard ring formed a good electrical barrier.

3.6.2 Earthing and Shielding

When measuring samples of such high resistance care must be taken to screen the apparatus to minimise the effects of external electromagnetic radiation. It is also important to ensure that the apparatus is correctly earthed to prevent the occurrence of earth loops. The ideal system is an entirely coaxial arrangement, with the outer screen connected to earth at one point. In practice "cut and try" methods are normally necessary to find the best arrangement.

All the wires in the apparatus used in this investigation were screened, and the whole apparatus was earthed at one point, the electrometer. The ends of the work tube, which projected from the furnace tube, were surrounded by screening boxes and the wires to the back of the sample were all shielded by copper braiding from the point at which they left the screening box. The furnace case was connected to both of the screening boxes and also to the negative side of the regulated power supply. The lead-through was connected via a shielded plug and socket and a length of coaxial cable to the electrometer. This cable was wrapped several times around a ferrite rod to reduce the pickup of external interference. Thus the whole system was, as far as possible, a complete coaxial system, although the "outer shield" consisted of several separate parts.

At low temperatures the noise was often as large as, or larger than, the D.C. signal it was desired to measure and it was only possible to take current measurements by drawing a "trend line" through a very noisy trace on the chart recorder output. The noise problem was generally much less severe at higher temperatures where the sample resistance was much lower and the currents measured correspondingly higher.

3.7 Temperature Measurement

The temperature of the sample was measured using a platinum/platinum + 13% rhodium thermocouple welded to the platinum gauze about 2mm away from the back of the sample. The cold junction was a brass block whose temperature was measured by a mercury-in-glass thermometer. The thermocouple E.M.F. was measured on a Solartron digitial voltmeter with a resolution of 2.5μV - this corresponds to about one quarter of a centigrade degree. It is estimated that the sample temperature was known within a few centigrade degrees at all temperatures encountered in this investigation.

4. CONDUCTIVITY MEASUREMENTS

The conductivity of the samples was calculated from the measured conductance using the formula:-

$$\sigma = G \frac{l}{a} \qquad (4.1)$$

where σ is the conductivity (Sm^{-1})
G is the conductance (S)
l is the sample thickness (m)
a is the contact area (m^2)

Different methods of measuring G were used in different measurement runs; these are described below. The sample thickness was measured with a micrometer, and an average of four measurements was taken.

The contact area, a, was taken to be the area of the sputtered platinum centre contact, which was measured with a travelling microscope. It was noted that, after a measurement run, the platinum coating had become much thinner, probably due to evaporation. This caused the sheet resistance of the contacts to increase by several orders of magnitude. The effect of high resistance contacts has been theoretically investigated (25), and it was concluded that the effect is only of consequence when the sample conductance is high, i.e. at high temperatures. It has also been reported that at higher temperatures the resistance of the electrodes is not critical (26), as they are shorted out by surface and gas conduction. It is estimated that errors due to the change of the resistance and effective area of the electrodes were less than a factor of two throughout the measurements of this investigation.

For all measurement runs the sample temperature was measured with a platinum/platinum -13% rhodium thermocouple. It is estimated that the temperature of the sample was known to within a few degrees. The errors in the measurements of "G", "l" and "a" led to an error in the estimation of the conductivity which was probably less than a factor of two.

The relative accuracy, however, is better than this. Fig. 14 shows the results of measurements made on a nominally pure sample. The measurements, which will be discussed further below, were all made while the sample was cooling, and the scatter is less than ±30% except for measurement runs started near the "knee" region. The presence of the "knee" is identified in section 7 with the valence change of iron impurities in the sample and so the variation of conductivity in this region is due to changes in the state of the sample, not experimental error. Thus it appears that any differences greater than about 50% between measurement runs made under the same conditions may be attributed to a real change in the sample and not to experimental error.

The conductivity measurements were divided into two phases: those taken while the sample was continuously cooling and those taken while the sample temperature was held constant. For convenience the results of the two phases are discussed separately.

4.1 Measurements with Sample Temperature Continuously Falling

The results of the first two measurement runs are shown in Figs. 14 and 15. All of these measurements were made by heating the sample, applying a voltage across it, and then monitoring the current and temperature as the sample cooled. Voltages of both polarities up to about 350V were used and the cooling rate varied from about $5^{\circ}C$ per minute at $1000^{\circ}C$, to about $1^{\circ}C$ per minute at $300^{\circ}C$.

During the course of these measurements it was noticed that the results indicated the presence of a "background current", i.e. when the input voltage was reduced to zero there was still a residual reading on the meter. At low temperatures currents flowing in the opposite direction to that expected were occasionally measured. The exact cause of this "background current" was not known, although contact potentials and external interference were suspected. The presence of a "background current" has been reported before (8).

Several measurement techniques which enabled the measurement of this "background current" were tried. The simplest was to reduce the input voltage to zero and measure the "background current" directly. This method worked quite well at the higher temperatures, but at lower temperatures, where the effect was thought to be more important, the time taken for the current to decay to the background level was too long to allow the results to be considered with any confidence. Other methods involved switching the input voltage between two or three different values as the sample cooled and then interpolating values from the curves obtained to find the "background current" and the conductivity. These methods suffered from a similar drawback to the method mentioned previously: that of long time decays at low temperatures.

Despite these difficulties it was possible to obtain conductivity results which, it is felt, are representative of the sample conductivities. Measurements were made in argon and oxygen ambients. No systematic variation of conductivity with ambient was found and so all the measurements are considered together.

4.1.1 Nominally Pure Sample

The results of measurements on a nominally pure sample are shown in Fig. 14. All the measurement points are not shown, as measurements were made every few degrees as the sample cooled. The plotting of each point would be extremely tedious and not very useful. One set of measurements is represented by one line, to within a few per cent.

Most of the results are seen to fall near two straight lines (a) and (b). In the range $0.9 < 10^3/T < 1.3$ the results follow line (a) which has a slope equivalent to an activation energy of about 2.9eV. The results for $10^3/T < 0.9$ fall a little below an extrapolation of this line, and have a slope corresponding to about 2.5eV.

The form of the results at lower temperatures is quite interesting. If the sample was cooled from any temperature above about 700°C ($10^3/T \approx 1.0$) and the conductivity monitored as the sample cooled, then the results followed line (a). If the sample was left at about 600°C ($10^3/T \approx 1.15$) for several hours, then subsequent cooling would give results as line (b). If the sample was held at lower temperatures for some time after cooling from a high temperature then intermediate lines such as (c) and (d) were found. The slope of line (b) is equivalent to an activation energy of about 1.4eV.

4.1.2 Chromium-Doped Sample

The results of measurements on the chromium-doped sample, as shown in Fig. 15, are seen to be of a similar form to those of the nominally pure sample, but they are not so closely grouped. This variation of the results was mainly due to a slow decrease of the conductivity with time, over a period of a few weeks. The measurements in the range $0.9 < 10^3/T < 1.3$ have slopes corresponding to activation energies in the range 2.7 to 2.95eV. At higher temperatures the slope is a little lower, 2.2 to 2.4eV.

Again at lower temperatures there are two main sets of measurements. The group of higher conductivity results have slopes corresponding to activation energies of 1.3 to 1.5eV. The lower conductivity branch is an extrapolation of higher temperature results.

Comparing the results of Figs. 14 and 15 we see that the general forms of the curves are similar. The slopes of the lines agree quite well in both the high and low temperature regions. In the region $0.7 < 10^3/T < 0.8$ the measured values of conductivity are very close. At lower temperatures ($0.9 < 10^3/T < 1.3$) the conductivity of the chromium-doped sample was about one order of magnitude higher than that of the nominally pure sample, for both the upper and lower branches of the curve. The conductivity of the chromium-doped sample appeared to be decaying towards that of the nominally pure sample.

Although the existence of a good straight line fit to conductivity data is not necessarily a guarantee of the presence of only one conduction mechanism (115, 116), in the absence of evidence to the contrary it would seem reasonable to suppose that the conduction processes in the two samples are similar.

As these two sets of results are fairly simple in their form, they will be used as "standards" when discussing later measurements.

4.2 Measurements with Sample Temperature Constant

It was felt that the presence of a "background current" and the existence of long time-constant current decays, as had been indicated by the measurements just discussed, might severely affect conductivity measurements at low temperatures where it is necessary to measure only very small currents. In order to study the "background current" and decay phenomena in more detail it was necessary to take a series of measurements on samples held at constant temperature. This was impossible using the original A.C. powered furnace, and so a regulated D.C. power supply was built. This has been described in section 3. Using this supply it was possible to hold a sample at a constant temperature ($\pm 2^{\circ}C$) for several days and a new series of measurements was undertaken.

It soon became clear that measurements made at constant temperature were very difficult to interpret. At any temperature between $200^{\circ}C$ and $1000^{\circ}C$ the current was found to decay slowly after a change of applied voltage. At the lower temperatures especially, the current did not always tend towards a well-defined equilibrium value. In these cases the actual value of current taken to correspond to any given applied voltage was, to some extent, arbitrary. In order to obtain results in a reasonable time some criterion had to be applied. For example, as will be discussed later, the decay curves were not generally exponential. However, the initial decay could be approximated to an exponential

decay, the current left to decay for five or more "time constants" and the value of current then flowing was recorded, even if the current were still falling at a faster rate than would be expected for a true exponential decay. This enabled comparative measurements to be made at different temperatures. The method was not felt to be completely satisfactory however, as it was not entirely objective.

For some of the later results, theoretical decay curves were fitted to the measurements in an attempt to find the equilibrium current. It was not usually possible to fit one decay formula to one set of measurements for all values of time, and so the formula which fitted best at the longer measurement times was used. The study of the current decays will be discussed in the next section.

During these measurements the non-ohmic behaviour of the samples was noted. As an estimate of the magnitude of this effect the incremental conductivities at high voltages (near 500V) and at low voltages were calculated. The difference between the two values of conductivity was generally less than a factor of five, except in a few instances which will be specifically mentioned. As will be noted in the next section, no useful analysis of the non-ohmic behaviour has been possible, and so in plotting Figs. 16 to 19 an average value has been used.

4.2.1 Chromium-doped Sample

The measurements shown in Fig. 16 were all carried out on a chromium-doped sample. The lines represent the results of two separate heatings of the furnace although the sample was not removed from the furnace between heatings. The points were measured by applying a voltage across the sample and monitoring the current flowing. Graphs of the current decays were drawn and extrapolated to give an estimate of the equilibrium current. It was at this time that it was noticed that the form of the current decay could not be adequately described by one simple decay formula,

and different decay formulae were tried. The one that fitted best at the longer measurement times was used. As a general rule the current seemed to approach an equilibrium value more quickly at higher temperatures and so the high temperature results were felt to be more reliable. However, the results obtained were fairly consistent, all within a factor of three of the lines shown, with the exception of the first measurements at about 200°C ($10^3/T \simeq 2.0$), when the current showed no sign of levelling off after 50 minutes. The conductivities were calculated from the ratio of the applied voltage and the extrapolated value of equilibrium current (the non-ohmic behaviour had not been noted at this time).

Comparing these results with those made while the sample temperature was continuously falling, as shown in Figs. 14 and 15, we see that the conductivity values in the range $0.8 < 10^3/T < 1.0$ agree quite well with those of the pure sample (Fig. 14) and are a little lower than those of the chromium-doped sample (Fig. 15). Although the magnitudes agree quite well the activation energy is a little lower (2.5eV). At lower temperatures ($10^3/T > 1.0$) the results do not coincide with an extrapolation of the higher temperature results, but follow a line of lower activation energy (1.35eV), similar to the upper branches of the results of Figs. 14 and 15. This is to be expected as the samples were allowed to reach thermal equilibrium before measurements were made. The magnitude of these results is about half that of the results previously measured on the chromium-doped sample and five times greater than those measured on the nominally pure sample.

These results are in broad agreement with those previously discussed: there is a change from a high activation energy mechanism to one with a low activation energy at around 600 to 700°C which is only measured when the sample is cooled slowly. The downward trend of conductivity, noted earlier, appears to have continued.

The results shown in Fig. 17 were measured on the same sample after the contacts had been re-sputtered. The conductivity values were calculated using the method described immediately above, and also from the slopes of measured voltage-current characteristics.

Measurements were started at about 180°C ($10^3/T \simeq 2.2$). The initial current flowing was very high and decayed for the next 115 hours without reaching an equilibrium value. The equivalent conductivity change is shown by line (a) but it must be noted that no point on this line represents an equilibrium value. It is felt that this current decay may be due to the annealing out of damage caused by sputtering the contacts. On heating, the conductivity followed line (b) and then line (c). Line (c) was traversed in both directions and then, on further heating, measurements jumped to a parallel line (d) which was followed on subsequent heatings and coolings. Line (e) was followed on all coolings and there is some evidence of a low activation energy region at the lowest temperatures (line (f)).

Some non-ohmic characteristics were recorded during these measurements, principally in the range 400°C to 600°C ($1.5 > 10^3/T > 1.1$). The high voltage (near 500V), and low voltage (near 0V), incremental conductivities were calculated. Generally the difference between the values was less than a factor of five, and the average value is plotted on Fig. 17.

Comparing these results with those of the previous runs (Figs. 14 to 16) we see that the results represented by lines (a) and (b) do not agree with any previous results. In addition they are not retraced on cooling. These two observations suggest that these results are due to a mechanism which is annealed out at higher temperatures. This mechanism could be related to the sputtering process, and may be due to induced lattice damage causing a change of vacancy concentration, or altering the charge state of impurity ions. Without confirmatory evidence, preferably

using a method which could examine the mechanical structure of the material, it is very difficult to draw any conclusions.

The line (c) represents measurements higher than any others in the same temperature range. It has the same slope as line (d), equivalent to about 2.5eV, but has a magnitude about a factor of ten greater. The sudden jumping down to line (d) is very difficult to explain. It seems unlikely that it has a mechanical cause, such as 90% of the platinum becoming detached from the centre contact, because the conductivity values were stable after this. So we must assume that either the carrier density or the carrier mobility suddenly decreased by a factor of ten. No explanation of this is offered.

Line (d) has approximately the same slope as the previous measurements and the magnitude agrees reasonably well with some of the earlier measurements shown in Fig. 15. This is evidence of a reversal of the downward trend of the conductivity noted above.

Line (e) has a similar slope to previous measurements, about 1.3eV. In magnitude it agrees with the results shown in Fig. 15, and the line continues down to about 300°C ($10^3/T \simeq 1.7$).

The results represented by line (f) do not correspond to any previous results. The slope is, however, similar to that of line (b). If, as was suggested above, the results represented by line (b) are due to sputter damage which is then annealed out at higher temperatures, this agreement of slopes is probably fortuitous. It seems unlikely that further annealing is occurring at about 300°C after the sample had been heated to over 1000°C.

4.2.2 Nominally Pure Sample

The results of Fig. 18 were measured on a nominally pure sample. The techniques used were the same as those described for the previous run. Again non-ohmic characteristics were observed, in the region 400 to 650°C, especially on the

first few measurements on heating, line (a). At the last point of line (a) the low voltage slope conductivity was about a hundred times greater than that at high voltage (about 500V across 0.9mm). Line (a), drawn through results at lower temperatures, passes through the conductivity found at the lower voltages.

After line (a) had been traced the sample was inadvertently cooled to about 300°C for a few hours. On reheating the line (b) is followed; an extrapolation of this line passes close to the point representing the high voltage conductivity at the top of line (a). On cooling lines (c), (d) and (e) are traced.

The results represented by line (a) do not agree with any of the previous results; they are much higher than most other measurements in this temperature region. The fact that they are not repeated on reheating suggests that the conduction mechanism is annealed out at higher temperatures. Again, this mechanism could be connected with the sputtering process.

The results represented by lines (b) and (c) are of approximately the same magnitude as the results found on previous runs but the two slopes are different, lower on heating and higher on cooling. The results of line (d) are of a similar magnitude to those shown by lines (b), (c) and (d) of Fig. 15, but these results seem to fall on an average of the three lines, rather than agreeing with any one set of data. There is again evidence for a low activation energy mechanism at low temperatures, but the data points do not form a convincing straight line.

4.2.3 Iron-doped Sample

The results of measurements of an iron-doped sample are shown in Fig. 19. The conductivity values were calculated from the slopes of voltage-current characteristics. The current was measured after the initial decay had died away (25).

The results at the lowest temperatures ($1.9 > 10^3/T > 1.5$) are adequately represented by a single straight line (a). Similarly the results at the highest temperatures ($1.0 > 10^3/T > 0.7$) are also represented by a single straight line (c). The results in the intermediate region, however, fall into two groups, those which fall near extrapolations of lines (a) and (c), and those which are represented by line (b).

When these results are compared to the previous results we see that line (a) falls very close to the results of Fig. 14 at high temperature and line (b) agrees fairly well with an average of lines (b), (c) and (d) of Fig. 15 although there is no true coincidence with any one of the three lines. Again we see some evidence of a low temperature, low activation energy mechanism.

4.3 Summary

The results of all the measurements of this investigation, except for the very high conductivities sometimes obtained during the initial heating of the sample, are shown on Fig. 20. This figure illustrates the basic similarity of the results obtained. At the higher temperatures ($0.7 < 10^3/T < 1.1$) most of the results have a slope corresponding to an activation energy of about 2.5eV, although the values of conductivity measured at any one temperature vary by a factor of about twenty. At lower temperatures ($1.2 < 10^3/T < 1.7$) results taken on samples which had cooled slowly through the region near $600^{\circ}C$ ($10^3/T \simeq 1.1$) generally follow lines of lower slope, corresponding to activation energies of about 1.4eV. In this region the variation of conductivity values is greater, as much as two orders of magnitude.

Although there is obviously a large variation in the different sets of measurements, underlying similarities are apparent, and these will be discussed in section 7, which is concerned with identification of the possible conduction mechanisms.

The results of this investigation may be compared to other published conductivity measurements on single crystal magnesia, as shown on Fig. 2. Most of the published results are at temperatures greater than 700°C ($10^3/T < 1.0$). In this temperature region the measurements of this investigation agree quite well with the published results. At lower temperatures the few published results available coincide with extrapolations of those at higher temperatures. Results showing activation energies of about 1.4eV as found in this investigation, have not been reported before.

5. OTHER MEASUREMENTS

Although this investigation was mainly concerned with the conductivity of magnesia, other measurements were made during the course of the work. These are described and discussed in this section.

Most of these measurements were made on the samples used for the conductivity measurements during the conductivity measurement runs, but the measurements described in sub-sections 5.1 and 5.2 were made on different samples taken from the same crystals.

5.1 Chemical Analysis

Samples of the crystals, from which the conductivity samples were prepared, were etched in orthophosphoric acid and sent to the Atomic Energy Establishment (A.E.E.) Winfrith for partial chemical analysis. The results of the analyses are presented in Table 3.

As can be seen there is considerable variation in the impurity levels, even between two samples from the same crystal. The iron content of the iron-doped samples is seen to vary by a factor of five, and the iron content of one nominally pure sample (crystal 1) is almost as high as that of one of the iron-doped samples.

Such variation makes accurate correlation of conductivity (or any other property of magnesia) and impurity content impossible and only agreement to within an order of magnitude can be expected.

5.2 Electron Spin Resonance Measurements

The technique of electron spin resonance (E.S.R.) has been used by other workers to study the behaviour of various defects in magnesia (36 - 47). It was decided to use the E.S.R. technique to study the behaviour of three impurity ions after various heat treatments. The impurity ions studied were Fe^{+++}, Cr^{+++} and Mn^{++}. The first two of these

were studied in an attempt to investigate the Fe^{+++}: Fe^{++} and Cr^{+++}: Cr^{++} ratios as a function of temperature. Manganese was studied as previous investigations had found it to be stable during heat treatment (38) and thus it could be used as a "reference" when assessing the measurements of the iron and chromium contents. Small samples (about 10mm x 1mm x 1mm) were cleaved from all four of the crystals and etched in boiling orthophosphoric acid. The E.S.R. spectra were all measured at room temperature on a Varian E.S.R. measurement rig.

The detailed theory of E.S.R. measurements will not be presented here, but a simplified explanation of the technique may be useful. Consider a crystal containing a defect (impurity ion, interstitial ion, etc.) having an unpaired electron. This electron has an energy level associated with it. If a magnetic field is applied the energy level splits, by an amount proportional to the magnetic field strength (Zeeman splitting). If the sample is now irradiated, energy will be absorbed by the defect when this splitting is equal to the energy of the incident photons.

The absorption spectrum is usually measured by placing the sample in a tuned microwave cavity and slowly varying the magnetic field applied to it. The field strength(s) at which absorption takes place is (are) characteristic of the defect, and the strength of the absorption is proportional to the number of defects in the sample.

The absorption spectra of the samples were measured at room temperature and the characteristic spectra of Fe^{+++}, Cr^{+++} and Mn^{++}, were identified by reference to published works (128). The samples were then subjected to different heat treatments and the spectra measured again. By comparing the size of the absorption peaks the fractional change in the concentrations of the impurities was found.

The heat treatments entailed heating the samples to 400°C, 600°C and 900°C in ambients of oxygen and argon.

One sample from each crystal was treated at each temperature and in each ambient, making a total of twentyfour samples. The duration of the heat treatments was greater than 40 hours, and at the end of this period the samples were quenched by pulling them rapidly out of the furnace and tipping them onto an alumina substrate. It is estimated that the samples cooled to below 100°C in less than ten seconds. By quenching the samples in this manner it was hoped to freeze in the defect structure (especially the charge state of the iron and chromium ions) that had existed at the temperature of the heat-treatment. The E.S.R. spectra were measured less than thirty minutes after the samples had been removed from the heat-treatment oven.

The results of this investigation are shown on Figs. 21 to 23. As can be seen, there is no clear trend in any of the results. The results of previous workers (36 - 39) had suggested that the Mn^{++} concentration would remain constant, that the Fe^{+++} concentration would change as the Fe^{+++}: Fe^{++} ratio changed with temperature, and that the Cr^{+++} concentration would change as the Cr^{+++}:Cr^{++} ratio similarly changed. The results of this investigation indicate that the Mn^{++} concentration changed to the greatest degree and the Cr^{+++} and Fe^{+++} concentrations to a lesser extent.

The reasons for this lack of conclusive results are not clear. It may be that the experimental technique was at fault. In particular the quenching rate may have been too low and the durations of the heat treatments may have been too short (see comments below in section 5.3).

Although the author was unable to obtain any useful results from this technique it is felt that such measurements could yield valuable information, especially if the E.S.R. spectra and conductivity results of similar samples could be correlated. However, it may be that the experimental techniques will need refining.

5.3 Ambient Gas Effects

As noted in the section describing the conductivity results, some of these measurements were performed in oxygen and some in argon. In general the differences measured were less than the scatter of the results and it has been impossible to draw any firm conclusions on the effect of the ambient on the conductivity.

Some measurements of the change in current flowing when the ambient was suddenly changed from one gas to the other were made. At first this seemed a reasonable method of obtaining comparative results, but further investigation revealed that the technique had several disadvantages. Firstly, although the gas flows could be turned on and off rapidly there was considerable mixing in the gas pipes and the gas drying equipment. Thus the gas passing over the sample was an undefined mixture for some unknown time after the intended changeover. This disadvantage could perhaps be overcome by a redesign of the gas system. Secondly, the different thermal conductivities of the gases, combined with slightly different flow rates changed the temperature of the sample. This would cause a change of current for two reasons:

a) the sample conductance would change;

b) a thermoelectric EMF would be set up owing to a small thermal gradient across the sample.

This difficulty could perhaps be overcome by using a separate thermostatically controlled ambient gas heater placed inside the work tube. There may be severe practical problems with this arrangement. Thirdly, there would be an EMF set up across the cell due to the galvanic cell action when there are different oxygen partial pressures on the two sides of the sample.

Lastly, in the time taken for these measurements, the gas would probably only have had time to affect the surface properties of the sample. As the measurement system was designed to measure the bulk conductivity of the sample

and to be insensitive to surface properties, no change of conductivity would be noted.

When considering the times required for a change of ambient to have an effect on the bulk of a single crystal sample it is worth while considering the diffusion rates of the ions and vacancies present. The "diffusion length" $l = \sqrt{Dt}$ is a useful measure of the rate of diffusion. When a species is diffusing into a crystal, the concentration of the diffusing species falls to a quarter of that at the surface at a distance of one diffusion length from the surface. Thus the time taken for the diffusion length to equal the thickness of a sample is a reasonable estimate of the time taken for the diffusing species to reach an approximately uniform distribution throughout the sample.

In these measurements samples approximately 1mm thick were used. For these calculations it will be assumed that the oxygen ion vacancy concentration, and the magnesium ion vacancy concentration, are both 100 ppm, and that the tracer diffusion coefficients are as given by extrapolations of the published diffusion measurements, as discussed in Section 6. The times calculated for a temperature of 1000°C are approximately 3 months, 600 years and 90 years for magnesium ion vacancy, oxygen ion vacancy, and iron ion diffusion respectively. At 800°C the corresponding times are 60 years, 6.10^4 years and 10^4 years, respectively. (Iron was chosen as an example here because it is an impurity with one of the highest diffusion coefficients in magnesia).

It is known that oxygen diffuses more quickly along grain boundaries than through the bulk (54 - 56), and so the equilibration time for oxygen motion in real samples will be shorter than the value calculated above. However, it is felt that the calculations do indicate that long annealing times are necessary below 1000°C for single crystal samples to come into equilibrium after a change of ambient gas.

After consideration of the above factors, it was decided that the measurements of this investigation had not shown any real changes of bulk conductivity resulting from a change of sample ambient. The high values of equilibration time calculated, although only estimates of the behaviour of real samples, show that no change of bulk conductivity could be expected in the time taken for these measurements. It is more likely that the changes of sample conductance actually observed were caused by the other factors discussed above i.e. changing sample temperature, thermoelectric E.M.F.s and galvanic cell effects. It was therefore decided not to attempt to analyse the effects of a change of sample ambient, and to consider all the bulk conductivity measurements together.

5.4 Non-Ohmic Effects

Voltage-current characteristics were measured on nominally pure, chromium-doped and iron-doped samples. Ohmic and non-ohmic behaviour was found and some examples of these measurements are shown in Figs. 24 to 28. Both convex (incremental conductivity increasing with increasing applied voltage) and concave (incremental conductivity decreasing with increasing applied voltage) non-ohmic characteristics were measured. The non-ohmic characteristics all appeared in the temperature range 350°C to 600°C. This temperature range is the one in which the conductivity measurements show an activation energy of about 1.4eV; i.e. the region just below the "knee". Outside this temperature range the results appeared to be ohmic up to fields of about 500V/mm.

The convex characteristics are not be be confused with the occurrence of dielectric breakdown in the sample. Breakdown effects were also observed; the current increased very rapidly with applied voltage and occasionally large current spikes, separated from each other by a few seconds, were recorded. The fields involved (approximately 500V/mm) seem too low for this effect to be breakdown of the bulk material (8, 9) and so it seems likely that the sample was breaking down around the edge.

The measurements of voltage-current characteristics obviously necessitated the measurement of current for several values of applied voltage. It was noted earlier that after a change of applied voltage the current decayed slowly, usually (but not always) to an equilibrium value. In order to obtain voltage-current characteristics in a reasonable time it was necessary to truncate these decays, and thus a non-equilibrium value of current was found. To reduce the errors introduced by such truncation, measurements were often taken for rising and falling steps of voltage, and for voltages of both polarities. The resulting measurements usually gave a loop when plotted (see Fig. 28),

and there was often noticeable asymmetry of the characteristics, see Figs. 27 and 28. The incremental conductances were computed by measuring the slopes of the "best" straight lines fitted to the measured data at high and low voltages. Usually the fitting was done by eye. Occasionally a least squares curve-fitting analysis was used; the difference between the values of conductivity obtained was negligible.

Due to the existence of the loops in the characteristics and the uncertainty in the true values of the equilibrium current, no attempt was made to fit the voltage-current curves to any theoretical model, e.g. Schottky-type injection. Previous attempts at such fitting (8, 9) have proved unsuccessful.

Although most previous workers have found, or assumed, magnesia to be ohmic, non-ohmic behaviour has been reported before. Lewis and Wright (8, 9) studied the conductivity of magnesia up to 900kV/mm and found convex voltage-current characteristics above 10kV/mm. The samples they used were very thin (down to 30μm) and were ground to form from both sides. The severe mechanical stresses induced in the crystals by grinding almost certainly created many dislocations, which may have affected the conductivity seriously. They reported ohmic behaviour up to fields of about 10kV/mm and so it appears that phenomena different from those found in this work were observed.

Osburn and Vest (10) found that their single- and bi-crystal samples were ohmic up to 400V/mm, but that their polycrystalline samples were non-ohmic. The voltage-current characteristics they found were concave and a qualitative explanation of partially blocking electrodes and a current flow determined by a rate-limiting reaction at the electrodes was presented.

It is known that the measured conductivity of solid electrolyte systems is strongly influenced by the nature of the electrodes used (see for example Ref. 123) and also that

non-ohmic characteristics can be caused by the use of electrode materials which are blocking to the moving species. The electrode material used throughout this work was sputtered platinum and this would be blocking to any other moving cation. These electrodes would not be blocking to electrons (or holes), or to oxygen ions, as the porous nature of the platinum would allow the escape of oxygen gas at the anode, and the cathode would not be blocking if oxygen atoms were available there.

The processes occurring at the electrodes would be:

$$\left.\begin{array}{ll} 2O^{--} \rightarrow O_2\uparrow + 4e^- & \text{at the anode} \\ O_2 + 4e^- \rightarrow 2O^{--} & \text{at the cathode} \end{array}\right\} \quad (5.1)$$

The possible occurrence of oxygen ion conductivity is discussed in section 6.

Non-ohmic characteristics have also been observed at metal-electrolyte interfaces where electronic conduction occurs (e.g. Schottky-type injection).

Thus the existence of non-ohmic behaviour does not then confirm or deny the existence of electronic or ionic conduction mechanisms.

It was not possible in this investigation to examine further the non-ohmic behaviour of magnesia. This investigation was able to examine only briefly what appeared to be complex phenomena. A more detailed examination might yield some interesting results. However, the making of accurate, repeatable results would be a lengthy undertaking due to the current decays found after a change of voltage. The occurrence of these decays would make measurements difficult at all temperatures, but the difficulties would be most severe at low temperatures.

5.5 Current Decay Measurements

As has been mentioned before, when the voltage applied to a sample was changed the current flowing did not reach an

equilibrium value immediately, but generally followed a decay curve. (The general term "decay" will be used, although when the voltage applied to a sample was suddenly reduced the current at first decreased and then rose towards its steady state value). This phenomenon was first noticed during the measurement of voltage-current characteristics and the decays were recorded so that the measurements could be extrapolated to determine the equilibrium value of the current. At first the decay curves were fitted by trial and error, using logarithmic and semi-logarithmic graph paper. It was noticed, however, that relatively small variations of the fitted lines led to relatively large variations in the estimated value of the equilibrium current. Later a computerised curve-fitting routine was used in an attempt to obtain less subjective results (see Appendix 3).

This enabled one set of data to be fitted to different decay curves and estimates of the "goodness of fit" to be obtained. In general the ratio of the transient to the equilibrium current decreased as the temperature increased so that it was necessary to wait a shorter time for the current to fall to within a given percentage of the steady state value. At the lower temperatures the current did not always appear to be decaying to an equilibrium value and often experiments were truncated without a reasonable estimate of the equilibrium current being obtained.

Figures 29 - 31 show some examples of measured current decays and the results of computerised curve-fitting analyses of the data. When considering these graphs and interpreting the results several points should be borne in mind. The taking of these measurements is extremely time-consuming. The results shown in Fig. 31, for example, span nearly three days and the longest decay curve measured spanned nearly eight days before measurements were halted, and even then the current had not reached an equilibrium value. The length of time involved brings problems of sample temperature control. At times greater than a few

hours after the application of the voltage to the sample the current is changing very slowly and small fluctuations of temperature will cause the current to change by more than the tail of the decay originally observed. At low temperatures the currents flowing are very small (see the scale of Fig. 15) and the decay current will be superimposed on a relatively large noise signal, necessitating the use of severe filtering. At higher temperatures the decay current will be small compared to the steady state value and, although this allows the equilibrium current to be measured more quickly, it is necessary to measure accurately small changes in a large current in order to study the decay in any detail.

Figures 29(a) - 29(d) show the decays measured consecutively on one sample at 293°C after four changes of applied voltage. The measured data points are shown together with the results of fitting curves to the data at large values of time. Two types of decay curve have been fitted to each set of data:

$$I = I_\infty + I_0\, t^{-m} \qquad \text{(in Figs. 29(a) and 29(b))} \quad (5.2)$$

$$I = I_\infty + I_0 \exp(-t/\tau) \quad \text{(in Figs. 29(c) and 29(d))} \quad (5.3)$$

Current decays following similar expressions have been observed in alkali halides and other insulators (129 - 132).

It can be seen that both forms of curve can be made to fit the later data quite closely, although neither fits the measurements at low values of time very well, expression (5.2) predicting values too high and (5.3) values too low. (It should be noted that expression (5.2) predicts an infinite value of current at t = 0, so it is to be expected that measurements at low values of time will be less than predicted). When one considers the "goodness of fit" of the curves, the model represented by expression (5.2) is generally better, but it is impossible to say that the difference is significant without analysing many more results.

Considering figures 29(a) and 29(b) where expression (5.2) is fitted to the data we see that the values of "m" obtained vary considerably (from 0.92 to 1.54) despite the fact that all these measurements were made on one sample within a few hours, and that the individual errors in the values of "m" are in the range 2% to 4%. (All errors stated on Figs. 29(a) - 29(d) are the standard errors estimated from the scatter of the data points about the fitted curve). Similar variations were noted on other measurements and values of "m" between 0.52 and 1.75 were found.

Next, considering figures 29(c) and 29(d) where expression (5.3) is fitted to the data, we see a similar spread of values for the parameter "τ" - from 544s to 802s, despite the individual errors being much less, in the range 3% to 7%. This variation was found in other measurements, and values of "τ" in the range 500s to 2900s were found during this investigation.

Figure 30 shows a current decay measured at a much higher temperature (625^{o}C). Expression (5.2) did not fit the data well and a value of τ = 734s allowed expression (5.3) to be fitted reasonably well to the later measurements. It should be noted that this graph has a false zero and that the current falls to within 10% of the (predicted) equilibrium value within 700 seconds. This is to be compared with estimated times of about 3000 seconds (from the $\exp(-t/\tau)$ model) and 8000 seconds (from the t^{-m} model), for the current to fall within 10% of the (predicted)equilibrium values for the measurements at 293^{o}C.

Figure 31 is included to demonstrate the form the current decay can take at lower temperatures. The current fell by three orders of magnitude in three days and still showed no sign of tending towards an equilibrium value. The form of this curve, where the current fell steeply again after appearing to level off, was observed several times and indicates that several decay processes are present simultaneously in the sample, and that the one which is dominant varies with the time of measurement. The last

measurements of this curve show the scatter due to the noise which is superimposed on very small currents.

The variation in the values of parameters obtained from measurements on a single sample under seemingly identical conditions was as large as or larger than the differences between measurements on different samples, or on the same sample at different temperatures. For example, compare the values of "τ" found at 293°C (544s to 802s) with the value found at 625°C (734s). The reason for part of this variation of results may lie in the nature of fitting exponential curves to data points. The procedure appears to be ill-conditioned, i.e. many sets of parameters fit almost as well as the best set. This behaviour has been reported before (119). For example, before the data of curve (4) of Fig. 29(b) was analysed by computer a hand-fitting exercise was carried out to find the values of the parameters. A curve which seemed to fit the data well had parameters I_∞=0.726 pA and m = 1.01; had a computer program not been available these values would have been accepted as satisfactory. The optimum values from the computer program were I_∞ = 0.684 pA and m = 0.92. The differences are approximately 10%, which is not large considering the spread of values found, but this does indicate that the results must be interpreted with care.

The ill-conditioned nature of the system also means that the fitting is sensitive to small changes of the input data. Thus the noise, temperature drift, and measurement accuracy problems mentioned above become very important. This is especially true when attempting to fit the sum of two exponentials to a set of data. This is a notoriously ill-conditioned case and very small fluctuations in the data will cause large variations in the values of the parameters found. Also if the initial estimates of the parameters are not reasonably good, the procedure may diverge away from a solution, instead of converging towards one.

This investigation of current decays started when it was noticed that they approximated to simple decay laws, at least

for a restricted range of the measurements. A computerised fitting procedure was used in order to obtain unbiased estimates of the parameters. As has been discussed above, quite good fits were obtained, but a clear picture of the phenomenon did not immediately emerge. In view of the time required to make the measurements, transfer them to punched cards, run the computer program and analyse the results, it was felt that further work would not produce useful results in the time available and so the investigation was discontinued. The only positive result is that the existence of these long decays indicates the existence of ionic, rather than electronic, conductivity in the temperature range studied. It is difficult to postulate a theory of electronic conduction mechanisms with long time constants such as have been measured here.

Despite the fact that the results of this brief investigation were not sufficiently consistent for the temperature- or impurity-dependence of the parameters "m" and "τ" to be proved or disproved the author feels that further investigation of this phenomenon could yield useful results. There is obviously much information in the decay curves, but the interpretation is very difficult. Any investigation will necessarily be very lengthy and would preferably use an automated method of data collection to obviate the transference of information from chart-recorder rolls to punched cards. This investigation considered only two simple decay formulae (and a brief investigation into the sum of two similar terms). The use of other formulae might meet with more success. However, the decay formulae should be kept simple; one may fit a set of measurements to almost any form of equation, provided there are enough variable parameters, but the significance of the result decreases as the number of parameters increases. The fitting of several simple formulae to restricted parts of the decay curve may well prove more fruitful than attempting to fit one general formula with many parameters to the complete curve.

6. THEORETICAL CONDUCTIVITY CALCULATIONS

In this section the values of conductivity expected from various conductivity mechanisms are calculated. The discussion will be broken into five sub-sections.

6.1 General Conductivity Relationships

6.2 Intrinsic Electronic Conduction

6.3 Intrinsic Ionic Conduction

6.4 Extrinsic Electronic Conduction

6.5 Extrinsic Ionic Conduction

Note that, unless it is specifically stated otherwise, the term "electronic" is used to describe processes involving electrons and/or holes.

6.1 General Conductivity Relationships

The conductivity of any material in which there are several mechanisms may be expressed as:

$$\sigma = \sum_{j} z_j \, q \, n_j \, \mu_j \qquad (6.1)$$

where σ is the conductivity (Sm^{-1})

z_j is the charge of the current carrier in units of q

q is the modulus of the electronic charge ($+1.602\ 10^{-19}C$)

n_j is the carrier concentration (m^{-3})

μ_j is the carrier mobility ($m^2V^{-1}s^{-1}$)

and the total conductivity is found by summing over j for all the different mechanisms.

Thus for any calculation of the conductivity expected from any given mechanism estimates of z, n, and μ are needed. The method of estimating these three quantities varies according to the class of the mechanism involved.

There are four fundamentally different classes of conduction mechanism, i.e. intrinsic electronic, intrinsic ionic, extrinsic electronic, and extrinsic ionic. For magnesia

the current carriers in these four cases are, respectively: electrons and holes arising from direct transitions between the conduction and valence bands, across the energy band gap; mobile magnesium and oxygen ions; electrons and/or holes arising from the presence of isolated energy levels in the energy band gap, caused by lattice defects; impurity ions moving through the lattice.

We will now consider the methods of estimating z, n, and μ for these four classes of conduction mechanism.

6.1.1 Carrier Charge z

This is generally the easiest of the three quantities to estimate. For electrons and holes z is always unity. For ionic mechanisms z depends on the valence state of the ion concerned. The intrinsic ions Mg^{++} and O^{--} both correspond to z = 2. The valence state of impurity ions can generally be established fairly easily; most ions have only one stable valence in magnesia (e.g. calcium, Ca^{++}, z = 2); but some ions are of variable valence (e.g. iron, Fe^{++}, z = 2 and Fe^{+++}, z = 3), and this fact necessitates separate consideration of the different valence states of the ion.

6.1.2 Carrier Concentration n

6.1.2.1 Intrinsic Electronic

The intrinsic electronic carrier concentrations may be calculated by treating magnesia as a wide band gap semiconductor and using the standard equations derived from solid state physics to calculate the electron and hole densities. If we assume that the effective masses of the electrons and holes are both equal to the rest mass of the electron, an assumption which should not be in error by more than an order of magnitude, then (133):

$$n_e = n_h = 2 \left[\frac{2\pi MkT}{h^2}\right]^{1.5} \exp(-E_g/2kT) \qquad (6.2)$$

where n_e = concentration of electrons in the conduction band (m^{-3})

n_h = concentration of holes in the valence band (m^{-3})

M = rest mass of the electron ($9.108.10^{-31}$kg)

k = Boltzmann's constant ($1.380\ 10^{-23}$ J K^{-1} = $8.617\ 10^{-5}$ eV K^{-1})

T = absolute temperature (K)

h = Planck's constant ($6.625\ 10^{-34}$ Js)

E_g = energy gap (eV)

This reduces to

$$n_e = n_h = 5.10^{21}\ (T)^{1.5}\ \exp(-E_g/2kT)\ m^{-3} \qquad (6.3)$$

There have been several estimates of the energy band gap, E_g. The best estimate now available appears to be that of Whited et al (92), 7.775 ± 0.01eV. For calculations in this section a value of 7.8eV will be used; the small rounding error is insignificant. Thus we have

$$n_e = n_h = 5.10^{21}\ (T)^{1.5}\ \exp(-3.9eV/kT)\ m^{-3} \qquad (6.4)$$

6.1.2.2 Intrinsic Ionic

The carrier concentration in these two cases will be the concentration of magnesium or oxygen ions in the lattice. It is known from lattice parameter measurements that the concentration of magnesium ion sites, and that of oxygen ion sites, is approximately $5.4.10^{28}$ m^{-3}.

6.1.2.3 Extrinsic Electronic

The concentration of extrinsic electronic carriers will be dependent on both the concentration of the isolated energy levels and their state of ionisation. The concentration of the isolated energy levels is directly related to the concentration of the defect causing them: each defect will give rise to one energy level (134). The state of ionisation will depend on the energy level - band edge separation and the temperature. The conditions in magnesia are different from those obtaining in a semiconductor at normal

temperatures and so the usual equations must be re-formulated for the calculations. The details of the calculations are given in Appendix 2, and the results are shown in Tables 4 and 5.

6.1.2.4 Extrinsic Ionic

The carrier concentration in this case may be determined by chemical analysis. The impurity concentration is usually expressed in % $^{w}/_{w}$, occasionally in atomic% or molecular %. For conversion the following relationships are used:

$$\left.\begin{array}{ll} 1 \text{ at } \% \equiv 1.08\ 10^{27}\ m^{-3} & 1 \text{ at ppm} \equiv 1.08\ 10^{23}\ m^{-3} \\ 1 \text{ mole } \% \equiv 5.4\ 10^{26}\ m^{-3} & 1 \text{ mole ppm} \equiv 5.4\ 10^{22}\ m^{-3} \\ 1\%\ ^{w}/_{w} \equiv \frac{218}{W}\ 10^{26}\ m^{-3} & 1 \text{ ppm } ^{w}/_{w} \equiv \frac{218}{W}\ 10^{22}\ m^{-3} \end{array}\right\} \quad (6.5)$$

where W is the atomic weight of the impurity ion.

6.1.3 Carrier Mobility μ

6.1.3.1 Electronic

There have been two investigations into the mobility of electronic charge carriers in magnesia. Yamaka et al (95) performed Hall effect measurements on samples in which the carriers were photoinduced. They found that the carriers were holes and obtained mobility values of 10^{-4} to 2.10^{-4} $m^2V^{-1}s^{-1}$ (presumably at room temperature although this is not stated).

The group of papers by Pomerantz et al (96 - 99) describe a study of the electrical conductivity induced in single crystal samples by electron beam bombardment. An expression for the mobility as a function of temperature in the range 200°K to 600°K is given in reference 97 and his following two papers describe the extension of measurements down to 100°K and refinements of the mathematical analysis, but do not explicitly state the values of mobility measured. In the higher temperature region (> 500°K) an extrapolation of the results is adequately described by

$$\mu = 4.5\ 10^{-5} \exp(0.148eV/kT)\ m^2V^{-1}s^{-1} \qquad (6.6)$$

The room temperature value of mobility as measured by Pomerantz et al. is about $6.10^{-3}\ m^2V^{-1}s^{-1}$, i.e. about thirty to sixty times larger than the value found by Yamaka et al., and so by using expression (6.6) we should obtain the upper limit of mobility (and hence conductivity) values.

For the purpose of these calculations it will be assumed that the hole and electron mobilities are equal; there is no direct evidence that this is true, but measurements on germanium and silicon suggest that the two mobilities are within an order of magnitude of each other. Even if the mobilities are greatly different then one would expect the higher of the two mobilities to have been measured in the experiments mentioned above, and so by assuming the lower mobility to have a value equal to that of the higher an error of less than a factor of two will be made when calculating the intrinsic electronic conductivity. When calculating the extrinsic conductivity values no distinction is made between electrons and holes and thus by using the values predicted by expression (6.6) we should obtain an upper limit on the conductivity.

6.1.3.2 Ionic

There are no published values known to the author, of experimental measurements of the mobilities of ionic species in magnesia. However, there have been many measurements of diffusion coefficients, see section 2.5 and Figs. 4 and 5, and the mobility may be calculated from the diffusion coefficient by use of the Einstein relationship (115)

$$\mu = D.\ \frac{zq}{kT} \qquad (6.7)$$

where D is the diffusion coefficient (in m^2s^{-1}) and the other quantities are as already defined.

In order to estimate ionic mobilities over a wide temperature range it has been necessary to extrapolate the measured diffusion results to lower temperatures.

6.1.4 Sources of Error in the Calculation of Conductivity Values

There are several possible sources of error in the estimation of the values of carrier concentration and mobility, and this leads to uncertainty in the calculated values of conductivity. These sources of error will now be discussed.

a) Expression (6.4) and expression (A2.8) in Appendix 2, used for calculating the electronic carrier concentrations, have been shown to give fairly accurate results when calculating the electron and hole concentrations in semiconductors such as germanium and silicon, but the accuracy of their application to materials with a large band gap, such as magnesia, does not seem to have been proved. However, one would expect the results to be of the correct order of magnitude.

b) The estimation of the mobility of the electronic carriers, by use of expression (6.6) is an extrapolation of the published results for all temperatures above about $600^{\circ}K$, i.e. for most of the temperature range of interest in this thesis. Extrapolation of results in such a manner is not usually advisable, but as there is no other method of obtaining the mobilities, we must accept these extrapolated values as the best available estimates.

c) A similar comment applies to the extrapolation of diffusion measurements to obtain values for ionic mobilities at all the temperatures of interest. Again we must accept the values obtained as the best available estimates.

d) The measurement of diffusion coefficients, when such measurements are made by following the diffusion of (usually radio-active) tracer ions, are subject to errors due to the correlation of successive jumps of the tracer

ions (135). The errors due to this effect are less than 25% for the magnesia lattice (135) and so are negligible for the purposes of this thesis.

e) The Einstein relationship, expression (6.7), does not hold true if there are many neutral defects, such as vacancy pairs, in the crystal. Such neutral defects will contribute to the diffusion but not to the conductivity. There is no evidence of large concentrations of such neutral defects in magnesia and so we shall ignore any possible error due to this effect.

f) The conductivity data presented in this thesis, and those presented in most of the literature, are plotted with the logarithm of the conductivity along the vertical axis and reciprocal absolute temperature along the horizontal axis, a log (σ) - T^{-1} graph.

If the data plotted are determined by an expression of the form:

$$\sigma = \sigma_o \exp(-Q/kT) \qquad (6.8)$$

then all the data points will fall on a straight line whose slope will be proportional to the activation energy, Q.

Lidiard (115) has shown that the temperature variation of the diffusion coefficient is given by an expression of the form:

$$D = D_o \exp(-Q'/kT) \qquad (6.9)$$

Combining the expression with expressions (6.1) and (6.7), assuming a constant carrier concentration, leads to an expression of the form:

$$\sigma T = \sigma_o' \exp(-Q'/kT) \qquad (6.10)$$

Plotting data of this form on a log (σT) - T^{-1} graph will yield a straight line; however, plotting them on a log (σ) - T^{-1} graph will yield a gentle curve. Fortunately due to the overriding influence of the exponential factor the

presence of the "T" term on the left hand side of (6.10) has very little effect on the appearance of the graph, and the curve is very shallow.

If data described by expression (6.8) are plotted on a log (σT) - T^{-1} graph, or data described by expression (6.10) plotted on a log (σ) - T^{-1} graph, the difference of the slope at any given value of T^{-1} corresponds to a difference in the value of Q of kT, i.e. 0.11eV at 1000°C and 0.05eV at 300°C. This small error is generally less than the errors in the estimated value of Q due to the scatter of the experimental points.

A similar situation exists with the electronic conductivity data. The mobility has been approximated by expression (6.6) and the intrinsic carrier concentration by expression (6.4) This latter expression contains a $T^{1.5}$ term and so plotting the data on a log (σ) - T^{-1} graph would lead to an error of Q of 1.5kT, again negligible for the purpose of this work.

If it were desired to analyse accurate, repeatable data with a very low activation energy it would be necessary to take into account any T or $T^{1.5}$ terms in expressions describing the conductivity. Such data do not exist for conductivity measurements of magnesia and so the decision to plot the data on log (σ) - T^{-1} graphs is considered justified.

6.2 Intrinsic Electronic Conduction

The expected values of intrinsic electronic conductivity as a function of reciprocal temperature are shown plotted in Fig. 32. The values represented by the line were computed by assuming that the electron and hole concentrations, which are equal for a purely intrinsic mechanism, are given by expression (6.4), and that the mobilities, assumed equal, are given by expression (6.6). Also drawn on Fig. 32 are the limits of single crystal conductivity measurements. The previously published results shown in Fig. 2, and those of this investigation, shown in Fig. 20, all lie between these limits.

As can be seen the calculated values lie well below even the lowest of the measured values, by two orders of magnitude at $10^3/T = 0.5$, and by more than four orders of magnitude near $10^3/T = 1.2$. It does not seem likely that the calculation of the carrier concentration is in error to this degree and a mobility of about 1 $m^{-2}V^{-1}s^{-1}$ seems too large for an electron or hole in an ionic crystal. Thus we may conclude that it is very unlikely that intrinsic electronic conductivity has been observed in magnesia.

6.3 Intrinsic Ionic Conduction

There are two possibilities for intrinsic ionic conduction: the movement of magnesium ions Mg^{++}, and the movement of oxygen ions O^{--}. The view generally held is that the movement of the small magnesium ions is more likely than that of the oxygen ions, although oxygen ion conductivity has been suggested (18). In magnesia the ionic radii of Mg^{++} and O^{--} are 0.72Å and 1.40Å respectively (136).

The two cases will be considered separately below.

6.3.1 Magnesium Ion Conduction

As stated in section 6.1.2.2 the concentration of magnesium ions in magnesia is $5.4\ 10^{28}\ m^{-3}$. The mobility of the magnesium ions can be calculated using the published diffusion data and expression (6.7).

There have been three papers published on the diffusion of Mg^{++} ions in magnesia (50 - 52); the results of these papers are shown in Fig. 4. The final work by Harding and Price (52) extends the measurements up to 2350°C and explains their earlier results (51) and those of Lindner and Parfitt (50). The results and conclusions of this work are very relevant to this thesis and so they will be discussed below in some detail.

It is generally considered that magnesium ions (and most other cations) diffuse through magnesia by a vacancy

mechanism (51, 52, 64) and thus the diffusion coefficient is proportional to the magnesium ion vacancy concentration (133). Evidence to support this belief comes from the failure to find appreciable concentrations of interstitial magnesium ions in un-irradiated crystals, and also from the fact that the estimated energy of formation of a cation Frenkel defect (magnesium ion vacancy plus magnesium ion interstitial), 6.3eV (105), is much higher than the estimates of the energy of formation of a Schottky defect (magnesium ion vacancy plus oxygen ion vacancy), 3.8eV (52) and 4.0eV (106).

The work of Harding and Price (52) identifies three temperature regions in which the magnesium ion vacancy concentration, and thus the magnesium ion diffusion coefficient, is controlled by different factors. The three regions are:

I: The intrinsic region - oberved above 1900°C. The Mg^{++} vacancy concentration is determined by the concentration of Schottky defects. The observed activation energy, 3.46eV, is the sum of the energy of motion of a Mg^{++} ion and half the energy of formation of a Schottky defect.

II: The extrinsic region - observed in the temperature range 1500°C to 2100°C. The Mg^{++} vacancy concentration, which is constant, is determined by the concentration of aliovalent impurity ions in the crystal. The observed activation energy, 1.56eV, is equal to the energy of motion of a Mg^{++} ion.

IV: The precipitation region - observed at temperatures below about 1500°C. The Mg^{++} vacancy concentration is again determined by the aliovalent impurity ions, but

is not constant as the impurities form precipitates and/or segregate to grain boundaries as the crystal cools. It is difficult to deduce the significance the observed activation energy, 3.2eV, but it is at least partially dependent on the energies of solution of the impurities concerned.

By comparing the observed activation energies in regions I and II the energy of motion of a Mg^{++} ion, Q_m, is estimated to be 1.56eV, and the energy of formation of a Schottky defect, Q_S, to be 3.8eV. These values agree quite well with previous estimates of 1.5eV and 4.0eV respectively (118).

When the values of conductivity expected from Mg^{++} ion motion are calculated using the published results of Harding and Price we find that the whole of the temperature range of interest in this work falls into the precipitation region (region IV). Harding and Price published two sets of diffusion coefficients in this region. One set of measurements was made using an "as received" tracer solution having an aluminium content of 2000µg/ml, and the other with a diluted tracer solution containing 100µg/ml of aluminium. It was estimated that the aluminium content introduced by the latter solution was less than the grown-in aliovalent impurity content of the samples used.

The diffusion coefficients measured using the "as received" tracer solution formed a good straight line on the Arrhenius plot in the temperature range 1130°C to 1450°C. When conductivity values are calculated from extrapolations of these diffusion measurements, values represented by line 1 on Fig. 33 are obtained. The values generally fall within the band of published results, but the activation energy, 3.1eV, does not agree with any published value.

The diffusion coefficients measured using the diluted tracer solution fell on a parallel straight line on the Arrhenius plot in the temperature range 1400°C to 1550°C. In the

temperature range 1130°C to 1400°C, however, a lower activation energy was observed. This is in accordance with an observation made by Lindner and Parfitt (50). When conductivity values are calculated by extrapolating these lower temperature measurements, the values represented by line 2 on Fig. 33 are obtained. The magnitudes of the calculated and measured values agree very well, and there is also good agreement of the slopes. It thus seems reasonable to conclude that Mg^{++} ion motion, controlled by the behaviour of impurities in the crystal, is a likely conduction mechanism.

The dependence of the diffusion coefficient, and hence conductivity, on the concentration and detailed behaviour of impurities would explain the differences in the values of conductivity found by different workers. It is also known that the state of impurities in magnesia is dependent on the thermal history of the sample: this would explain the large changes in the conductivity of a single sample before and after heat treatment, as observed during the measurements of this work.

It is possible to analyse further the results of Harding and Price to estimate the conductivity values due to Mg^{++} ion motion at any given constant vacancy concentration. These calculated conductivity values will be used in later discussion. The details of the calculation are given below.

The diffusion coefficient of Mg^{++} ions is (as noted above) proportional to the magnesium ion vacancy concentration. Thus we may write,

$$D_{Mg} = A.\exp(-Q_m/kT) \; . \; f \qquad (6.11)$$

where D_{Mg} is the diffusion coefficient of Mg^{++} ions;

A is a constant: a function of the jump frequency, jump distance, etc.;

Q_m is the energy of motion of a magnesium ion;

f is the ratio of the Mg^{++} ion vacancies to the total Mg^{++} ion concentration (i.e. in mole. fraction);

and the other quantities are as defined previously.

It is the variation of f, the fractional vacancy concentration, which causes the different behaviour of the diffusion coefficient in the three regions discussed above. By analysis of the results of Harding and Price in the intrinsic region (region I) it is possible to estimate the value of A, as follows.

In the intrinsic region the Mg^{++} vacancy concentration is, by definition, determined by the concentration of intrinsic defects in the crystal. Thus, if we ignore any second-order effects, such as vacancy - vacancy interaction, the fractional Mg^{++} vacancy concentration is given by the expression (115, 138)

$$f = C \cdot \exp(-Q_s/2kT) \qquad (6.12)$$

where C is a constant, a function of the coefficient of thermal expansion of the crystal and the change of lattice vibration frequency due to the presence of the defect. This constant has a value of about 1000 (within an order of magnitude) for materials such as magnesia (138).

Q_s is the energy of formation of a Schottky defect.

Thus in the intrinsic region, using the estimate of Q_s (3.8eV) from the results of Harding and Price, we have

$$f = 1000 \cdot \exp(-1.9eV/kT) \qquad (6.13)$$

Harding and Price find that in the intrinsic region

$$D_{Mg} = 7.43.10^{-6} \cdot \exp(-3.46eV/kT)\ m^2s^{-1} \qquad (6.14)$$

Combining expressions (6.11), (6.13) and (6.14), and using the estimate of Q_m (1.56eV) from the results of Harding and Price, we have

$$D_{Mg} = A \cdot \exp(-1.56eV/kT) \times 1000 \cdot \exp(-1.9eV/kT)$$
$$= 7.43.10^{-6} \cdot \exp(-3.46eV/kT) \qquad (6.15)$$

$$\therefore \quad A \simeq 7.10^{-9} \ m^2 s^{-1} \qquad (6.16)$$

and by combining expressions (6.11) and (6.16) we have

$$D_{Mg} = 7.10^{-9} \cdot \exp(-1.56eV/kT) \cdot f \quad m^2 s^{-1} \qquad (6.17)$$

Thus we may calculate the diffusion coefficient of Mg^{++} ions for any value of vacancy concentration by using expression (6.17).

As a check on the value calculated for A we may compare the measured diffusion coefficients in the extrinsic region (region II), where f is constant, with the value calculated from expression (6.17).

In the extrinsic region Harding and Price find that

$$D_{Mg} = 7.48 \cdot 10^{-10} \cdot \exp(-1.56eV/kT) \ m^2 s^{-1} \qquad (6.18)$$

Combining expressions (6.17) and (6.18) we have

$$D_{Mg} = 7.10^{-9} \cdot \exp(-1.56eV/kT) \cdot f$$

$$= 7.48 \ 10^{-10} \cdot \exp(-1.56eV/kT) \qquad (6.19)$$

$$\therefore \quad f \simeq 0.1 \text{ mole. fraction} \qquad (6.20)$$

(It must be noted that this last result is not general. It only holds for the samples used by Harding and Price).

Harding and Price estimated that the aluminium impurity in their tracer solution led to an Al^{+++} ion concentration of 0.15 mole fraction. This implies a Mg^{++} vacancy concentration of 0.075 mole fraction for charge compensation. The concentration of other impurities was much less than that of aluminium and so their presence would alter this value only a little. The agreement of this value of 0.075 mole fraction and the calculated value of 0.1 mole fraction in expression (6.20) is very good. This implies that the value calculated for A, and by inference the value selected for C in expression (6.12), is reasonable.

From the values of diffusion coefficient calculated from expression (6.17), values of mobility can be calculated for any value of $\dot{M}g^{++}$ vacancy concentration, using expression (6.7). The concentration of Mg^{++} ions, n_{Mg}, is given by the expression

$$n_{Mg} = 5.4 \cdot 10^{28} \cdot (1-f)\ m^{-3} \qquad (6.21)$$

where $5.4 \cdot 10^{28}\ m^{-3}$ is the concentration of Mg^{++} ion sites in the crystal and (1-f) is a "dilution factor" due to the presence of vacancies. This latter term approximates to unity for most cases of practical importance.

Thus values of conductivity due to Mg^{++} ion motion, for any vacancy concentration can now be calculated. The calculated values for several vacancy concentrations are shown in Fig. 34. For clarity the lines are drawn to span the whole temperature range, but these calculations must be interpreted with caution. Each is only valid for a constant vacancy concentration, and this condition will not occur in the intrinsic and precipitation regions.

When these calculated values are compared to the conductivity measurements of this investigation, as shown in Fig. 20, some measure of agreement is found. This will be discussed further in section 7.

6.3.2. Oxygen Ion Conduction

The diffusion of O^{--} ions in magnesia has been measured by several workers (53 - 57) but only two measurements have been performed on single crystal samples (53, 57). The results of the radio-active tracer measurements of Oishi and Kingery (53) are considered to represent extrinsic diffusion. The diffusion measurements of Narayan and Washburn (57), measured by monitoring the rate of change of dislocation loops, are considered to represent intrinsic diffusion. By considering the activation energies found by these two groups of workers, the energy of formation of a Schottky defect is estimated to be 4.0eV. This agrees well with the values estimated from

magnesium diffusion measurements (see section 6.3.1), and thus the interpretation of these results is consistent with other measurements.

The concentration of oxygen ions in the magnesia lattice is $5.4 \cdot 10^{28}$ m^{-3} (see section 6.1.2.2). To calculate oxygen ion mobility we take the diffusion results of Oishi and Kingery (53), and use expression (6.7). The values of conductivity expected from oxygen ion motion can thus be calculated using expression (6.1). The results of these calculations are shown by line 3 in Fig. 33. The calculated values of conductivity are about two orders of magnitude lower than the lowest measured value. It does not seem likely that the sample used by Oishi and Kingery had an impurity content a hundred times less that those used by other workers for conductivity results and it is therefore reasonable to conclude that oxygen ion conduction has not been observed in single crystal magnesia. It should be noted, however, that other published diffusion results (54 - 56) show oxygen ion diffusion to be much faster along grain boundaries than through the bulk. This suggests that oxygen ion motion might be an important conduction mechanism in polycrystalline material.

6.4 Extrinsic Electronic Conduction

Extrinsic electronic conductivity arises from the motion of electrons and/or holes which originate from isolated energy levels in the energy band gap. These energy levels are due to lattice inhomogeneities and their behaviour is similar to that of donor and acceptor levels in a semiconductor.

For calculation of the expected values of conductivity, estimates of the mobility and concentration of the carriers are needed. The mobility values are taken to be as given in expression (6.6) and the carrier concentration is discussed in section 6.1.2.3 and calculated in Appendix 2. The results of the calculations in Appendix 2 are tabulated in Tables 4 and 5. On examining Table 5 we see that, at any given temperature, and for any given energy level - band

edge separation, the concentration of free electronic carriers is approximately proportional to the square root of the concentration of the energy level. Thus in order to calculate the values of conductivity it is necessary to know the concentration of the energy level. To be definite we shall choose a value of $5 . 10^{24}$ m^{-3}, i.e. about 100 mole. ppm. This value is entirely arbitrary and the conductivity values expected at any other concentration may be obtained by scaling the values by the square root of the ratio of the concentration to $5 . 10^{24}$ m^{-3}. The calculated conductivity values for a number of energy level - band edge separations are shown in Fig. 35. The slopes of the lines are equivalent to activation energies of approximately half the energy level - band edge separation.

By comparing the calculated values with the limits of conductivity measurements, also shown on Fig. 35, we see it is quite possible that extrinsic electronic conductivity has been observed in magnesia. Energy level - band edge separations in the range 2 to 6eV give conductivity values with slopes close to observed values. In order to give conductivity values of the correct magnitude the concentration of energy levels 2eV from the band edge would need to be about $5 . 10^{9}$ m^{-3} (i.e. 1 level per 10^{19} Mg^{++} sites), and the concentration of energy levels 6eV from the band edge about $5 . 10^{27}$ m^{-3} (i.e. 1 level per 10 Mg^{++} sites). These calculations will be referred to in section 7.

6.5 Extrinsic Ionic Conduction

Measurements of the diffusion coefficients of impurity cations have been published by several workers (58 - 70). Their results are collected together in Fig. 5. The mobility of any given ion can be computed from the measured diffusion coefficient by use of expression (6.7).

The impurity content of a sample can be determined by chemical analysis and the equivalent carrier density calculated by use of expressions (6.5). In this section we

will calculate the conductivity values expected for an impurity content of 100 ppm $^{w}/_{w}$. This is a fairly high concentration of most impurities in the majority of reasonably pure samples, and so the values obtained will generally represent the upper limit of the values expected in practice. Calculation of the conductivity of any other impurity content is simply a matter of scaling up or down, except in the cases when the diffusion coefficient varies with concentration. These cases will be specially noted in the following discussion.

Typical chemical analyses of magnesia crystals can be found in references 1 and 70.

The following discussion will deal separately with normally monovalent, normally divalent, normally trivalent, and normally tetravalent ions. The valency state of iron is known to be variable and so the behaviour of iron will be discussed separately.

6.5.1 Normally Monovalent Ions

The author has found no published measurements of diffusion of monovalent cations and so it is impossible to estimate with any accuracy their contribution to the conductivity. However, analyses of crystals (1, 70) show that in undoped crystals the monovalent impurity concentration is generally low, < 1 ppm $^{w}/_{w}$. Also, with the exception of lithium, the concentration of which is usually less than 1 ppm, the ionic radii of monovalent ions are rather larger than that of Mg^{++} (136). This suggests that the diffusion coefficients are smaller than that of Mg^{++}. Taking these observations into consideration it is probably reasonable to assume that the mobile monovalent impurity ions play little part in the conductivity of undoped crystals.

6.5.2 Normally Divalent Ions

Several measurements of the diffusion of divalent ions have been published. The various elements are considered separately below.

6.5.2.1 Barium Ba^{++}

Only one measurement of Ba^{++} diffusion has been reported: that of Harding (65). He found two diffusion coefficients; one for small penetrations, which he referred to as the "lattice diffusion coefficient", and a second at larger penetrations which describes "dislocation - influenced diffusion". Taking the larger of these two coefficients (i.e. the latter) and calculating the conductivity values for an assumed impurity content of 100 ppm $^{w}/_{w}$ gives values represented by line 1 in Fig. 36. Also shown on Fig. 36 are the limits of conductivity measurements.

The calculated values fall below the measured values at all temperatures above 550°C ($10^3/T \simeq 1.2$). Below this temperature the calculated values are a little higher than the lowest measured values. However, the concentration of barium in undoped crystals is generally closer to 1 ppm $^{w}/_{w}$ than to 100 ppm $^{w}/_{w}$ (1), and so the contribution to the conductivity by barium is probably as much as two orders of magnitude less than the values shown by line 1 in Fig. 36. Thus we may conclude that barium ion conductivity has not been observed in magnesia.

6.5.2.2 Beryllium Be^{++}

The diffusion coefficient of beryllium has a lower activation energy (1.6eV) (64) than that of the diffusion coefficients of most other divalent cations in magnesia. This has led to the suggestion (64) that it does not diffuse in the same manner as most of the other cations discussed in this section. The small ionic radius of 0.35 Å (136) would suggest that interstitial diffusion is possible.

The conductivity values calculated from the diffusion coefficient, assuming an impurity content of 100 ppm $^{w}/_{w}$, are shown by line 2 on Fig. 36. These values are similar in slope and magnitude to some of the measurements of this investigation, especially in the region $10^3/T > 1.2$.

However, beryllium is not usually present in magnesia in concentrations above 1 ppm $^{w}/_{w}$ (1). Thus the expected conductivity of an undoped sample is at least two orders of magnitude less than that shown by the line. No such measurements have been reported. It is thus unlikely that beryllium ion conduction has been observed, although gross contamination (perhaps from beryllium copper electrodes) might affect the conductivity.

6.5.2.3 Cadmium Cd^{++}

The values of conductivity as calculated from the diffusion measurements of Harding and Bhalla (69), assuming a cadmium content of 100 ppm w/w, are represented by line 3 on Fig. 36. As can be seen, the calculated values fall several orders of magnitude below the measured results at all temperatures. Thus we may conclude that cadmium ion conduction has not been observed in magnesia.

6.5.2.4 Calcium Ca^{++}

The diffusion of calcium in magnesia has been measured by Rungis and Mortlock (64). The values of conductivity calculated using their results and assuming a calcium content of 100 ppm w/w are shown by line 4 on Fig. 36. The measured results at all temperatures are more than an order of magnitude greater than the calculated values, even for a relatively large calcium content. Thus we may conclude that calcium ion conduction has not been observed in magnesia.

6.5.2.5 Cobalt Co^{++}

There have been two investigations of the diffusion of cobalt in magnesia. Wuensch and Vasilos (58) found that the diffusion coefficient was independent of the cobalt concentration, but Zaplatynsky (59) found a concentration dependence, the diffusion coefficient increasing as the colbalt concentration increased. Taking the larger values of diffusion coefficient, those of Zaplatynsky, and

calculating the conductivity expected for a cobalt content of 100 ppm $^{w}/_{w}$ we obtain the values shown by line 5 in Fig. 36. At all temperatures the measured results exceed the calculations by at least two orders of magnitude. The typical cobalt content of an undoped crystal is less than 10 ppm $^{w}/_{w}$ (1, 70) and so we may conclude that cobalt ion conduction has not been observed.

6.5.2.6 Manganese Mn^{++}

Manganese can exist in several valence states, but it has usually been reported as a divalent ion in magnesia (38) and is thus considered with other divalent ions.

The diffusion of manganese in magnesia has been studied by Tagai et al. (61). The conductivity values calculated from their results, assuming a manganese content of 100 ppm $^{w}/_{w}$ are shown by line 6 in Fig. 36. We see that, in the region $10^3/T < 0.8$, the calculated values are lower than the measured results. In the range $0.8 < 10^3/T < 1.2$ the calculated values are of the right magnitude, but no measurements of the same slope (1.0eV) have been reported. At lower temperatures, however, the calculations predict conductivity values higher than those measured. This would imply that the conductivity of single crystals is dominated by manganese ion conduction at temperatures below about 550°C.

As will be discussed in section 7 there is evidence to suggest that another mechanism is responsible for conductivity measurements of similar activation energies in this temperature region. If this is so it implies that the calculated values of Mn^{++} ion conductivity are incorrect. The most likely reason for this would be a change of the diffusion mechanism which leads to lower values of diffusion coefficient, and hence conductivity, below 550°C, than those obtained by a simple extrapolation of the high temperature results. As the results of Tagai et al. were all made at or above 1300°C, this hypothesis is not unreasonable.

6.5.2.7 Nickel Ni^{++}

There have been four determinations of the diffusion coefficient of nickel in magnesia (58, 59, 66, 68). Zaplatynsky (59) and Blank and Pask (66) reported that the diffusion coefficient was a function of the nickel concentration. Wuensch and Vasilos (58, 68) found no concentration - dependence. This disparity they attributed to the difference in nickel concentration levels used in their experiments. The work of Wuensch and Vasilos was carried out at low nickel concentrations and so their results are probably more representative of the behaviour of nickel in undoped crystals. For this reason it is their results which are used for the conductivity calculations.

Calculating the conductivity expected for 100 ppm $^{w}/_{w}$ of nickel gives the values represented by line 7 in Fig. 36. The results are well below the measured values at all temperatures, even for a relatively high nickel content. Thus we may conclude that nickel ion conduction has not been observed in magnesia.

6.5.2.8 Zinc Zn^{++}

Wuensch and Vasilos measured the diffusion of zinc in magnesia (62). Calculating the conductivity for a zinc content of 100 ppm $^{w}/_{w}$ gives the values shown by line 8 in Fig. 36. At the higher temperatures, $10^{3}/T > 1.0$, the calculated values are greater than the lowest of the measured values. However, zinc is usually present in concentrations in the range 1 to 5 ppm $^{w}/_{w}$ and so the expected values of conductivity in undoped crystals will be as much as two orders of magnitude less than the values shown by line 8. It thus seems very unlikely that zinc ion diffusion has ever been observed in magnesia.

6.5.3 Normally Trivalent Ions

Measurements of aluminium (70) and chromium (61, 67) diffusion have been reported. The presence of trivalent ions in the lattice causes a charge imbalance and thus tends

to favour the formation of cation vacancies for charge compensation. If diffusion proceeds by a vacancy controlled process then the diffusion coefficient will be an increasing function of the concentration and specialised graphical techniques are needed for calculation of the diffusion coefficient (67, 70).

6.5.3.1 Aluminium Al^{+++}

The results of Whitney et al. (70) show that the diffusion coefficient of aluminium in magnesia is linearly dependent on the aluminium concentration. Extrapolating these results to obtain a value for the diffusion coefficient at 100 ppm $^{w}/_{w}$ and calculating the conductivity as before, the results represented by line 9 in Fig. 36 are obtained. The calculated results are much less than the measured results at all temperatures.

It should be noted that the linear dependence of the diffusion coefficient on concentration implies that the aluminium ion conductivity varies as the square of the aluminium content at high aluminium concentrations. Aluminium is not usually found in concentrations exceeding 100 ppm $^{w}/_{w}$ in undoped crystals (1, 70) and so we may conclude that aluminium ion conduction has not been observed in magnesia.

6.5.3.2 Chromium Cr^{+++}

Chromium normally exists in magnesia in the trivalent state, although reduction to the divalent form may occur in some ambient conditions (40). Chromium diffusion has been measured by Tagai et al. (61) and by Greskovich (67). The former workers reported no concentration dependence, but Greskovich found that the diffusion coefficient was exponentially dependent on the chromium concentration. An extrapolation of his results gives values of diffusion coefficient which are approximately three times larger than the measurements of Tagai over the temperature range of interest. Calculating conductivity values from the results

of Greskovich gives the values shown by line 10 in Fig. 36. These values fall well below the lowest values of conductivity measured.

Again, due to the concentration - dependence of the diffusion coefficient, the conductivity will increase more rapidly than the chromium concentration, especially at high concentration (> 1 mole %). The chromium content of undoped crystals is however generally less than 100 ppm $^{w}/_{w}$ (1, 70) and so we may conclude that chromium ion conduction has not been observed in magnesia. Even at the concentrations found in the chromium-doped samples used in this investigation (750 ppm $^{w}/_{w}$) the predicted conductivity values are only one order of magnitude higher than the values discussed above, i.e. at least two orders of magnitude below the lowest measured values.

6.5.4 Normally Tetravalent Ions

The author has been unable to find any published measurements of the diffusion of tetravalent ions in magnesia. Silicon in particular is found in concentrations of the order of a hundred parts per million in magnesia (1, 70). Several tetravalent ions have relatively small ionic radii, which would suggest the possibilty of fast interstitial diffusion. However, the large extra charge in the lattice might cause the impurities to be trapped in (cation vacancy) - (impurity)-(cation vacancy) complexes which would probably be able to move only slowly through the lattice. Separate investigations would be necessary to clarify these points.

It is thus not possible at present to estimate with any accuracy the contribution made to the conductivity by tetravalent ions.

6.5.5 Iron

Iron is a very common impurity in magnesia, and its concentration can exceed 100 ppm $^{w}/_{w}$, even in nominally pure samples (1). It is found in several forms (see below) and

the effect on the conductivity of changes of form, especially the transition between the ferric and ferrous states, has been considered by previous authors (5, 21). In view of the complex behaviour of iron, it is considered separately from other impurities.

Many investigations of the state of iron impurities in magnesia have been carried out. The electron spin resonance technique, described previously, has been used several times to study the behaviour of iron (36, 38, 40, 41, 45, 48). Other techniques, such as measurements of the Mössbauer effect (the measurement of nuclear resonance fluorescence during the recoil-less emission and resonant reabsorption of γ-rays) (110) and analysis of the hardness of crystals (109) have also been used to determine the effect of heat treatments on iron impurities in magnesia. We will not consider in detail the methods used, but only the results of the investigations.

Iron has been detected in magnesia in many forms: Fe^{+} (38), Fe^{++} (38, 40, 84, 109, 110), Fe^{+++} (38, 40, 109), metallic iron (109, 110), inclusions of magnesioferrite $MgFe_2O_4$ (66, 109, 110), and inclusions of ferric oxide Fe_2O_3 (110). Although there is not a complete agreement about the detailed behaviour of iron, it is generally agreed that Fe^{++} tends to be the stable form at high temperatures and in reducing or neutral atmospheres, and that Fe^{+++} is more stable at low temperatures; the transition temperature has been estimated to be approximately 560°C ($10^3/T \simeq 1.2$) (107). In strongly reducing atmospheres the iron may be reduced further to Fe^{+} and to metallic iron (109, 110). Fe^{++} ions are very soluble in the magnesia lattice; the complete range of FeO-MgO solid solutions is known to exist. The solubility of Fe^{+++} is much more limited, about 0.3 to 0.5 atomic % at 900°C (110), and if iron is converted to the trivalent state by heating in air or oxygen, precipitates of magnesioferrite may form on cooling (109, 110).

The transition between the divalent and trivalent states does not take place instantaneously. There have been many

references to the time taken for iron impurities in magnesia to come into equilibrium with the surroundings. Soshea (84) reported that it was necessary to leave a 0.5mm thick crystal at 1400°C for an hour to come into equilibrium. Hansler et al. (40) found it necessary to hold their sample at 1100°C for six hours to remove the Fe^{+++} spectrum. Chiba et al. (48) observed the rate of formation of Fe^{+++} in magnesia in air. They found that the times taken to achieve 50% of the final concentration change were about 100min., 50min., and 20min. at 1200°C, 1300°C and 1500°C respectively.

It is thus possible to find iron in magnesia in its non-equilibrium form i.e. Fe^{+++} at high temperatures following rapid heating, and Fe^{++} at low temperatures after rapid cooling. Observations of the latter condition are more likely as the higher diffusion rates at high temperatures would allow the system to reach equilibrium more quickly than would be possible at lower temperatures. These observations will be discussed in section 7.

6.5.5.1 Ferrous Ion (Fe^{++}) Conduction

There have been three investigations of iron diffusion in magnesia which have been attributed to Fe^{++} ion motion (58, 61, 66).

The results obtained by Wuensch et al. (58) and by Tagai et al. (61) are basically very similar. Neither group of workers found any concentration dependence: the activation energies of the two sets of results are very close, and the difference between measured values at any one temperature is less than a factor of five. The highest values were obtained by Tagai et al. when using oxidised ferric chloride as a source of iron.

Calculating the conductivity from these values, assuming an iron content of 100 ppm $^{w}/_{w}$, all present as Fe^{++} ions, we obtain the results represented by line 1 in Fig. 37. In the temperature region $10^3/T < 1.1$ these calculated values are less than the lowest measurements. At lower

temperatures the calculations lead to values a little higher than the lowest measurements.

It would thus seem that Fe^{++} motion is a possible conduction mechanism, especially in the temperature region $10^3/T > 1.1$. However, the valence change known to occur at about 560°C ($10^3/T \simeq 1.2$) means that the extrapolation of these results is probably more prone to error than are the other extrapolations discussed so far. The calculated conductivity values for temperatures below 560°C are likely to be too high because the Fe^{++} ion concentration will decrease as the temperature falls, due to the formation of the more stable Fe^{+++} ions.

We may thus conclude that it is unlikely that Fe^{++} ion conductivity has been observed in undoped single crystal magnesia.

The third investigation of iron diffusion attributed to Fe^{++} motion was by Blank et al. (66). Their results are very different from those discussed immediately above. The diffusion coefficient was found to be concentration-dependent and the activation energy measured was quite different. Extrapolating these results to find the value of diffusion coefficient at 100 ppm $^{W}/_{W}$ iron content, and calculating the conductivity as before we obtain the values represented by line 2 in Fig. 37. These calculated values are less than the measured values at high temperatures and are of approximately the same magnitude as the measured values below the "knee", although the agreement of the slopes is not good.

A possible reason for the differences between these results and those discussed above is found when the experimental procedures are examined. Wuensch et al. and Tagai et al. used relatively low surface concentrations of iron for their diffusion sources. Blank et al. buried magnesia crystals in iron powder and relied on the reaction

$$xFe + MgO \rightarrow Fe_xO + Mg \uparrow \qquad (6.22)$$

for the production of Fe^{++} ions. The iron concentrations measured were very high, up to 25 atomic % and it thus seems reasonable to conclude that these measurements do not accurately represent the diffusion of Fe^{++} ions in a crystal of fairly low iron content. Hence it also seems likely that the values of conductivity calculated from these results will not be observed in any but the most highly doped crystals.

6.5.5.2 Ferric Ion (Fe^{+++}) Conduction

Blank et al. also measured iron diffusion due to Fe^{+++} motion (66). The iron concentrations encountered were much lower than those found during measurements of Fe^{++} ion motion, due to the limited solubility of Fe^{+++} ions in the lattice. The diffusion coefficient was found to be independent of iron concentration.

Calculating the conductivity values as before, assuming an iron concentration of 100 ppm w/w, all present as Fe^{+++} ions, we obtain the values represented by line 3 in Fig. 37. The calculated values are close to the measured results at high temperatures, but the calculations fall well below the measurements at lower temperatures. It would at first seem that Fe^{+++} ion motion is a possible conduction mechanism at high temperatures, but Fe^{+++} is the less stable form of iron at high temperatures. Therefore the Fe^{+++} ion concentration will be much less than the total iron concentration due to the existence of the more stable Fe^{++} ions. Thus the conductivity values at high temperatures will be less than those shown by line 3, and so it is reasonable to conclude that Fe^{+++} ion conduction has not been observed in magnesia.

6.6 Summary

In this section the values of conductivity expected from a wide range of possible conduction mechanisms have been calculated. The list is not exhaustive due to the lack of published information. There are many impurity ions found in magnesia, for which there are no published diffusion

data (e.g. silicon, titanium). It is thus impossible to estimate their contribution to the total conductivity. It is also possible that the calculated values are considerably in error, as it has been necessary to extrapolate published results to temperatures far above or below those at which the measurements were made. The author believes, however, that the values obtained here represent the best estimates at present available. As new information becomes available the calculated values may easily be modified, should this be required.

The conduction mechanisms which were found to lead to conductivity values which agree, at least to some extent, with measured values were found to be:

Mg^{++} ion conduction
extrinsic electronic conduction
Mn^{++} ion conduction

The results obtained in this section will be referred to in section 7, which is concerned with the identification of possible conduction mechanisms.

7. DISCUSSION

In this section the nature of the conductivity of magnesia is discussed. Identification of the most likely conduction mechanisms is made by considering measurements made on magnesia, both by the present author, and by other workers.

It was noted in sections 4 and 5 that the current flowing after the application of a voltage to the sample generally decayed from a high initial value towards a lower equilibrium value. There are two theories which have been proposed to explain the existence of these decays. The "space-charge polarisation" theory states that the initial current is representative of the true conductivity and that the decay is due to the build up of a space-charge near the electrodes. The "dielectric relaxation" theory, on the other hand, states that the equilibrium value of the current represents the true conductivity and that the current decay is due to a change in the dielectric constant of the material with time.

The two theories have coexisted since the 1920's and, although there has been considerable investigation of this phenomenon in alkali halides (see, for example, Ref. 129 and the references therein), it has not been established which of the two theories is valid for conduction in magnesia. Previous workers have generally measured the current flowing after the decay of the initial transient. In the measurements made at constant temperature during the present investigation the equilibrium value of current was used to calculate the conductivity. The response time of the apparatus available did not allow the measurement of the current flowing immediately after the application of a voltage to the sample. Measurements made as the sample cooled cannot be truly representative of the equilibrium current. The discrepancy between the current measured and the equilibrium current is a function of both the cooling rate of the sample and the decay time constants occurring at the temperature of measurement.

It was not the object of this investigation to establish which of the two theories is valid for magnesia and so the conductivities calculated as described above will be discussed in this section. Conductivity values calculated from the initial currents flowing would obviously be larger, by a factor which varies with the temperature at the time of measurement.

In addition to the measurements of conductivity two other measurement techniques which are capable of giving information about the conduction mechanisms are considered. Transport number measurements and thermoelectric E.M.F. measurements are discussed in sub-sections 7.1 and 7.2 respectively. Conductivity measurements are discussed in sub-section 7.3; the nature of the conductivity and the identification of conduction mechanisms are considered in sub-section 7.4.

7.1 Transport Number Measurements

The transport number of a current carrier in a material is defined as the fraction of the total conductivity of that material which is due to the carrier. In general, the transport number will be a function of temperature, the sample ambient, the defect structure of the material, etc.

We may thus define the transport number, t_j, of any conduction mechanism, j, to be

$$t_j = \frac{\sigma_j}{\sigma} \qquad (7.1)$$

where σ_j is the conductivity due to mechanism j,
and σ is the total conductivity of the material.

If we sum all the terms like expression (7.1) then we obtain the relationship

$$\sum_j t_j = \frac{\sum_j \sigma_j}{\sigma} = 1 \qquad (7.2)$$

Two transport numbers which are often used are the ionic and the electronic transport numbers, t_i and t_e, respectively. We have

$$t_i = \frac{\sigma_i}{\sigma} \tag{7.3}$$

$$t_e = \frac{\sigma_e}{\sigma} \tag{7.4}$$

$$t_i + t_e = 1 \tag{7.5}$$

where σ_i is the conductivity due to ionic motion
and σ_e is the conductivity due to electronic motion

Obviously knowledge of the magnitude of the transport numbers would be of great assistance when attempting to identify the conduction mechanisms present in a material.

Three techniques have been used to measure ionic and electronic transport numbers in magnesia. These three techniques will be discussed separately.

7.1.1 Electrolytic Cell Technique

The theory of the operation of electrolytic cells has been described in detail elsewhere (see for example references 121, 138 and the references therein) and so only a simplified description of their operation will be given here.

If an electrolyte which is a perfect ionic conductor (i.e. $t_i = 1$) is placed between two electrodes of different chemical potential there is an E.M.F. developed across the cell which is directly related to the free energy change of the reaction between the constituents of the electrodes. If the electrolyte is not a perfect ionic conductor the E.M.F. is reduced by approximately the fraction of electronic conduction present. Thus, by choosing electrode materials whose reaction is well characterised, it is possible, in principle, to determine the ionic and electronic transport numbers. It is not possible to determine whether the moving ions are anions or cations.

7.1.1.1 Measurements on Magnesia

There have been several investigations of electrolytic cells using magnesia as the electrolyte (6, 27 - 32). Only those measurements using single crystal samples (6, 28 - 30, 32) will be considered here.

Two systems have been used for measurements of magnesia: cells of the general type (29, 30, 32)

$$Pt \mid Me_1, Me_1O \mid MgO \mid Me_2, Me_2O \mid Pt \qquad (I)$$

and those of the general type (6, 28)

$$Pt\ (P'_{O_2}) \mid MgO \mid Pt\ (P''_{O_2}) \qquad (II)$$

In the first type of cell Me_1, Me_2 are metals, and Me_1O, Me_2O their oxides; nickel, cobalt and iron are metals typically used. Usually the magnesia electrolyte is held between two metal/metal oxide pellets while measurements are made. In cells of type II the two sides of the electrolyte are exposed to different oxygen partial pressures, P'_{O_2} and P''_{O_2}, and the E.M.F. generated is given by the expression (138)

$$E = \frac{kT}{4q} \log_e \left(\frac{P'_{O_2}}{P''_{O_2}} \right) \qquad (7.5)$$

This configuration is often preferred as it is possible to change the oxygen partial pressure near the sample fairly easily and so make several sets of measurements on the same sample.

Most workers have reported that the E.M.F.'s measured did not reach an equilibrium value instantaneously, and equilibration times of about 15 minutes at 1300°C (6), and up to 15 hours at about 900°C (32), have been reported. It has also been reported (32) that the behaviour of the samples is altered by a heat-treatment at about 1100°C. These reports are consistent with observations made by several workers concerning conductivity measurements.

Alcock et al. (32) summarised the results of previous electrolytic cell measurements on magnesia. The results are all consistent with a maximum value of the ionic transport number near 1000°C. The results of Alcock et al., measured with Ni/Fe and Ni/Co electrodes, agree fairly well with those of Mitoff (6), measured on a sample exposed to air and oxygen atmospheres. The results on a sample using Cr/Mn electrodes were, however,much lower, although they still show a maximum value at about 1000°C.

7.1.1.2 Discussion of Measurements

At first this technique seems to offer an ideal method of studying the transport phenomena in solid electrolytes, but there are several difficulties, both theoretical and practical.

a) The electrode used in cells of type I may react with the magnesia electrolyte. This behaviour has been reported (32) and is probably due to interdiffusion of the cations. The effect is therefore most marked in systems where the interdiffusion coefficient is high. This diffusion of impurity ions into the sample can seriously affect the conduction processes and so lead to the measurement of transport numbers which are not representative of the original sample (121).

b) Small concentrations of impurities in the metal/oxide electrodes can lead to large variations in the values of E.M.F. measured.

c) The measurements of Mitoff (6) suggest that the ionic transport number is dependent on the oxygen partial pressure, and so measurements made using a type II cell will yield a value of ionic transport number which is valid at some indeterminate intermediate oxygen partial

pressure. This difficulty can be minimised by choosing the atmospheres such that the oxygen partial pressures are not very different, but this reduces the E.M.F. developed and may lead to measurement problems.

d) There must be no gas leakage around the edge of the sample or the differential oxygen partial pressure across the electroyte will be reduced, leading to smaller values of E.M.F. than would otherwise be measured. The problems of obtaining a gas-tight seal on both sides of a ceramic sample at high temperatures are considerable.

e) Both types of cell require the use of electrical and volume guards to prevent surface and gas conduction from affecting measurements. The difference between measurements made on guarded and unguarded systems has been demonstrated by Mitoff (6, 28). The importance of using a guarded system has also been shown by Brook et al. (26) in their work on alumina. Their guarded measurements show an ionic transport number indistinguishable from unity in the temperature range 1000°C to 1400°C; whereas their unguarded measurements indicate values which fall almost to zero near 1400°C.

f) At low temperatures (<1000°C) both types of cell suffer from the problem of long equilibration times. This can lead to values of transport number which are not representative of the equilibrium state of the crystal.

g) Although in the simplified description given above it was stated that the effect of electronic conduction is to reduce the E.M.F. by the fraction of electronic conduction present, it has been reported by Steele (121)

that an electronic transport number as low as 0.005 can lead to erroneous results. Steele also stated (121) "... Even for these [qualitative] applications, however, the properties of MgO are not very favourable ...". It may be that a more refined theory of electrolytic cells is necessary before reliable measurements of transport numbers can be obtained for materials such as magnesia.

In view of the problems discussed above, the author feels that the results obtained from electrolytic cell measurements are not very useful. There are several fundamental difficulties and severe practical problems. It would appear that there is some ionic conduction occurring, as zero E.M.F. would be found if the conduction were entirely electronic. However the author does not feel that electrolytic cell measurements are at present capable of yielding accurate estimates of the electronic and ionic transport numbers in magnesia.

7.1.2 Electrode Weight Change Technique

If a material is a perfect ionic conductor ($t_i = 1$) then one gram-equivalent of the material will be decomposed for every Faraday of charge which passes through the material. This will lead to a transfer of mass between the electrodes. By weighing the electrodes before and after the passage of an electric current, the sign of the mobile ion can be determined. Often three crystals are used to overcome the problem of the crystal becoming attached to one electrode; each electrode and its adjacent crystal are weighed together. If the material is not a perfect ionic conductor ($t_i < 1$) then t_i gram-equivalents will be decomposed per Faraday. This technique was used in some of the early work on alkali halides (139).

Giutronich et al. (33) performed such experiments on single crystal magnesia samples in the temperature range 1200°C to

1500°C. They found values of ionic transport number similar to those found by Mitoff (6), and were able to determine the moving ionic species to be a cation, which they identified as Mg^{++}.

This type of measurement, although it may seem very simple at first, is, in fact, very difficult to interpret. The problem of gas and/or surface conduction is again encountered. The results obtained may be determined as much by the environment as by the sample. In order to obtain measurements which are truly representative of the bulk material, surface and volume guards must be used at every interface. Giutronich et al. did not use such guards and so the author feels that their results do not accurately describe the ionic transport number of bulk magnesia.

7.1.3 Crystal Face Movement Technique

This technique is, in principle, the same as that discussed immediately above. The difference lies in the fact that, instead of the mass of the transferred material being measured, the volume change caused by the transfer is monitored. Due to the small distances involved very sensitive measurement techniques are necessary.

Gauthier et al. (34) used this technique to measure the ionic transport number in magnesia between 1100°C and 1450°C. They showed that the ionic current carrier was Mg^{++}, and the values of ionic transport number they obtained were about half the values found by Mitoff (6).

Again this technique is liable to errors caused by gas and surface conduction. The problems are similar to those discussed immediately above: a guarded system is necessary if results which describe the behaviour of the bulk material are to be obtained.

7.1.4 Summary

It has been shown that all the methods used to date for measuring the ionic and electronic transport numbers are

liable to several different types of error. The problems have been outlined in the preceding discussion. The author feels that, owing to the existence of these problems and to the fact that no single set of measurements has been made using an experimental procedure which eliminates all the major problems of sample contamination, surface conduction, gas conduction and gas leakage, none of the measurements discussed above can be considered to be truly representative of the behaviour of bulk magnesia. At temperatures above about 1000°C it appears that gas and surface conduction are the main sources of error. At lower temperatures the long equilibration times probably affect the results obtained.

Mitoff (6) combined conductivity and electrolytic cell measurements in an attempt to separate the electronic and ionic contributions to the conductivity. These measurements will be discussed more fully below, but it should be noted that the conductivity values obtained for the electronic mechanism could not be explained by any of the mechanisms discussed in section 6. The only explanation appears to be that of a surface conduction mechanism. These observations support the supposition that the transport number measurements have been seriously affected by the surface properties of the samples.

The author feels that these measurement techniques may be capable of yielding useful information, but the practical and theoretical problems outlined above will need to be solved before the results are capable of aiding identification of the conduction mechanisms.

7.2 Thermoelectric E.M.F. measurements

There have been four measurements of thermoelectric E.M.F. in magnesia (4, 12, 14, 20). The two measurements on single crystal samples by Yamaka et al. (4) and Afzal et al. (12) indicate that the current carriers are negatively charged over the temperature range 850°C to 2000°C.

However, both of these measurements were made using unguarded measurement systems and so were subject to errors of gas and surface conduction. The author feels that these results are not truly representative of the bulk material and that it will be necessary to devise a guarded method of measuring thermoelectric E.M.F.s before useful results can be obtained.

7.3 Conductivity Measurements

In Fig. 2 are shown the results of all the conductivity measurements of single crystal magnesia that the author has been able to find. As will be seen, most workers have chosen to make their measurements at temperatures above 700°C ($10^3/T < 1.0$). It is in this region that the conductivity is fairly high and the current decay problems less severe.

Above 700°C the spread of measured values at any one temperature extends over one or two orders of magnitude. However, most of the measurements have slopes equivalent to activation energies in the range 2.4eV to 2.8eV, and so there is, despite the variation in magnitude, an underlying similarity linking most of the measurements.

The most obvious exception to this general rule is the set of results by Mitoff (5), measured on a high purity sample, (iron - 7.9 ppm, other impurities $\sim$ 10 ppm), which show the existence of a distinct "knee" in the conductivity. The knee occurs at about 1050°C and the activation energies above and below the knee are 3.5eV and 0.9eV respectively. Mitoff identified the upper branch with an electronic mechanism, and it is interesting to note that these measured values are close to the values of electronic conductivity he calculated from his subsequent conductivity and electolytic cell measurements (6). The validity of transport number measurements made by the electrolytic cell technique has been discussed previously, and it was concluded that such measurements are probably not reliable. However, it is useful to attempt to explain these results using the

methods and calculations of section 6. This will now be done.

The three sets of results by Mitoff, while varying somewhat in slope and magnitude, all suggest the presence of an electronic mechanism, having an activation energy of about 3.5eV, and leading to conductivity values of about 10^{-3} S m^{-1} at $10^3/T = 0.55$. There are two possible electronic conduction mechanisms: intrinsic and extrinsic.

The intrinsic model (see section 6.2) leads to an activation energy of about 3.8eV, i.e. approximately correct, but the magnitude of the conductivity is about 2.10^{-7} S m^{-1} at $10^3/T = 0.55$ (see Fig. 32). This is more than three orders of magnitude too small and so we conclude that intrinsic electronic conductivity was not observed.

The results of extrinsic electronic conductivity calculations are discussed in section 6.4 and shown in Fig. 35. For this mechanism to give rise to an activation energy of 3.5eV the band edge - energy level separation must be about 7eV.

The calculated conductivity at $10^3/T = 0.55$, for a density of energy levels equal to $5 . 10^{24}$ m^{-3}, is shown in Fig. 35 to be about $2 . 10^{-7}$ S m^{-1}. The conductivity is proportional to the square root of the energy level density (see Appendix 2), and so for the calculated conductivity to equal the measured value, the energy level density must be greater than 10^{32} m^{-3}. This is equivalent to more than 1000 energy levels per molecule and is clearly unreasonable.

Thus there appears to be no electronic mechanism which satisfactorily explains the measurements. The only ionic mechanism which would give measurements of the right slope and magnitude is that of intrinsic magnesium ion motion, but for this to be measured at such temperatures the impurity content of the sample would need to be less than 1 part in 10^9. It was reported that the sample was not of this (exceptionally high) purity.

The lower branch of these measurements is also difficult to explain, and no similar results have been obtained by other workers. The most likely explanation of these results is that surface and/or gas conduction affected the measurements. Mitoff used 2- and 4- terminal systems for all these measurements, and these techniques do not eliminate the effects of gas and surface conduction. A possible explanation of a sample of this purity apparently showing such high surface conduction below 1050°C could lie in the methods of sample preparation. The sample may not have been chemically etched for fear of contamination, leading to a high surface defect density, and thus to high surface conductivity. This is pure speculation, but no other explanation can be offered.

There have been two sets of measurements in the temperature range $10^3/T > 1.0$. The results of Osburn et al. (10) extended down to 550°C ($10^3/T \simeq 1.2$) and coincided with extrapolations of higher temperature results. The results of Lewis et al. (8, 9) extended down to 350°C ($10^3/T \simeq 1.55$). Their results followed a straight line down to 420°C; below this temperature an activation energy of 1.5eV was found.

The measurements of this investigation, as shown in Fig. 20, are in general agreement with other published results in the temperature region $0.7 < 10^3/T < 1.1$. At lower temperatures the results fall into two main groups. One group, measured on samples cooling relatively quickly, coincides with extrapolations of higher temperature measurements. The second group, measured on samples cooled more slowly through the region near $10^3/T = 1.1$, are generally higher in value and show a lower activation energy of about 1.4eV.

At the lowest temperatures the few measurements made suggest the presence of a lower activation energy mechanism (<1eV).

All these measurements will be discussed in the following sub-section.

7.4 The Nature of the Conductivity

In this sub-section the conductivity measurements, both those made by the author and other published results, are considered and compared to the conductivity values expected from different conduction mechanisms, as calculated in section 6. Identification of the most likely conduction mechanism is made and other possible mechanisms are also considered.

This discussion falls naturally under five headings:

7.4.1 The High Temperature Region (>700°C)

7.4.2 The Intermediate Temperature Region (300°C to 700°C). Measurements with activation energies of about 2.5eV.

7.4.3 The Intermediate Temperature Region (300°C to 700°C). Measurements with activation energies of about 1.5eV.

7.4.4 The Low Temperature Region (<300°C)

7.4.5 Other Possible Conduction Mechanisms

Each of these will be discussed separately.

7.4.1 The High Temperature Region (>700°C)

In this temperature region the results of this investigation, shown in Fig. 20, agree reasonably well with other published results, shown in Fig. 2. There is a variation of about two orders of magnitude at any one temperature, but the activation energies of all the measurements, except those of Mitoff which have been discussed in section 7.3, are similar, about 2.5eV. The measurements of this investigation were all made at temperatures below 1100°C. Other published results extend to above 2000°C.

When the measured values of conductivity are compared to the values calculated in section 6 we find that there are two mechanisms which lead to conductivities of about the right magnitude and activation energy: extrinsic electronic conduction and magnesium ion conduction.

The conductivity values predicted by extrinsic electronic conduction are seen to agree with the measured values reasonably well if the energy level - band edge separation is assumed to be about 4.5eV to 5eV (see Fig. 35). The conductivity values predicted by magnesium ion conduction, and represented by line 2 on Fig. 33, agree quite well with the measured values of this investigation, and with those of other workers.

There is no direct evidence to disprove the existence of either of these mechanisms. Transport number measurements, which in theory could distinguish the electronic and ionic contributions to the conductivity, were discussed in section 7.1 and the measurements made to date were shown to be incapable of giving quantitative results. No other techniques which can isolate the electronic from the ionic conductivity are known to the author. However, it is felt that the ionic conduction mechanism is the most likely for two reasons.

Firstly, the slow current decays reported by several workers suggest the existence of ionic carriers. The current decays observed when electronic conduction mechanisms are dominant are usually much faster.

Secondly, the values of conductivity calculated in the upper part of this temperature region (above 1150^{o}C) are based on measured values of diffusion coefficient, not extrapolated values. There is, thus, strong evidence that conduction due to Mg^{++} ion motion is present. Even if an electronic mechanism does exist, one would still expect to observe some ionic conduction. In contrast to this there is no positive identification of energy levels which would give rise to the electronic conductivity. It should be noted that any identification of conductivity measurements with an extrinsic electronic mechanism is very tenuous without independent evidence of the existence of the energy levels. Almost any conductivity results may be explained if the energy level - band edge separation and energy level density

are chosen correctly. (It should be noted that more than fifty energy levels have been found by various workers. See section 2.6).

The nature of the conductivity will thus be discussed in sections 7.4.2 and 7.4.4 on the basis that the conductivity is due to magnesium ion motion. It will be shown that several features of the conductivity can be satisfactorily explained on this basis, but it should be borne in mind that the existence of an extrinsic electronic mechanism cannot be positively ruled out.

7.4.1.1 Variation of Published Conductivity Results

As was discussed in section 6.3.1 the diffusion coefficient of magnesium below 1500°C is determined by the precipitation behaviour of impurities in the sample. This implies that the actual diffusion coefficient (and thus the mobility and conductivity) measured in a sample will depend not only on the impurity content of the sample, but also on factors such as its thermal history, dislocation density, etc., all of which will affect the state of the impurities. The author believes that it is this dependence of the conductivity on the concentrations and interaction of such factors which leads to the large variations in the measurements of different workers.

7.4.1.2 The Conductivity of Chromium-doped Samples

It was noted in sections 4.1.1 and 4.1.2 that the measured conductivity of a chromium-doped sample, shown in Fig. 15, was higher than that of a nominally pure sample, shown in Fig. 14. It was found that the conductivity of the chromium-doped sample tended to decay towards that of the nominally pure sample, over a period of some weeks. This behaviour will now be shown to be consistent with the theory of magnesium ion motion and with published observations of the behaviour of chromium impurities in magnesia.

Chromium is normally present as Cr^{+++} ions in magnesia; it

is not easily reduced to the Cr^{++} state (38, 40). The Cr^{+++} ions occupy Mg^{++} sites and the extra positive charges on the Cr^{+++} ions necessitate the formation of Mg^{++} vacancies in the lattice for charge compensation. There will be one extra vacancy for every two Cr^{+++} ions. As discussed in section 6.3.1 the diffusion coefficient of magnesium, and hence the conductivity due to Mg^{++} ion motion, is proportional to the Mg^{++} vacancy concentration. Thus the observed increase of conductivity in a chromium-doped sample is consistent with Mg^{++} ion motion.

Chromium ions are known to form associates of the type (Cr^{+++} ion) - (Mg^{++} vacancy) - (Cr^{+++} ion) (85) and it will be demonstrated that the formation of these associates is consistent with the observed slow decay of the conductivity of the chromium-doped sample.

For simplicity, first consider a chromium-doped sample with the Cr^{+++} ions and the Mg^{++} vacancies uniformly distributed throughout the lattice. In the region near each Cr^{+++} ion there is a local charge imbalance of plus one electronic charge, and near every Mg^{++} vacancy there is a local charge imbalance of minus two electronic charges. Mg^{++} ion diffusion occurs by Mg^{++} ions moving into the vacancies. This is an energetically favourable situation as a vacancy is effectively doubly negatively charged, and a Mg^{++} ion doubly positively charged.

As the Cr^{+++} ions and the Mg^{++} vacancies diffuse through the lattice there will be occasions when a Cr^{+++} ion is adjacent to a Mg^{++} vacancy. The total local charge imbalance will now be minus one electronic charge. The vacancy is still available for Mg^{++} ion diffusion although the situation is less energetically favourable than that involving an isolated Mg^{++} vacancy, and so the vacancy will tend to remain close to the Cr^{+++} ion, forming an associate.

As the diffusion processes continue further there will be occasions when a second Cr^{+++} ion is adjacent to the same vacancy. A (Cr^{+++} ion) - (Mg^{++} vacancy) - (Cr^{+++} ion)

associate is then formed. This is electrically neutral with respect to the lattice and, as such, is stable. It would be energetically unfavourable for either a Cr^{+++} ion to move away, or for a Mg^{++} ion to move into the vacancy. The two Cr^{+++} ions thus "trap" the vacancy and the concentration of Mg^{++} ion vacancies available for Mg^{++} ion diffusion is reduced. Thus the diffusion coefficient of Mg^{++} ions (and hence the conductivity) is also reduced.

As it is energetically unfavourable for the associate to break up, the concentration of associates will increase with time, leading to a decay of the conductivity, as observed. A rough estimate of the time scale of the formation of these associates may be obtained by considering the time required for the diffusion length, $l = \sqrt{Dt}$, to equal the average separation between Cr^{+++} ions. The author made measurements on the sample in the temperature range 350°C to 1050°C, and so a "mean" temperature of 900°C will be used for the calculation.

The chromium content of the samples used was approximately 750 ppm $^{w}/_{w}$. Assuming that the chromium is uniformly distributed, the separation between the Cr^{+++} ions is $5 \cdot 10^{-7}$ m. Extrapolating the diffusion measurements of Greskovich et al. (67) to 900°C we find that the diffusion coefficient is approximately $7 \cdot 10^{-20}$ $m^2 s^{-1}$. The time for the diffusion length to equal $5 \cdot 10^{-7}$ m is thus about 40 days.

Although this can only be regarded as a very rough estimate, and the value calculated varies considerably with the temperature at which the diffusion coefficient is calculated (600 days at 800°C, 4 days at 1000°C), this calculation does show that the time scale of the observed conductivity decay is of the same order of magnitude as that expected for chromium ion associate formation.

The above discussion is only a very simplified explanation of the behaviour of chromium in magnesia. The presence of other impurity ions, especially those of variable valence,

e.g. iron, will alter the Cr^{+++} ion : Mg^{++} vacancy equilibrium and may cause the breakup of the associates. Also any mechanical working or sputtering of the sample can cause dislocations which may affect the Cr^{+++} ion : Mg^{++} vacancy equilibrium. However, the author feels that the explanation presented above does give some insight into the processes occurring in chromium-doped magnesia.

7.4.1.3 The Effect of Other Impurity Ions

The addition of impurity ions to magnesia will only affect the conductivity by changing the Mg^{++} vacancy concentration. It can be seen from Fig. 36 that most impurity ions have diffusion coefficients too low to affect the conductivity directly.

The role of trivalent ions is similar to that of Cr^{+++} discussed above, except that the formation of associates does not necessarily occur. Divalent ions will require no charge-compensating vacancies and so, in general, will not have a great effect on the conductivity. The addition of small quantities of monovalent ions will aid the charge-compensation of the trivalent ions, normally present in larger concentrations (1), and thus may cause the conductivity to fall. Mitoff (6) reported that the addition of lithium, Li^{+}, to a single crystal sample reduced the conductivity below $1350^{\circ}C$.

7.4.1.4 Summary

It has been shown that the most likely conduction mechanism in the high temperature region appears to be that of magnesium ion conduction. The motion of the magnesium ions, and hence the conductivity, is determined by the concentration of magnesium ion vacancies in the lattice, which is in turn determined by the behaviour of impurity ions and other lattice defects. The large variation of conductivity values found by different workers is therefore probably due, at least partially, to the different defect structures of the actual samples used.

It has been shown that the slow decay of the conductivity of chromium-doped samples, observed in this investigation, can be explained by the formation of associates, each comprising a magnesium ion vacancy and two chromium ions.

The addition of monovalent and trivalent impurity ions is seen to affect the magnesium ion vacancy concentration, and thus the conductivity. The presence of divalent impurity ions will not generally affect the conductivity to a large extent.

7.4.2 The Intermediate Temperature Region (300°C to 700°C) Measurements with Activation Energies of about 2.5eV

The only previously published results which extend more than a few degrees below 700°C are those of Osburn et al. (10) and Lewis et al. (8, 9). These measurements will be discussed first, and those of the present investigation afterwards.

The measurements of Osburn et al. were made at temperatures down to 550°C, and their results in this temperature region coincide with extrapolations of the higher temperature measurements. It would thus seem that the same conduction mechanism which is dominant at the higher temperatures, Mg^{++} ion motion, is still dominant at these temperatures.

The results of Lewis and Wright showed the same activation energy down to about 420°C ($10^3/T \approx 1.4$). Below this temperature an activation energy of 1.5eV was found at conductivity levels near 10^{-16} S m^{-1}. Lewis et al. interpreted their measurements between 420°C and 600°C as being due to the diffusion of oxygen ions via a "hopping mechanism". This explanation seems to be unlikely, as the conductivity values calculated from oxygen ion diffusion data are at least two orders of magnitude lower than the lowest measured values (see section 6.3.2 and Fig. 33).

It is true that the method of sample preparation used by Lewis and Wright, that of grinding the crystal to the required

shape, may well have led to a large density of dislocations within the sample, and thus to enhanced oxygen ion diffusion (54 - 56). If, however, the conductivity were controlled solely by the density of dislocations in the sample, then one would expect the activation energy of measurements of polycrystalline samples to be very similar to that of measurements of single crystals, the only difference between the conductivities being a simple scaling factor equal to the ratio of the grain boundary densities in the samples. Lewis and Wright reported measurements of both single crystal and polycrystalline samples taken under identical conditions. Not only are the magnitudes different, but the activation energies are also at variance, (single crystal 2.9eV, polycrystalline 1.2eV). This indicates the existence of two separate mechanisms which makes the suggestion of hopping oxygen ion conduction in single crystal material seem very unlikely. A more probable conduction mechanism is that of magnesium ion motion, as discussed above.

The measurements made by the author in this particular temperature range only coincided with extrapolations of the higher temperature results if the samples were cooled relatively quickly. Again the conclusion is that magnesium ion motion is the dominant conduction mechanism.

Measurements made by the author in this temperature region which showed a lower activation energy are discussed below.

7.4.3 The Intermediate Temperature Region (300°C to 700°C) Measurements with Activation Energies of about 1.5eV

There is only one set of previously published measurements known to the author which shows an activation energy of about 1.5eV below 700°C, that of Lewis and Wright (8, 9). These workers measured conductivity levels in the range 10^{-15} to 10^{-17} S m^{-1} below 420°C. The measurements were made at high field strengths on samples containing a high dislocation density (see section 7.4.2) and the conduction mechanism was not identified. The measurements made by the

author showed an activation energy of about 1.5eV at much higher temperatures and conductivity levels. These measurements will now be discussed.

It was noted in section 4.1 that the values of conductivity measured below about 600°C by the author while the sample was continuously cooling depended on the temperature from which the sample had been cooled. The conductivities of samples cooled from above 800°C were as shown by line (a) on Fig. 14. The conductivities of samples held near 600°C for several hours before further cooling were as shown by line (b) on Fig. 14 and lines (b), (c), (d) on Fig. 15. This dependence of the conductivity on the cooling rate of the sample through the temperature region in which the $Fe^{++} \rightarrow Fe^{+++}$ transition is known to take place (see section 6.5.5) led to the supposition that the valence state of iron impurities in the sample was influencing the conductivity.

A theory of iron - influenced conduction by Mg^{++} ion motion below 600°C will now be presented, and the measurements of this investigation compared with the predictions of the theory. Other conduction mechanisms which might also be present will be considered in section 7.5.

7.4.3.1 The Effect of the Valence State of Iron on the Conductivity

Consider an iron-doped sample heated to about 1000°C. The discussion of section 6.5.5 has shown that most of the iron will be present as Fe^{++} ions, and only a small proportion as Fe^{+++} ions. There will, therefore, be only a small number of Mg^{++} vacancies present to charge-compensate for the Fe^{+++} ions. The Mg^{++} vacancy concentration, and thus the Mg^{++} diffusion coefficient and the conductivity, will be determined by the other impurities in the sample. (This was discussed in section 7.4.1).

The transition between the Fe^{++} state and the Fe^{+++} state is known to be fairly slow (see section 6.5.5) and so if the sample is cooled rapidly the iron will be "frozen in" as Fe^{++} ions and the conductivity will continue to be

determined by the other impurities in the sample.

If, however, the sample is cooled much more slowly, or held near 600°C for some hours, the $Fe^{++} \rightarrow Fe^{+++}$ transition will be able to proceed, to an extent determined by the cooling rate of the sample. The existence of Fe^{+++} ions in the lattice will necessitate the formation of extra Mg^{++} vacancies for charge-compensation (see section 7.4.1). Fe^{+++} ions do not form associates with Mg^{++} vacancies (109), and so the extra vacancies formed will be available for Mg^{++} ion diffusion. Thus the diffusion coefficient, and the conductivity, are increased by the presence of the Fe^{+++} ions.

If, after being held for some hours at 600°C, a sample is cooled rapidly, the $Fe^{++} \rightarrow Fe^{+++}$ transition will not be able to proceed to any great extent during the cooling, and so the conductivity values measured will be consistent with a constant Mg^{++} vacancy concentration. If, however, conductivity measurements are made on a sample which is held at a constant temperature for several hours during each measurement, then the Fe^{++} : Fe^{+++} equilibrium will have moved between successive measurements and the conductivity values measured will not be consistent with a constant Mg^{++} vacancy concentration. Both of these cases will be discussed below.

7.4.3.2 Comparison of the Measurements with Theoretical Predictions

The measurements shown in Figs. 14 and 15 were all made while the sample was continuously cooling. Thus, by the theory proposed above, the measurements represented by line (b) on Fig. 14 and by lines (b), (c) and (d) on Fig. 15 should all correspond to a constant Mg^{++} vacancy concentration. When we compare these results with the calculated values of conductivity expected for constant Mg^{++} vacancy concentrations as shown in Fig. 34 (see section 6.3.1), we see that the agreement of activation energies is very good.

The results of Fig. 14, measured on a nominally pure sample;

are closely grouped and correspond to a vacancy concentration of about 10 mole. ppm. The results of Fig. 15, measured on a chromium-doped sample, show more variation. The measurements represented by line (a) were made on a sample which had been cooled from above 1000°C several hours before. There is evidence of a partial transition to the upper branch of the measurements; the conductivity corresponds to a Mg^{++} vacancy concentration of 6 mole. ppm. Lines (b), (c) and (d) represent successive sets of measurements, between which the sample was not heated above 600°C. Lines (b) and (c), measured on the same day, correspond to Mg^{++} vacancy concentrations of about 100 and 150 mole. ppm respectively. Line (d), measured on the following day, corresponds to a Mg^{++} vacancy concentration of about 400 mole. ppm.

Bearing in mind that the calculations represented in Fig. 34 are only accurate to about one order of magnitude it is possible to say that the measurements discussed above support the theory of Fe^{+++} - influenced conductivity quite well. Each set of measurements corresponds to a constant Mg^{++} vacancy concentration, and there is evidence that the concentration increases slowly with time, consistent with the $Fe^{++} \rightarrow Fe^{+++}$ transition moving slowly to the right.

The measurements shown on Figs. 16 to 19 were all made by allowing the sample to come into equilibrium before conductivity measurements were made. It was thus possible for the Fe^{++} : Fe^{+++} equilibrium to have changed between the successive measurements. This is reflected in the generally lower activation energies of the results.

The conductivity results shown on Fig. 16, measured on a chromium-doped sample, show a change of Mg^{++} vacancy concentration of 40 mole. ppm at 600°C ($10^3/T \simeq 1.15$) to 100 mole. ppm at 300°C ($10^3/T \simeq 1.75$).

The results shown by line (e) on Fig. 17, measured on the sample after previous heating to above 1000°C, have a similar

slope. The conductivity values at 600°C and 300°C correspond to Mg^{++} vacancy concentrations of about 120 and 500 mole. ppm respectively.

The results of measurements taken on cooling a nominally pure sample, as shown in Fig. 18, are equivalent to Mg^{++} vacancy concentrations of 6 and 150 mole. ppm at 600°C and 300°C respectively.

The conductivity measurements of an iron-doped sample, as shown in Fig. 19, exhibit a lower activation energy below about 360°C, but if we extrapolate the results a little to obtain comparative results we find that line (b) represents conductivity values equivalent to 5 and 400 mole. ppm of Mg^{++} vacancies of 600°C and 300°C respectively.

Thus we find that all the measurements of this investigation made on samples which had previously been heated above 800°C agree qualitatively with the predictions of the proposed conduction mechanism. The quantitative agreement is not quite so good. The calculated values of vacancy concentration are reasonable; i.e. of the same order as the measured iron content (see Table 3), but there is not complete correlation between the iron content and the measured conductivity. One would expect the iron-doped sample to show greater conductivity than the chromium-doped and nominally pure samples, which have lower iron contents; this is found not to be so. The reasons for the lack of full agreement may include: different cooling rates during the measurement runs; different concentrations of other aliovalent impurities in the crystals, which may affect the Fe^{++} : Fe^{+++} equilibrium; different dislocation densities which would probably affect the rate of production of Mg^{++} vacancies; and the limited solubility of Fe^{+++} ions in the lattice which might lead to proportionately lower vacancy concentrations at higher iron concentrations. The measurement problems associated with the slow current decays, as discussed in sections 4 and 5, add further uncertainty to the measured results.

However, the author feels that the proposed theory does explain the important points of the conductivity measurements, and agreement within an order of magnitude is encouraging.

7.4.3.3 Summary

Conductivity measurements showing an activation energy of about 1.5eV have only been observed in the temperature range 300°C to 700°C on samples which are either cooled very slowly, or held at about 600°C before subsequent rapid cooling. The values of conductivity measured are consistent with the values calculated for magnesium ion conduction. The dependence of the conductivity on the cooling rate of the sample near 600°C has been shown to be consistent with the valence change of iron impurities known to take place at approximately that temperature. If a sample is cooled quickly, then the iron is "frozen" in the divalent state and has little effect on the conductivity. When a sample is cooled more slowly, the iron impurities change to the trivalent state at about 600°C. This necessitates the formation of magnesium ion vacancies for charge compensation, and the increase in vacancy concentration leads to a higher magnesium ion mobility, and hence to higher values of conductivity.

7.4.4 The Low Temperature Region (<300°C)

The author has been unable to find any published conductivity measurements in this temperature range and so the discussion below is based entirely on the measurements of this investigation.

The conductivity results in this temperature region tend to follow lines of low slope, corresponding to activation energies of less than 1eV. The results are often rather scattered and the lines drawn through the data points do not always fit very well. Although the individual activation energies were found to vary, 0.58eV, 0.34eV and 0.77eV, the results measured on all the samples fall in the

same general area and could perhaps all be reasonably represented by the same "best fit" straight line.

This agreement of magnitude could be interpreted as evidence of a conduction mechanism common to all the samples, but it may also be due to a limitation of the measurement rig. In this temperature range the resistances of the samples are of the order of 10^{17} to 10^{18} Ω, and although the errors introduced by gas and surface conduction are greatly reduced by the three-terminal measurement system used, they are not entirely eliminated. For example, the leakage resistance between the centre contact and the guard-ring would have to be greater than 10^{12} Ω for the error in the measurement of the bulk resistance to be less than 10% (see Appendix 1). It does not seem unreasonable that leakage resistances of this order were present. For example the resistance of the cable used was of the order of 10^{13} Ω. Measurements in this temperature range are also subject to the difficulties discussed in section 4 and 5, those of very slow current decays and noise. These factors add further uncertainty to the measured results.

There is little additional evidence available from other measurements to aid the identification of any possible conduction mechanism. The existence of slow current decays suggests an ionic mechanism, but photo-induced conductivity measurements (96 -99) have shown that the presence of electronic conductivity cannot be ruled out. The mobility of electronic carriers is much higher than that of any ionic carrier at these temperatures and thus only a very low concentration of carriers is necessary to give these levels of conductivity. A conductivity of 10^{-15} S m^{-1} implies an electron density of about 10^{7} m^{-3} (i.e. about 1 per 10^{21} Mg^{++} sites). It would be difficult to identify the source of such a small concentration of carriers by correlation with the concentrations of impurities, lattice defects etc.

In view of the uncertainties involved and the lack of additional information the author feels that the evidence is

insufficient at the present to support any definite theory of conduction. Further work is necessary before conduction processes at such temperatures may be better understood.

7.4.5 Other Possible Conduction Mechanisms

It was noted in section 6 that three conduction mechanisms predicted values of conductivity close to the measured values. These mechanisms were Mg^{++} ion conduction, Mn^{++} ion conduction and extrinsic electronic conduction. In the discussion of this section it has been possible to explain most of the observed conduction phenomena assuming that the conductivity is due to the motion of Mg^{++} ions. However, the other mechanisms will now be considered further, and the values of conductivity predicted by them compared to the measured values.

For convenience the discussion will be split into two sections: the first deals with mechanisms having an activation energy of about 2.5eV, and the second with mechanisms having an activation energy of about 1.5eV.

7.4.5.1 Mechanisms with Activation Energies of about 2.5eV

It was noted in section 7.4.1 that the values of conductivity above 700°C could be explained by extrinsic electronic conduction arising from isolated energy levels separated from the band edge by 4.5eV to 5eV. Such energy levels are caused by lattice defects, e.g. impurity atoms, dislocations etc. In general, each lattice defect would give rise to one isolated energy level (134). The density of energy levels which would give rise to conductivities of the correct magnitude is of the order 10^{24} to 10^{25} m^{-3}, i.e. about 1 level per 10^{4} Mg^{++} sites or 100 mole. ppm. This is of a similar magnitude to the impurity concentrations reported by several workers, and so the presence of extrinsic electronic conduction is seen to be possible. It has not yet been possible to measure accurately the separate electronic and ionic contributions to the conductivity (see section 7.1) and so no definite conclusion can be drawn at present.

However, the time constants of the observed current decays are much longer than those generally observed when electronic conduction is taking place, and so the author feels that ionic conduction is probably dominant, although the possibility of some simultaneous electronic conductivity cannot be ruled out.

The discussion of section 6 showed that no ionic conduction mechanism having an activation energy close to 2.5eV, except that of Mg^{++} ion motion, gave rise to conductivity values of the correct magnitude.

7.4.5.2 Mechanisms with Activation Energies of about 1.5eV

Measurements with activation energies of 1.5eV could only be observed below 600°C on samples which had cooled fairly slowly. This dependence of the conductivity on cooling rate has been shown above to be consistent with the change of valence of iron impurities affecting the mobility of Mg^{++} ions. The author knows of no other phenomenon which is likely to give rise to two distinct branches of conductivity values, and so any other conduction mechanism considered must also be influenced by the valence state of iron ions in magnesia.

Ionic and electronic mechanisms will be considered separately.

a) Ionic Mechanisms

The discussion of section 6 showed that the only ionic mechanism which may give conductivity values of approximately the right magnitude and activation energy is that of manganese ion motion.

The values of conductivity calculated from Mn^{++} ion motion have an activation energy of about 1eV and exceed the measured values at temperatures below about 400°C, (see section 6.5.2.6 and Fig. 36). The fact that the measured conductivity of samples cooling fairly rapidly is several orders of magnitude less than the calculated values leads to the conclusion that the

calculated values are in error. The most likely cause of the error is that the extrapolation of the diffusion coefficient measurements, all performed above 1300°C, is not valid. Manganese is known to be stable in many valence states, from Mn^{++} to Mn^{7+}. Most of these valence states have not been reported in magnesia, but the presence of the variability of the structure of the manganese ion does suggest that the mechanism of manganese ion motion may change between 500°C and 1300°C. From the evidence of the conductivity measurements it would appear that the diffusion coefficient of manganese is much lower at temperatures below 500°C than an extrapolation of higher temperature measurements would suggest.

However, further investigation would be necessary before any definite conclusion could be drawn.

b) Electronic Mechanisms

When the iron impurities change from the Fe^{++} to the Fe^{+++} state, there must be a rearrangement of the electrons in the crystal. We must now consider the behaviour of the electrons lost by the iron ions during the $Fe^{++} \rightarrow Fe^{+++}$ transition. The presence of Mg^{++} vacancies in the lattice will also lead to isolated energy levels in the energy band gap and the effect of these is also considered.

The presence of an iron ion in the magnesia lattice will, in general, lead to the existence of an isolated energy level which is closer to the valence band than to the conduction band (134). The level will be occupied by an electron when the iron is in the divalent state, and empty when the iron is in the trivalent state. To use the terminology of semiconductor physics, the energy level acts as an acceptor level. At high temperatures, when the iron is in the divalent state, the level is ionised, and at lower temperatures, when the iron is

trivalent, the level traps a free hole from the valence band.

This hole must have been released from a second (unidentified) trap a short time before, because the conductivity calculated by assuming that the hole mobility is equal to that of electrons, as measured by Pomerantz et al. (96 - 99), and that there is one hole per iron atom, typically gives values a factor of 10^{12} higher than the measured values. It thus appears that the Fe^{++} ion is a very efficient hole trap at temperatures below the $Fe^{++} \rightarrow Fe^{+++}$ transition temperature, and that no free carriers are generated by the iron ions during the $Fe^{++} \rightarrow Fe^{+++}$ transition.

The presence of Mg^{++} vacancies in the lattice also leads to the existence of isolated acceptor - like energy levels in the energy band gap (134). Their behaviour will be similar to that of the levels due to the presence of iron ions discussed immediately above.

Thus we see that the energy levels caused by both the Fe^{+++} ions and the Mg^{++} vacancies, are unlikely to lead to free electronic carriers as the $Fe^{++} \rightarrow Fe^{+++}$ transition takes place. However, it will be shown that only a very small concentration of energy levels is necessary to account for the observed levels of conductivity. We must therefore consider the possibility that a small proportion of the Fe^{+++} ions or the Mg^{++} vacancies are capable of forming associates with other (unidentified) lattice defects, and forming energy levels capable of generating free carriers.

Comparing the measured results, as shown in Figs. 14 and 15, with the values of conductivity calculated for extrinsic electronic mechanisms, as shown in Fig. 35, we find that to explain the observed conductivity results the energy level - band edge separation must be about 3eV, and the density of levels about $5 \cdot 10^{14}$ m^{-3} (i.e. 1 per 10^{14} Mg^{++} sites). If we assume an iron content

of 50 mole. ppm, the Fe^{+++} ion concentration is approximately $3 . 10^{24}$ m^{-3}, and the Mg^{++} vacancy concentration necessitated by the presence of Fe^{+++} ions is half this, $1.5 . 10^{24}$ m^{-3}. Thus only one Fe^{+++} ion or Mg^{++} vacancy in about 5.10^{9} forms an associate leading to a suitable energy level.

It is only possible to guess at the identity of the lattice defect with which the Fe^{+++} ion or Mg^{++} vacancy forms the associate. It may be an impurity ion, or a structural defect, such as a dislocation or a stacking fault. It may even be a combination of two of these, implying that the final associate is composed of three different lattice defects. Observation of these associates would be extremely difficult as defect concentrations of the order of 1 in $5 . 10^{9}$ can only be detected by optical, E.S.R. and Mössbauer techniques, and it is probably fair to say that there are many defects present in such low concentrations. The task of identifying the defect by correlation of optical, E.S.R., and/or Mössbauer measurements with conductivity measurements is somewhat daunting.

In summary, we may say that it is possible to postulate an electronic mechanism which predicts values of conductivity close to those measured. There is, however, no independent evidence of the existence of the postulated energy levels, or of the existence of the associates. The theory of Mg^{++} ion motion, presented earlier in the discussion, requires fewer unsupported suppositions, and the author feels therefore that this is the most likely conduction mechanism.

7.4.6 Summary

The most likely conduction mechanism in magnesia is that of Mg^{++} ion motion. The diffusion coefficient of Mg^{++} ions, and thus the mobility and the conductivity, is proportional to the Mg^{++} vacancy concentration. At all temperatures below $1800^{\circ}C$ the Mg^{++} vacancy concentration

is determined by the behaviour of aliovalent impurities in the lattice. The variation in the values of conductivity measured by various workers is partly attributed to differences in the impurity contents of the different samples, and partly to the different thermal histories of the samples.

Divalent ions, which require no charge compensation, have little effect on the conductivity. The presence of monovalent and trivalent ions, however, affects the conductivity by altering the Mg^{++} vacancy concentration. The slow decay of the conductivity of chromium-doped magnesia, observed during this investigation, is consistent with the formation of (Cr^{+++} ion) - (Mg^{++} vacancy) - (Cr^{+++} ion) associates in the lattice.

Iron impurities can only affect the conductivity when the iron is in the ferric (Fe^{+++}) state. Iron is usually found as Fe^{++} ions in samples above 700°C, and in samples which have been cooled fairly rapidly to below this temperature. Fe^{+++} ions are found in samples which are cooled more slowly through the 600°C to 700°C region and the extra Mg^{++} vacancies formed for charge compensation lead to increased Mg^{++} diffusion, and thus increased conductivity.

It is also possible to explain the measured values of conductivity by extrinsic electronic conduction, but no identification of the energy levels is possible at present.

7.5 The Conductivity of Polycrystalline Samples

Although this investigation was mainly concerned with the behaviour of single crystal magnesia, it is of interest to consider the conductivity of polycrystalline samples. There are extra factors which may influence the conductivity of polycrystalline material that do not need to be considered in single crystals, e.g. grain size, degree of sintering, porosity etc. In many of the earlier studies the authors did not use especially pure samples and did not report the impurity content. In view of these factors it will not be possible to discuss the measurements of the

polycrystalline material in as much detail as those of single crystal material.

Several published conductivity measurements are shown in Fig. 3. Comparing these results with those measured on single crystal samples, as shown in Fig. 2 we see that at high temperatures ($10^3/T < 0.9$) all the results are of a similar character although there is a spread over two orders of magnitude at any given temperature. The results of Surplice and Jones (20) are an extension of this general agreement down to $10^3/T \simeq 1.2$. At lower temperatures ($10^3/T > 1.2$) there are two sets of measurements which follow the lines of lower slope. They have a similar appearance to the results shown in Figs. 14 and 15 but a closer comparison reveals them to be about 2 or 3 orders of magnitude higher.

The higher temperature results suggest that the same conduction mechanism is present in polycrystalline material as in single crystals, i.e. Mg^{++} ion motion with the mobility of the ion controlled by the precipitation rate of the impurities in the crystal. The agreement of the results implies that the motion of Mg^{++} ions is similar in both types of material. This does not seem an unreasonable supposition. The diffusion measurements of Zaplatynsky (71) indicate that cation diffusion is not affected by the presence of grain boundaries, although O^{--} ions are known to diffuse much faster along grain boundaries than through the bulk (54 - 56). Again the actual value of the Mg^{++} ion diffusion coefficient (and thus mobility) in any one sample will be determined by the behaviour of the impurities present in that sample; this would again explain the large variation of the results reported by different authors.

The later electrolytic cell measurements of Mitoff (28) suggested the presence of an electronic surface conduction mechanism. We cannot rule out the possibility of such a mechanism and would expect it to be more important in polycrystalline samples than in single crystals owing to

the increased surface area of the crystallites. Variations in grain size between samples would lead to differences in the surface area and thus to differences in conductivity. By comparison with Fig. 35 we see that the values of conductivity predicted by the model of extrinsic electronic conduction due to energy levels about 4 to 5eV from the band edge fit the measured results fairly well.

If we now consider the results at lower temperatures ($10^3/T > 1.2$) where there is evidence that the activation energy is lower, we see that the results are of a similar character to those shown on Figs. 14 and 15. It thus seems reasonable to attempt to explain these results by magnesium ion motion with the vacancy concentration controlled by an impurity in the sample. However, comparing the results of Fig. 3 with the models as shown on Fig. 34 we find that the agreement of the slopes is not particularly good and that very high vacancy concentrations (10^4 to 10^5 mole. ppm) are necessary to explain the observed levels of conductivity. These very high concentrations (up to 1 in 10 Mg^{++} sites) would appear very unlikely, especially as the previous discussion has noted that grain boundaries do not affect the Mg^{++} diffusion coefficient, which implies that they do not affect the vacancy concentration. None of the extrinsic ionic conduction models discussed in section 6 predicts conductivity values as high as these results, but extrinsic electronic models with energy levels about 3eV and 2eV from the band edge at concentrations of $5 . 10^{21}$ m^{-3} (0.1 mole. ppm) and $5 . 10^{12}$ m^{-3} (10^{-10} mole. ppm) give a reasonable fit to the upper and lower lines respectively. If we assume that the slopes of the lines do truly represent the conductivity and are not representative of the non-equilibrium state of the samples (note that we would expect electronic equilibration to be faster than that of ionic processes) then it seems that we have indications of two energy levels. These energy levels are not present in such high concentrations in single crystals, as the levels of conductivity are much too high, and so we may assume that their presence is directly influenced by grain boundaries

or other features unique to polycrystalline material. Also the existence of two different energy levels in two samples shows that the levels are not solely due to the grain boundaries but must be due to another feature whose concentration varies from sample to sample. The most obvious choice for this other feature is an impurity atom.

In conclusion we may say that at high temperatures the conduction mechanism in polycrystalline material appears to be the same as that in single crystals i.e. magnesium ion motion. Measurements on single crystals indicate that there might also be an electronic mechanism which leads to significant surface conduction. At lower temperatures it is possible to explain the higher conductivity measurements by extrinsic electronic models. However it should be noted that as almost any conductivity measurements in this general region can be fitted to an extrinsic electronic model by choosing the energy level concentration and energy level - band edge separation correctly, the identification of these levels is not made positively, and it is considered that further independent evidence of any energy level detected by conductivity measurements would be necessary before any positive identification could be made.

8. RECOMMENDATIONS FOR FURTHER WORK

There are several areas of work which could be investigated in order to increase the knowledge of electrical conduction in magnesia. Some of this work should consist of extensions of the methods reported here, and some should be in related fields which would aid the understanding of the "simple" conductivity measurements.

For any further bulk conductivity measurements it is recommended that a fully volume guarded three-terminal measurement system be used. This system greatly reduces the effect of gas and surface conduction and thus assists study of the properties of the bulk material. The use of evaporated, rather than sputtered, platinum electrodes is also recommended.

A study of the surface conductivity of magnesia would also be of interest, both as an independent study which would aid the understanding of the conduction mechanisms, and also as an aid to assessing the accuracy of the bulk conductivity, and other electrical measurements. The surface conductivity would show the effects of changing ambient gases much more rapidly than does the bulk conductivity, and a study of surface conductivity as a function of temperature and ambient may prove very fruitful. In order to overcome the lack of repeatability of results found in this work it would be advantageous to design the sample and measurement rig such that the surface and bulk conductivities could be measured on the same sample within a short time.

As was noted earlier the electrode materials of samples used for conductivity measurements can influence the conductivity measurement considerably (123). There does not appear to have been very much work in this area with magnesia. This is probably due to the fact that only inert electrodes (usually platinum or carbon) can be used at high temperatures, where the conductivity is fairly high. Work with magnesium electrodes would be limited to low temperatures due to the low melting point of magnesium ($\sim 650^{\circ}C$). The

possibility of using solid solutions of magnesium and another metal does not appear to have been considered. A detailed study of electrode/magnesia interfaces would probably yield useful information about the current carriers. (For a review of electrode processes see Ref. 123).

Any further conductivity measurements should include measurements on samples held at constant temperature and also measurements made with the sample temperature slowly falling. It was by combining these two types of measurement that identification of the valence state of iron as a factor influencing the conductivity was possible in this work. The conductivity, as measured when the sample temperature is falling rapidly, appears to be controlled mainly by the state of the sample just before the cooling started. By annealing a sample at progressively lower temperatures before the measurements are made on cooling it may be possible to follow the course of important reactions (e.g. $Fe^{++} \rightarrow Fe^{+++}$) with temperature. Conductivity measurements made while the sample temperature is held constant enable the study of current - voltage characteristics and the time decay of the current flowing. Both of these features were considered briefly in this work and the author feels that a deeper study of both these phenomena could well prove worthwhile.

There are several techniques for gaining information about the current carriers which do not depend on measuring the conductivity. Two techniques which have been used are the measurements of thermoelectric E.M.F.s and of the Hall effect. Both of these can yield information on the sign of the current carrier but their usefulness is limited for materials such as magnesia by the effects of surface and gas conduction. If guarded methods which eliminate these effects could be devised the identification of the current carriers would become much easier.

In a general sense any work which provides information about the structure of magnesia is useful for identifying features

of the conductivity. Thus work on the diffusion of ionic species through magnesia, Mössbauer and E.S.R. techniques in particular would be very useful. If measurements using the last two techniques could be extended to higher temperatures so that the behaviour of impurities (such as chromium and iron) could be directly studied as a function of temperature then a much clearer picture of the interaction of lattice defects in magnesia could be formed.

9. CONCLUSIONS

The main purpose of this investigation was to identify the electrical conduction mechanisms present in single crystal magnesia. To aid this identification a survey of the literature dealing with measurements of many properties of magnesia was carried out. The findings of this survey have been presented and the most relevant published results discussed.

The construction of the measurement rig used for making conductivity measurements has been described. The techniques of sample preparation and the electrical system used for measuring the conductivity have also been described and discussed.

The conductivity of several single crystal magnesia samples, nominally pure, iron-doped and chromium-doped, has been studied at temperatures up to 1000°C. Conductivity measurements were made on the samples both at constant temperature, and as the temperature fell slowly. It was noted that measurements at temperatures less than about 600°C fell broadly into two groups. The first group, made on samples cooling relatively quickly from about 1000°C, coincided with an extrapolation of higher temperature measurements. The second group, made on samples held at about 600°C for several hours before cooling, or cooled slowly from above 600°C, were much higher and had a lower slope on an Arrhenius plot. Such measurements have not been reported before.

The current decay which occurred after applying a voltage to the samples was studied. The decay waveforms which resulted were generally complex, showing the existence of several distinct decay processes. Some of the results were analysed by fitting curves to the measured data points. An iterative computerised curve fitting routine was used to obtain the parameters of the "best fit" curve over a limited range of the measurements. Generally the data points fitted a curve of the type $I = I_\infty + I_0 \exp(-t/\tau)$ or $I = I_\infty + I_0 t^{-m}$ at long values of time. However no useful analysis

of the variation of values of τ and m was possible.

Current-voltage characteristics of the samples were measured. Ohmic and two types of nonohmic behaviour were found i.e. the incremental conductivity would either remain constant, decrease or increase with increasing voltage, depending on the sample and the temperature of measurement. The uncertainty in the values of current measured, often due to the current decays mentioned above, prevented the fitting of any theoretical curves (e.g. for Schottky-type current injection) to the data points.

The results of electron spin resonance measurements and of the effect of changing the sample ambient have also been discussed.

The values of conductivity expected from several possible conduction mechanisms were calculated. The existence of electronic and ionic mechanisms, both intrinsic and extrinsic, was considered. The carrier densities and mobilities were calculated from theoretical expressions, or from published measurements, these published results being extrapolated, of necessity, to higher and lower temperatures.

By comparison of the predicted conductivity values with those measured in this investigation and those published by other workers the most likely conduction mechanism for all single crystal samples was found to be that of magnesium ion motion. The mobility of the magnesium ions is determined by the behaviour of impurity ions in the crystal; these impurity ions control the magnesium ion vacancy concentration at any given temperature. The wide spread of published results was thus attributed to the difference of impurity content between samples, the differences in thermal history, and the different cooling rates of the samples during measurement. The slow decay of the conductivity of the chromium-doped samples found in this investigation was shown to be consistent with the formation of Cr^{+++} ion - Mg^{++} vacancy - Cr^{+++} ion associates in the sample.

The existence of two branches of the conductivity results below 600°C was identified with the transition of iron from the divalent state at temperatures above about 600°C to the trivalent state below this temperature. The transition is known to be slow and so in a sample cooling relatively quickly the iron is trapped in the divalent state. The iron thus has no effect on the magnesium ion vacancy concentration, or on the conductivity. If, however, the sample is cooled at a rate such that the transition to the trivalent state can take place then extra magnesium ion vacancies are formed in the lattice for charge compensation and thus the magnesium ion mobility is increased, resulting in the higher conductivity values measured.

At temperatures below about 300°C the conductivity values measured in this investigation were very similar in all the samples. It was shown that this could be due to electronic conduction or to leakage resistances in the measurement rig.

It was noted that most of the conductivity measurements could also be explained by postulating extrinsic electronic conduction mechanisms, but that independent evidence of the existence of the energy levels would be necessary before it would be possible to state definitely that the conductivity was electronic. It was concluded that the mechanism of magnesium ion motion explained the measurements equally well, and required fewer unsupported suppositions.

The published results of conductivity measurements on polycrystalline material were briefly reviewed. Above about 600°C the published results are broadly similar to the single crystal measurements. It is known that grain boundaries are unlikely to affect magnesium ion motion and so it was concluded that the predominant conduction mechanism was again that of magnesium ion motion. It was shown that conductivity measurements below about 600°C could only, on the basis of present knowledge, be explained by extrinsic electronic conduction, but no attempt to

identify the source of the carriers could be made.

Recommendations for further work, especially on the behaviour of defects in magnesia and its surface conductivity, were made.

10. REFERENCES

1. C. T. Butler, B. J. Sturm, R. B. Quincy Jr. — Report No. ORNL-4547 Oak Ridge National Laboratory, Oak Ridge, Tennessee, U.S.A., 1970.

2. N. F. Mott, R. W. Gurney — Electronic Processes in Ionic Crystals. Dover Publications, New York, 1964

3. A. Lempicki — Proc. Phys. Soc. 66B 281-3, 1953.

4. E. Yamaka, K. Sawamoto — J. Phys. Soc. Japan 10 176-9, 1955.

5. S. P. Mitoff — J. Chem. Phys. 31 1261-9, 1959.

6. S. P. Mitoff — ibid. 36 1383-9, 1962.

7. P. Zirkind, E. S. Freeman — ibid. 41 906-7, 1964.

8. T. J. Lewis, A. J. Wright — J. Phys. D 1 441-7, 1968.

9. T. J. Lewis, A. J. Wright — ibid. 3 1329-39, 1970.

10. C. M. Osburn, R. W. Vest — J. Am. Ceram. Soc. 54 428-35, 1971.

11. J. S. Choi, H. Y. Lee, K. H. Kim — J. Phys. Chem. 77 2430-3, 1973.

12. F. A. Afzal, J. E. Giutronich — J. Phys. E. 7 579-82, 1974.

13. J. R. Hensler, E. C. Henry — J. Am. Ceram. Soc. 36 76-83, 1953

14. R. Mansfield — Proc. Phys. Soc. 66B 612-4, 1953.

15. W. Weigelt, G. Haase — Ber. Deut. Keram. Ges. 31 45-8, 1954.

16. V. N. Eremenko, A. M. Beinish — Russ. J. Inorgan. Chem. 1 2118-30, 1956.

17. A. N. Lulichev, F. I. Chuprinin, S. I. Kovalenko — Zavodskaya Laboratoriya 23 931, 1957.

18. M. O. Davies — J. Chem. Phys. 38 2047-55 1963.

19. J.-P. Loup, A.-M. Anthony — Ref. Hautes Temp. et Refract. 1 193-9, 1964.

20. N. A. Surplice, R. P. Jones — Brit. J. Appl. Phys. 15 639-42, 1964.

21. P. P. Budnikov, V. K. Yanovskii — J. Pract. Chem. of the U.S.S.R. 37 1249-57, 1964.

22. L. B. Khoroshavin, G. A. Sapeev — Ogneupory 6 44-9, 1966.

23. D. M. Shakhtin, E. V. Levintovich, T. L. Pivovar, G. G. Eliseeva — High Temperature 5 454-7, 1967.

24. D. R. Lamb, T. G. Read — Wolfson Industrial Unit Report No. 681/1, University of Southampton, 1975.

25. D. R. Lamb — Wolfson Industrial Unit Report No. WIU 781, University of Southampton, 1977.

26. R. J. Brook, J. Yee, F. A. Kröger — J. Am. Ceram. Soc. 54 444-51, 1971.

27. S. F. Pal'guev, A. D. Neuimin — Sov. Phys. Sol. State 4 629-32, 1962.

28. S. P. Mitoff — J. Chem. Phys. 41 2561-2, 1964.

29. H. Schmalzried — ibid. 33 940, 1960.

30. S. P. Mitoff — ibid. 33 941, 1960.

31. V. P. Luzgin, A. G. Frolov, A. F. Vishkarev, V. I. Yavoyskii — Ogneupory 4 42-4, 1965.

32. C. B. Alcock, G. P. Stavropoulos — J. Am. Ceram. Soc. 54 436-43, 1971.

33. J. E. Giutronich, F. A. Afzal — Nucleus 8 77-85, 1971.

34. M. Gauthier, P. Fabry, C. Deportes — Electrochim. Acta. 19 103-9, 1974.

35. B. Henderson — Defects in Crystalline Solids Edward Arnold, London, 1972.

36. J. E. Wertz, P. Auzins — Phys. Rev. 106 484-8, 1957.

37. J. E. Wertz, P. Auzins, R. A. Weeks, R. H. Silsbee — ibid. 107 1535-7, 1957.

38. J. E. Wertz, P. Auzins, J. H. E. Griffiths, J. W. Orton — Disc. Farad. Soc. 26 66-71, 1958.

39. J. E. Wertz, P. Auzins, J. H. E. Griffiths, J. W. Orton — ibid. 28 136-41, 1959.

40. R. L. Hansler, W. G. Segelken — J. Phys. Chem. Solids 13 124-31, 1960.

41. J. E. Wertz, J. W. Orton, P. Auzins — J. Appl. Phys. Supp. 33 322-8, 1962.

42. J. E. Wertz, G. Saville, P. Auzins, J. W. Orton — J. Phys. Soc. Japan 18 Supp. 2 305-311, 1963.

43. J. E. Wertz, R. E. Coffman — J. Appl. Phys. 36 2959-61, 1965.

44. P. W. Kirklin, P. Auzins, J. E. Wertz — J. Phys. Chem. Solids. 26 1067-74, 1965.

45. B. Henderson, J. E. Wertz, T. P. P. Hall, R. D. Dowsing — J. Phys. C. 4 107-16, 1971.

46. O. F. Schirmer — J. Phys. Chem. Solids 32 499-509, 1971.

47. R. Martens, F. Freund, E. G. Derouane — Proc. 2nd. International Conference on Solid Surfaces. Japan. J. Appl. Phys. Supp. 2. Pt. 2 471-4, 1974.

48. Y. Chiba, N. Shinbori — J. Phys. Soc. Japan. 38 1219, 1975.

49. Y. Chen, M. M. Abraham, L. C. Templeton, W. P. Unruh — Phys. Rev. B 11 881-90, 1975.

50. R. Lindner, G. D. Parfitt — J. Chem. Phys. 26 182-5, 1957.

51. B. C. Harding, D. M. Price, A. J. Mortlock — Phil. Mag. 23 399-408, 1971.

52. B. C. Harding, D. M. Price — ibid. 26 253-60, 1972.

53. Y. Oishi, W. D. Kingery — J. Chem. Phys. 33 905-6, 1960.

54. J. B. Holt, R. H. Condit — Mat. Sci. Res. 3 13-29, 1966.

55. D. R. McKenzie, A. W. Searcy, J. B. Holt, R. H. Condit — J. Am. Ceram. Soc. 54 188-90, 1971.

56. H. Hashimoto, M. Hama, S. Shirasaki — J. Appl. Phys. 43 4828-9, 1972.

57. J. Narayan, J. Washburn — Acta. Metall. 21 533-8, 1973.

58. B. J. Wuensch, T. Vasilos — J. Chem. Phys. 36 2917-22, 1962.

59. I. Zaplatynsky — J. Am. Ceram. Soc. 45 28-31, 1962.

60. E. B. Rigby, I. B. Cutler — J. Am. Ceram. Soc. 48 95-9, 1965.

61. H. Tagai, S. Iseki, M. Saho, S. Iwai — Radex Rundschau. 4 577-83, 1965.

62. B. J. Wuensch, T. Vasilos — Am. Ceram. Soc. Bull. 44 303, 1965.

63. B. C. Harding, A. J. Mortlock — J. Chem. Phys. 45 2699-700, 1966.

64. J. Rungis, A. J. Mortlock — Phil. Mag. 14 821-7, 1966.

65. B. C. Harding — ibid. 16 1039-48, 1967.

66. S. L. Blank, J. A. Pask — J. Am. Ceram. Soc. 52 669-75, 1969.

67. C. Greskovich, V. S. Stubican — J. Phys. Chem. Sol. 30 909-17, 1969.

68. B. J. Wuensch, T. Vasilos — J. Chem. Phys. 54 1123-9, 1971.

69. B. C. Harding, V. K. Bhalla — Phil. Mag. 24 485-8, 1971.

70. W. P. Whitney II, V. S. Stubican — J. Phys. Chem. Sol. 32 305-12, 1971.

71. I. Zaplatynsky — J. Appl. Phys. 35 1358, 1964.

72. W. T. Peria — Phys. Rev. 112 423-33, 1958.

73. H. Weber — Z. Phys. 130 392-402, 1951.

74. H. R. Day — Phys. Rev. 91 822-7, 1953.

75. J. H. Hibben — Phys. Rev. 51 530, 1937.

76. J. S. Prener — J. Chem. Phys. 21 160-1, 1953.

77. E. Yamaka — Phys. Rev. 96 293-6, 1954.

78. P. D. Johnson — Phys. Rev. 94 845-6, 1954.

79. B. D. Saksena, L. M. Pant — Proc. Phys. Soc. B67 811-6, 1954.

80. B. D. Saksena, L. M. Pant — J. Chem. Phys. 23 989-90, 1955.

81. A. S. Eisenstein — Phys. Rev. 93 1017-8, 1954.

82. F. P. Clarke — Phil Mag. 2 607-27, 1957.

83. G. H. Reiling, E. B. Hensley — Phys. Rev. 112 1106-11, 1958.

84. R. W. Soshea, A. J. Dekker, J. P. Sturtz. — J. Phys. Chem. Sol. 5 23-33, 1958.

85. A. M. Glass — J. Chem. Phys. 46 2080-91, 1967.

86. A. M. Glass, T. M. Searle — ibid. 46 2092-101, 1967.

87. T. M. Searle — J. Phys. Chem. Sol. 30 2143-52, 1969.

88. J. R. Nelson — Phys. Rev. 99 1902-3, 1955.

89. M. L. Cohen, P. J. Lin, D. M. Roessler, W. C. Walker — ibid. 155 992-6, 1967.

90. D. M. Roessler, W. C. Walker — ibid. 159 733-8, 1967.

91. C. Y. Fong, W. Saslow, M. L. Cohen — ibid. 168 992-9, 1968.

92. R. C. Whited, W. C. Walker — Phys. Rev. Lett. 22 1428-30, 1969.

93. J. R. Stevenson, E. B. Hensley — J. Appl. Phys. 32 166-72, 1961.

94. J. R. Stevenson — Thermionic and Photo-electric Emission from MgO. Ph.D. Thesis. University of Missouri, 1958.

95. E. Yamaka, K. Sawamoto — Phys. Rev. 101 565-6. 1956.

96. M. A. Pomerantz, R. A. Shatas, J. F. Marshall — ibid. 99 489-90, 1955.

97. J. F. Marshall, M. A. Pomerantz, R. A. Shatas — ibid. 106 432-4, 1957.

98. W. C. Schieve, M. A. Pomerantz — ibid. 122 808-14, 1961.

99. J. H. Pollard, D. L. Bowler, M. A. Pomerantz — J. Phys. Chem. Solids. 26 1325-41, 1965.

100. J. R. Townsend — Phys. Rev. 92 556-60, 1953.

101. K. Das Gupta — Report No. CALT-221-13. California Institute of Technology, 1965.

102. V. A. Fomichev, T. M. Zimkina, I. I. Zhukova — Soviet Physics Solid State 10 2421-7, 1969.

103. H. Watanabe — Phys. Rev. 95 1684-6, 1954.

104. C. G. Harkins, W. W. Shang, T. W. Leland — J. Phys. Chem. 73 130-41, 1969.

105. A. Roux, J. Elston, — C. R. Acad. Sci. Paris Ser C 270 505-8, 1970.

106. B. C. Harding — Phys. Lett. 40A 227-8, 1972.

107. J. Brynestad H. Flood — Z. Elektrochem. 62 953-8, 1958.

108. R. E. Carter — J. Am. Ceram. Soc. 44 116-20, 1961.

109. R. W. Davidge — J. Mat. Sci. 2 339-46, 1967.

110. V. G. Bhide, B. R. Tambe — ibid. 4 955-61, 1969.

111. T. K. Ghosh, F. J. P. Clarke — Brit. J. Appl. Phys. 12 44-50, 1961.

112. J. T. Milek — Report No. EPIC AD413809. Hughes Aircraft Co. Culver City, California, U.S.A., 1963

113. J. T. Milek — Proc. 7th Elec. Ins. Conf. I.E.E.E. Publication 32C 79-13, 1967.

114. M. Neuberger, D. B. Carter — Report No. EPIC AD 698343. Hughes Aircraft Co., Culver City, California, U.S.A., 1969.

115. A. B. Lidiard — Handbuch der Physik. 20 246-349, 1957.

116. R. G. Fuller — Ch. 3, Point Defects in Solids, Vol. I General and Ionic Crystals, Editors: J. H. Crawford, L. M. Slifkin. Plenum Press, 1972.

117. S. P. Mitoff — Prog. Ceram. Sci. 4 218-64, 1966.

118. A. B. Lidiard — Proc. Brit. Ceram. Soc. 9 1-14, 1967.

119. L. W. Barr, A. B. Lidiard — Ch. 3, Physical Chemistry - An Advanced Treatise, Vol. X Academic Press, N.Y., 1970.

120. B. Henderson, J. E. Wertz — Adv. Phys. 17 749-855, 1968.

121. B. C. H. Steele — Conference on Electromotive Force Measurements in Higher Temperature Systems. (Inst. of Mining and Metall) 1967. Publ. 1968. C. B. Alcock pp 3-27.

122. C. B. Alcock — ibid. pp 109-24.

123. D. O. Raleigh — Electroanalytical Chemistry A Series of Advances, Vol VI, 1972.

124.	G. F. J. Garlick	Handbuch der Physik 19, 1956.
125.	G. F. J. Garlick	ibid. 26, 1958.
126.	C. C. Klick	Science 150 451-6, 1965.
127.	J. A. Kitchener, J. O'M, Bockris	Disc. Farad. Soc. 4 91-100, 1948.
128.	W. Low	Sol. St. Phys. Supp. 2, 1960.
129.	P. H. Sutter, A. S. Nowick	J. Appl. Phys. 34 734-45, 1963.
130.	J. Lindmayer	ibid. 36 196-201, 1965.
131.	A. R. Allnatt, P. W. M. Jacobs, J. N. Maycock	J. Chem. Phys. 43 2526-32, 1965.
132.	L. B. Harris	J. Phys. Chem. Solids 32 59-70, 1971.
133.	C. Kittel	Introduction to Solid State Physics. Wiley. New York, 1956.
134.	F. A. Kröger, H. J. Vink	Sol. St. Phys. 3 307-435, 1956.
135.	R. J. Friauf	J. Appl. Phys. 33 Supp. 494-505, 1962.
136.	R. D. Shannon, C. T. Prewitt	Acta Cryst. B25 925-46, 1969.
137.	N. N. Greenwood	Ionic Crystals, Lattice Defects and Nonstoichiometry. Butterworths. London. 1968.

138. Collection of articles by S. V. Karpachev S. F. Pal'guev, L. D. Yushina, A. D. Neuimin and Z. S. Volchenkova. Trudy Inst. Elektrochim. Ural. Fil. Akad. Nauk. S.S.S.R. 1 63-106, 1960.

139. C. Tubandt — Handbuch der Experimentalphysik 12 (1) 383, 1932.

140. L. B. Valdes — Proc. I.R.E. 42, 1954.

141. N. M. Tallan, H. C. Graham, R. W. Vest — Rev. Sci. Inst. 33 1087-8, 1962.

142. K. G. Nichols, E. V. Vernon — Transistor Physics. Chapman and Hall, London. 1966.

143. W. E. Deming — Statistical Adjustment of Data. Dover Publications Inc. New York. 1964.

APPENDIX 1 TWO- THREE- AND FOUR- TERMINAL MEASUREMENT TECHNIQUES

The different electrical measurement systems which have previously been used for measuring the conductivity of ceramic samples will now be described, and their advantages and disadvantages briefly discussed. This appendix is intended to be only an introduction to the techniques described and so to avoid unnecessary complications only symmetrical samples of spatially constant conductivity will be considered.

A1.1 Two-Terminal Measurement Technique

This is the simplest conductivity measurement system. Conducting contacts are applied to both sides of the sample, a voltage applied across the sample and the total current flowing measured (see Fig. 38). The bulk conductivity is given by the expression:

$$\sigma_b = \frac{I_b}{V} \cdot \frac{l}{a} \qquad \text{(A1.1)}$$

where σ_b is the bulk conductivity (S m^{-1})

I_b is the current flowing in the bulk material (A)

$V = V_1 - V_2$ is the potential difference across the sample (V)

l is the length of the sample (m)

and a is the contact area (m^2)

This technique is suitable for measurement of the bulk conductivity in situations where the current flowing through the bulk material, I_b, is much greater than I_s, the current flowing on the surface of the sample, I_g, the current flowing through the surrounding gas, and I_l, the current flowing through any leakage resistances in parallel with the meter, M. If, however, any of I_g, I_s or I_l is significant when compared with I_b, then the measured current, I, will not be a good estimate of I_b and the conductivity value obtained will be erroneous.

When measuring the bulk conductivity of insulating materials, such as magnesia, the presence of a high surface conductivity cannot be discounted and errors due to gas conduction have been reported by several workers (19, 26). Also the leakage resistance, represented by R_l, due to the insulation resistance of the cable used, and perhaps to the leakage resistances of insulators, plugs and sockets, may be comparable to that of the meter, and so the leakage current I_l, will cause a significant error. This technique is thus not a recommended method of measuring the bulk conductivity of highly resistive samples.

A.1.2 Three-Terminal Measurement Technique

The three-terminal measurement technique has the advantage of reducing the errors due to gas and surface conduction, but a more complicated contact pattern, as shown in Fig. 39(a), is required. The basic system is as shown in Fig. 39(b).

The technique used is as for two-terminal measurements except that the guard-ring is raised to the same potential as the centre contact by a subsidiary voltage source V_2. This may be a manually adjusted source, or may be derived from the centre contact potential by a unity-gain amplifier.

Part of the current flowing through the bulk, I_{b2}, flows away to ground through V_2. The true bulk conductivity is given by the expression

$$\sigma_b = \frac{I_{b1}}{V} \cdot \frac{l}{a} \qquad \text{(A1.2)}$$

where I_{b1} is the current flowing through the bulk to the centre contact

and a is the area of the centre contact.

Any current, I_s, flowing along the surface flows to ground via voltage source V_2. No current flows between the centre contact and the guard ring, as they are at the same potential. Part of the current flowing through the gas, I_{g1},

also flows to ground via V_2. However, a portion of the current flowing through the gas, I_{g2}, may still reach the centre contact. The ratio of I_{g1} to I_{g2} will be determined by the sample and contact geometries. There is still a leakage current I_l, due to leakage resistance R_l.

An improved, "volume guarded", system is shown in Fig. 39(c). The centre contact is physically protected from gas conduction by a cylindrical shield. All the current flowing through the gas flows to ground via V_2. The current I_l still leads to an error in the calculation of the bulk conductivity.

The third, and most useful version of the three-terminal measurement technique is shown in Fig. 39(d). The guard-ring is connected directly to ground and thus no second voltage source is necessary. It is, however, essential for the meter M to have an electronic buffer amplifier used in the "fast", or "virtual earth", configuration. Such an amplifier will have a very low input voltage V_2. The Keithley 610C electrometer used in this investigation, when used in the "fast" mode, is guaranteed to have an input voltage of less than 10^{-4}V for current measurements of 10^{-14} A to $3 . 10^{-1}$ A F.S.D.

If the input voltage, V_2, is exactly zero then the current, I, measured by the meter is exactly equal to I_{b1} and the conductivity is calculated from expression (A1.2). If, however, V_2 is not exactly zero there are errors due to surface conduction between the centre contact and the guard-ring (represented by R_S) and to conduction through the leakage resistances (represented by R_l). The magnitude of this error may be appreciated by considering some typical figures.

Let V_1 = 100 V

$V_2 = 10^{-4}$ V (as for Keithley 610C)

R'_S = the parallel combination of R_S and R_l

R_b = the bulk resistance $\frac{1}{\sigma_b} . \frac{l}{a}$

Referring to Fig. 39(d) we have

$$I_{b1} = \frac{V_1 - V_2}{R_b} \simeq \frac{V_1}{R_b} \tag{A1.3}$$

$$\left.\begin{aligned} I &= I_{b1} - \frac{V_2}{R_s} - \frac{V_2}{R_1} \\ &= I_{b1} - \frac{V_2}{R'_s} \end{aligned}\right\} \tag{A1.4}$$

Thus the fractional error in the measurement of I_{b1} is

$$\frac{\left(\frac{V_2}{R'_s}\right)}{\left(\frac{V_1}{R_b}\right)} \tag{A1.5}$$

$$= \frac{V_2}{V_1} \cdot \frac{R_b}{R'_s} = 10^{-6} \cdot \frac{R_b}{R'_s} \tag{A1.6}$$

Thus it is possible to make measurements with an error of only 1% when the equivalent leakage resistance is a factor of 10^4 less than the resistance it is required to measure, R_b.

A1.3 Four-Terminal Measurement Techniques

The basic D.C. four-terminal measurement system is illustrated in Fig. 40. A known current, I, is passed between the two outer electrodes, and the voltage, V, developed between the two inner electrodes is measured. The conductivity of the sample may be calculated from a knowledge of I, V, and the geometry of the system.

This method is often used when it is difficult or impossible to obtain ohmic contacts between the sample and the measurement probes. e.g. when measuring semiconductor materials (140). Only a very small current passes through the two inner electrodes, and so unwanted contact potentials are reduced.

This method is not a preferred technique for making conductivity measurements on materials such as magnesia, because the problems of gas and surface conduction are as significant as for the two-terminal technique discussed previously.

It is noted here that an A.C. four-terminal measurement technique, similar to the three-terminal system described above, but with the addition of a guard on the back of the sample has been devised (10, 141). This thesis is mainly concerned with D.C. measurements and so this system will not be discussed in detail. For further information the original references should be consulted.

APPENDIX 2 EXTRINSIC ELECTRONIC CONDUCTION CALCULATIONS

In order to calculate the concentrations of free holes and/or electrons caused by the presence of isolated energy levels in the energy band gap it is necessary to consider the energy band picture of a semiconductor or insulator, as shown in Fig. 41. The equations describing the electron and hole equilibria have been derived and solved for several cases relevant to the conditions obtaining in a semiconductor (see e.g. Ref. 142). In this section the conditions obtaining in a wide band-gap material, such as magnesia, are considered.

The concentrations of free electrons in the conduction band, and of free holes in the valence band, are given by the expressions: (see Fig. 41 and Ref. 142)

$$n_e = N_c \exp(-(E_c-E_f)/kT) \qquad (A2.1)$$

$$n_h = N_v \exp(-(E_f-E_v)/kT) \qquad (A2.2)$$

$$N_c = 2\,(2\pi m_e kT/h^2)^{1.5} \qquad (A2.3)$$

$$N_v = 2\,(2\pi m_h kT/h^2)^{1.5} \qquad (A2.4)$$

where n_e is the concentration of electrons in the conduction band (m^{-3})

n_h is the concentration of holes in the valence band (m^{-3})

E_c is the energy at the conduction band edge (eV)

E_f is the energy at the Fermi level (eV)

E_v is the energy at the valence band edge (eV)

m_e is the effective mass of the electron in the conduction band (kg)

m_h is the effective mass of the hole in the valence band (kg)

and the other symbols have their usual meanings.

For n_e and n_h to be calculated the value of E_f, the position of the Fermi level, must be known. The general equation determining the position of the Fermi level is (142):

$$N_c \exp(-(E_c-E_f)/kT) + \frac{N_a}{1 + \exp((E_a-E_f)/kT)} =$$

$$N_v \exp(-(E_f-E_v)/kT) + \frac{N_d}{1 + \exp(-(E_d-E_f)/kT)} \qquad \text{(A2.5)}$$

where N_a is the concentration of acceptor levels (m^{-3})

N_d is the concentration of donor levels (m^{-3})

E_a is the energy at the acceptor level (eV)

E_d is the energy at the donor level (eV)

The intrinsic carrier concentration, n_i, is given by the equation (see section 6.1.2.1):

$$(n_i)^2 = N_c \, N_v \exp(-(E_c-E_v)/kT) \qquad \text{(A2.6)}$$

The electron and hole densities are related by the equation (142):

$$n_e \, n_h = (n_i)^2 \qquad \text{(A2.7)}$$

Equations A2.5, A2.6, A2.7 are general and hold for all semiconductors and insulators (or wide band-gap semiconductors). The specific case of the magnesia lattice containing donor levels will now be considered. The decision to choose the case of donor levels and to calculate the electron concentration arising from them is arbitrary: a corresponding situation exists for acceptor levels and holes. The calculations are essentially the same for both situations. To be definite a donor level concentration of $5 \cdot 10^{24}$ m^{-3} will be used for most of the calculations. This is equivalent to approximately 100 mole. ppm, the same order of magnitude as the typical impurity content of magnesia crystals. Each lattice defect caused by an impurity is expected to lead to one energy level (134), and so the values of electron density calculated should be representative of the values occurring

in practice. The effect of varying level concentrations will also be considered.

The values of intrinsic carrier concentration, n_i, are listed in Table 4. It can be seen that, even at high temperatures, n_i is very low. At $10^3/T = 0.4$ ($T \simeq 2230^{\circ}C$) $n_i = 9 \cdot 10^{18}$ m^{-3}; this is equivalent to 1 carrier per $6 \cdot 10^9$ molecules. The electron concentration, given by equation (A2.1) is generally much larger than n_i and so the hole concentration, n_h, as calculated from equation (A2.7), is negligible compared to n_e. Thus the third term in equation (A2.5) may be omitted.

As only donor levels are being considered, the acceptor level concentration, N_a, is zero. Therefore the second term of expression (A2.5) may be omitted.

Thus expression (A2.5) becomes:

$$N_c \exp(-(E_c-E_f)/kT) = \frac{N_d}{1 + \exp(-(E_d-E_f)/kT)} \qquad (A2.8)$$

$$\text{Let } U = \exp(-(E_c-E_f)/kT) \qquad (A2.9)$$

$$\text{and } V = \exp(-(E_c-E_d)/kT) \qquad (A2.10)$$

Combining equations A2.8, A2.9 and A2.10 we have:

$$N_e \cdot U = \frac{N_d}{1 + (U/V)}$$

$$\therefore \quad N_c U^2 + N_c V U - N_d V = 0$$

$$\therefore \quad U = \frac{-N_c V \pm (N^2_c V^2 + 4 N_c N_d V)^{\frac{1}{2}}}{2N_c} \qquad (A2.11)$$

This equation may be solved, ignoring the negative root as physically unrealisable, for different values of N_d and V (which is a function of (E_c-E_d), the energy level - band edge separation; see expression (A2.10)). The electron density n_e may then be calculated by noting that equation (A2.1) may be re-written:

$$n_e = N_c \cdot U \qquad (A2.12)$$

The values of n_e calculated when $N_d = 5 \cdot 10^{24}$ m^{-3}, for various values of energy level - band edge separation are listed in Table 4. The corresponding conductivities are plotted in Fig. 35 (see section 6.4).

The manner in which n_e varies with N_d is shown by Table 5. It can be seen that the electron concentration, n_e, is approximately proportional to the square root of the donor level concentration, N_d.

APPENDIX 3 COMPUTER PROGRAM USED FOR CURVE-FITTING

The computer program described in this appendix was developed by the author for fitting curves to measured data points. It was mainly used during the analysis of the current decay measurements (see section 5.5), but some voltage-current characteristics were also analysed. It may be used for fitting any form of curve to data points.

The procedure used is based on that described by Deming (143). The theory behind least-squares fitting is discussed at length in his work and so only a very brief discussion of the method used is given here. It is strongly recommended that the original book be consulted before the program described here is used.

A3.1 Program Description

The program described here may be used to fit any form of curve to any set of data. It is not limited to the fitting of polynomials. The procedure is, however, iterative and initial estimates of the parameters are therefore necessary.

A flow chart of the basic program is shown in Fig. 42. The final program, as listed in section A3.2 has extra loops to enable several sets of data to be analysed, or one set of data to be analysed several times. These need not be discussed here.

Initially the data points, their estimated errors and the initial estimates of the parameters are read in. The coefficients of the "normal equations" (see Ref. 143) are then calculated. These coefficients are calculated by summing cross-products of the partial derivatives of the function to be fitted over all the data points.

The normal equations are then solved to yield the "parameter residuals", and the new values of the parameters calculated by subtracting the parameter residuals from the previous estimates. The whole procedure is repeated until the parameters are found to the desired accuracy. The values

of the parameters, the "adjusted" data points, the values of the fitted curve and the confidence limits are then printed out.

In practice intermediate results are printed out to enable the progress of the program to be followed. The adjusted data points are printed out in three groups, to enable the "goodness of fit" to be compared at the two ends, and in the middle, of the range of the data. A typical output is shown in Fig. 43.

The main body of the program is the same for fitting any function. The fitting of different functions is achieved by putting different "inserts" into the program. These inserts contain the statements which define the calculation of the partial derivatives of the function. Some examples are given in section A3.3.

The program was found to work well in practice and most sets of data could be fitted to most functions which were of approximately the correct form. Some difficulty was encountered in fitting sums of exponential terms. This is due to the normal equations being ill-conditioned for this case, and this can cause the program to diverge from the solution.

A3.2 Program Listing and Notes

The program was written in the ICL version of Algol and a listing is given on the following pages. A few brief comments on the functions of the separate sections are also given.

```
'BEGIN''INTEGER'N,NX;
        SELECTINPUT(3);
        N:=READ;      NX:=READ;




'BEGIN''REAL''ARRAY'X,Y,RWX,RWY[1:N],XO[1:NX];
        'INTEGER'Z,NPARAM,DATASET;
        'REAL'DX,DY;

        'FOR'Z:=1'STEP'1'UNTIL'N'DO'
        'BEGIN'X[Z]:=READ;
                Y[Z]:=READ;
                DX:=READ;
                DY:=READ;
                RWX[Z]:=DX*DX;
                RWY[Z]:=DY*DY;
        'END';

        'FOR'Z:=1'STEP'1'UNTIL'NX'DO'      XO[Z]:=READ;

NEXTSET:DATASET:=READ;
        'IF''DATASET<0'THEN''GOTO'FINISH;

        NPARAM:=READ;



'BEGIN''INTEGER'J,K,L,IT,IRR,INN,IPSS,IMM,ISS,COUNT,ACC,N3,P,Q,R,
                CHECK2,LIM1,LIM2,FAST;
        'REAL'FX,FY  ,LL,S,SEEXT,SE,YO,SEY,CONF,LOG,DD,EPSS,MULT,AB,CD,
           EF,GH,IJ,KL,MN,EXPB,EXPD,EXPF,EXPH,EXPJ,EXPL,EXPN,LAMBDA,
              VX,VY,DO,TOL,F99,F95;
        'REAL''ARRAY'                    PARAM,RESID[1:NPARAM*2],
```

```
24              INV,SUM[1:NPARAM,1:NPARAM+1],FPARAM[1:NPARAM+1],
24                 AAA[1:NPARAM*NPARAM*2];
24              'INTEGER''ARRAY'IW[1:6*NPARAM];
25
25              'PROCEDURE' FPINDD(AA,IR,IN,D,EPS1,IPS,ABB,IM,IS,IW);
27              'REAL'D,EPS1,AA,ABB;
28              'INTEGER'IR,IN,IPS,IM,IS,IW;
29                          'EXTERNAL';
29
29
29              LOG:=1/LN(10);      COUNT:=0;
32
32              'FOR'J:=1'STEP'1'UNTIL'NPARAM'DO'      PARAM[J]:=READ;
34
34              IT:=READ;      TOL:=READ;      F99:=READ;      F95:=READ;
38              FAST:=READ;
39
39
39              WRITETEXT('('''('P')'INITIAL%%  VALUES%%  OF%%  PARAMETERS
39                        '('10S')'DATA%%SET%%%%')');
40              PRINT(DATASET,10,0);
41              NEWLINE(1);
42
42              'FOR'J:=1'STEP'1'UNTIL'NPARAM'DO'
43                   'BEGIN'NEWLINE(1);  PRINT(PARAM[J],0,10) 'END';
46
46      NEXTIT:'FOR'J:=1'STEP'1'UNTIL'NPARAM'DO'
47                   'FOR'K:=1'STEP'1'UNTIL'NPARAM+1'DO'      SUM[J,K]:=0;
49              S:=0;
50
50              WRITETEXT('('''('4C')'ITERATION%%NUMBER%%%%')');
51              PRINT(COUNT+1,4,0);
52
52              'FOR'J:=1'STEP'1'UNTIL'N'DO'
53      'BEGIN'
```

```
53        FY:=-1;     FX:=0;    DD:=-Y[J]+PARAM[1];
57        FPARAM[1]:=1;
58        'FOR'P:=2'STEP'2'UNTIL'NPARAM'DO'
59        'BEGIN'FPARAM[P]:=X[J]↑PARAM[P+1];
61               FPARAM[P+1]:=PARAM[P]*FPARAM[P]*LN(X[J]);
62               FX:=FX+PARAM[P]*PARAM[P+1]*↑PARAM[P]/X[J];
63               DD:=DD+PARAM[P]*FPARAM[P];
64        'END';
65
65        FPARAM[NPARAM+1]:=DD;
66
66
66
66
66               LL:=FX*FX*RWX[J]+FY*FY*RWY[J];
67               S:=S+FPARAM[NPARAM+1]*FPARAM[NPARAM+1]/LL;
68
68               'FOR'K:=1'STEP'1'UNTIL'NPARAM'DO'
69                    'FOR'L:=K'STEP'1'UNTIL'NPARAM+1'DO'
70                         SUM[K,L]:=SUM[K,L]+FPARAM[K]*FPARAM[L]/LL;
71        'END';
72
72               'FOR'K:=2'STEP'1'UNTIL'NPARAM'DO'
73                     'FOR'L:=1'STEP'1'UNTIL'K-1'DO'SUM[K,L]:=SUM[L,K];
75
75               'FOR'J:=1'STEP'1'UNTIL'NPARAM'DO'
76                    'FOR'K:=1'STEP'1'UNTIL'NPARAM'DO'   AAA[K+NPARAM*(J-1)]:=
77                                                             SUM[J,K];
78
78               'IF'FAST=0'THEN'
78               'BEGIN'
78               WRITETEXT('('''('2C')'COEFFICIENTS  %%OF  %%NORMAL%%  EQUATIONS
79                         '('1C')''')');
80
80               'FOR'J:=1'STEP'1'UNTIL'NPARAM'DO'
```

```
81              'BEGIN'NEWLINE(1);
83                    'FOR'K:=1'STEP'1'UNTIL'NPARAM+1'DO'  PRINT(SUM[J,K],0,10);
85              'END';
86
86              'END';
87
87              INN:=NPARAM;      DD:=0;     EPSS:=1&-20;     IPSS:=0;
91              'FOR'J:=1'STEP'1'UNTIL'NPARAM'DO'   RESID[J]:=SUM[J,NPARAM+1];
93              IM1:=ISS:=1;      IRR:=0;
95
95              FPINDD(AAAL1],IRR,INN,DD,EPSS,IPSS,RESID[1],IM1,ISS,IWW[1]);
96              'IF'INN=0'THEN''GOTO'OUT;
97
97              'FOR'J:=1'STEP'1'UNTIL'NPARAM'DO'
98                    'FOR'K:=1'STEP'1'UNTIL'NPARAM'DO'
99                          INV[J,K]:=AAA[K+(J-1)*NPARAM];
100
100
100             'IF'FAST=0'THEN'
100             'BEGIN'
100             WRITETEXT('('''('2C')'INVERSE  %%MATRIX'('1C')''')');
102
102             'FOR'J:=1'STEP'1'UNTIL'NPARAM'DO'
103             'BEGIN'NEWLINE(1);
105                   'FOR'K:=1'STEP'1'UNTIL'NPARAM'DO'  PRINT(INV[J,K],0,10);
107             'END';
108
108
108             'END';
109
109             WRITETEXT('('''('2C')'PARAMETER  %%RESIDUALS'('1C')''')');
110             'FOR'J:=1'STEP'1'UNTIL'NPARAM'DO'
111                   'BEGIN'NEWLINE(1);  PRINT(RESID[J],0,10);  'END';
115
115             WRITETEXT('('''('2C')'SUM%%  OF%%  SQUARES%%  %%S'('1C')''')');
```

```
116             'FOR'J:=1'STEP'1'UNTIL'NPARAM'DO'
117                  'BEGIN'NEWLINE(1);
119                         PRINT(S,0,10);
120                         S:=S-RESID[J]*SUM[J,NPARAM+1];
121                  'END';
122
122             NEWLINE(1);
123             PRINT(S,0,10);
124
124
124             'IF'S>0'THEN'SEEXT:=SQRT(S/(N-NPARAM)) 'ELSE'SEEXT:=0;
125
125             WRITETEXT('('''('2C')'STANDARD%%DEVIATION%%')');
126             PRINT(SEEXT,0,10);
127
127             WRITETEXT('('''('2C ')'NEW%%  VALUES%%  OF%%  PARAMETERS')');
128             NEWLINE(1);
129             'FOR'J:=1'STEP'1'UNTIL'NPARAM'DO'
130             'BEGIN'
130                   PARAM[J]:=PARAM[J]-RESID[J];
132                   NEWLINE(1);
133                   PRINT(PARAM[J],0,10);
134             'END';
135
135             ACC:=0;
136
136             'FOR'J:=1'STEP'1'UNTIL'NPARAM'DO'
137               'IF'ABS(RESID[J]/PARAM[J])>TOL 'THEN'ACC:=1;
138
138             COUNT:=COUNT+1;
139
139             'IF'ACC=1'AND'COUNT<IT'THEN''GOTO'NEXTIT;
140
140             PAPERTHROW;
```

```
141             WRITETEXT('('DATA%%SET%%%%')');
142             PRINT(DATASET,10,0);
143
143             'IF'ACC=1'THEN'WRITETEXT('('('3C')'PARAMETERS%%NOT%%FOUND%%TO%
143                  %%DESIRED%%ACCURACY%%%%')');
144             'IF'ACC=1'THEN'PRINT(TOL,0,3);
145
145             WRITETEXT('('('3C')'%%%X(OBSERVED)'('9S')'Y(OBSERVED)'('9S')'
145                    X%RESIDUAL'('10S')'Y%RESIDUAL'('10S')'X(ADJUSTED)
145                  '('9S')'Y(ADJUSTED)'('C')'')');
146
146             SEEXT:=S:=0;
147             N3:=N'/'3;
148             CHECK2:=0;
149       AGAIN :CHECK2:=CHECK2+1;
150             SEEXT:=SEEXT+S;
151
151             'IF'CHECK2=1'THEN''BEGIN' LIM1:=1; LIM2:=N3 'END';
154             'IF'CHECK2=2'THEN''BEGIN' LIM1:=N3+1; LIM2:=N-N3 'END';
157             'IF'CHECK2=3'THEN''BEGIN' LIM1:=N-N3+1; LIM2:=N; 'END';
161             'IF'CHECK2=4'THEN''GOTO'PRINTT;
162
162             S:=0;
163             'FOR'J:=LIM1'STEP'1'UNTIL'LIM2'DO'
164       'BEGIN'
164       FY:=-1;     FX:=0;    OO:=-Y[J]+PARAM[1];
168       FPARAM[1]:=1;
169       'FOR'P:=2'STEP'2'UNTIL'NPARAM'DO'
170       'BEGIN'FPARAM[P]:=X[J]↑PARAM[P+1];
172             FPARAM[P+1]:=PARAM[P]*FPARAM[P]*LN(X[J]);
173             FX:=FX+PARAM[P]*PARAM[P+1]*FPARAM[P]/X[J];
174             OO:=OO+PARAM[P]*FPARAM[P];
175       'END';
176
176       FPARAM[NPARAM+1]:=OO;
```

```
177             LL:=FX*FX*RWX[J]+FY*FY*RWY[J];
178
178             LAMBDA:=0;
179             'FOR'K:=1'STEP'1'UNTIL'NPARAM'DO'
180                  LAMBDA:=LAMBDA+FPARAM[K]*RESID[K];
181             LAMBDA:=(FPARAM[NPARAM+1]-LAMBDA)/LL;
182
182             VX:=RWX[J]*LAMBDA*FX;
183             VY:=RWY[J]*LAMBDA*FY;
184
184             NEWLINE(1);
185             PRINT(X[J],0,10);     SPACE(1);
187             PRINT(Y[J],0,10);     SPACE(1);
189             PRINT(VX,0,10);   SPACE(1);
191             PRINT(VY,0,10);   SPACE(1);
193             PRINT(X[J]-VX,0,10);   SPACE(1);
195             PRINT(Y[J]-VY,0,10);   SPACE(1);
197             S:=S+LL*LAMBDA*LAMBDA;
198     'END';
199
199             WRITETEXT('(''('2C')'STANDARD%%DEVIATION%%FOR%%THE%%ABOVE%%')');
200             PRINT(LIM2-LIM1+1,4,0);
201             WRITETEXT('('%%POINTS%%%=%%')');
202             PRINT(SQRT(S/(LIM2-LIM1+1)),0,10);
203             NEWLINE(1);
204             'GOTO'AGAIN;
205
205     PRINTT:SEEXT:=SQRT(SEEXT/(N-NPARAM));
206             WRITETEXT('(''('3C')'STANDARD%%DEVIATION%%FOR%%THE%%WHOLE%%
206                       CURVE%%%=%%')');
207             PRINT(SEEXT,0,10);
208
208             WRITETEXT('(''('5C')' NEW%%  VALUES%%  OF%%  PARAMETERS
208                       '('BS')'STANDARD%%  ERRORS   %%-%%FOR%%')');
209             PRINT(N-NPARAM,4,0);
```

```
210             WRITETEXT('('%%DEGREES%%OF%%FREEDOM'('10')'')');
211             'FOR'J:=1'STEP'1'UNTIL'NPARAM'DO'
212             'BEGIN'SE:=SEEXT*SQRT(INV[J,J]);
214                     NEWLINE(2);
215                     PRINT(PARAM[J],0,10);
216                     SPACE(15);
217                     PRINT(SE,0,10);
218             'END';
219
219
219             WRITETEXT('('''(' 5C12S')'FITTED%%CURVE'('35S')'CONFIDENCE%%
                        LIMITS%%-%%FOR%%')');
220             PRINT(N-NPARAM,4,0);
221             WRITETEXT('('%%DEGREES%%OF%%FREEDOM
221                             '('20?S')'X'('19S')'Y'('13S')'STANDARD%%  ERROR%%%
221                       %%%   99%%PER%%CENT'('7S')'95%%PER%%CENT'('3C')'')');
222
222                     F99:=SQRT(NPARAM*F99);      F95:=SQRT(NPARAM*F95);
224
224             'FOR'J:=1'STEP'1'UNTIL'NX'DO'
225             'BEGIN'
225
225
225
225
225     Y0:=PARAM[1];       FPARAM[1]:=1;
228     'FOR'P:=2'STEP'2'UNTIL'NPARAM'DO'
229     'BEGIN'FPARAM[P]:=XO[J]↑PARAM[P+1];
231             FPARAM[P+1]:=PARAM[P]*FPARAM[P]*LN(XO[J]);
232             Y0:=Y0+FPARAM[P]*PARAM[P];
233     'END';
```

```
234                     SEY:=0;
235
235                     'FOR'K:=1'STEP'1'UNTIL'NPARAM'DO'
236                          'FOR'L:=1'STEP'1'UNTIL'NPARAM'DO'
237                               SEY:=SEY+INV[K,L]*FPARAM[K]*FPARAM[L];
238                     SEY:=SEEXT*SQRT(SEY);
239
239                     NEWLINE(2);                PRINT(XO[J],0,10);   SPACE(1);
242                     PRINT(YO,0,10);   SPACE(1);
244                     PRINT(SEY,0,10);   SPACE(1);
246                     PRINT(YO+SEY*F99 ,0,10);  SPACE(1);
248                     PRINT(YO+SEY*F95 ,0,10);  SPACE(1);
250                     NEWLINE(1);  SPACE(60);
252                     PRINT(YO-SEY*F99 ,0,10);  SPACE(1);
254                     PRINT(YO-SEY*F95 ,0,10);  SPACE(1);
256               'END';
257
257          OUT:
257               NEWLINE(10);
258          'END';
259          'GOTO'NEXTSET;
260          FINISH;
260          'END';
261          NEWLINE(1 );
262          'END';
```

LINE	
3	N - number of data points NX - number of x values for which it is desired to print out the final curve
9 - 11	X[Z], Y[Z] - data points.
12 - 13	DX, DY - errors of data points.
14 - 15	RWX[Z], RWY[Z] - reciprocal weights of data points.
19 - 20	DATASET - reference number ; if negative then program halts.
21	NPARAM - number of parameters.
32	PARAM[J] - parameter values.
34	IT - maximum number of iterations allowed. TOL - relative accuracy to which parameter values are checked. F99, F95 - "F" values used for calculating confidence limits.
38	FAST - if 0 all intermediate results printed. - if 1 only some intermediate results printed.
53 - 65	Insert 1 (see section A3.3).
67	Sum of squares, S, calculated.
68 - 73	The coefficients of the normal equations are formed in SUM[K, L].
95	Procedure FPINDD is used to invert the matrix SUM, and to calculate the parameter residuals RESID[J].
98	INV[K, L] is the inverted matrix.
116 - 121	Reduced sum of squares calculated.

LINE

129 - 134 New values of parameters calculated.

135 - 139 Accuracy of parameters checked.

149 - 204 Adjusted data points, residuals and standard deviations printed out.

164 - 176 Insert 2 (see section A3.3).

219 - 256 Final curve and confidence limits printed out.

225 - 232 Insert 3 (see section (A3.3).

The data format required is given below:-

N - number of data points.

NX - number of x values for which it is desired to tabulate values of the final curve.

$\begin{bmatrix} X \\ Y \\ DX \\ DY \end{bmatrix}$ - data points and errors (N times).

$[XO]$ - x values for which the final curve is to be printed out (NX times).

DATASET - code number.

NPARAM - number of parameters.

$[PARAM]$ - initial values of parameters (NPARAM times).

IT - maximum number of iterations.

TOL - relative accuracy to which the parameter values are checked.

F99 - F_{99} (NPARAM, N-NPARAM)

F95 - F_{95} (NPARAM, N-NPARAM)

FAST - 1 or 0

negative integer.

A3.3 Program Inserts

The three program inserts contain all the statements specific to the function being fitted. The program was originally stored on punched cards and it was convenient to be able to change the function to be fitted by simply changing three short sections of the program.

As noted above, to form the coefficients of the normal equations it is necessary to evaluate the partial derivatives of the function to be fitted, at each of the data points. It is also necessary to calculate the residual (i.e. the difference beteen the measured and fitted values) at each data point. The purpose of insert 1 is to calculate the partial derivatives with respect to x (FX), y (FY), and the parameters (FPARAM[1], FPARAM[2], ...), and also to calculate the residual F_o, at each data point X[J], Y[J]. These values are then used to calculate the coefficients of the normal equations.

Insert 2, which is identical to insert 1, calculates values which are used in the calculation of the adjusted data points.

Insert 3, calculates the partial derivatives and the values of y at the values of x for which the final curve is tabulated. These values are used in the calculation of the confidence limits.

Two specific examples will be given, the first very simple, the other a little more complicated.

A3.3.1 $y = a + bx$

To fit a curve of the form $y = a + bx$ to a set of data points, write

$$F = -y + a + bx$$

Thus the partial derivatives are:-

$$F_y = -1$$

$$F_x = b$$

$$F_a = +1$$

$$F_b = x$$

and the residual is:-

$$F_o = -y + a + bx$$

Writing this in the notation of the program:-

```
FY : =    - 1 ;
FX : =    PARAM[2] ;
FPARAM[1]: =  1 ;
FPARAM[2]: =  X[J] ;
FPARAM[3]: =  -Y[J] + PARAM[1]
              + PARAM[2] * X[J] ;
```

inserts 1 and 2

```
FPARAM[1]: =  1 ;
FPARAM[2]: =  XO[J];
  YO : =  PARAM[1] + PARAM[2] * XO[J];
```

insert 3

A3.3.2 <u>$y = a + bx^c$</u>

This is one of the decay formulae discussed in section 5.5, when

$$a \equiv I_\infty$$

$$b \equiv I_o$$

$$c \equiv -m$$

We now have $F = -y + a + bx^c$

and $F_y = -1$

$F_x = b.c.x^{c-1} = b.c.F_b/x$

$$Fa = 1$$

$$F_b = x^c$$

$$F_c = b.x^c.\log_e(x) = b.F_b.\log_e(x)$$

Thus

```
FY : =   -1 ;
FPARAM[1] : =  1 ;
FPARAM[2] : =  X[J]↑ PARAM[3];
FX : = FPARAM[2] *  PARAM[2] *  PARAM[3]/X[J] ;
FPARAM[3] : =  PARAM[2] *  FPARAM[2] *  LN(X[J]);
FPARAM[4] : =  -Y[J] + PARAM[1]
               + PARAM[2] * FPARAM[2] ;
```

inserts 1 and 2

```
FPARAM[1] : =  1 ;
FPARAM[2] : = XO[J] ↑ PARAM[3] ;
FPARAM[3] : = PARAM[2] * FPARAM[2] * LN(XO[J]);
  YO : =  PARAM[1] + PARAM[2] * FPARAM[2];
```

insert 3

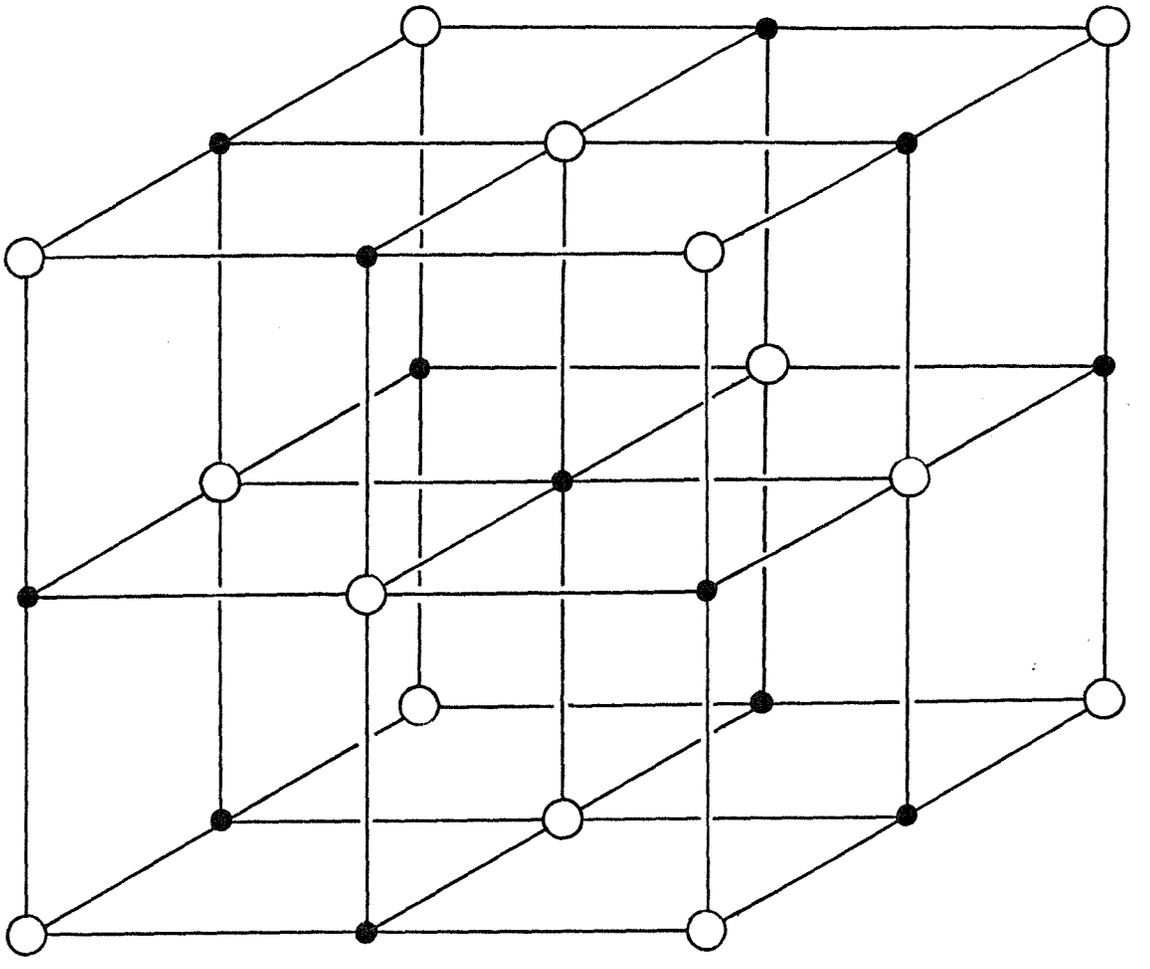

○ O^{--} ions

● Mg^{++} ions

FIGURE 1(a) THE MAGNESIA LATTICE

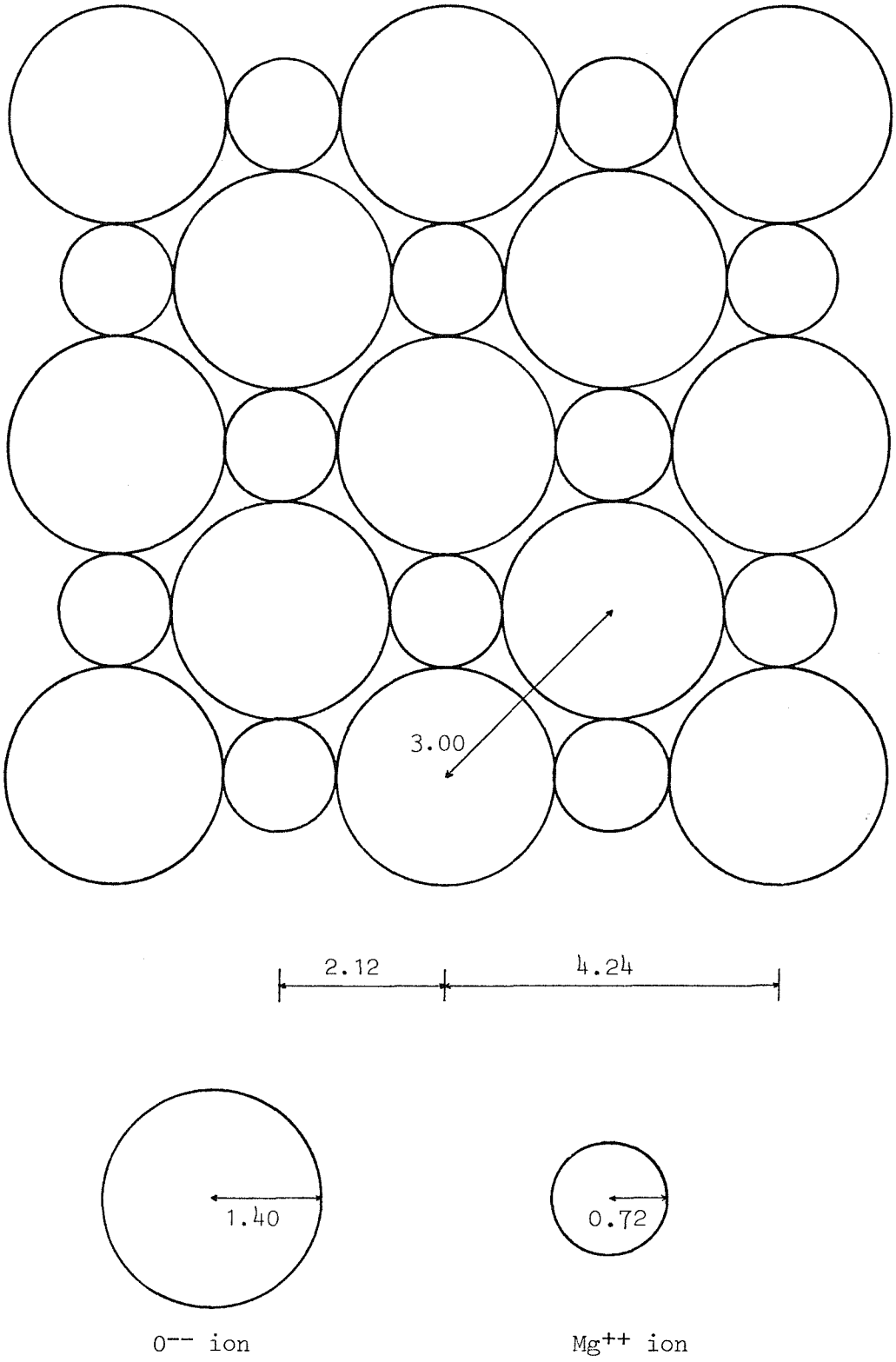

Distances in $\mathring{A}$ ($1\mathring{A} = 10^{-10}$ m)

FIGURE 1(b) TWO-DIMENSIONAL REPRESENTATION OF THE THE MAGNESIA LATTICE

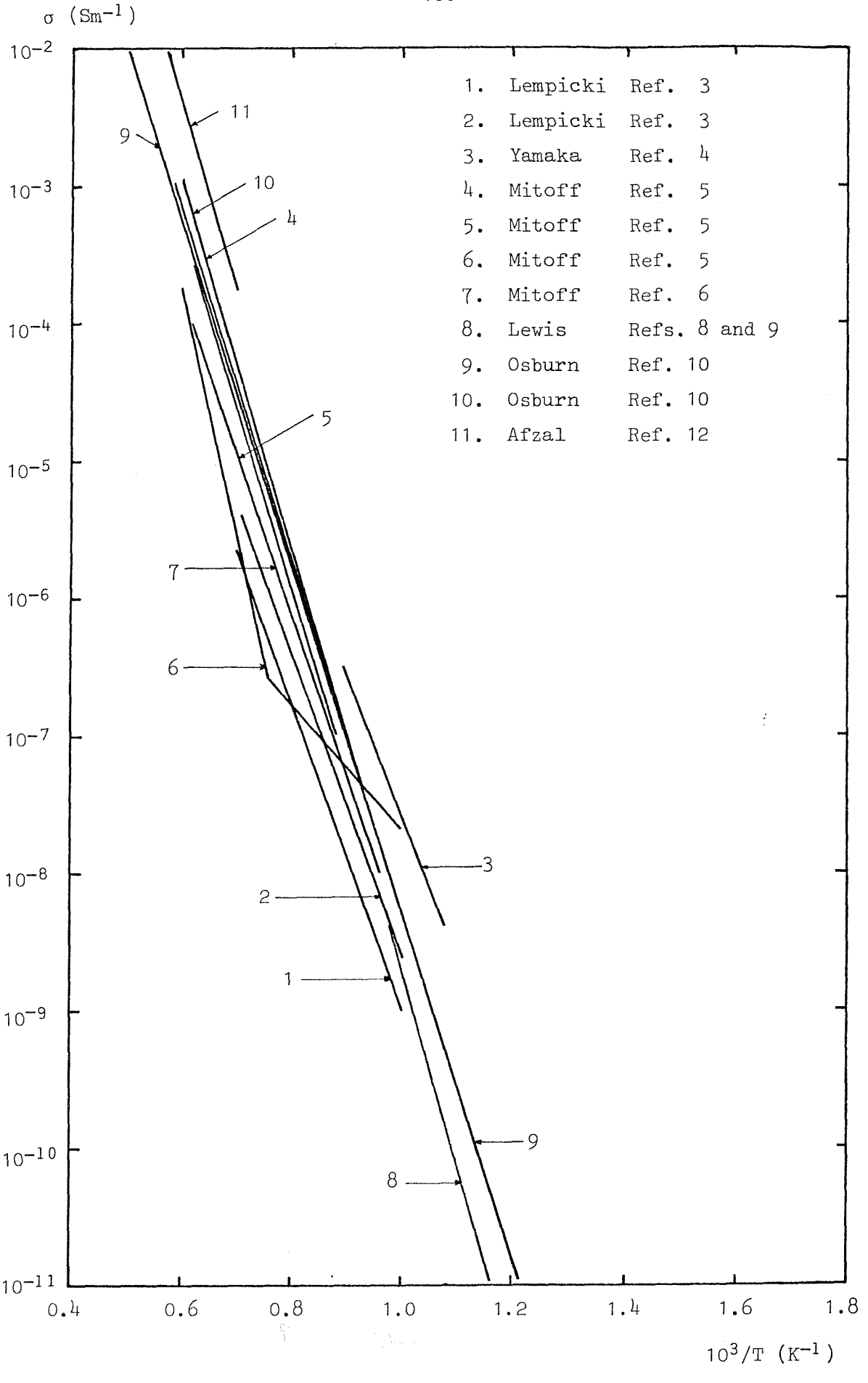

FIGURE 2 PREVIOUSLY PUBLISHED SINGLE CRYSTAL CONDUCTIVITY MEASUREMENTS

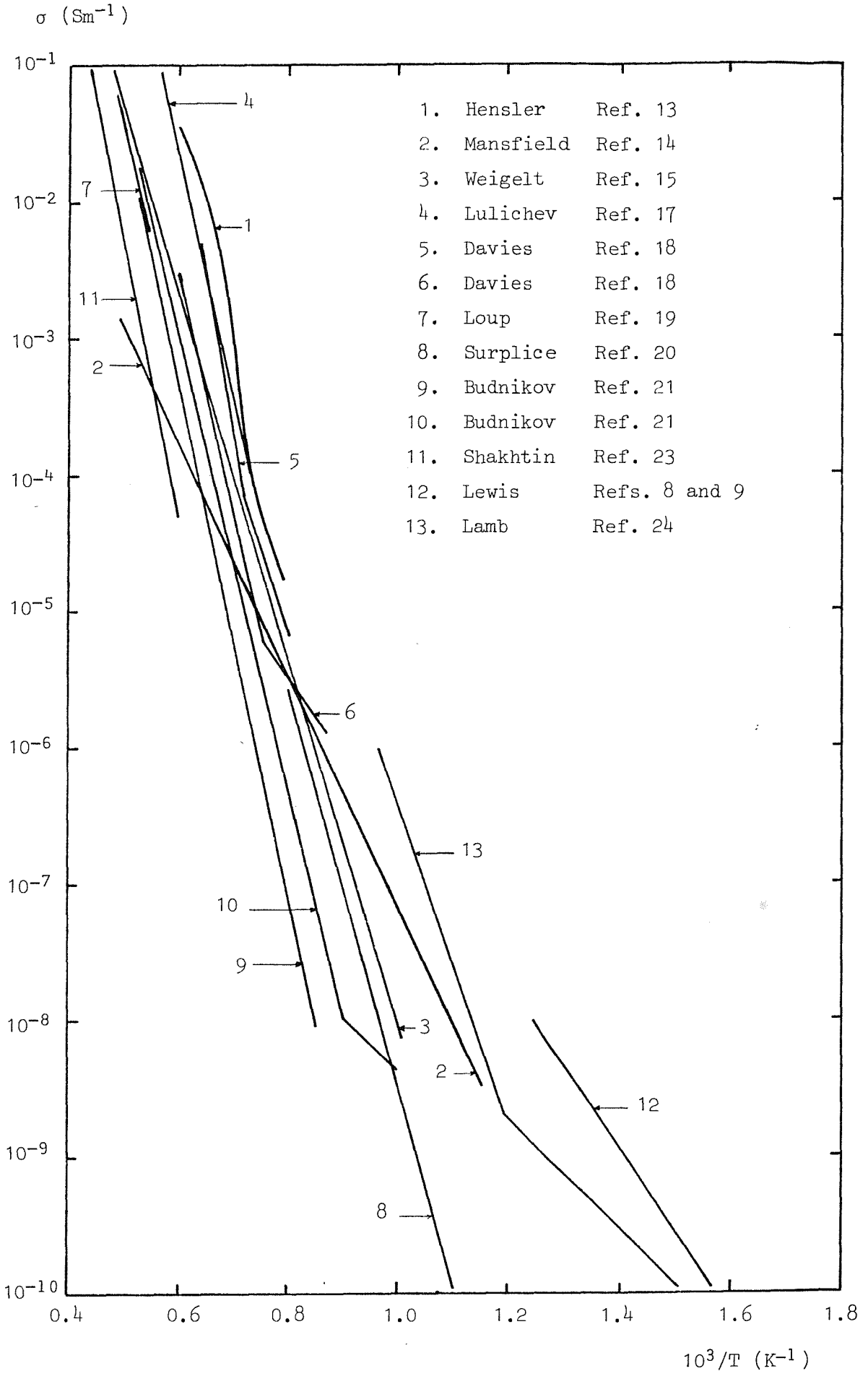

FIGURE 3 PREVIOUSLY PUBLISHED POLYCRYSTAL CONDUCTIVITY MEASUREMENTS

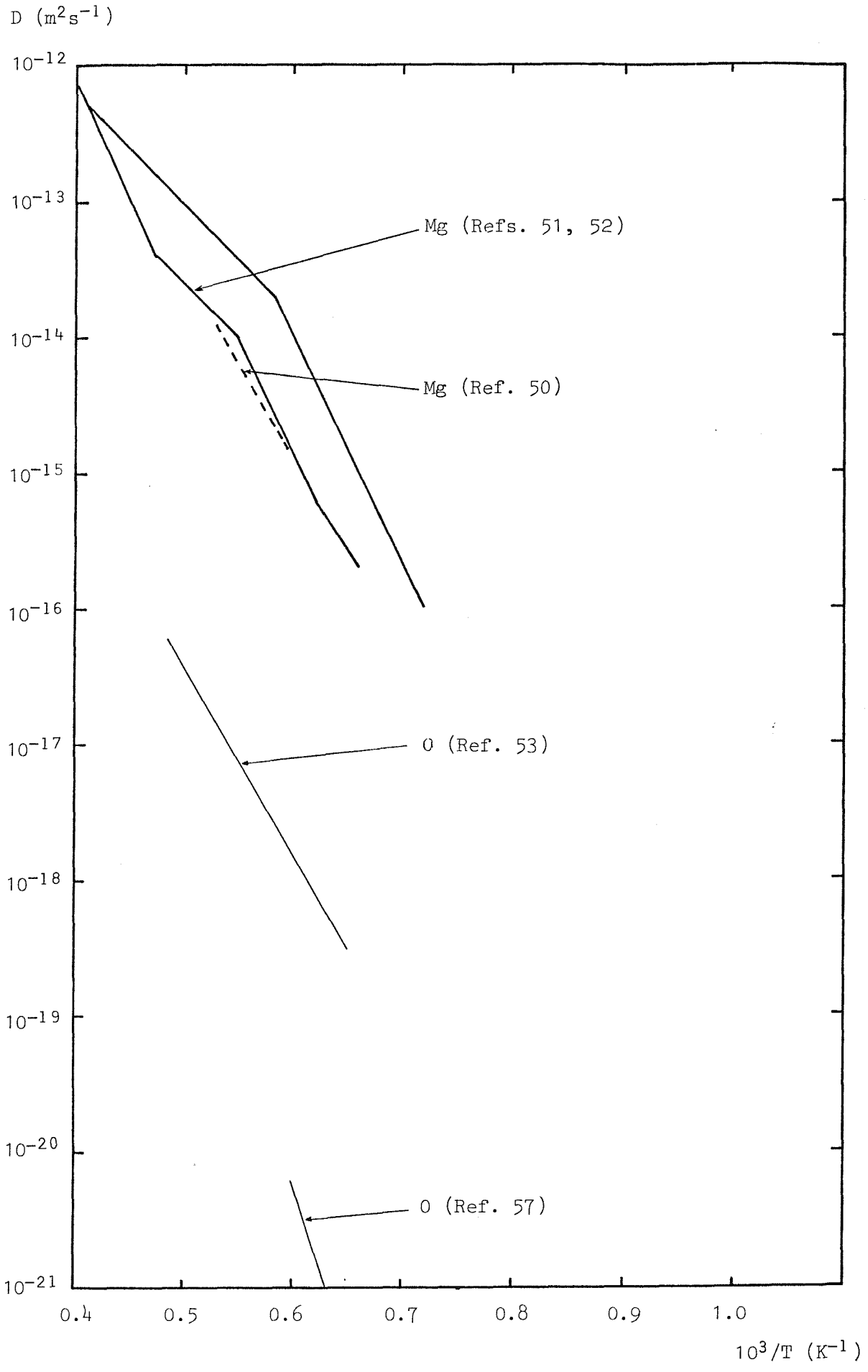

FIGURE 4 MAGNESIUM AND OXYGEN DIFFUSION COEFFICIENTS

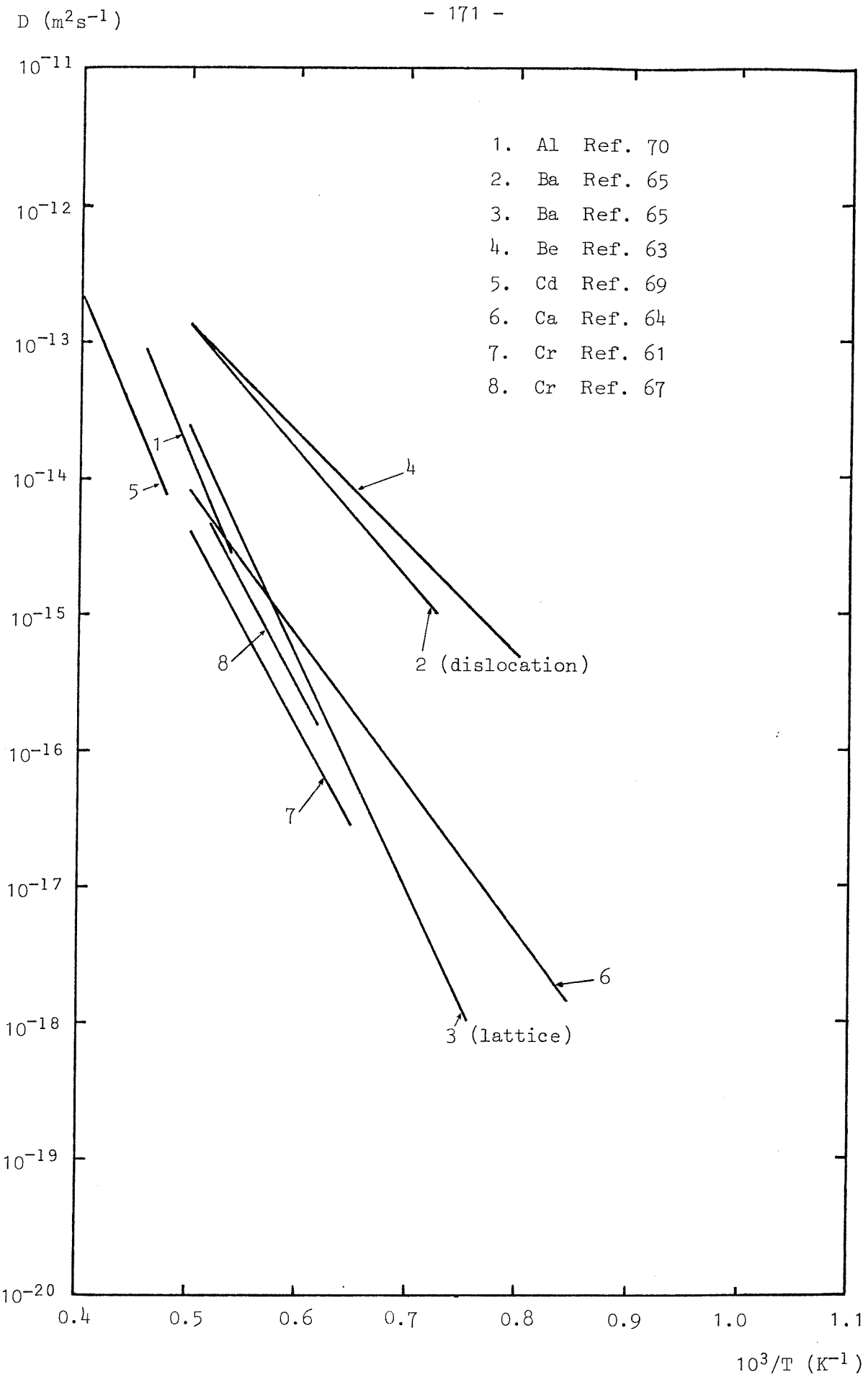

FIGURE 5(a) IMPURITY ION DIFFUSION COEFFICIENTS

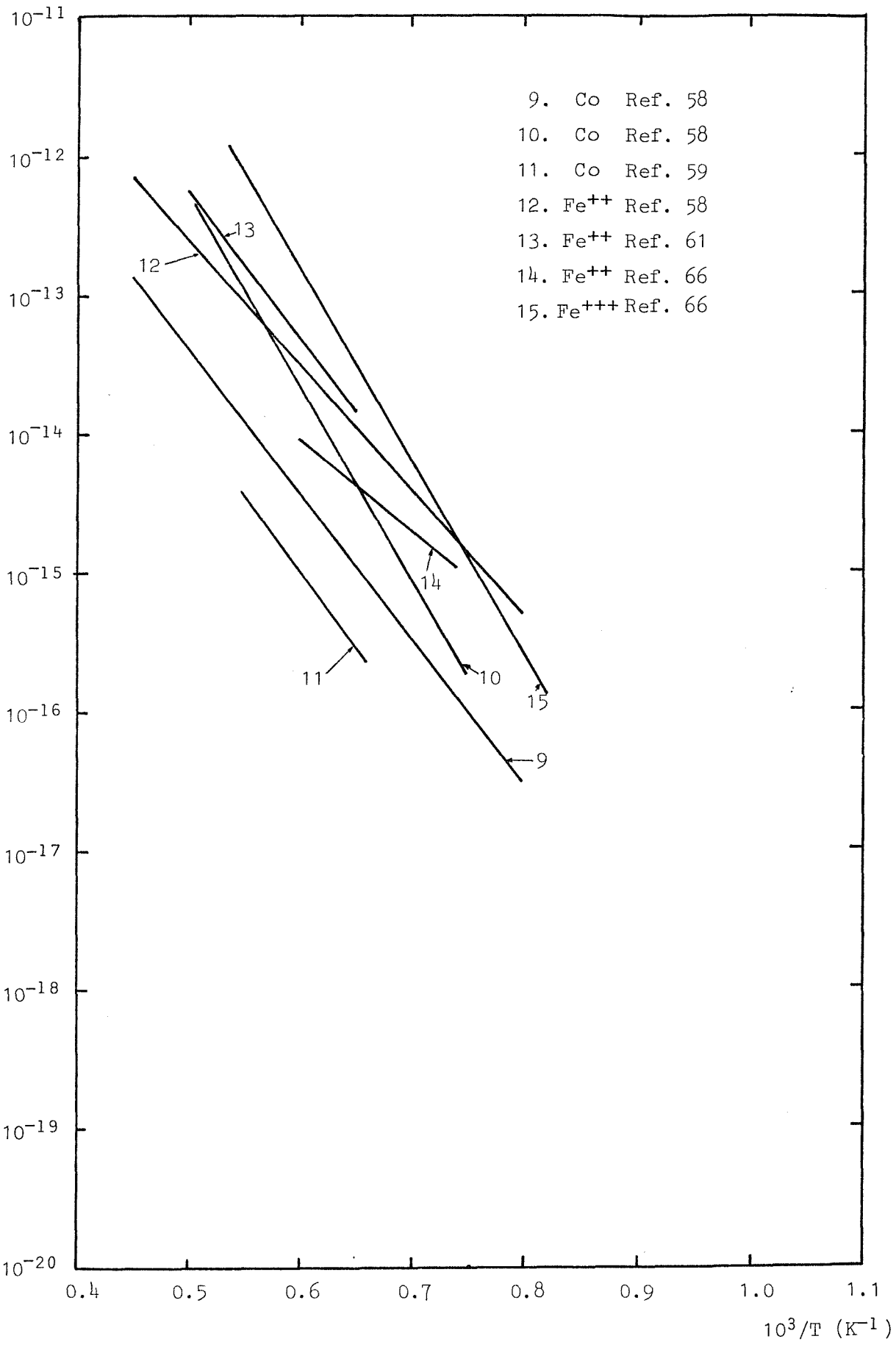

FIGURE 5(b) IMPURITY ION DIFFUSION COEFFICIENTS

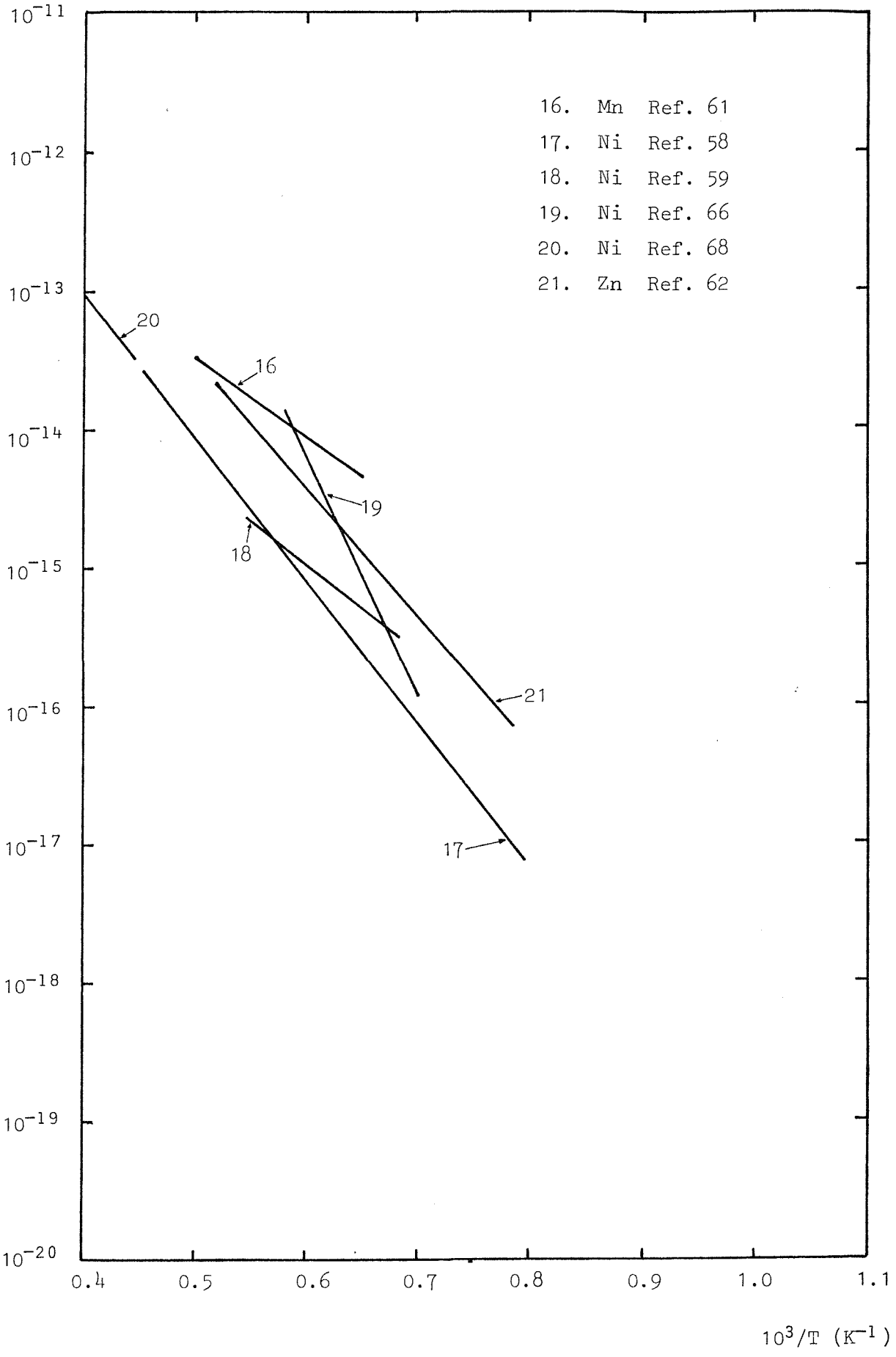

FIGURE 5(c) IMPURITY ION DIFFUSION COEFFICIENTS

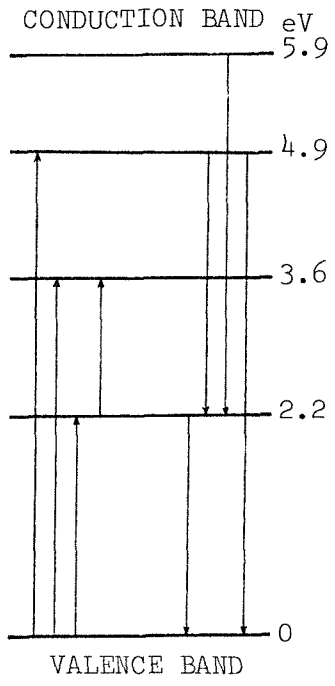

(a)
Saksena
Ref. 80

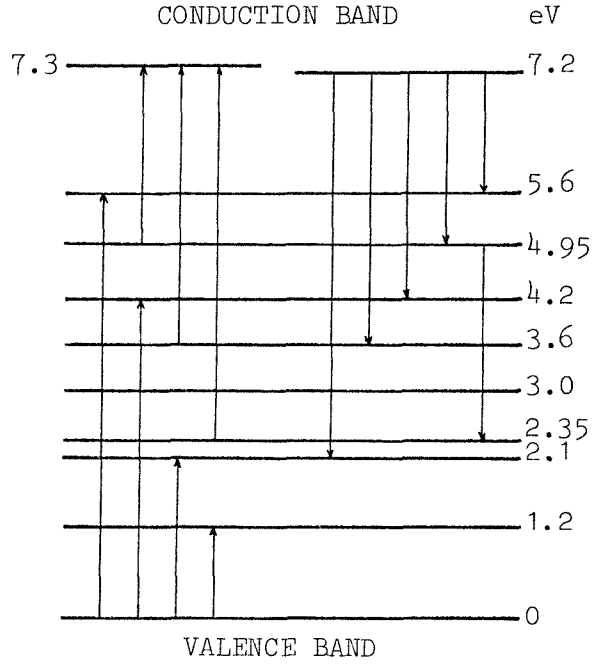

(b)
Clarke
Ref. 82

FIGURE 6 SOME PROPOSED ENERGY-BAND STRUCTURES

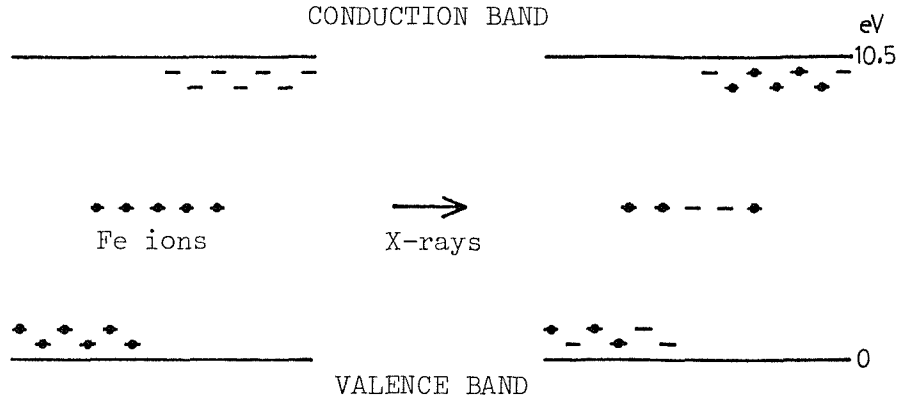

(c) Soshea Ref. 84

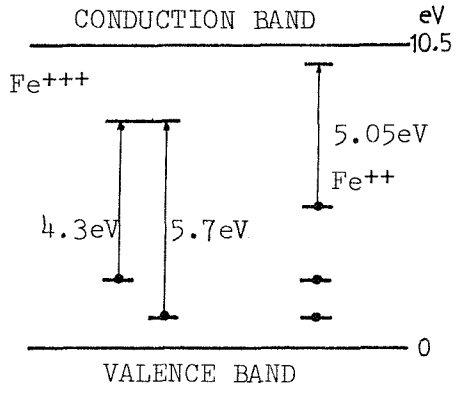

(d) Peria Ref. 72

FIGURE 6 SOME PROPOSED ENERGY BAND STRUCTURES (Cont.)

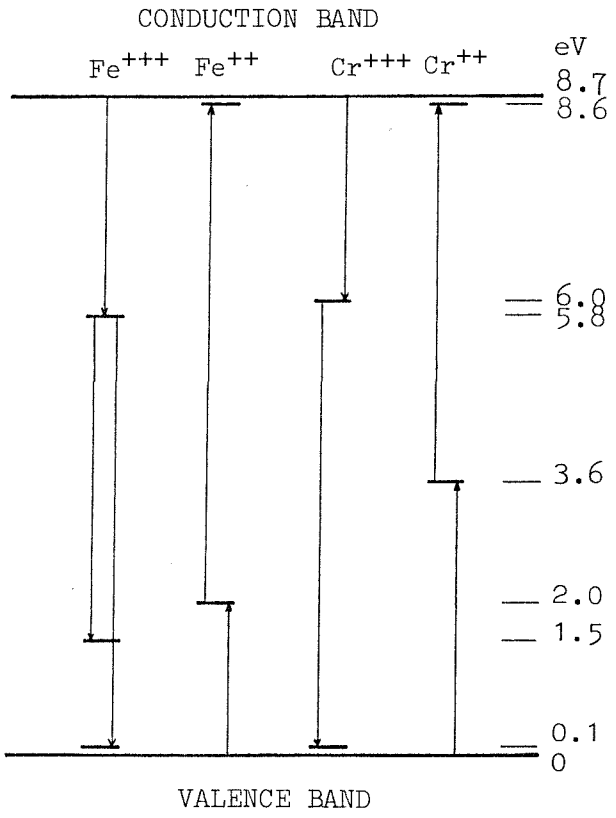

(e) Hansler Ref. 40

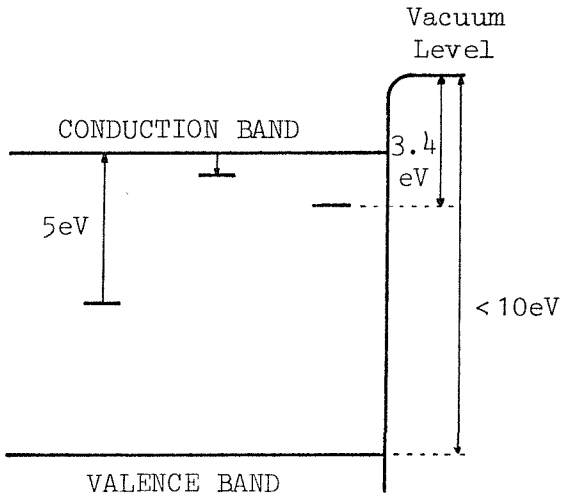

(f) Stevenson Refs. 93 and 94

FIGURE 6 SOME PROPOSED ENERGY LEVEL STRUCTURES (Cont.)

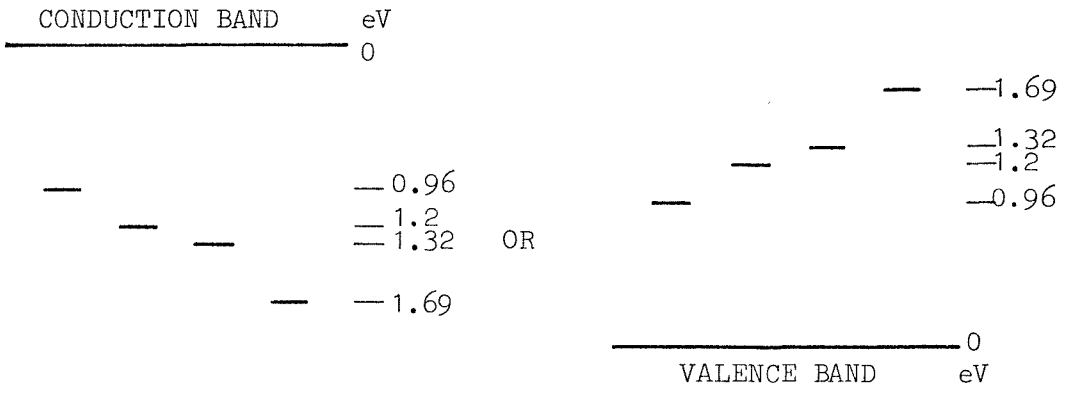

(g) Pomerantz Ref. 99

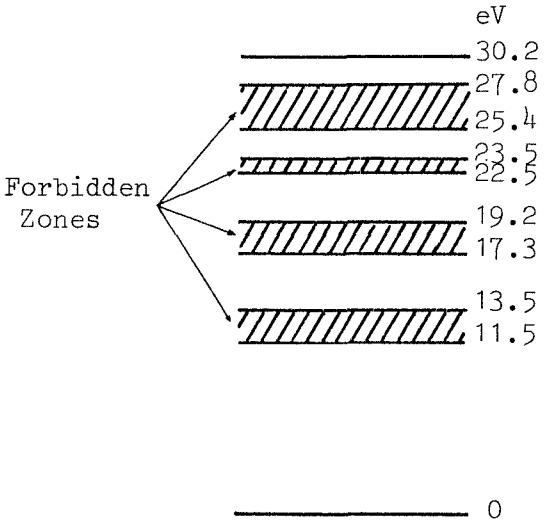

(h) Das Gupta Ref. 101

FIGURE 6 SOME PROPOSED ENERGY BAND STRUCTURES (Cont.)

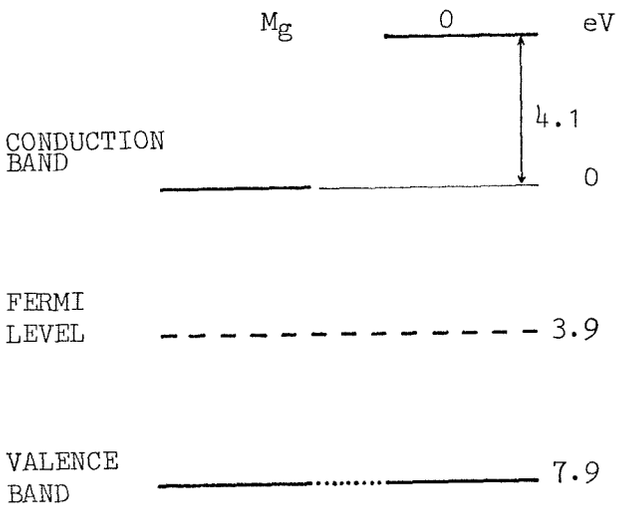

(i) Fomichev Ref. 102

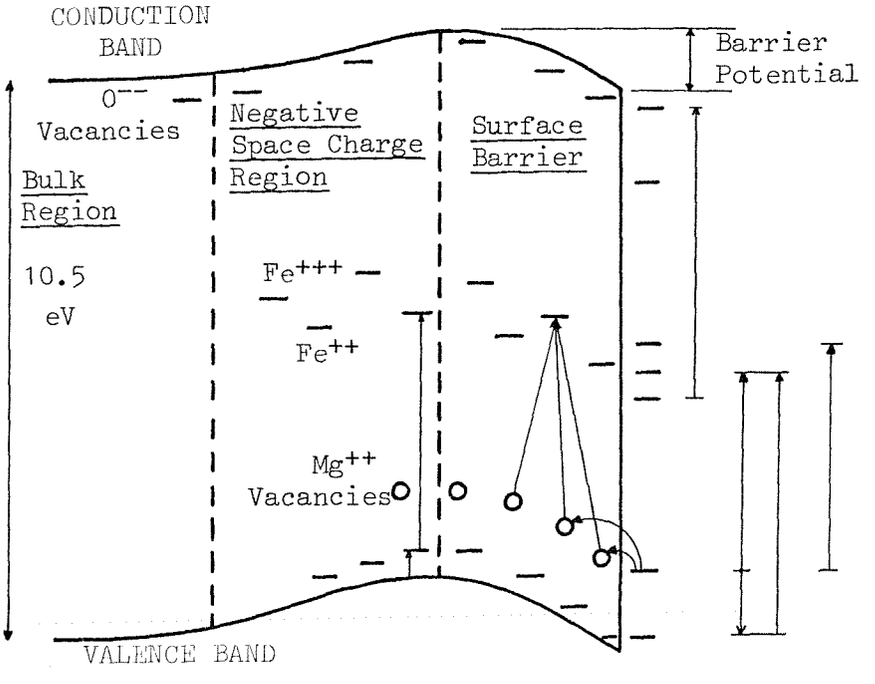

(j) Harkins Ref. 104

FIGURE 6 SOME PROPOSED ENERGY BAND STRUCTURES (Cont.)

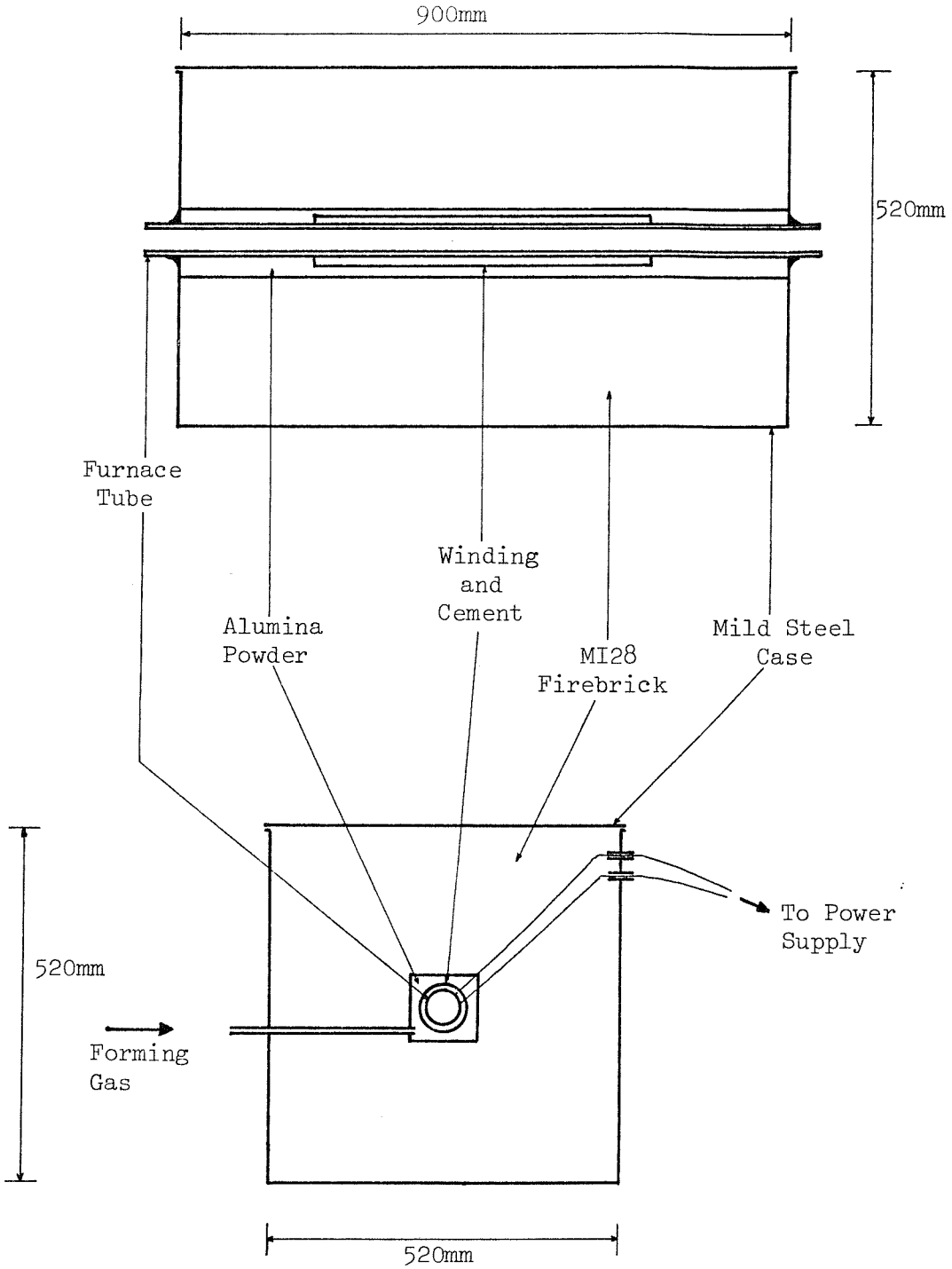

FIGURE 7 CROSS-SECTIONAL VIEWS OF THE FURNACE

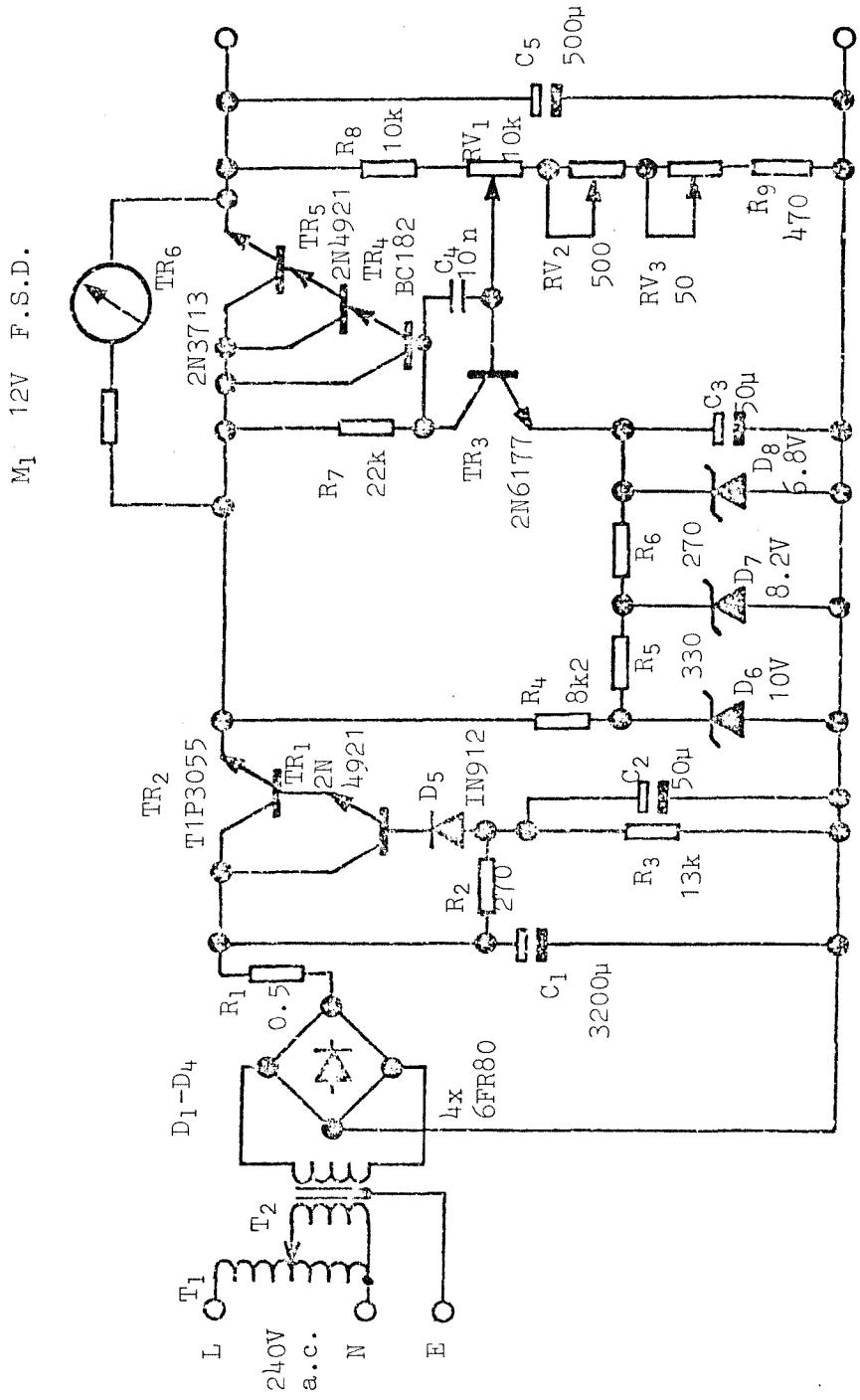

FIGURE 8 REGULATED D.C. POWER SUPPLY FOR FURNACE

NOT TO SCALE

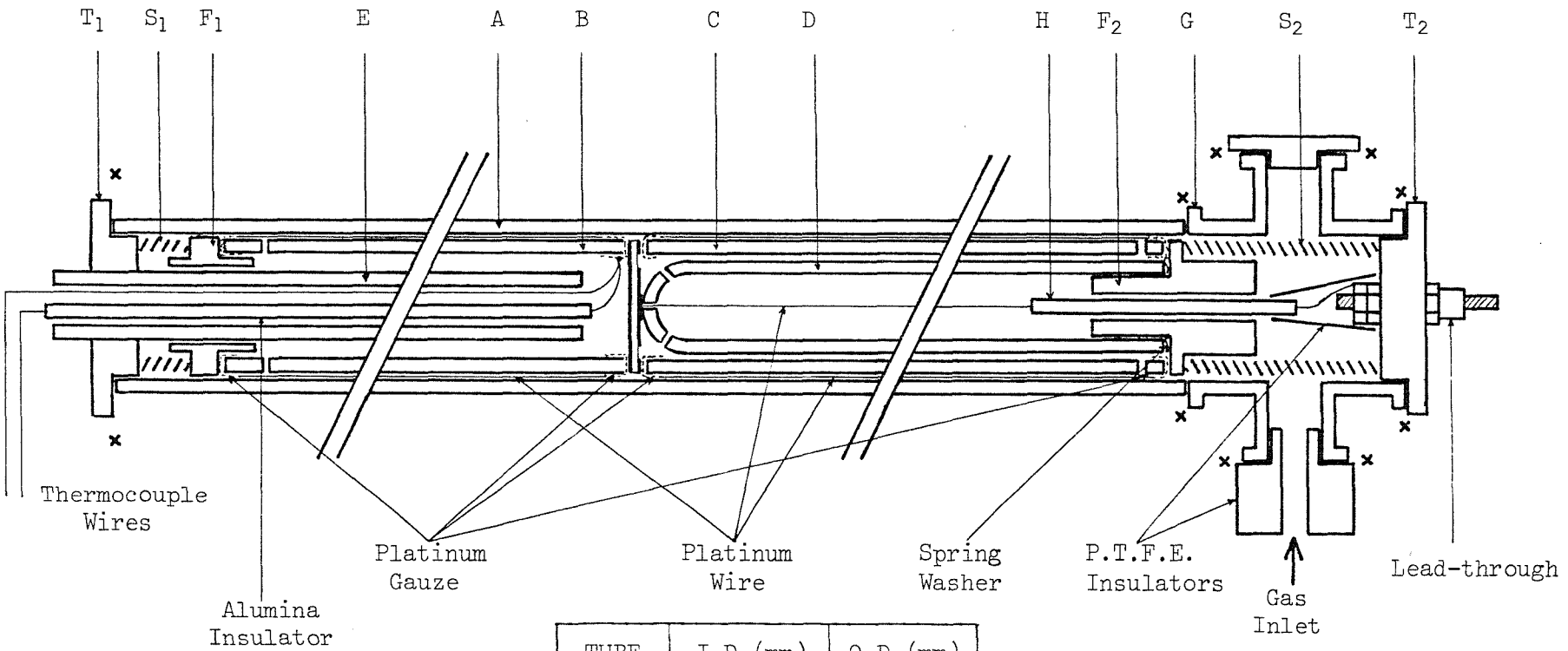

TUBE	I.D.(mm)	O.D.(mm)
A	22.5	28.5
B	15	21
C	15	21
D	8	12
E	6	10

FIGURE 9 THE WORK TUBE

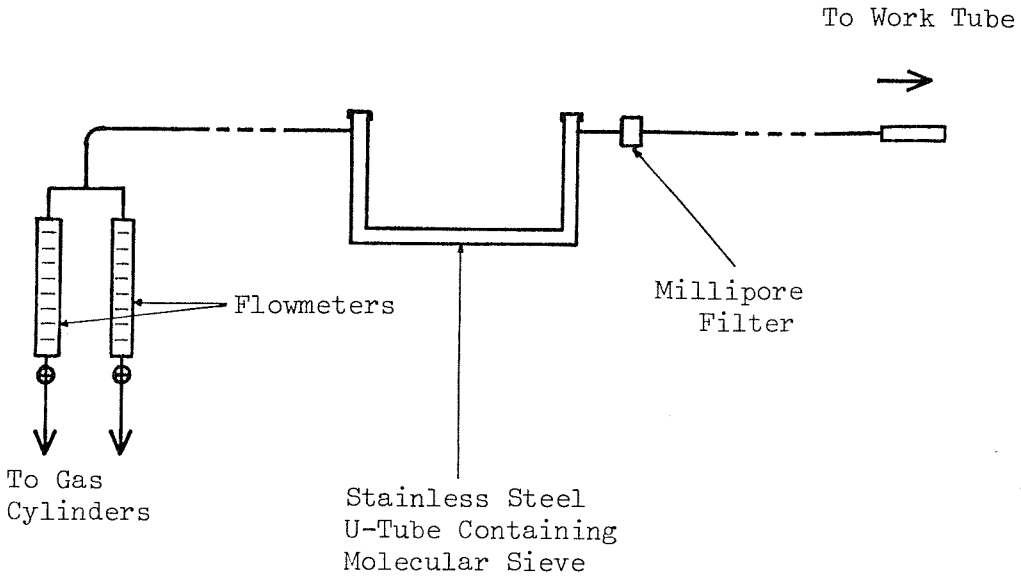

All Tubing Flexible Stainless Steel

FIGURE 10 THE SAMPLE AMBIENT GAS SYSTEM

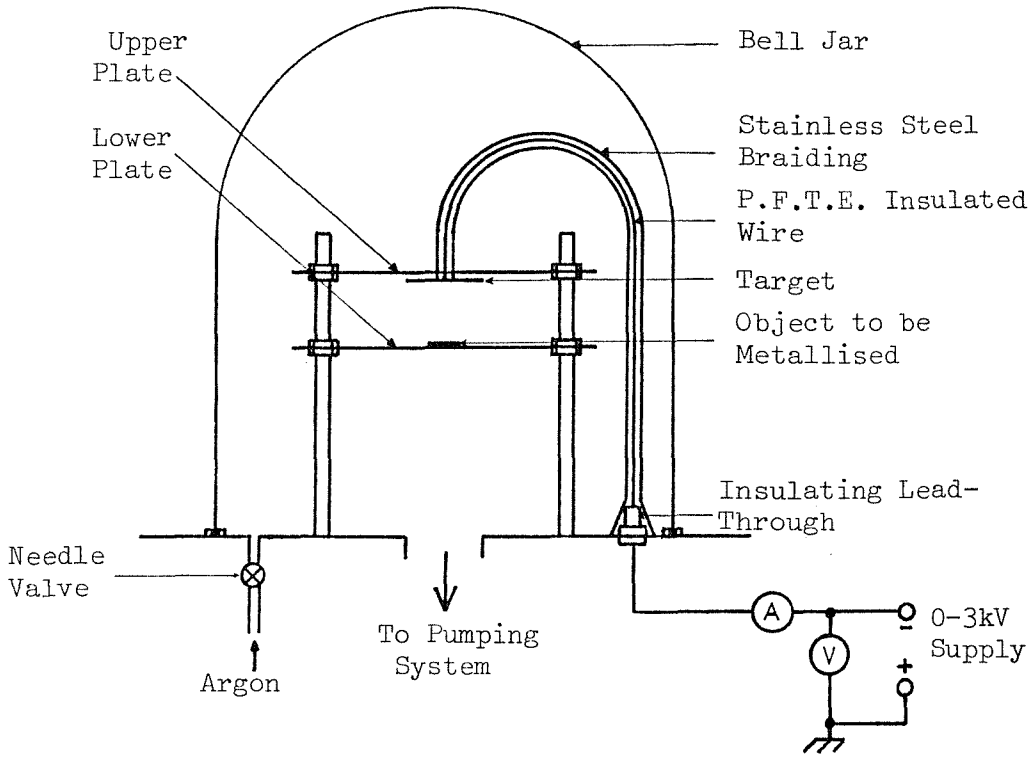

(a) General View

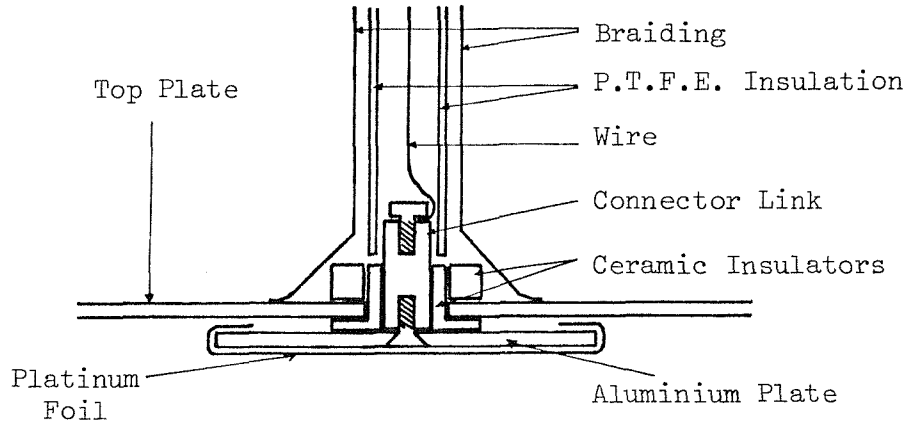

(b) The Target

FIGURE 11 THE SPUTTERING SYSTEM

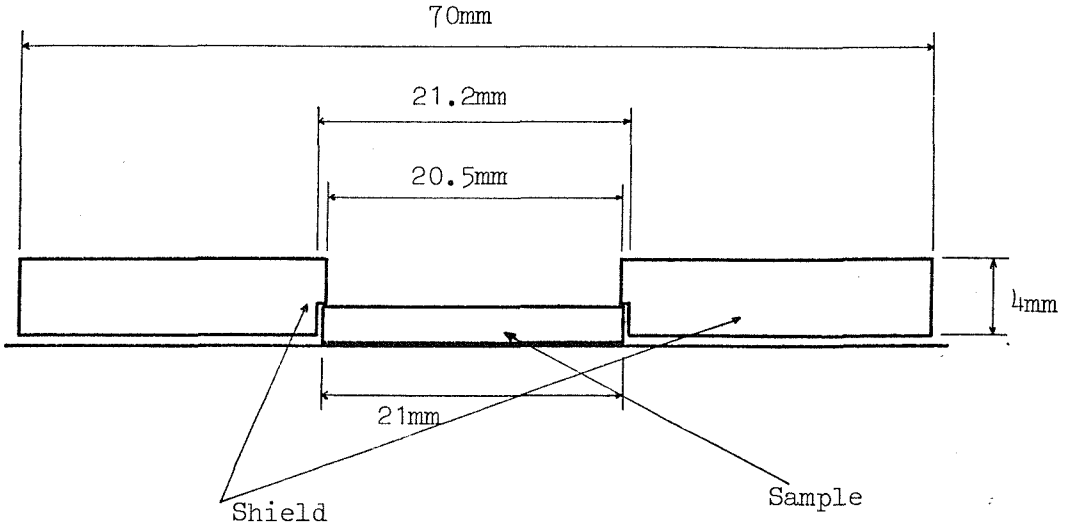

Cross-sectional View

FIGURE 12 THE SPUTTERING SHIELD

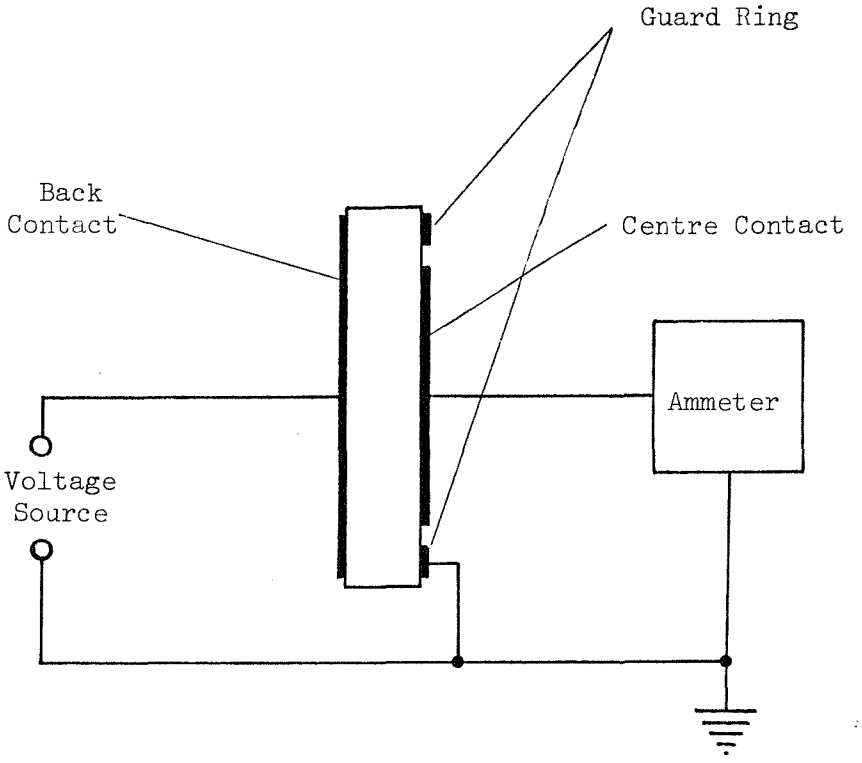

Cross Sectional View of Sample and Contacts

FIGURE 13 THE ELECTRICAL MEASUREMENT SYSTEM

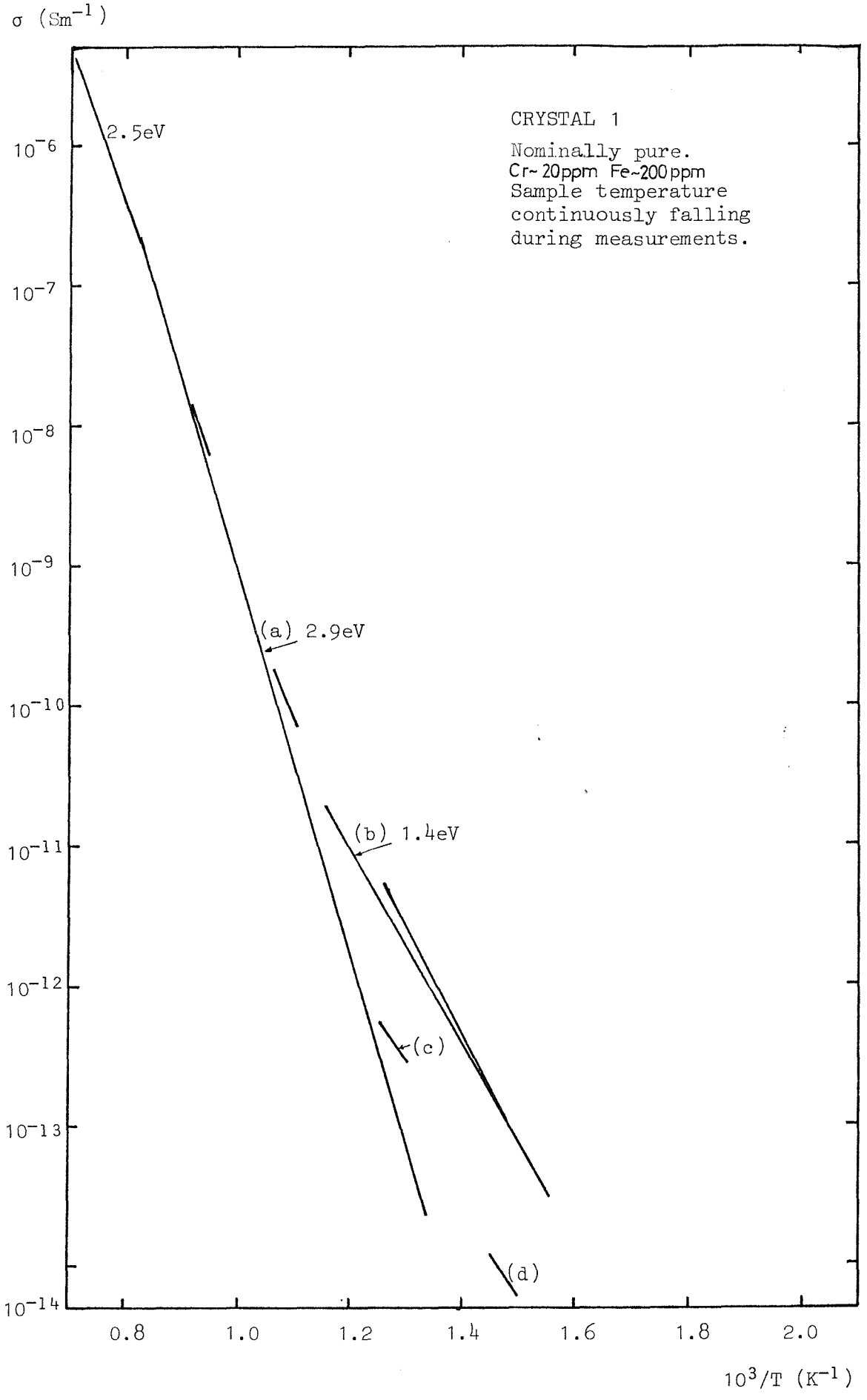

FIGURE 14 CONDUCTIVITY MEASUREMENTS OF NOMINALLY PURE SAMPLE

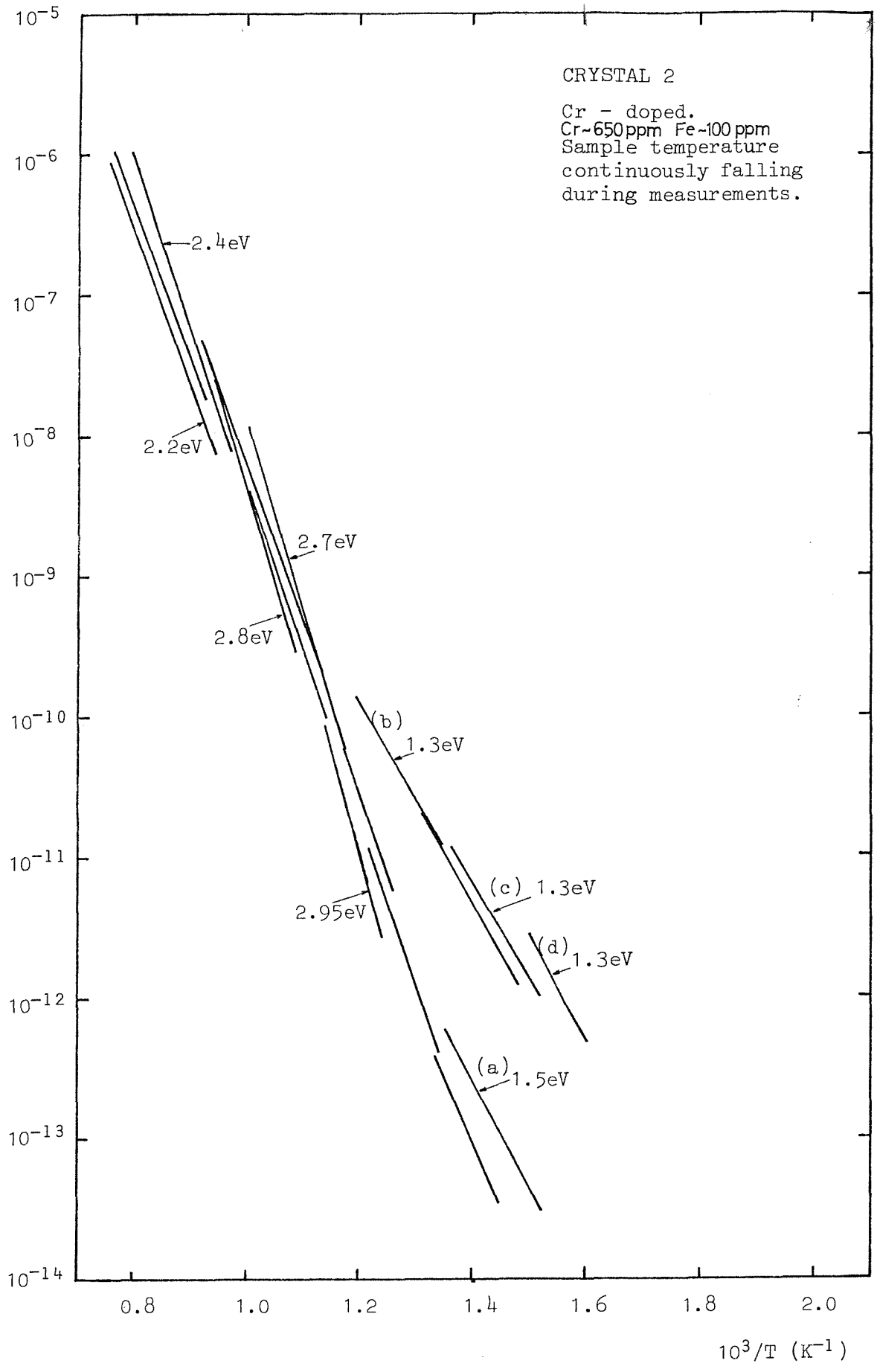

FIGURE 15 CONDUCTIVITY MEASUREMENTS OF CHROMIUM-DOPED SAMPLE

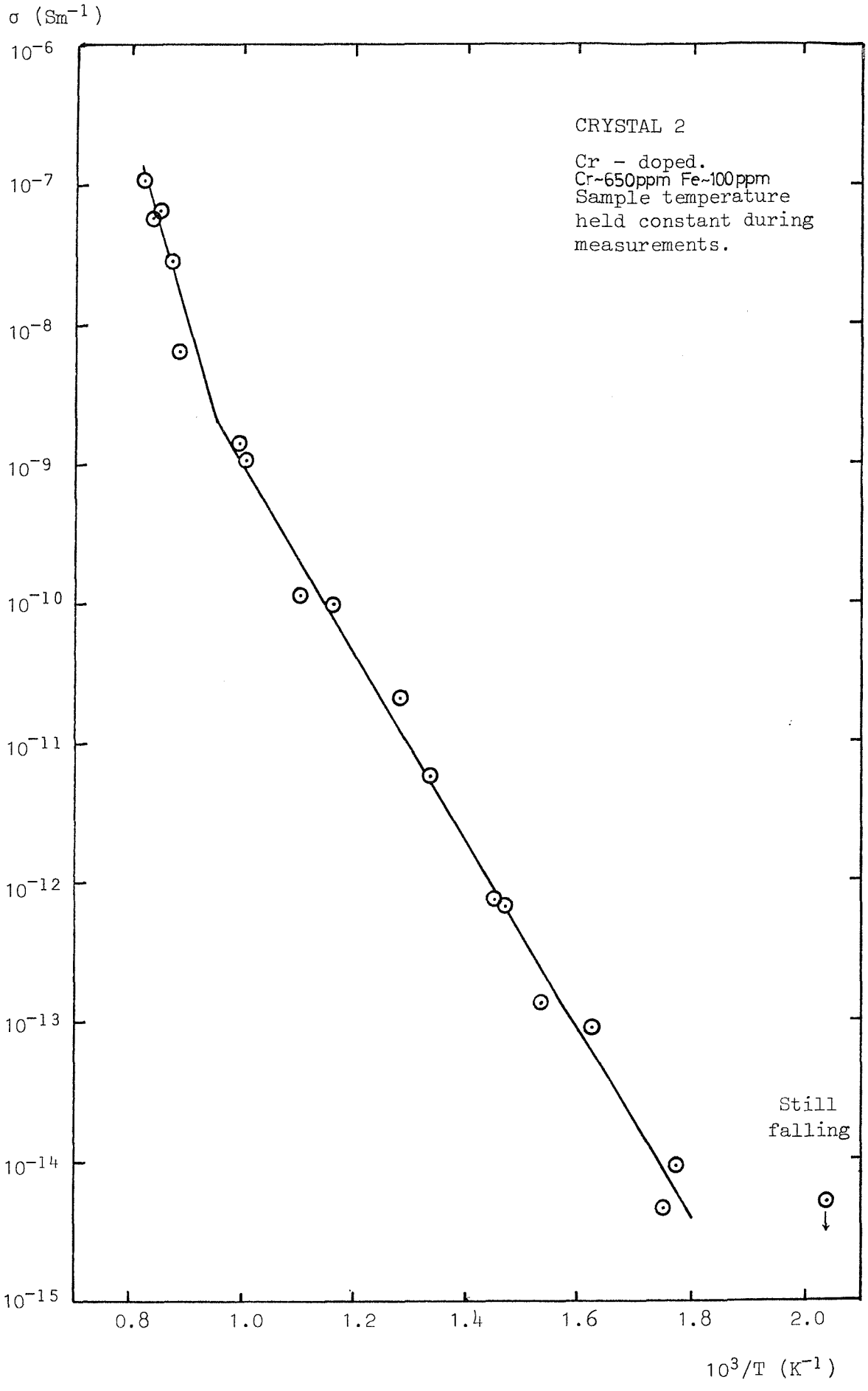

FIGURE 16 CONDUCTIVITY MEASUREMENTS OF CHROMIUM-DOPED SAMPLE

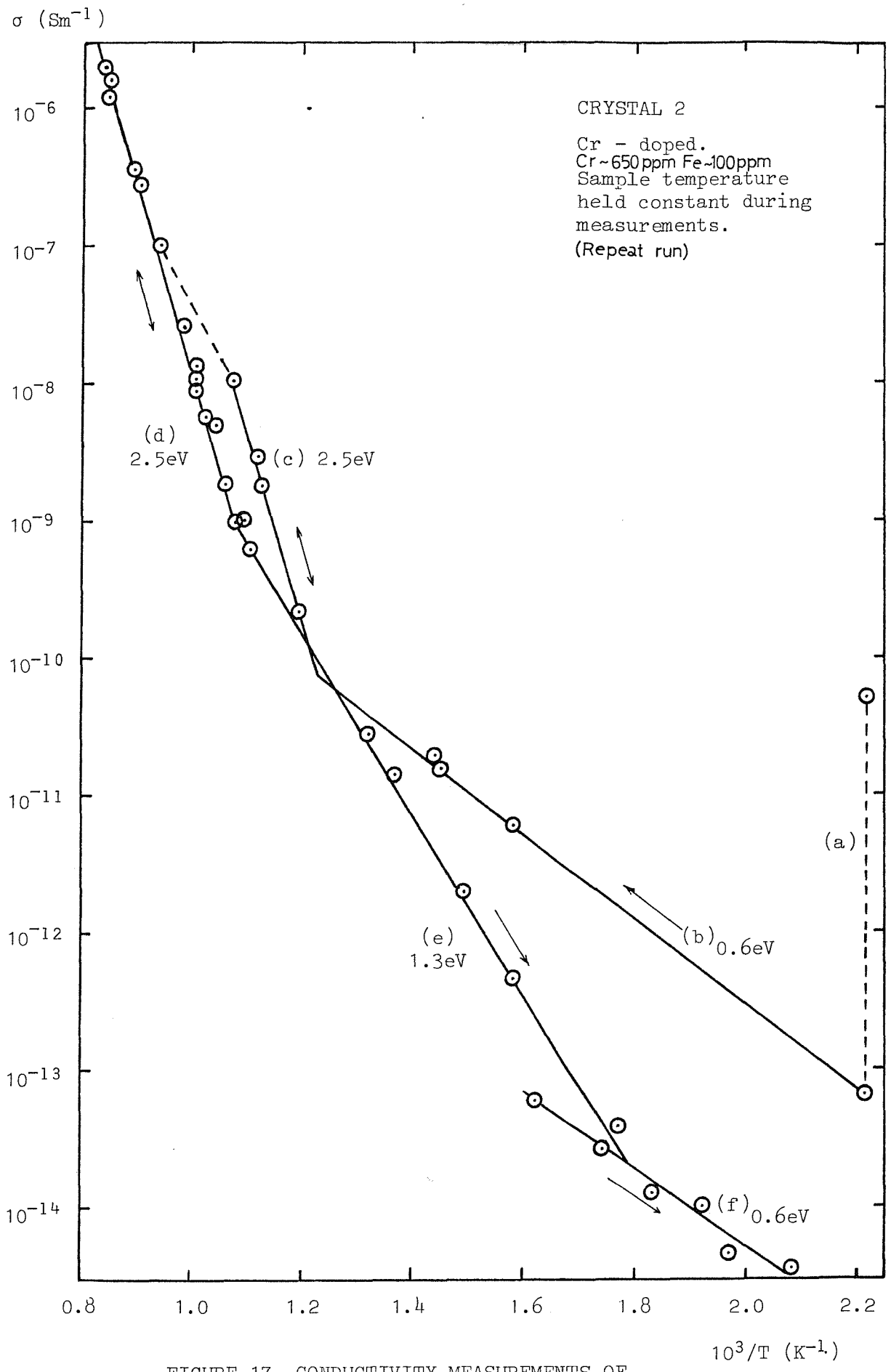

FIGURE 17 CONDUCTIVITY MEASUREMENTS OF CHROMIUM-DOPED SAMPLE

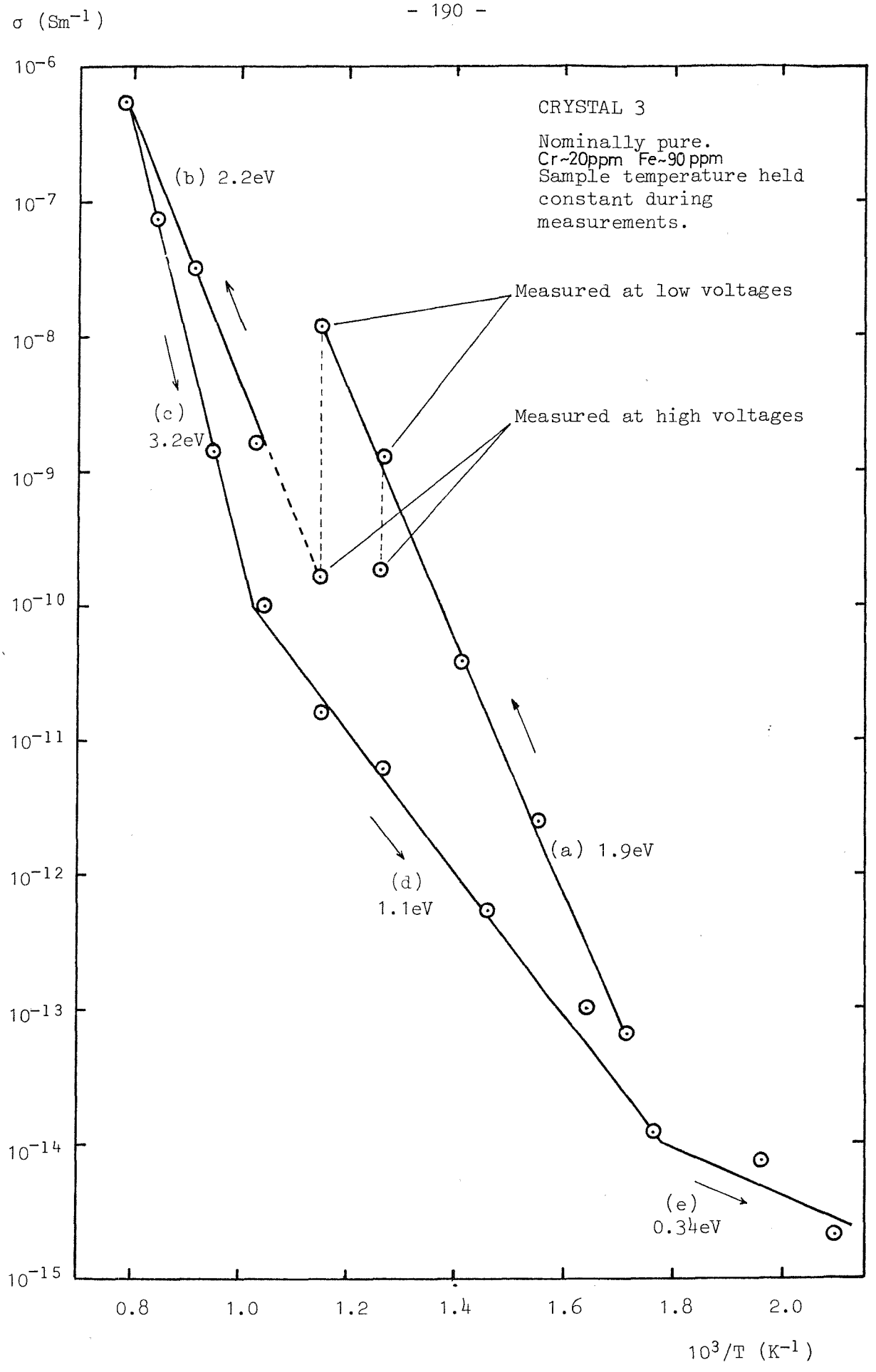

FIGURE 18 CONDUCTIVITY MEASUREMENTS OF NOMINALLY PURE SAMPLE

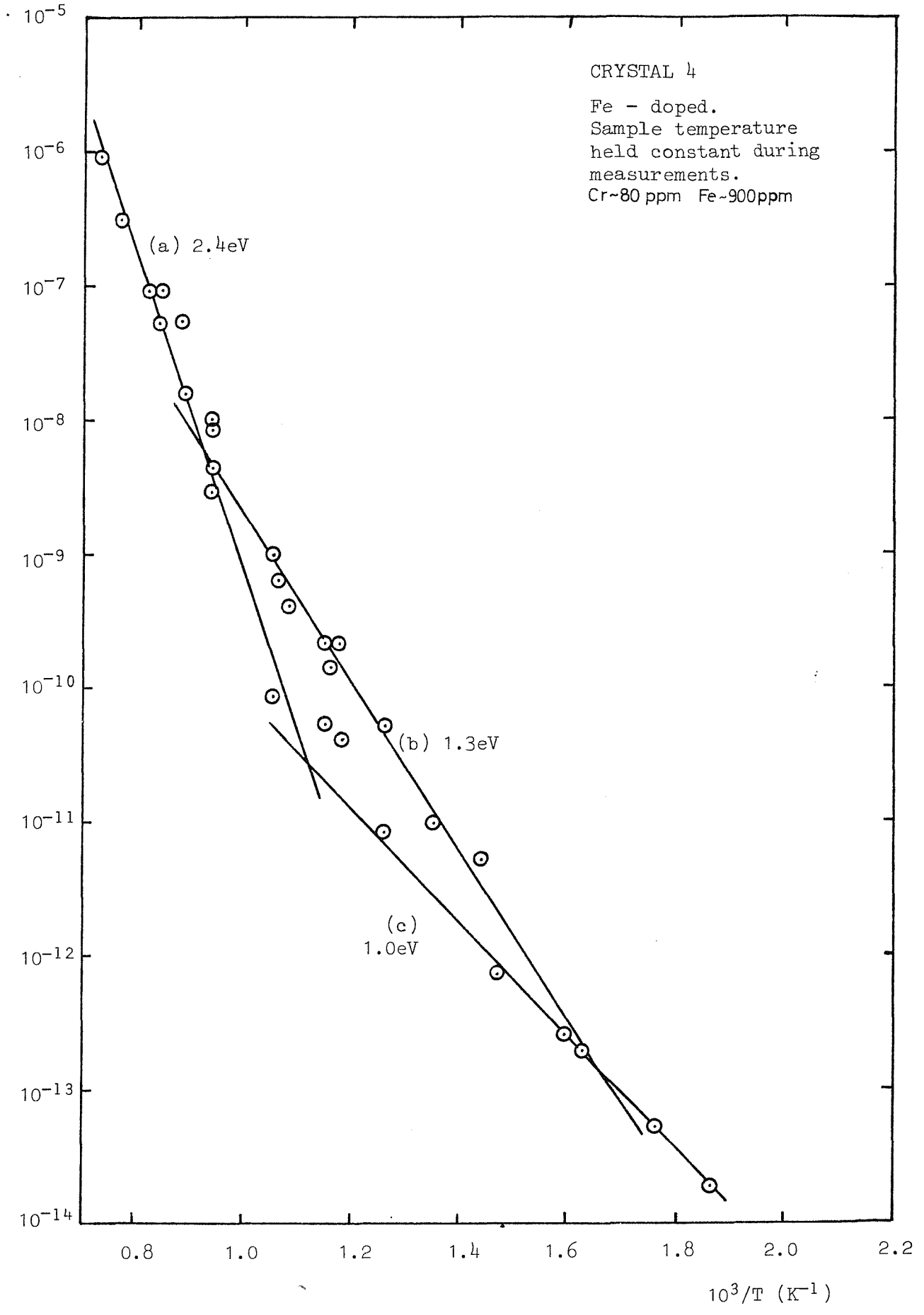

FIGURE 19 CONDUCTIVITY MEASUREMENTS OF IRON-DOPED SAMPLE

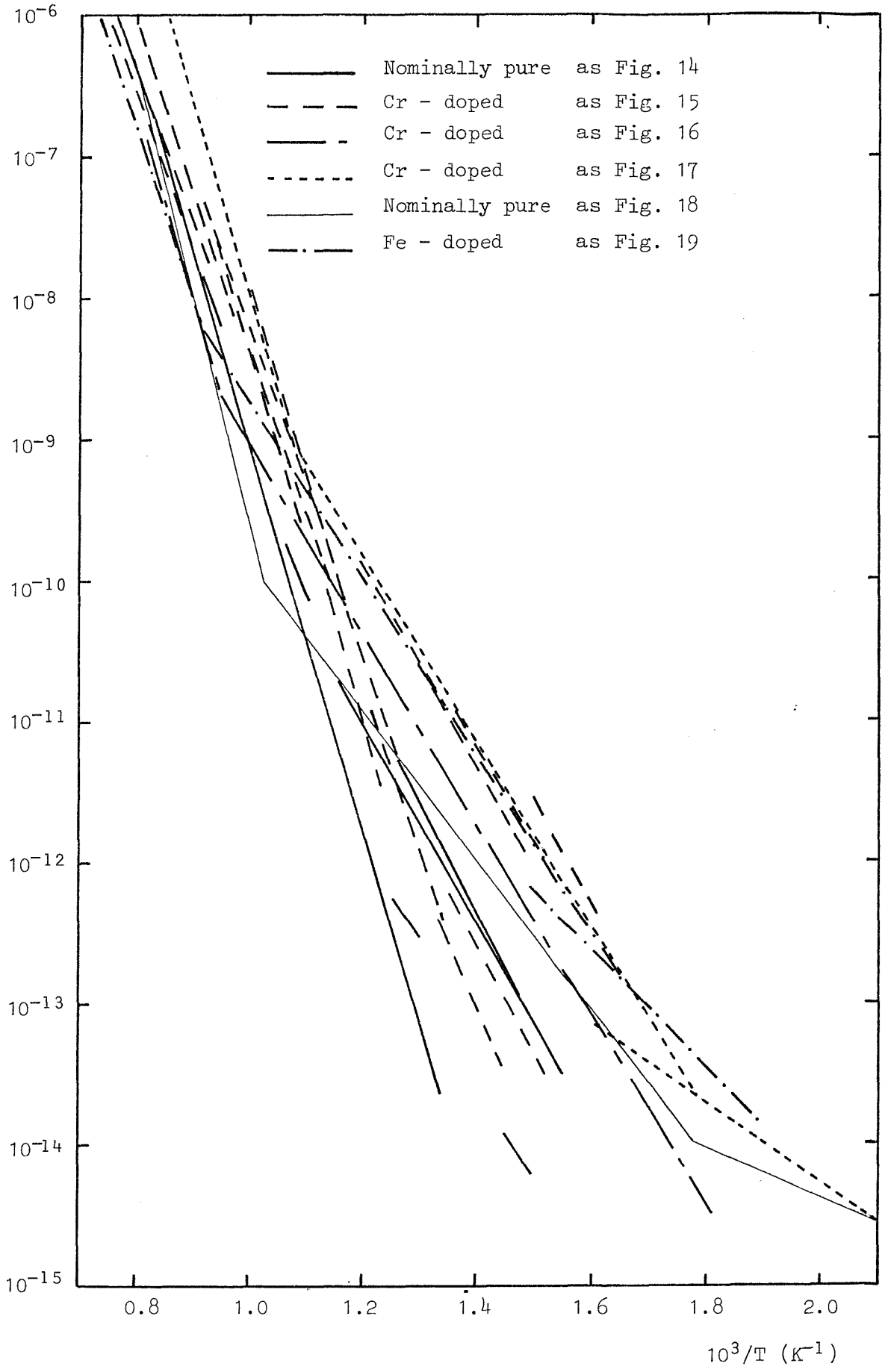

FIGURE 20 COLLECTED CONDUCTIVITY MEASUREMENTS

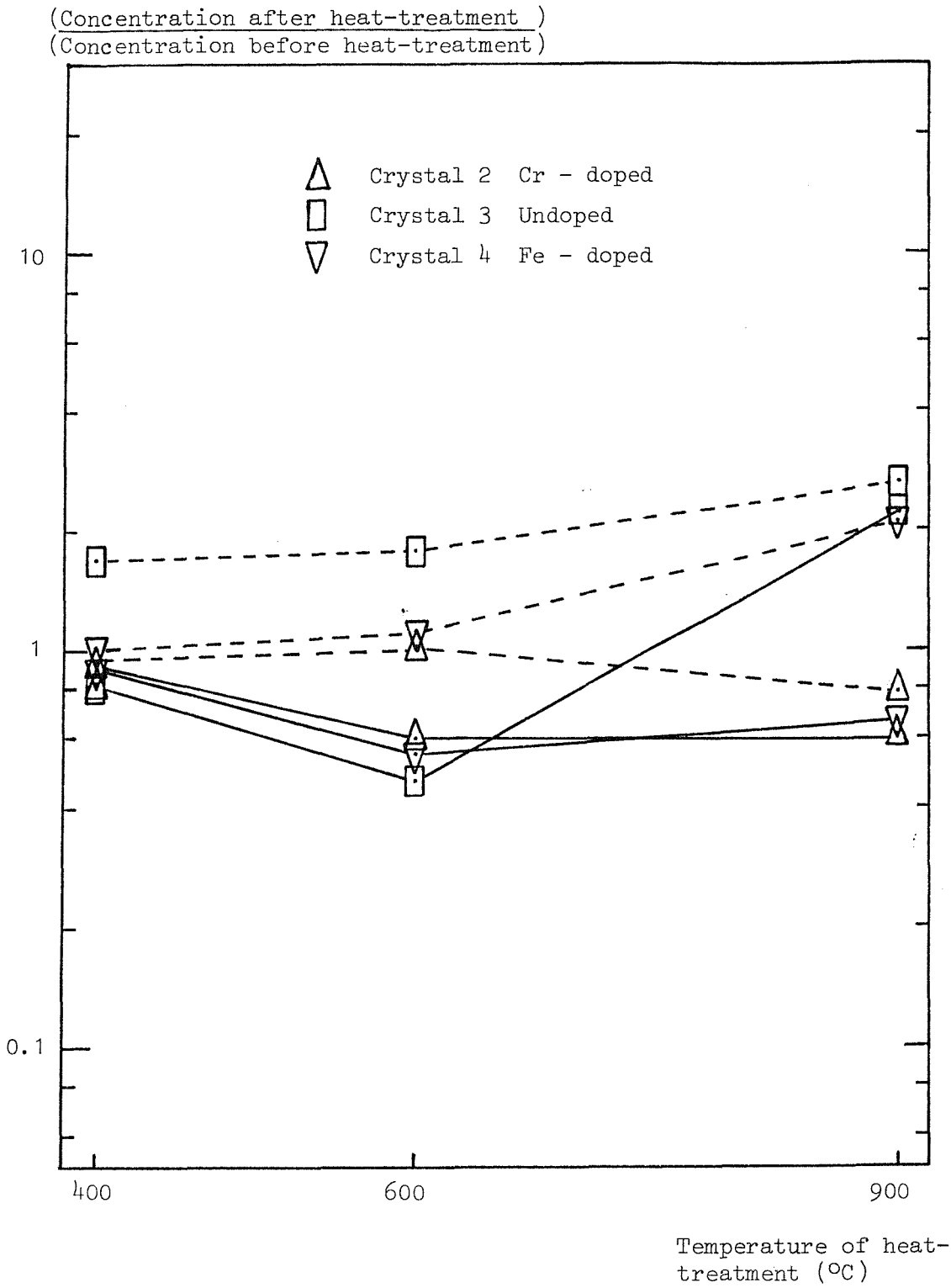

Full line: Crystals heated in oxygen

Broken line: Crystals heated in argon

FIGURE 21 EFFECT OF HEAT-TREATMENTS ON Fe^{+++} CONCENTRATION, AS MEASURED USING E.S.R. TECHNIQUES

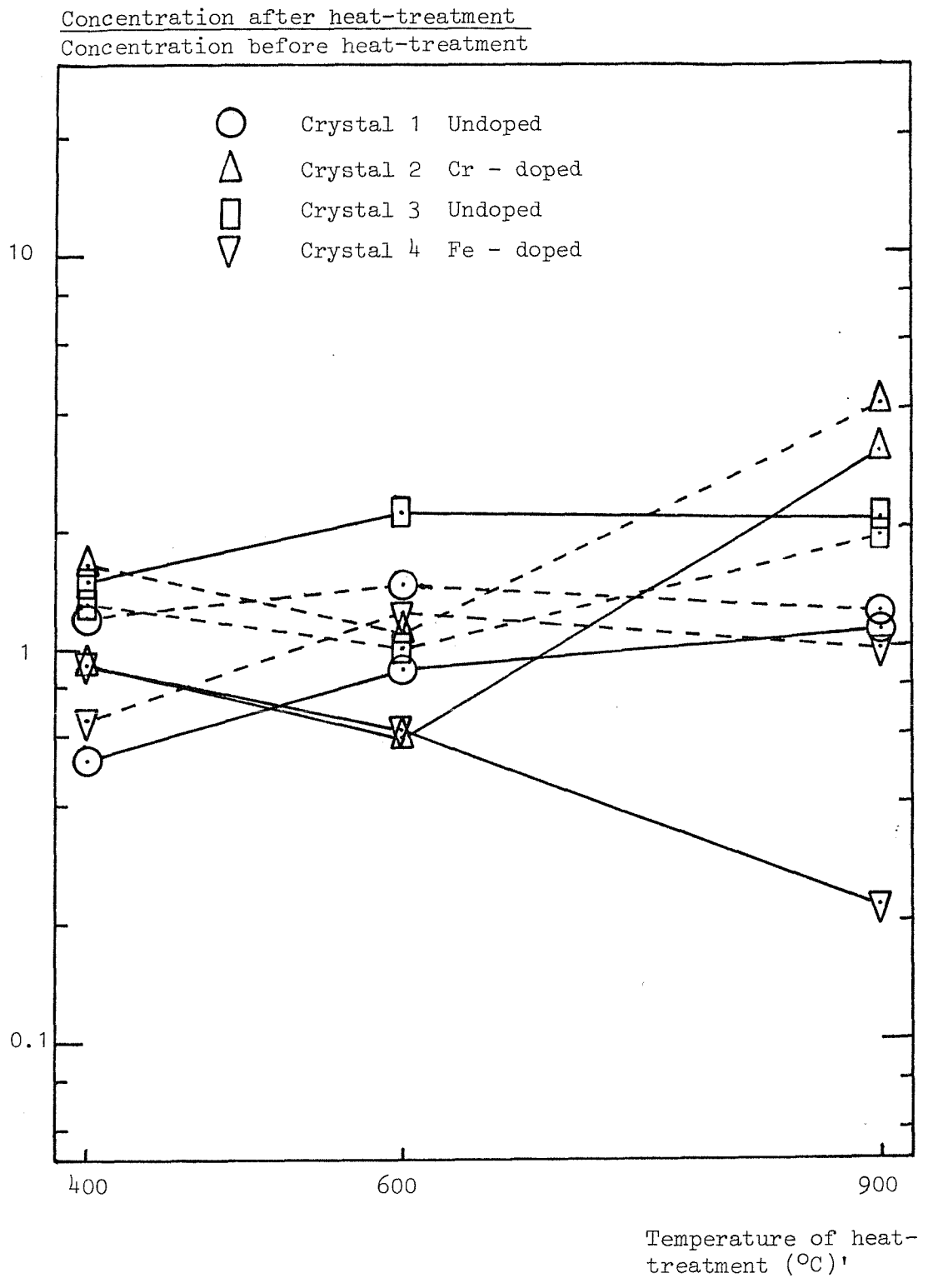

Full line: Crystals heated in oxygen

Broken line: Crystals heated in argon

FIGURE 22 EFFECT OF HEAT-TREATMENTS ON Cr^{+++} CONCENTRATION, AS MEASURED USING E.S.R. TECHNIQUES

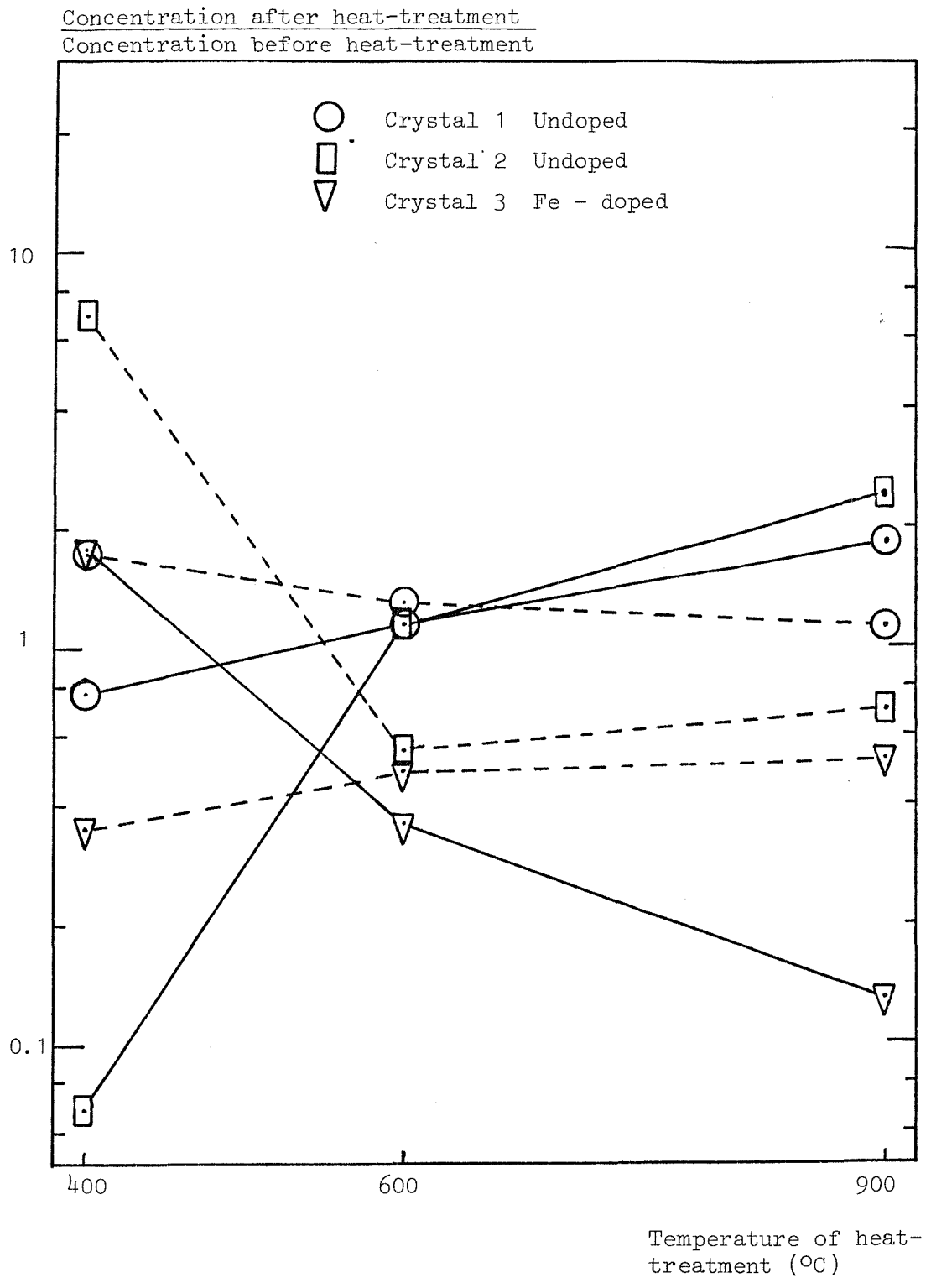

Full line: Crystals heated in oxygen

Broken line: Crystals heated in argon

FIGURE 23 EFFECT OF HEAT-TREATMENTS ON Mn^{++} CONCENTRATION, AS MEASURED USING E.S.R. TECHNIQUES

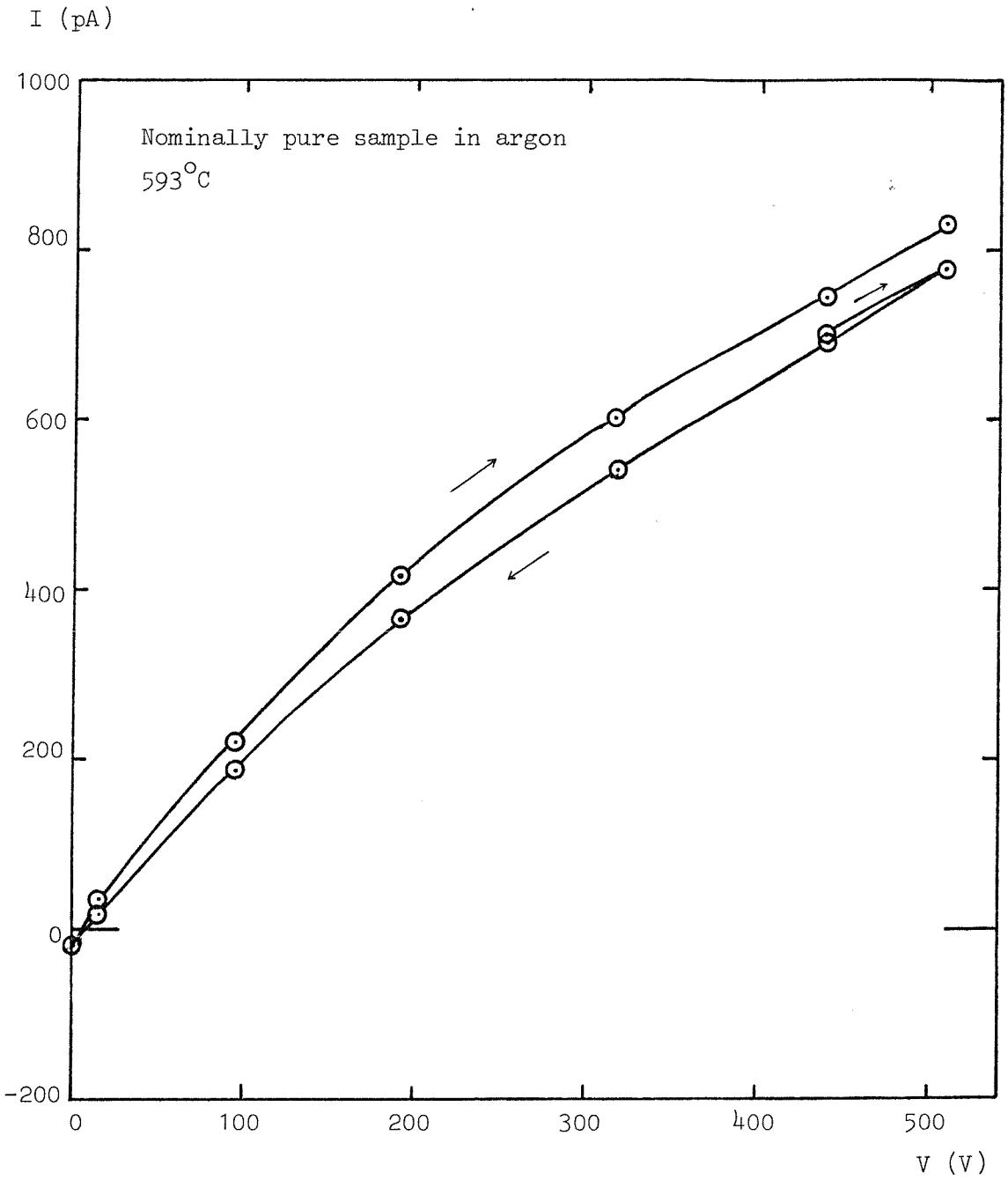

FIGURE 24 EXAMPLE OF VOLTAGE-CURRENT CHARACTERISTIC

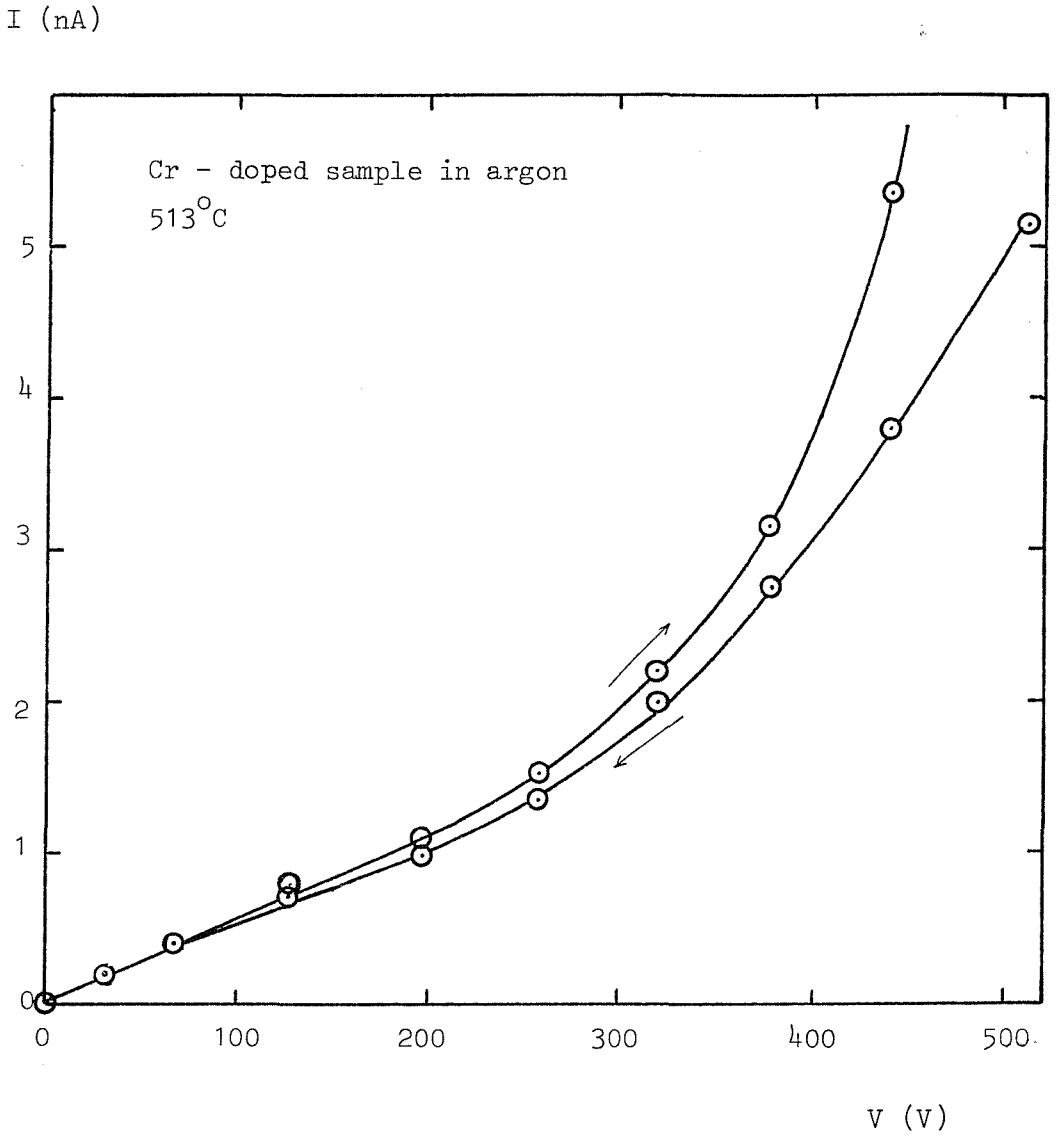

FIGURE 25 EXAMPLE OF VOLTAGE-CURRENT CHARACTERISTIC

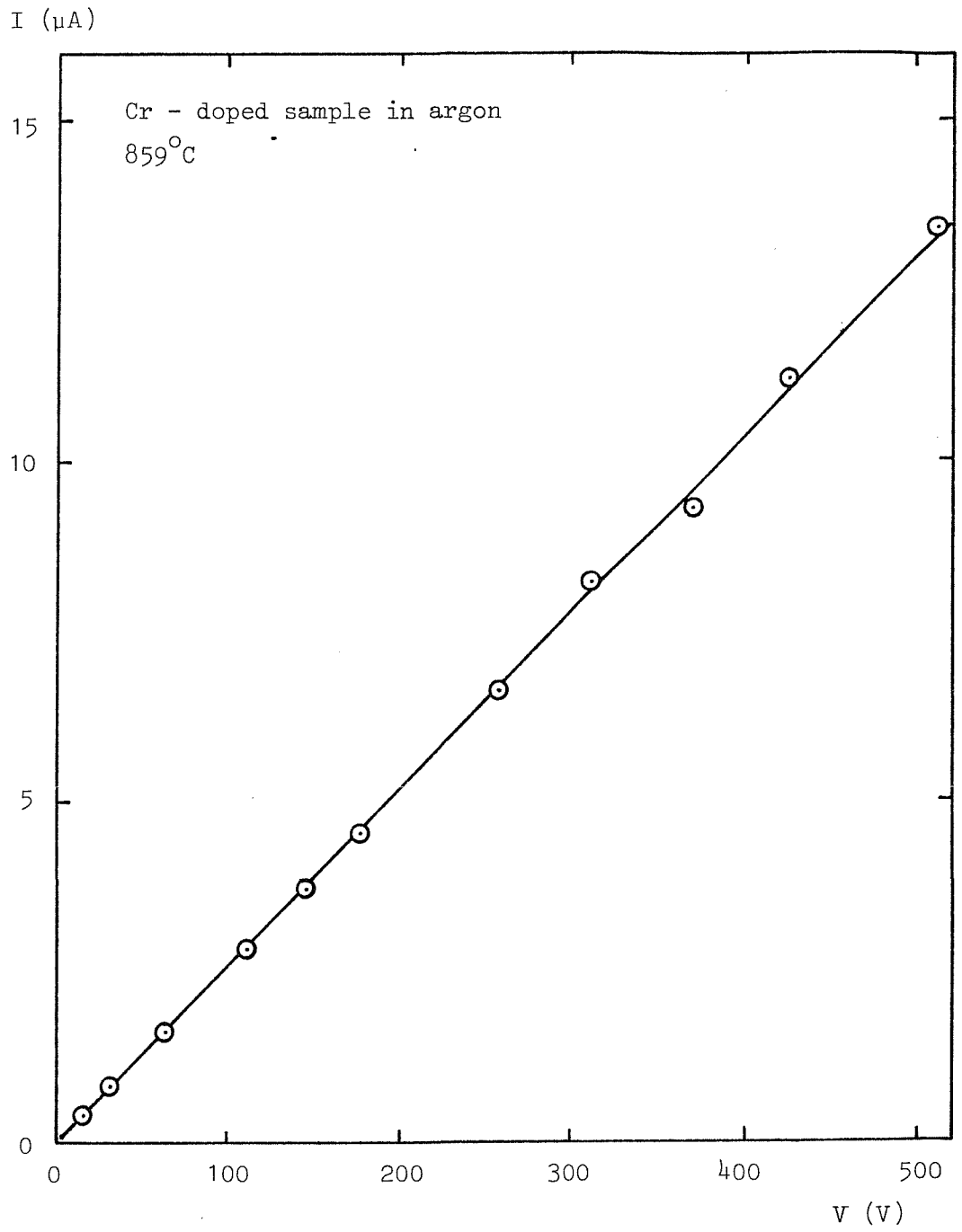

FIGURE 26 EXAMPLE OF VOLTAGE-CURRENT CHARACTERISTIC

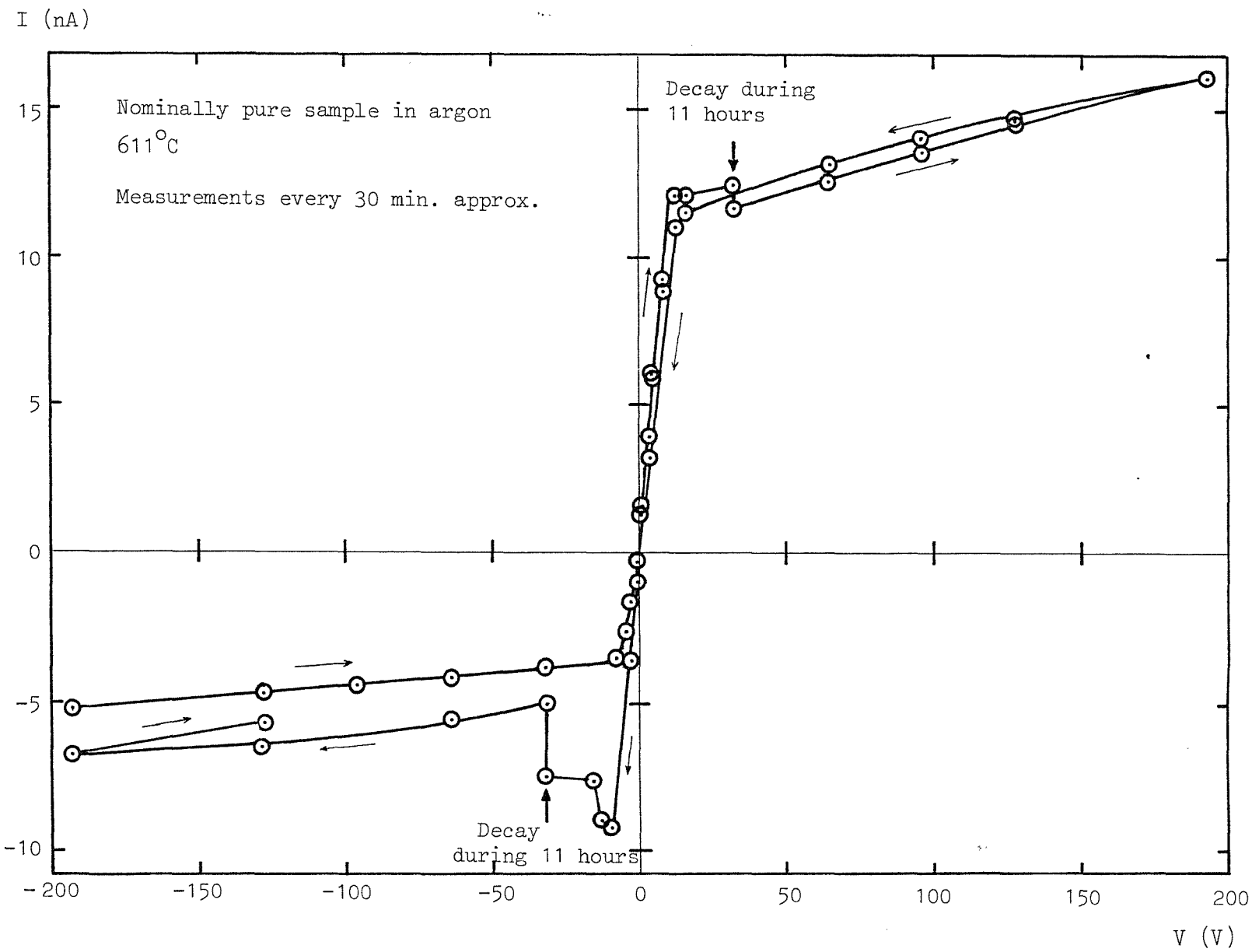

FIGURE 27 EXAMPLE OF VOLTAGE-CURRENT CHARACTERISTIC

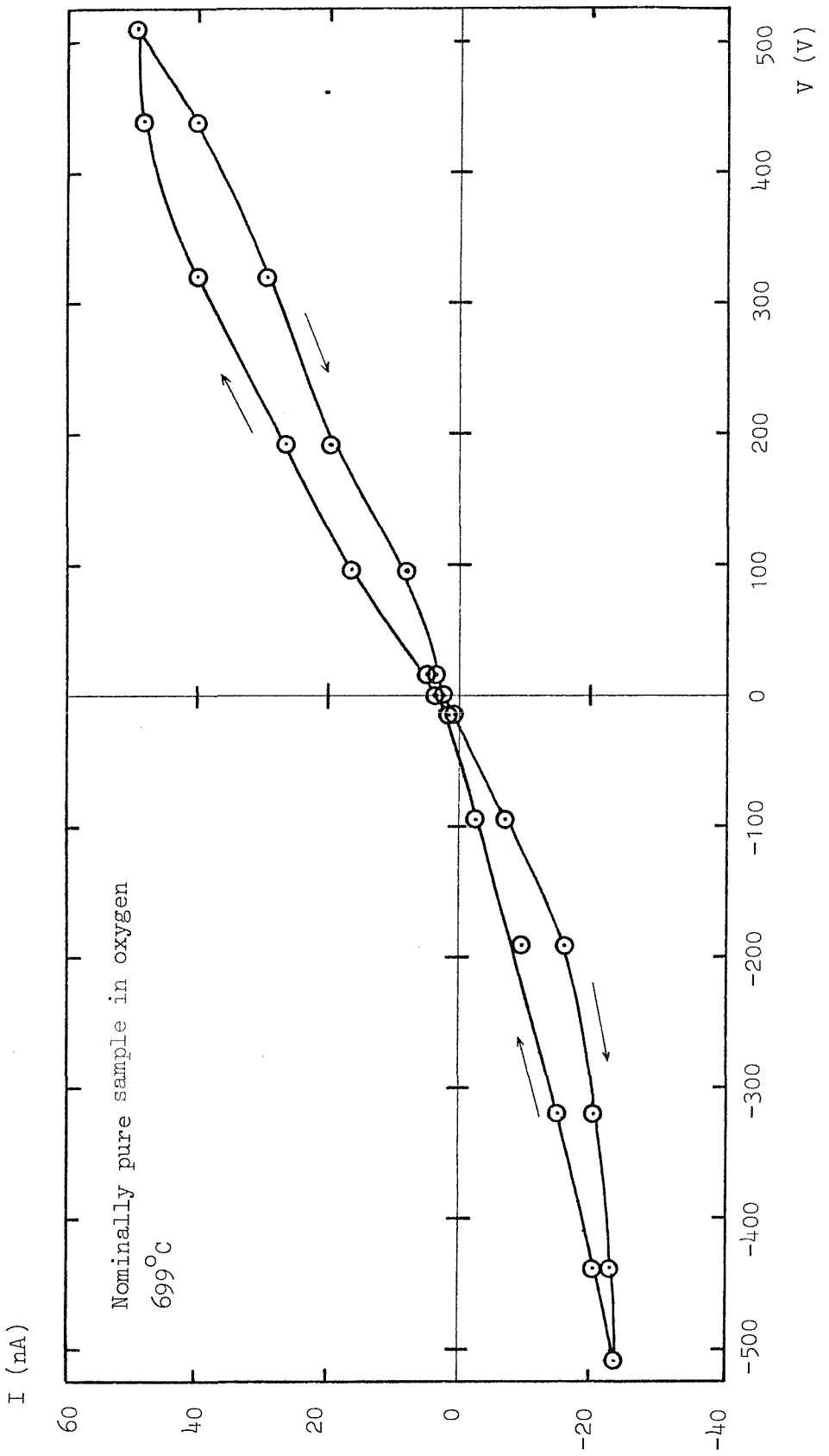

FIGURE 28 EXAMPLE OF VOLTAGE-CURRENT CHARACTERISTIC

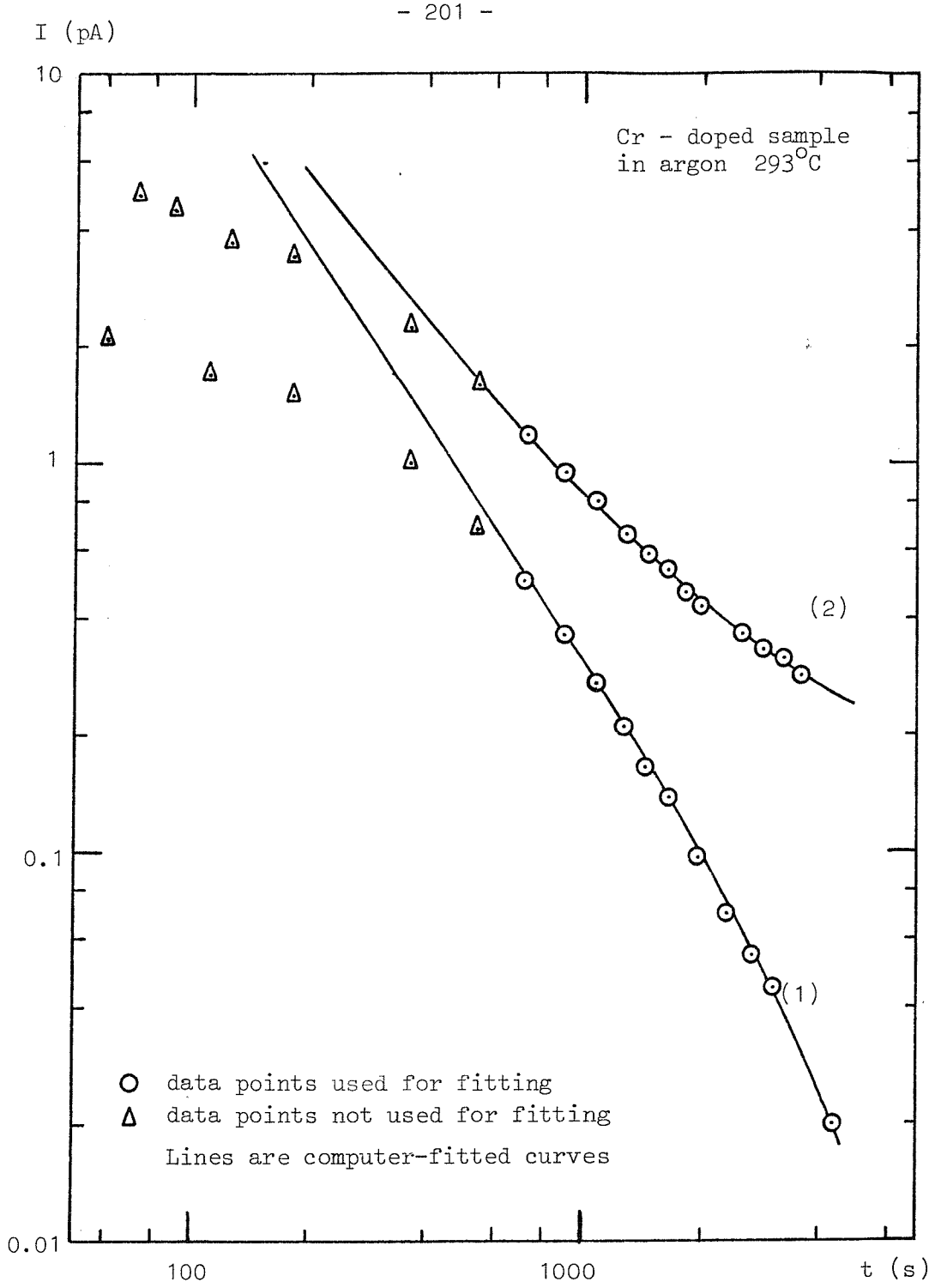

(1) Voltage change 0 - 64.3V

$I = (-0.013 + 13{,}068 \cdot t^{-1 \cdot 54 \pm 0 \cdot 04})pA$

(2) Voltage change 64.3 - 193V

$I = (0.157 + 4{,}946 \cdot t^{-1 \cdot 29 \pm 0 \cdot 05})pA$

FIGURE 29(a) EXAMPLES OF CURRENT DECAYS AND COMPUTER FITTING

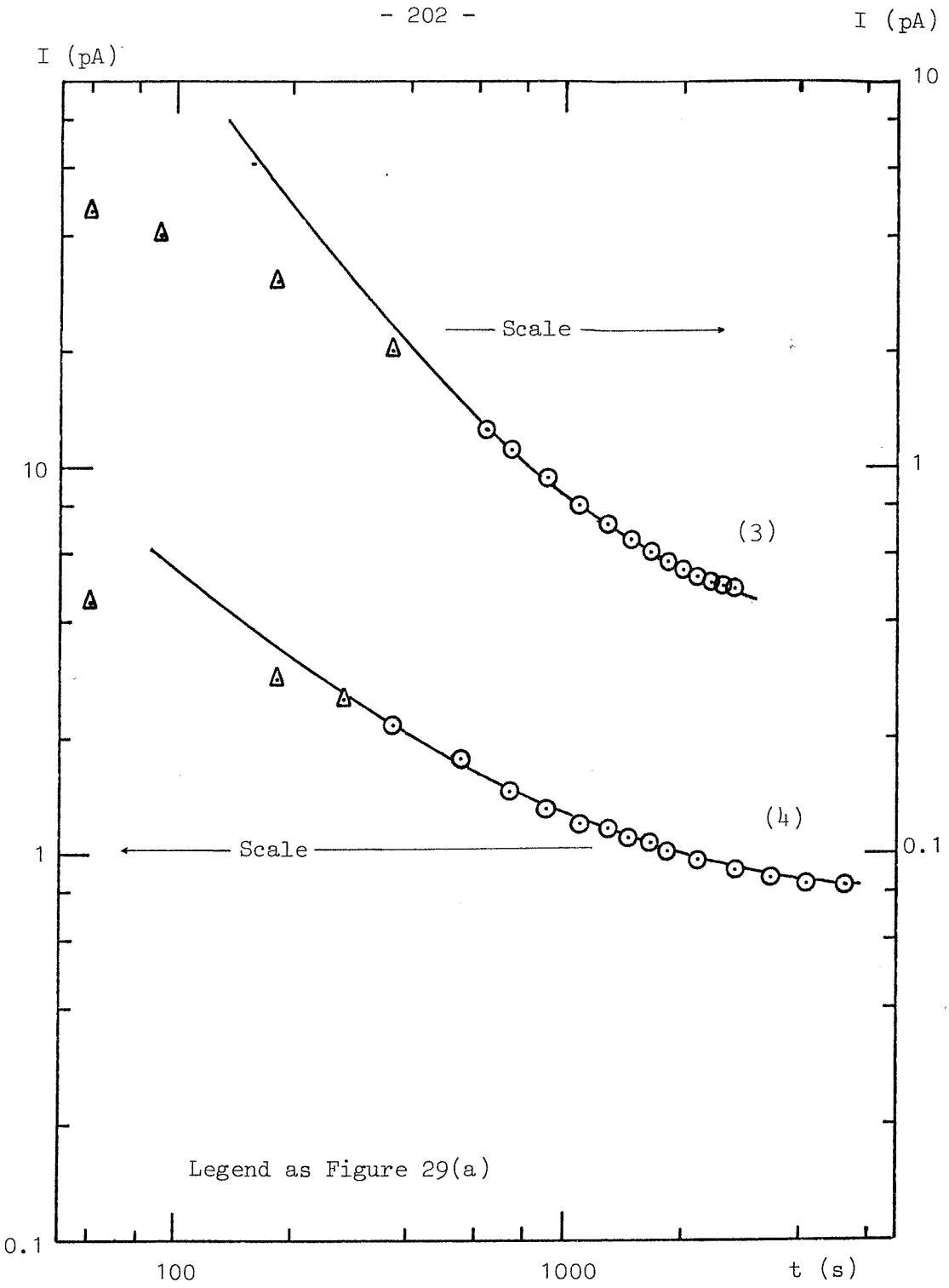

(3) Voltage change 193 - 319V

$I = (0.356 + 6{,}458 \cdot t^{-1 \cdot 38 \pm 0 \cdot 06})pA$

(4) Voltage change 319 - 439V

$I = (0{,}684 + 328.3 \cdot t^{-0 \cdot 92 \pm 0 \cdot 02})pA$

FIGURE 29(b) EXAMPLES OF CURRENT DECAYS AND COMPUTER FITTING

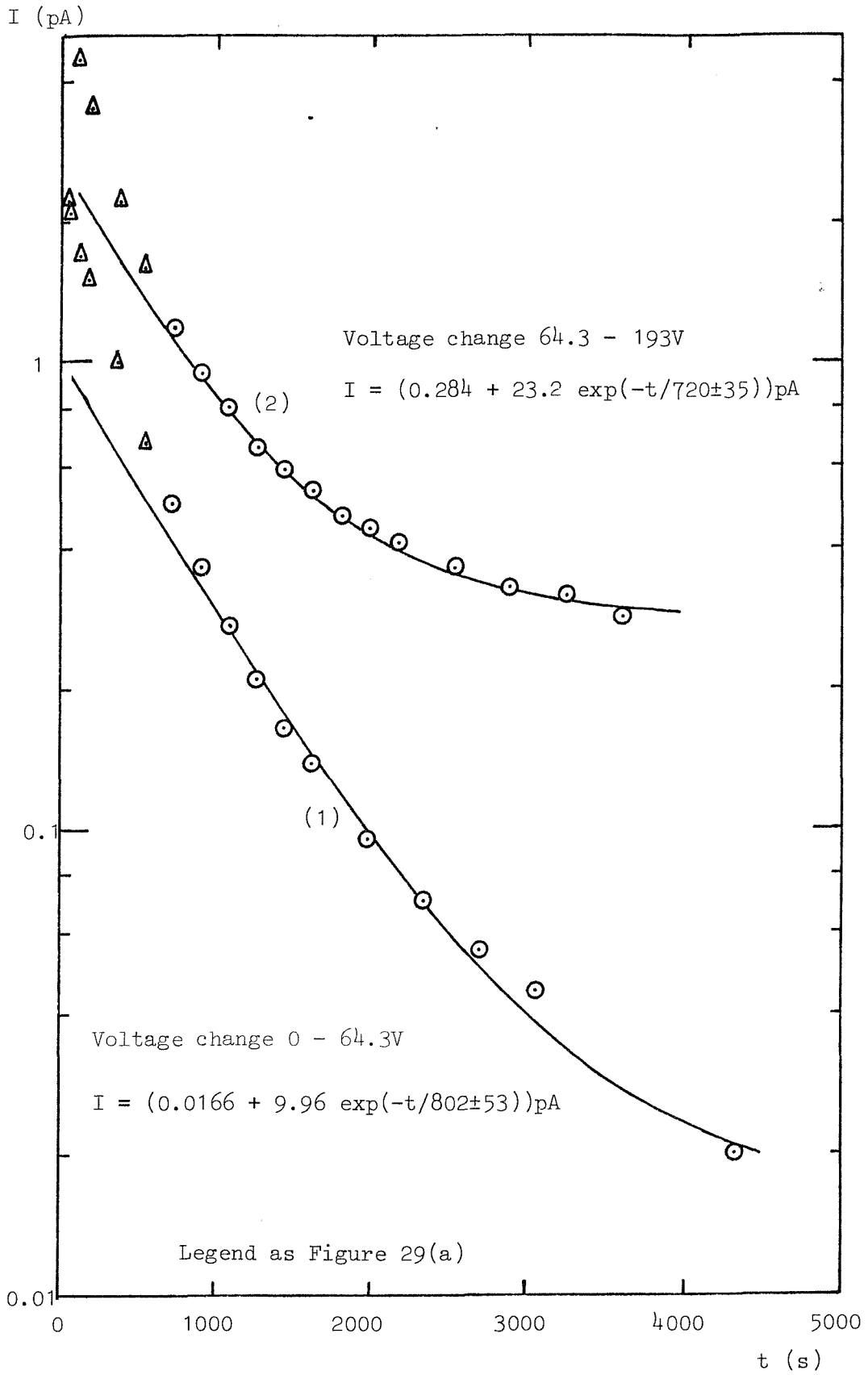

FIGURE 29(c) EXAMPLES OF CURRENT DECAYS AND COMPUTER FITTING

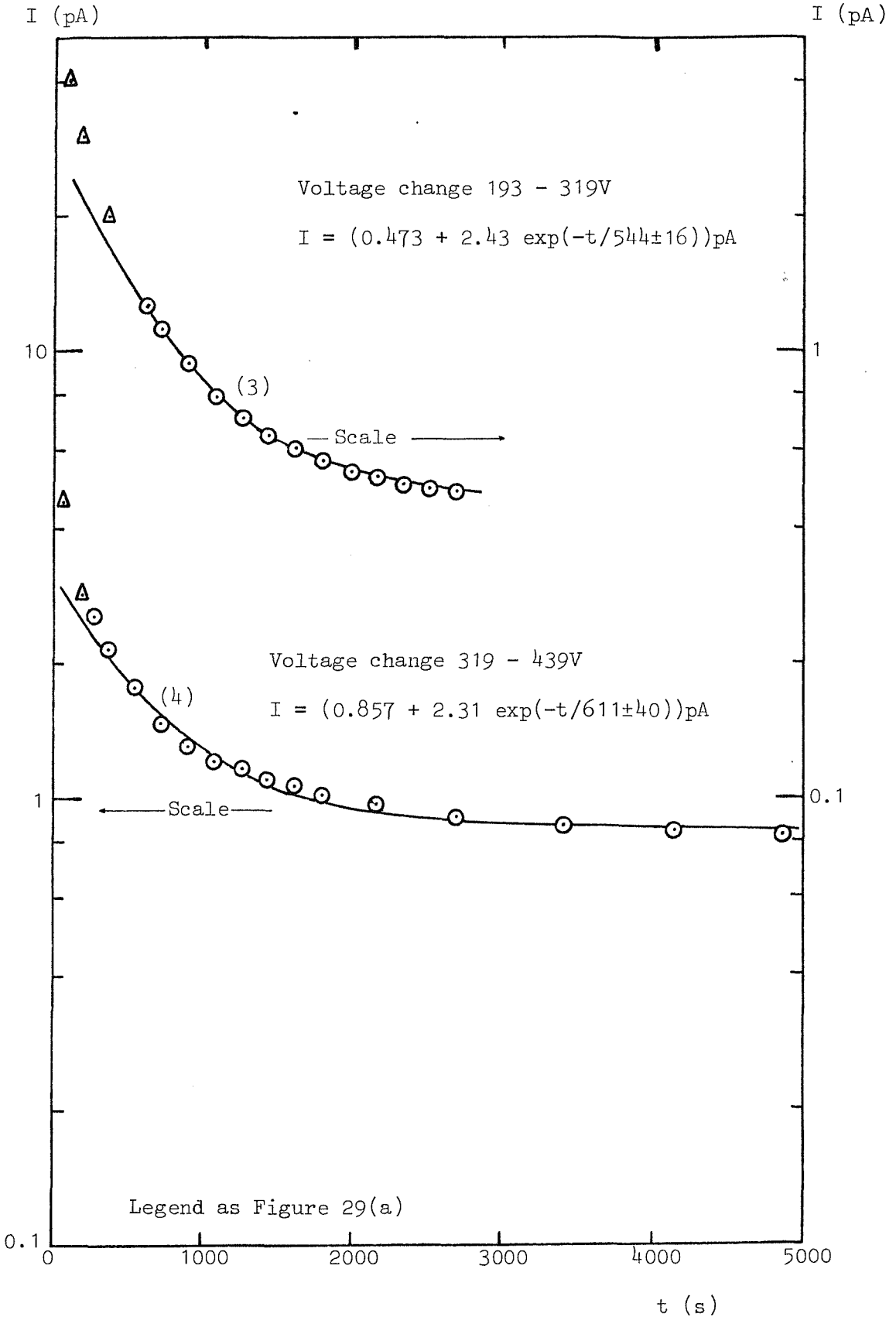

FIGURE 29(d) EXAMPLES OF CURRENT DECAYS AND COMPUTER FITTING

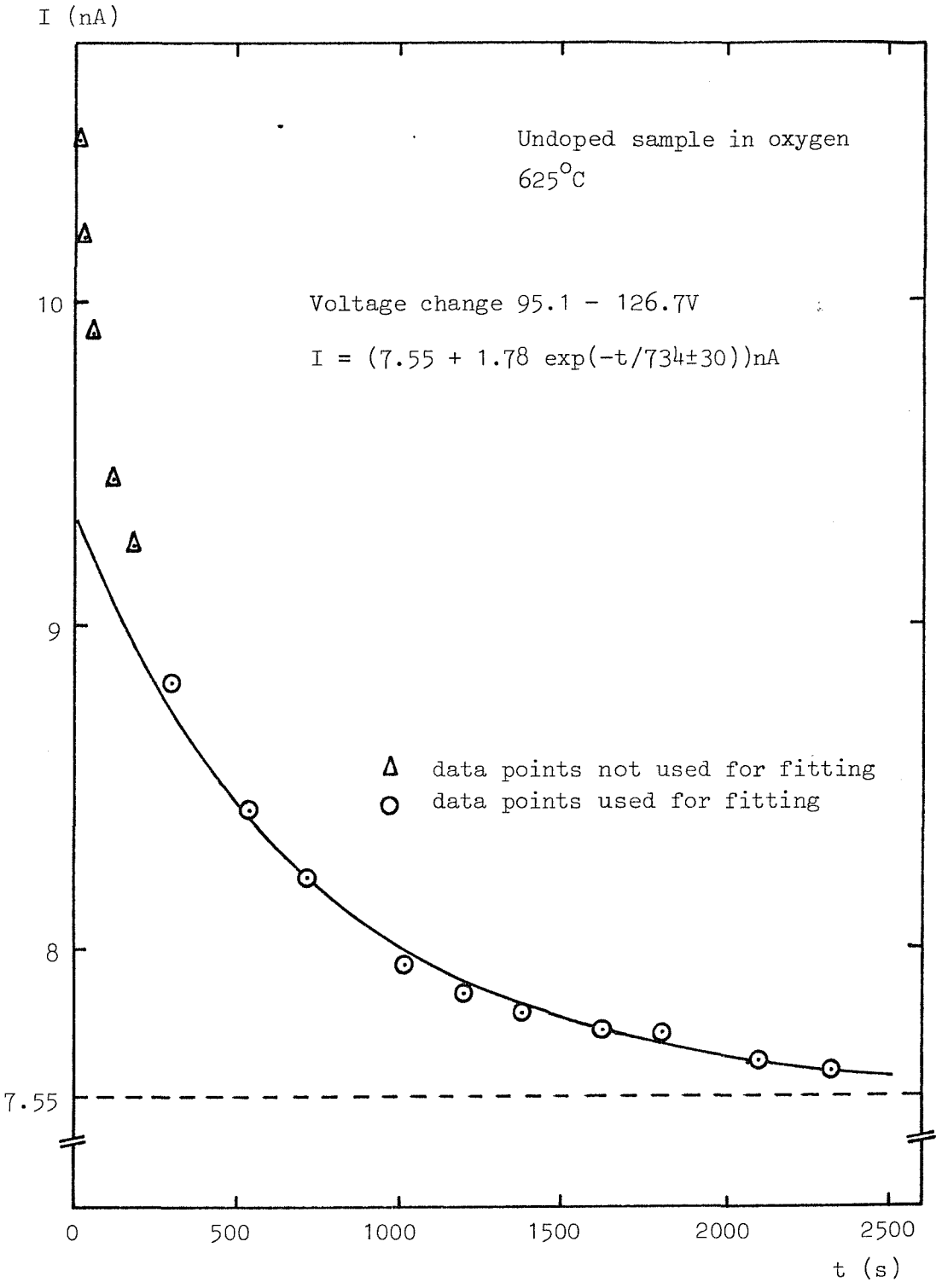

FIGURE 30 EXAMPLE OF CURRENT DECAY AND COMPUTER FITTING

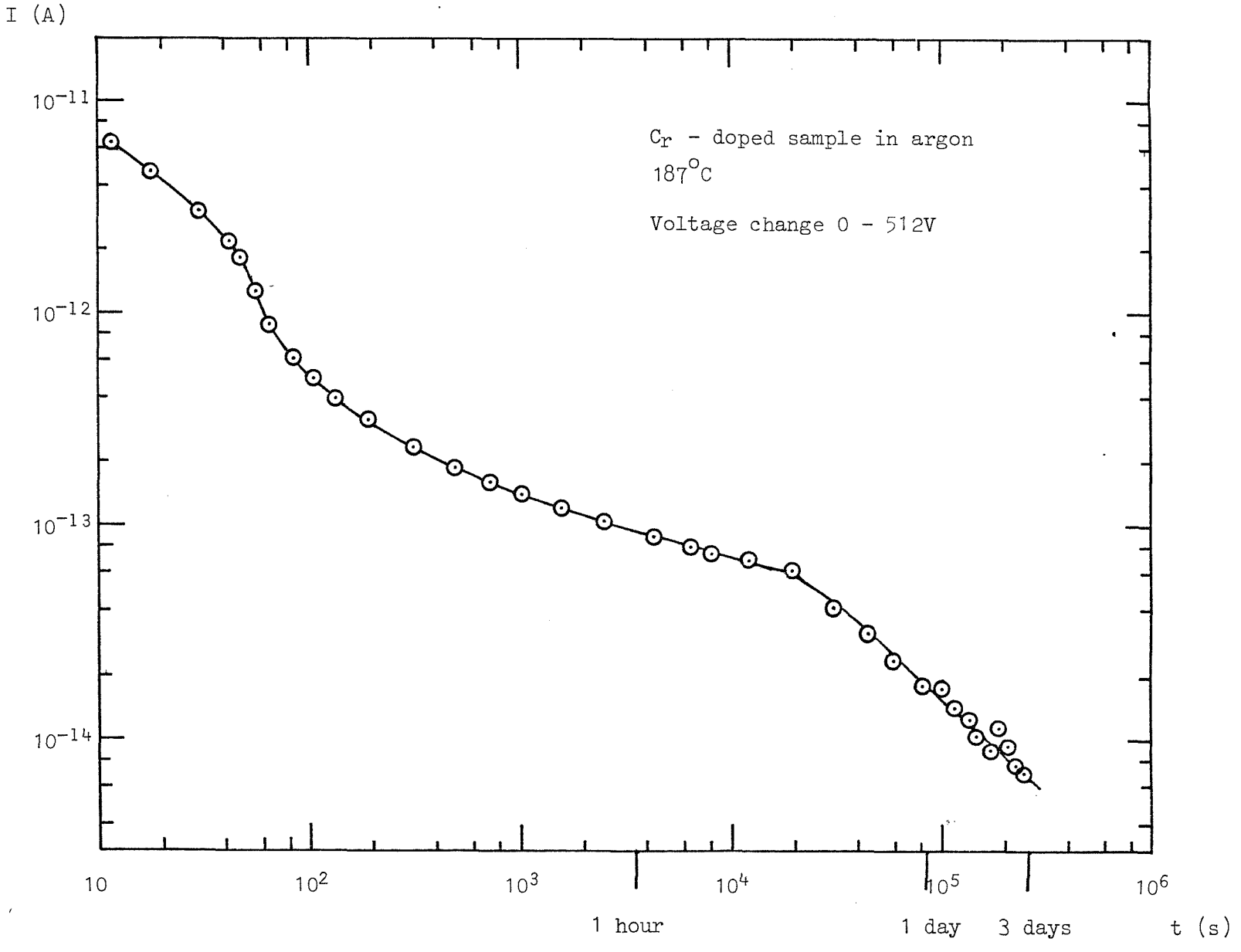

FIGURE 31 EXAMPLE OF CURRENT DECAY

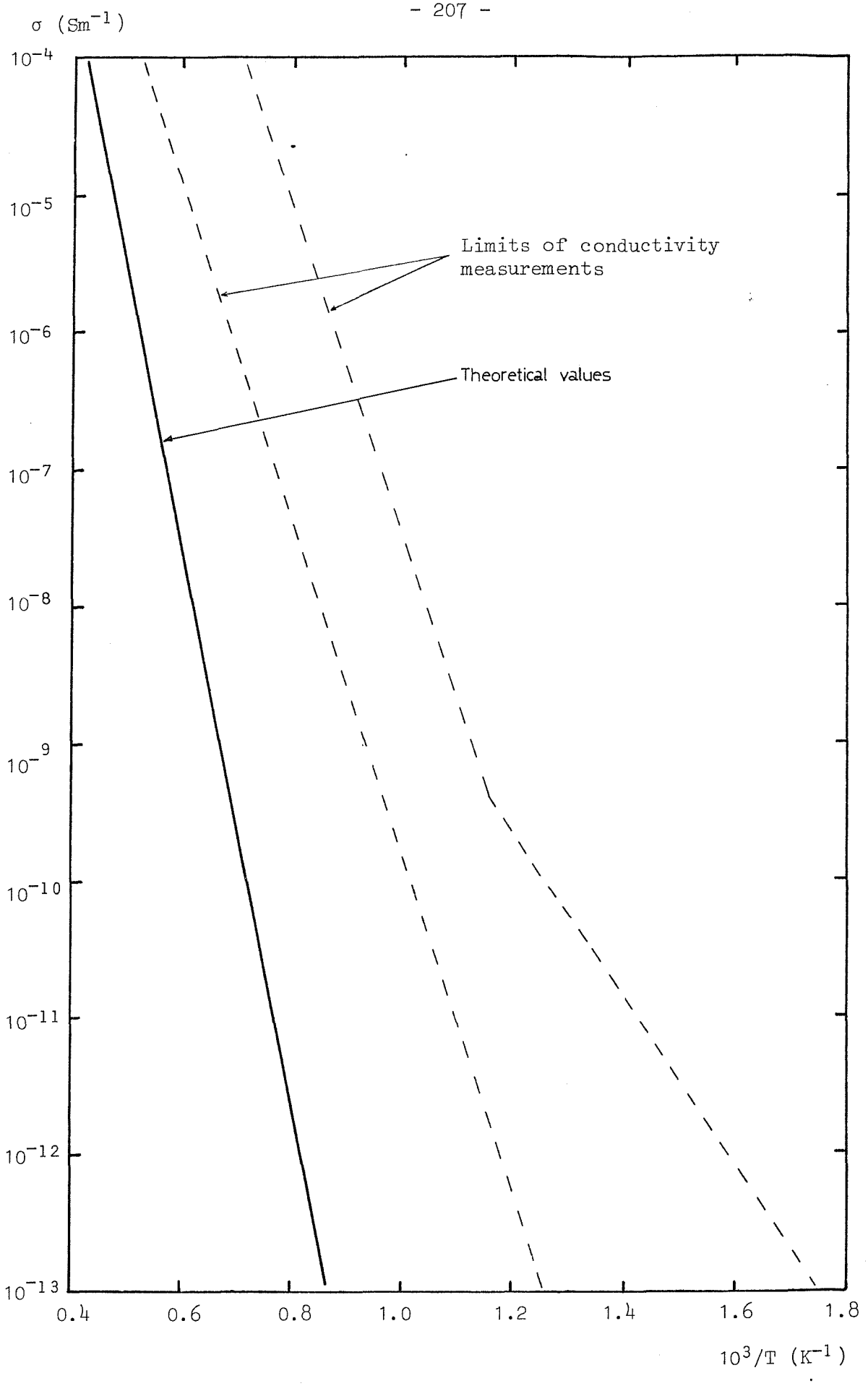

FIGURE 32 CONDUCTIVITY VALUES DUE TO INTRINSIC ELECTRONIC CONDUCTION

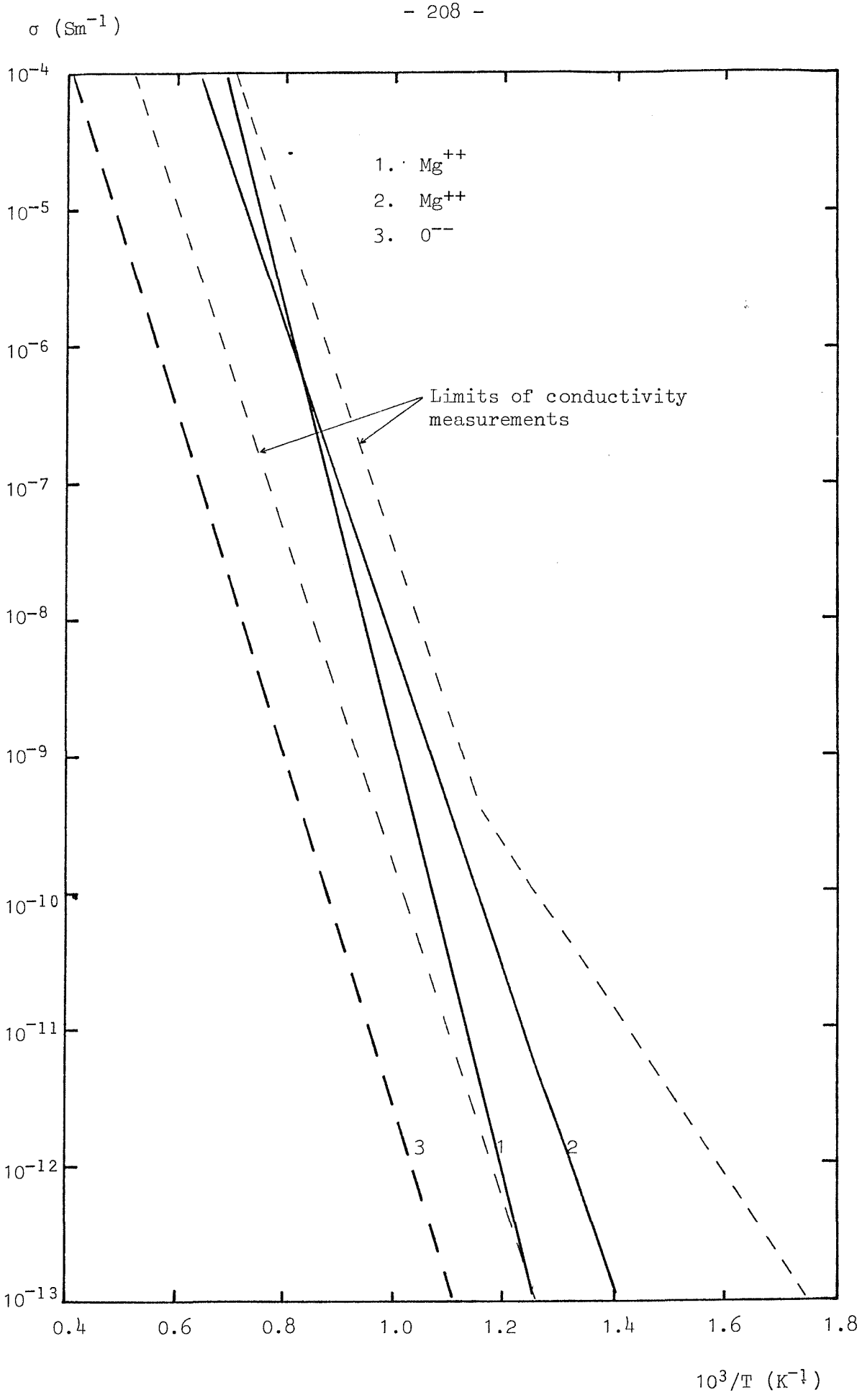

FIGURE 33 CONDUCTIVITY VALUES DUE TO INTRINSIC IONIC CONDUCTION

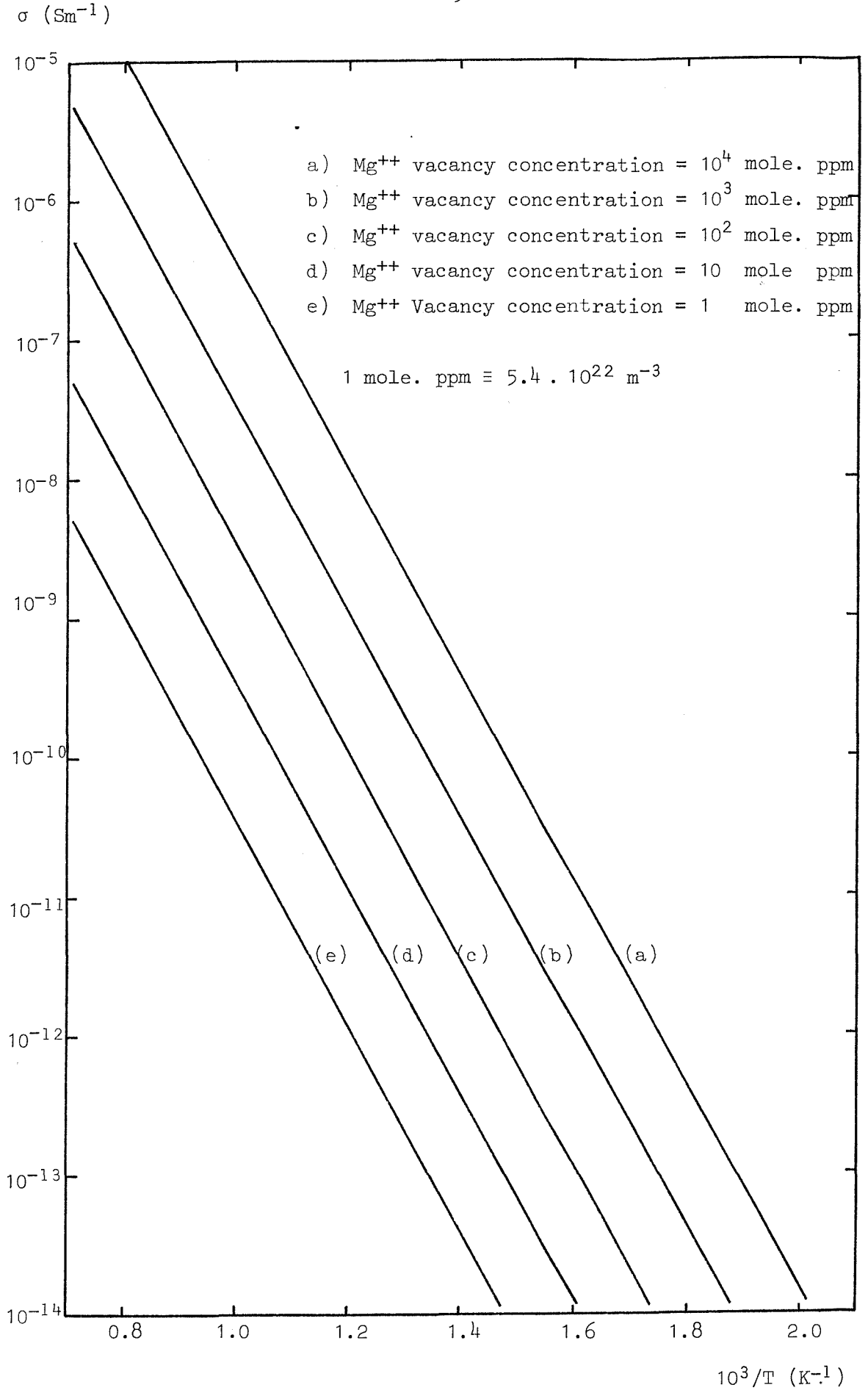

FIGURE 34 MAGNESIUM ION CONDUCTION AT CONSTANT VACANCY CONCENTRATIONS

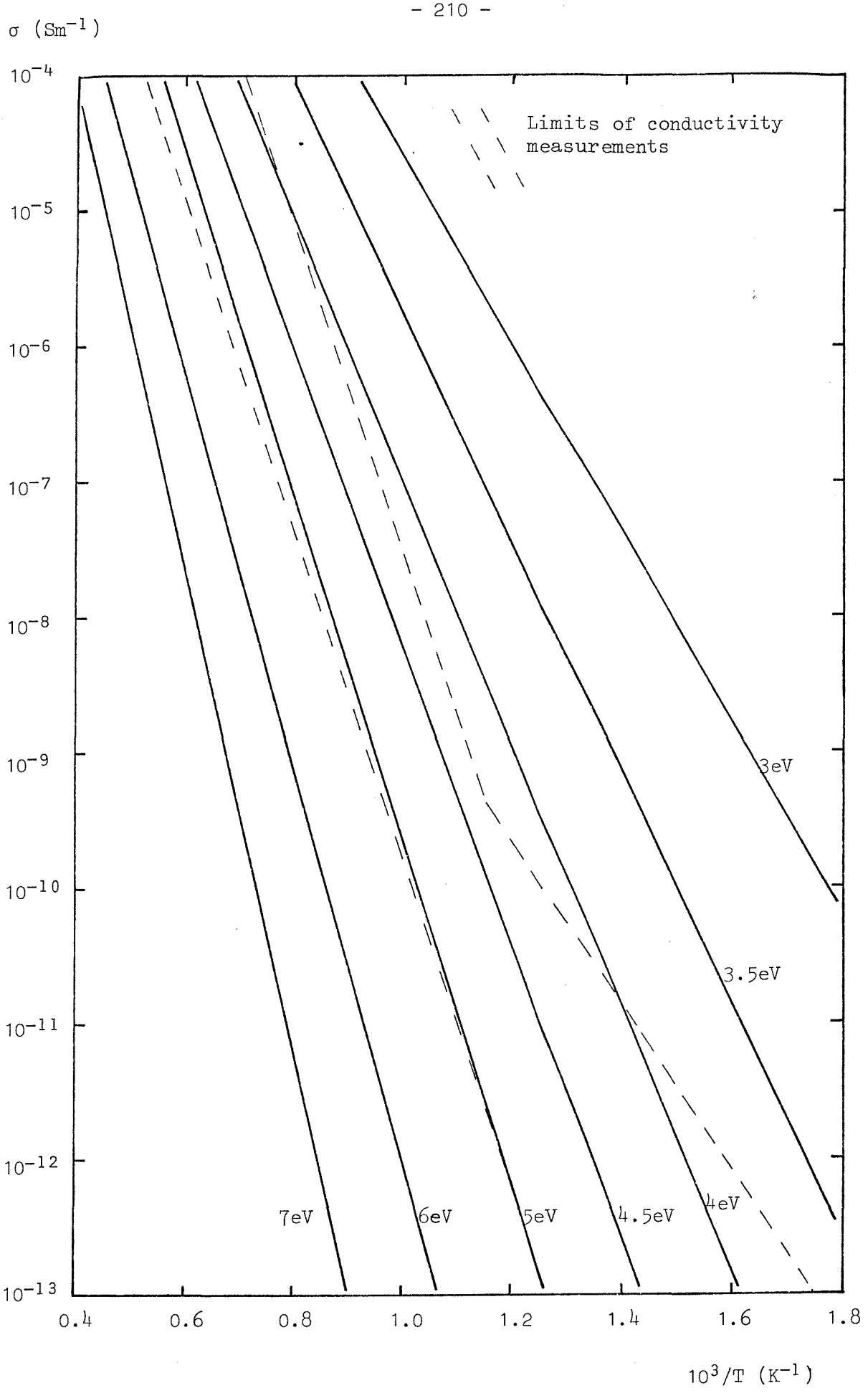

FIGURE 35 CONDUCTIVITY VALUES DUE TO EXTRINSIC ELECTRONIC CONDUCTION

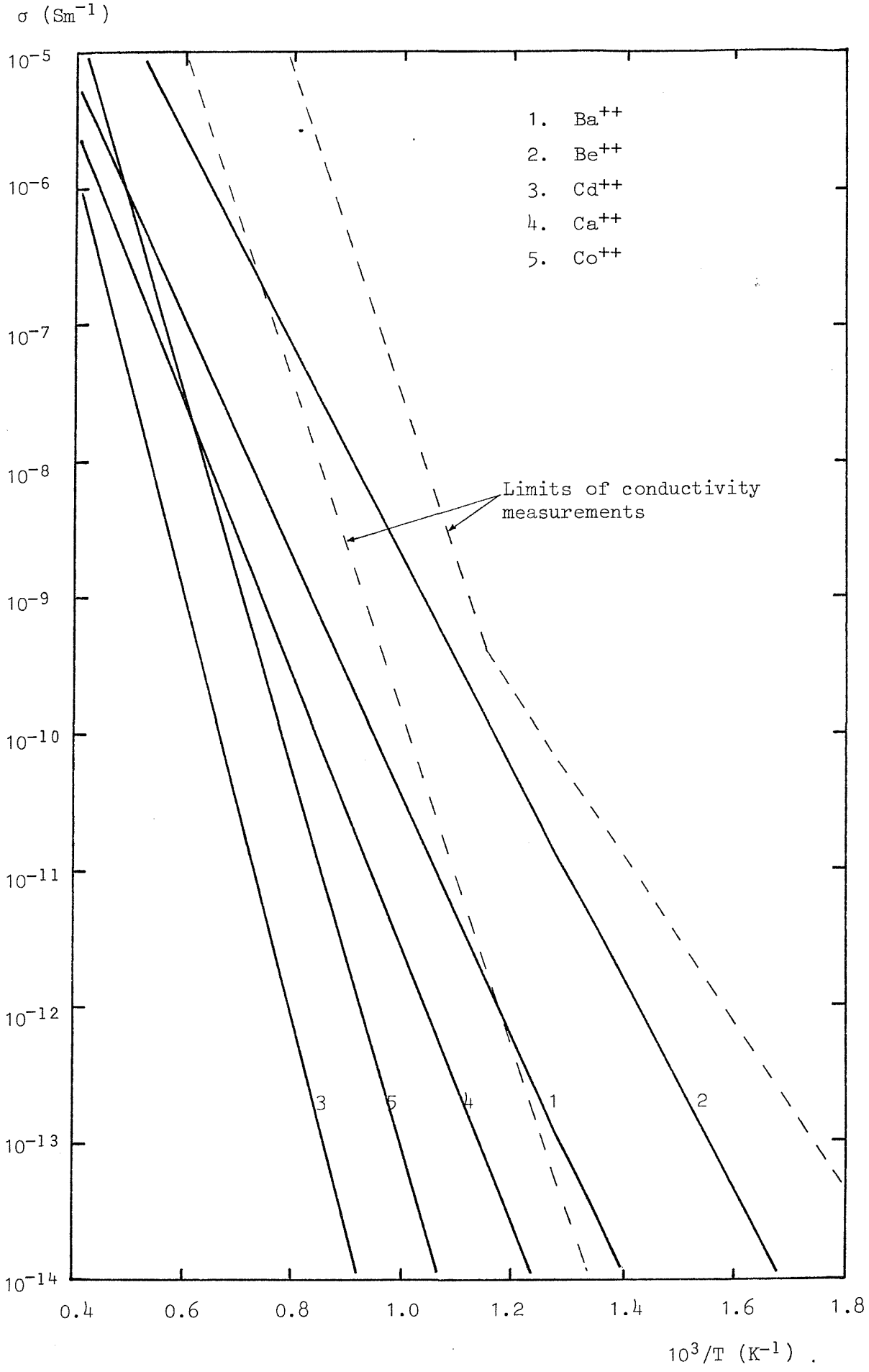

FIGURE 36(a) CONDUCTIVITY VALUES DUE TO EXTRINSIC IONIC CONDUCTION

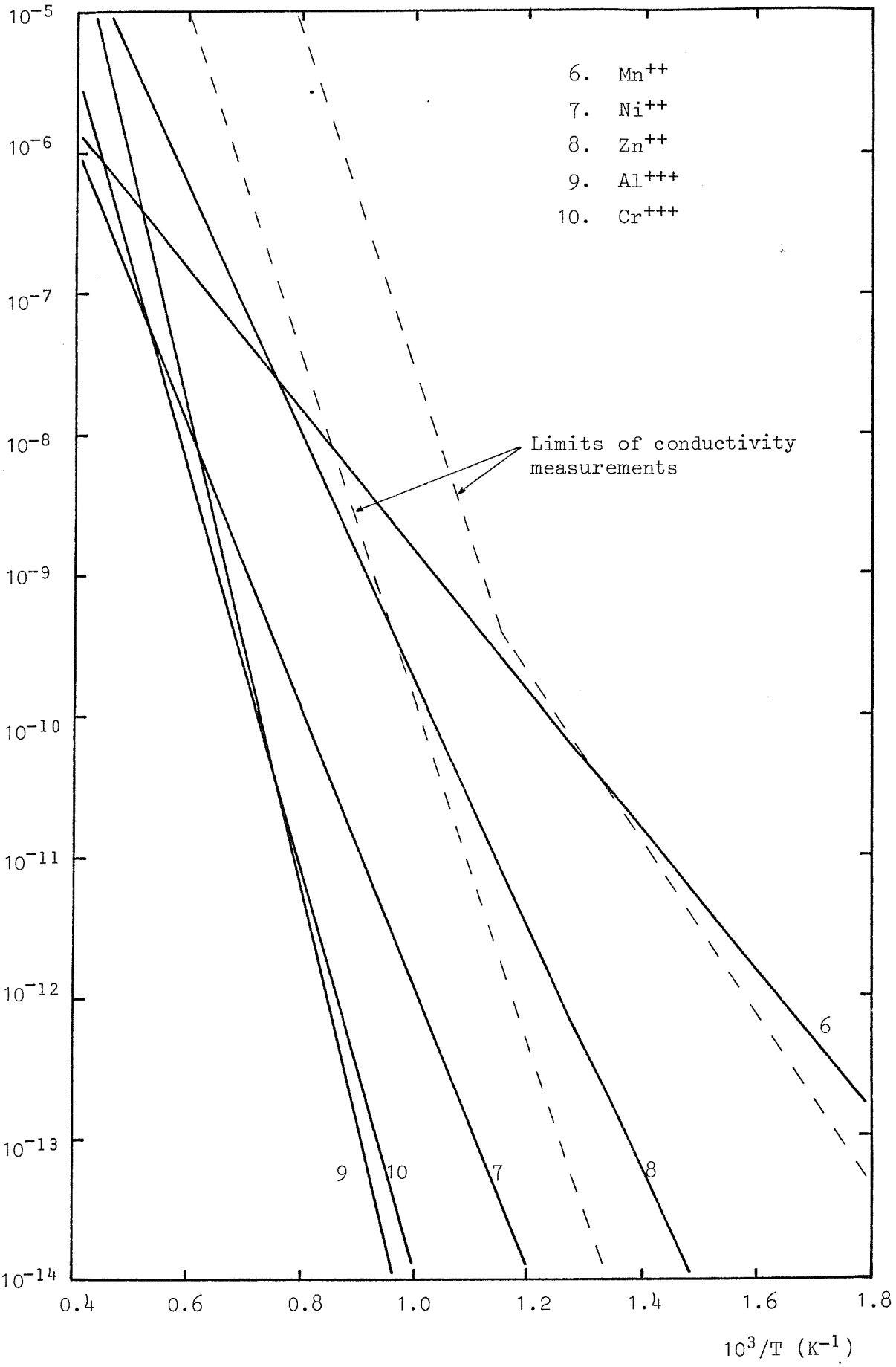

FIGURE 36(b) CONDUCTIVITY VALUES DUE TO EXTRINSIC ELECTRONIC CONDUCTION

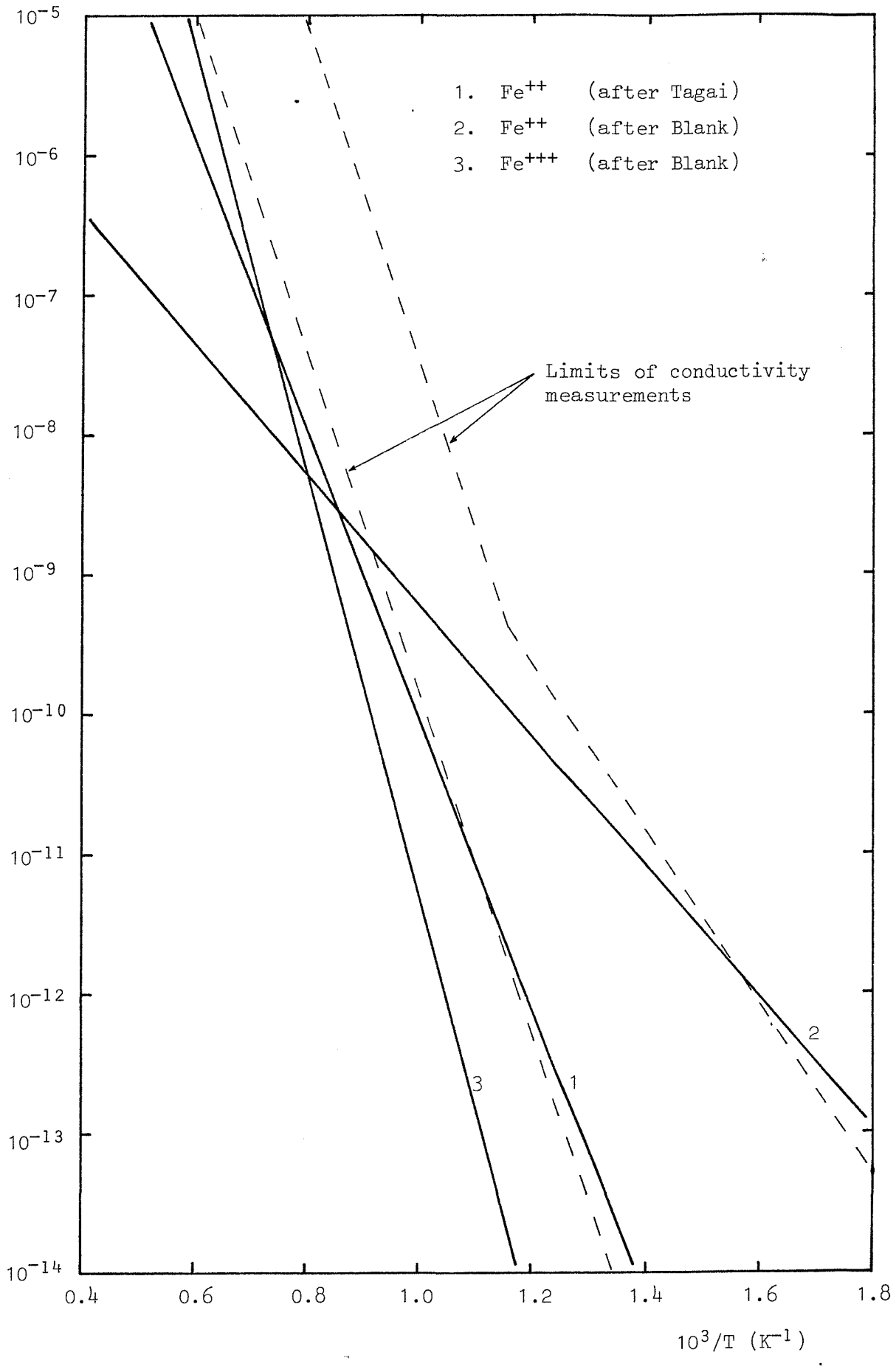

FIGURE 37 CONDUCTIVITY VALUES DUE TO IRON ION CONDUCTION

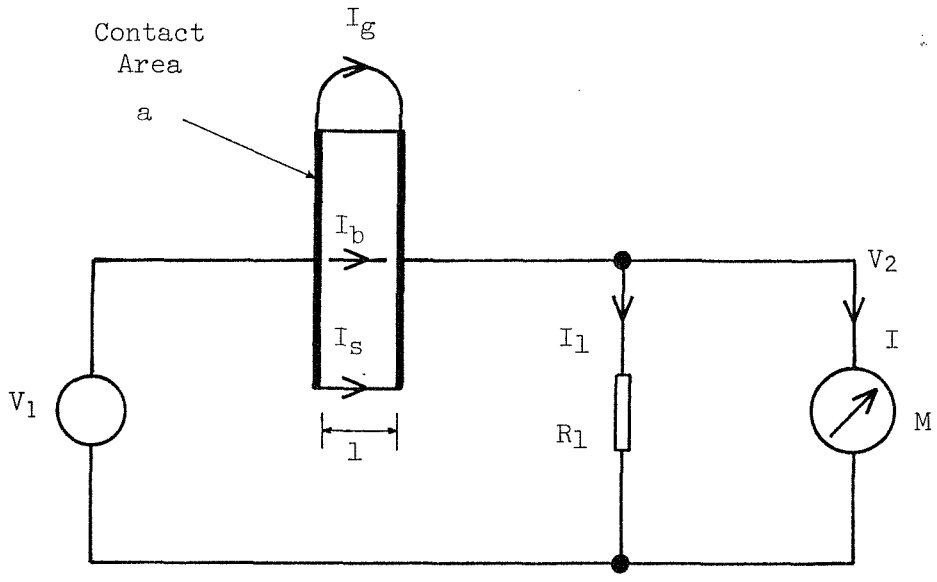

$$I = I_b + I_g + I_s - I_1$$

FIGURE 38 TWO TERMINAL MEASUREMENT SYSTEM

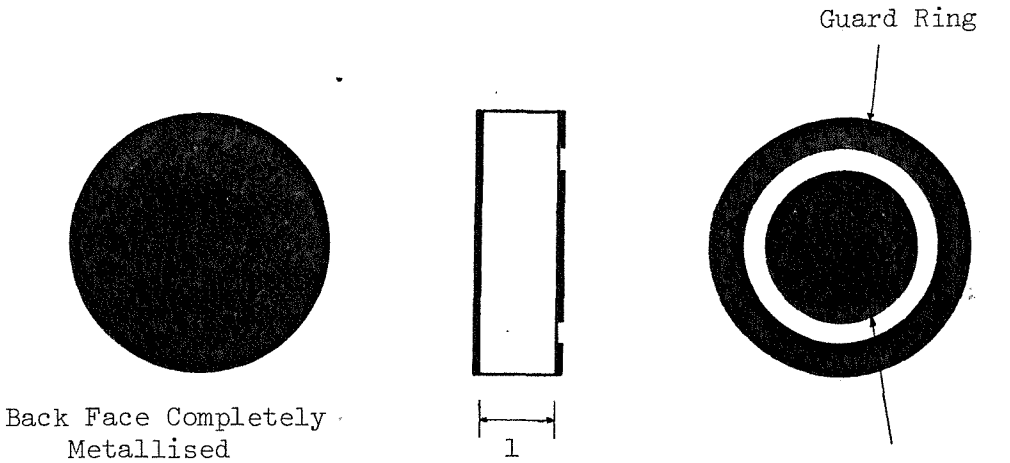

(a)
Contact Geometry

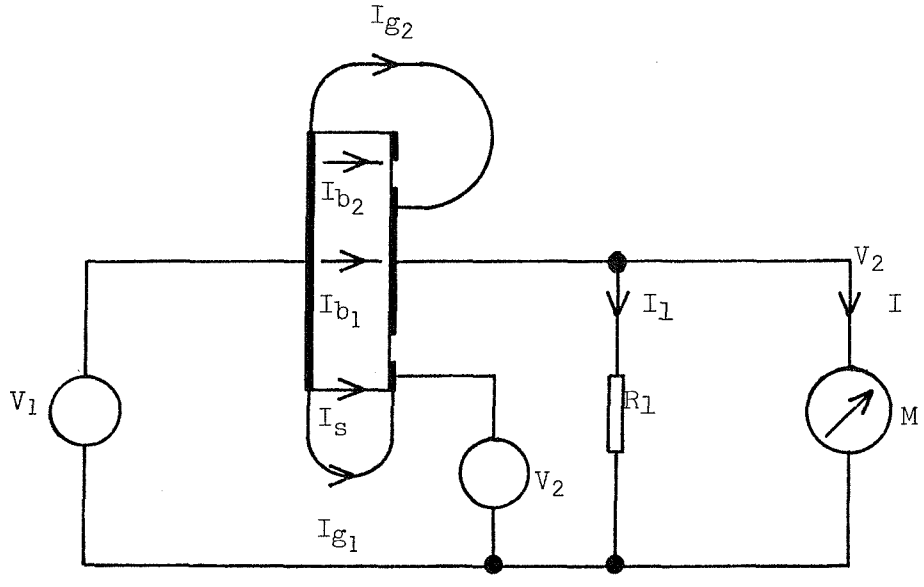

(b)
Basic System

FIGURE 39 THREE TERMINAL MEASUREMENT SYSTEMS

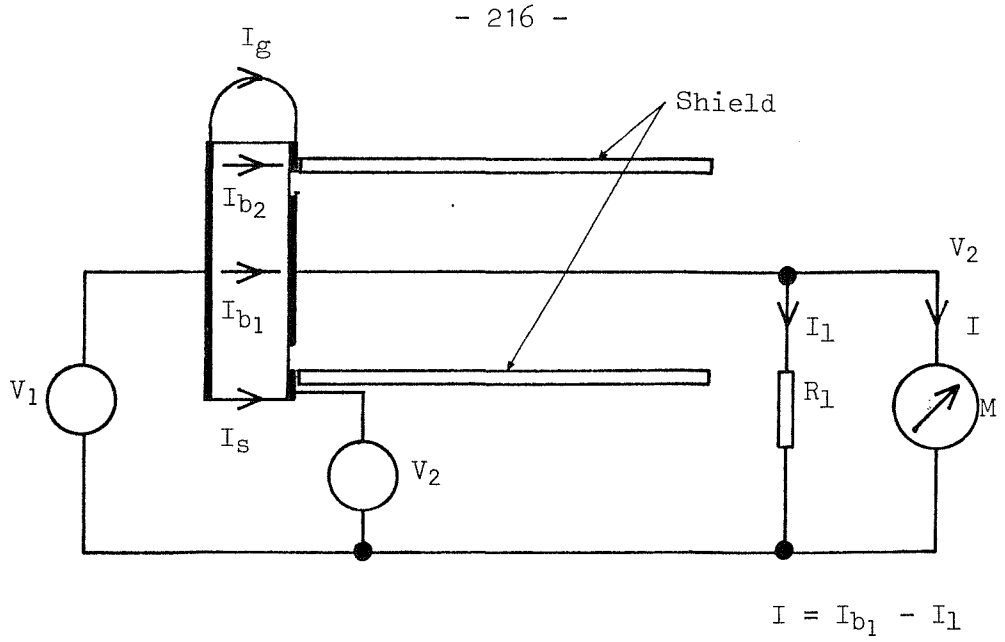

(c) Volume Guarded System

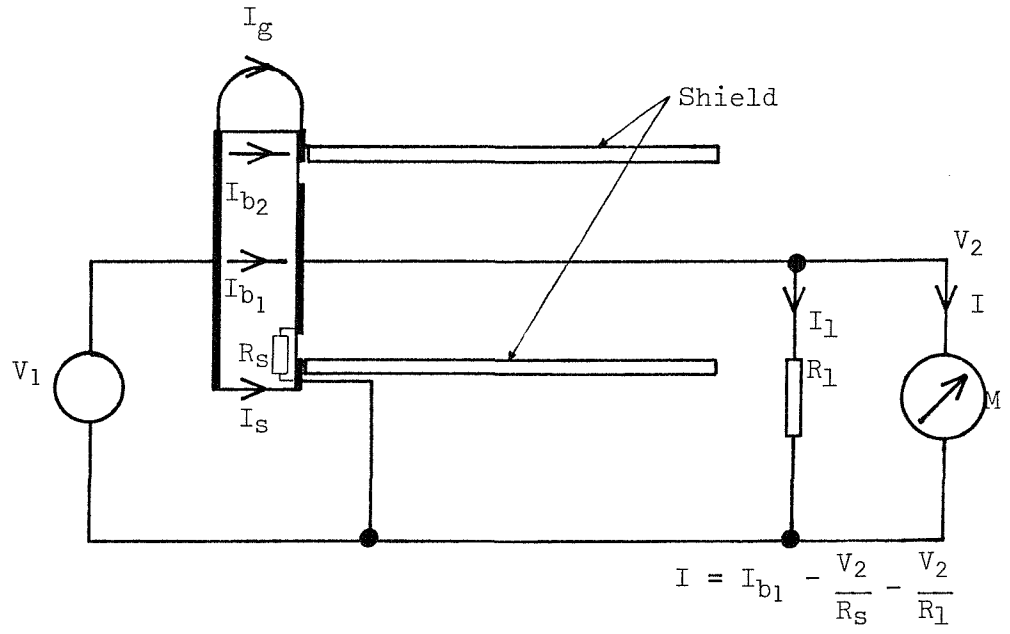

(d) Volume Guarded System using "Virtual Earth" Meter

FIGURE 39 THREE TERMINAL MEASUREMENT SYSTEMS (Cont.)

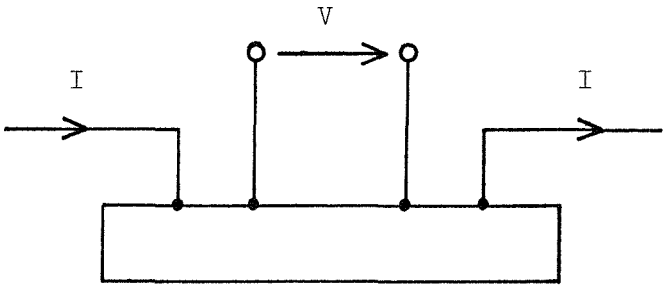

FIGURE 40 FOUR TERMINAL MEASUREMENT SYSTEM

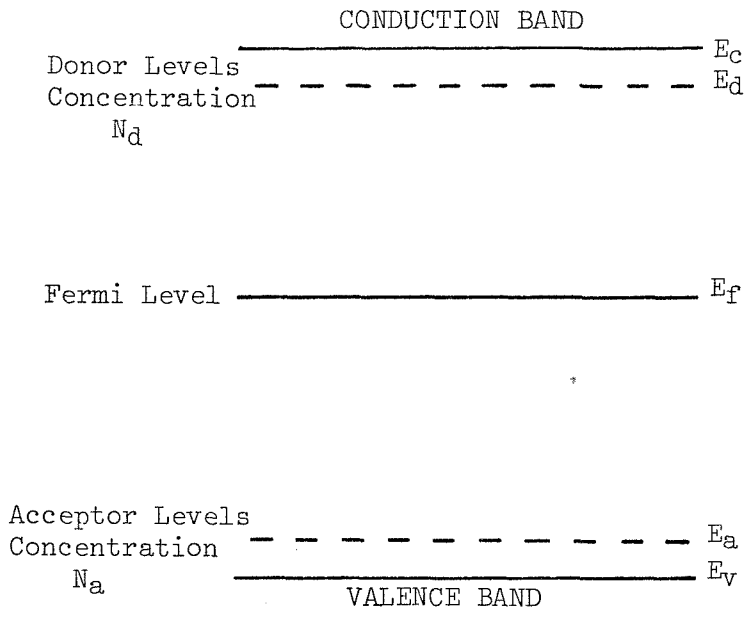

FIGURE 41 ENERGY BAND DIAGRAM

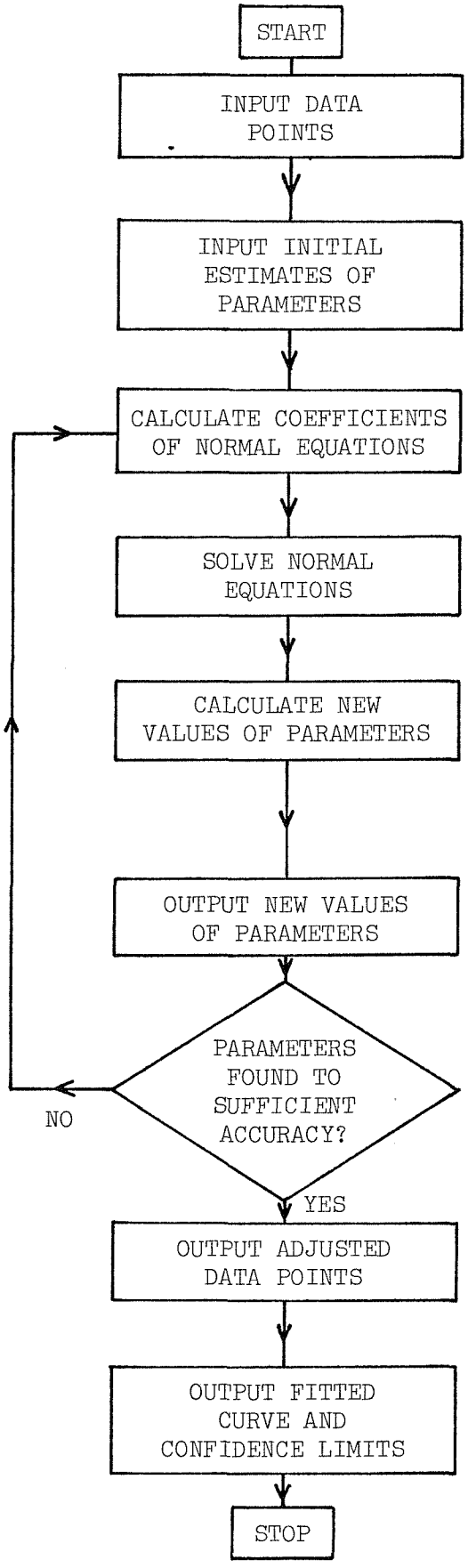

FIGURE 42 COMPUTER PROGRAM FLOW CHART

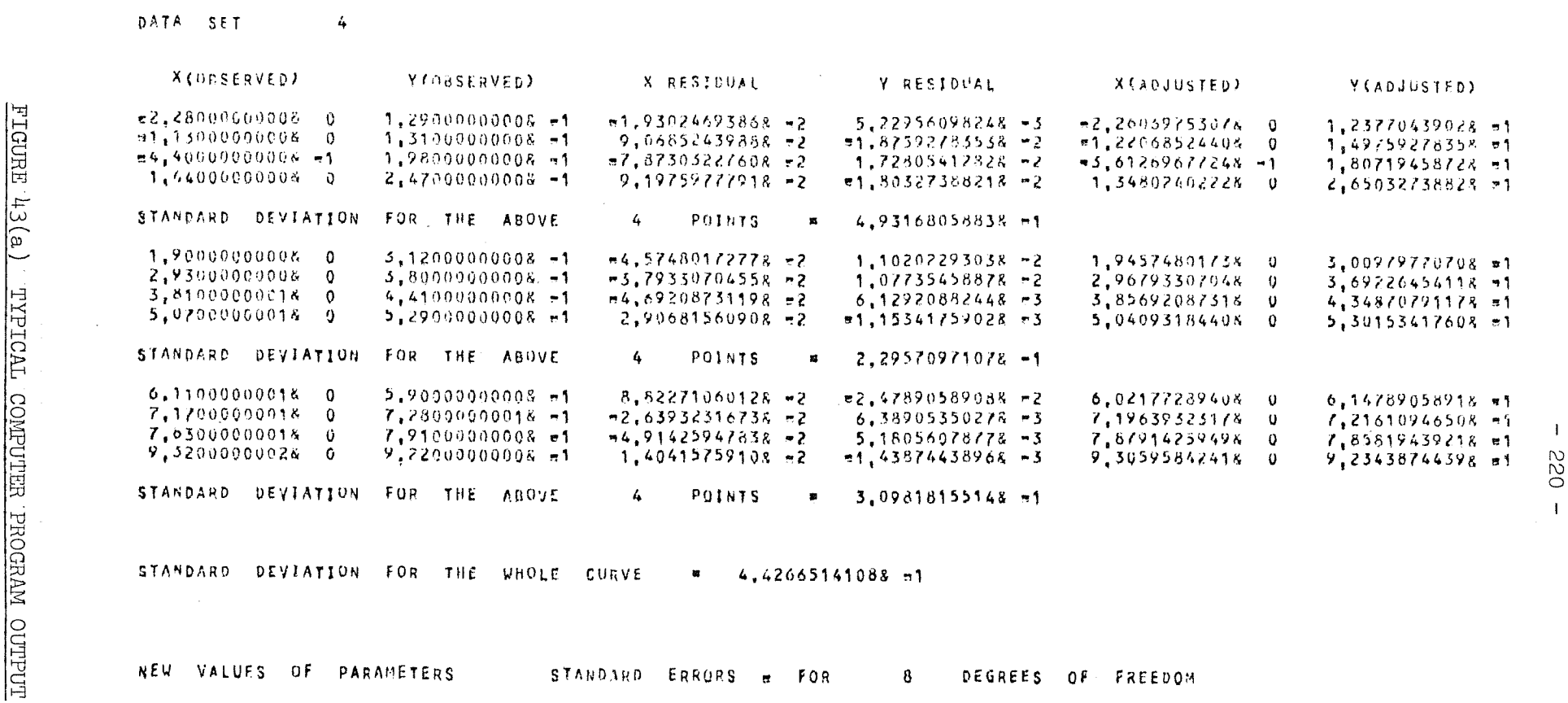

DATA SET 4

X(OBSERVED)	Y(OBSERVED)	X RESIDUAL	Y RESIDUAL	X(ADJUSTED)	Y(ADJUSTED)
-2,28000000008 0	1,29000000008 -1	-1,93024693868 -2	5,22956098248 -3	-2,26069753078 0	1,23770439028 -1
-1,13000000008 0	1,31000000008 -1	9,06852439888 -2	-1,87592783538 -2	-1,22068524408 0	1,49759278358 -1
-4,40000000008 -1	1,98000000008 -1	-7,87305227608 -2	1,72805412828 -2	-5,61269677248 -1	1,80719458728 -1
1,64000000008 0	2,47000000008 -1	9,19759777918 -2	-1,80327388218 -2	1,54807402228 0	2,65032738828 -1

STANDARD DEVIATION FOR THE ABOVE 4 POINTS = 4,93168058838 -1

1,90000000008 0	3,12000000008 -1	-4,57480172778 -2	1,10202293038 -2	1,94574801738 0	3,00979770708 -1
2,93000000008 0	3,80000000008 -1	-3,79330704558 -2	1,07735458878 -2	2,96793307048 0	3,69226454118 -1
3,81000000018 0	4,41000000008 -1	-4,69208731198 -2	6,12920882448 -3	3,85692087318 0	4,34870791178 -1
5,07000000018 0	5,29000000008 -1	2,90681560908 -2	-1,15341759028 -3	5,04093184408 0	5,30153417608 -1

STANDARD DEVIATION FOR THE ABOVE 4 POINTS = 2,29570971078 -1

6,11000000018 0	5,90000000008 -1	8,82271060128 -2	-2,47890589088 -2	6,02177289408 0	6,14789058918 -1
7,17000000018 0	7,28000000018 -1	-2,63932316738 -2	6,38905350278 -3	7,19639323178 0	7,21610946508 -1
7,03000000018 0	7,91000000008 -1	-4,91425947838 -2	5,18056078778 -3	7,87914259498 0	7,85819439218 -1
9,32000000028 0	9,22000000008 -1	1,40415759108 -2	-1,43874438968 -3	9,30595842418 0	9,23438744398 -1

STANDARD DEVIATION FOR THE ABOVE 4 POINTS = 3,09818155148 -1

STANDARD DEVIATION FOR THE WHOLE CURVE = 4,42665141088 -1

NEW VALUES OF PARAMETERS	STANDARD ERRORS = FOR 8 DEGREES OF FREEDOM
1,96146012888 -1	9,69091595418 -3
4,44901091708 -2	3,36766997178 -3
5,14720577558 -3	1,67766459128 -3
-1,64390200178 -4	1,68851580948 -4

FIGURE 43(a) TYPICAL COMPUTER PROGRAM OUTPUT

FIGURE 43(b) TYPICAL COMPUTER PROGRAM OUTPUT (Cont.)

FITTED CURVE				CONFIDENCE LIMITS - FOR 8 DEGREES OF FREEDOM		
X		Y	STANDARD ERROR	95 PER CENT	50 PER CENT	5 PER CENT
-2,00000000008	0	1,29069739248 -1	1,10108498928 -2	1,50651005038 -1 1,07488473458 -1	1,36494355338 -1 1,21645123168 -1	1,29320236088 -1 1,28819242418 -1
-1,00000000008	0	1,36967499688 -1	8,60862749358 -3	1,73840409578 -1 1,40094589808 -1	1,62772297208 -1 1,51162702178 -1	1,57163345968 -1 1,56771653418 -1
0,00000000008	0	1,96146012888 -1	9,69091595418 -3	2,15140208158 -1 1,77151817618 -1	2,02680597518 -1 1,89611428258 -1	1,96366481228 -1 1,95925544548 -1
1,00000000008	0	2,43618937638 -1	9,94495342068 -3	2,65111046538 -1 2,26126828928 -1	2,52324819728 -1 2,38913055548 -1	2,45845185328 -1 2,45392689948 -1
2,00000000008	0	3,04399932728 -1	9,32668247098 -3	3,22680230368 -1 2,86119635088 -1	3,10688914718 -1 2,98110950738 -1	3,04612114758 -1 3,04187750708 -1
3,00000000008	0	3,71502655968 -1	9,01623562748 -3	3,89174478798 -1 3,53830835138 -1	3,77582304648 -1 3,65423009288 -1	3,71707776328 -1 3,71297557608 -1
4,00000000008	0	4,45940769168 -1	9,80938001568 -3	4,65167153998 -1 4,26714384338 -1	4,52555234108 -1 4,39326504218 -1	4,46163932558 -1 4,45717605768 -1
5,00000000018	0	5,26727928108 -1	1,11385432608 -2	5,48559472898 -1 5,04896383318 -1	5,34238647828 -1 5,19217208388 -1	5,26981329968 -1 5,26474526248 -1
6,00000000018	0	6,12877792588 -1	1,19212162238 -2	6,38243376378 -1 5,89512206788 -1	6,20916268668 -1 6,04639316488 -1	6,13149000258 -1 6,12606584918 -1
7,00000000028	0	7,03404021418 -1	1,18458471318 -2	7,28621881788 -1 6,80186161038 -1	7,11391676138 -1 6,95416366698 -1	7,05673514438 -1 7,03134528398 -1
8,00000000018	0	7,97320273388 -1	1,30189606538 -2	8,22837456268 -1 7,71803110508 -1	8,06098958558 -1 7,88541588218 -1	7,97616454738 -1 7,97024092038 -1
9,00000000308	0	8,93640207298 -1	2,02479201408 -2	9,33326130768 -1 8,53954283818 -1	9,07293379848 -1 8,79987034748 -1	8,94100847478 -1 8,93179567108 -1

REFERENCE NUMBER	DOPANT ADDED																			
	Na	Cs	K	Li	Sr	Ba	Be	Ca	Co	Zn	Ni	Fe	Cr	Sc	Al	Ti	Zr	Th	Si
13											↓								
15	↑	↑	↑	↑	↑	↑	↑	↑			↑					↑	↑	↑	↑
16									↑				↑						
18									↑		↑								
20											↑								
21										↑	↑	↑		↑		=	=		
22												↑							
23												↑			=	↑	=		

TABLE 1 EFFECT OF DOPANTS ON CONDUCTIVITY OF POLYCRYSTALLINE SAMPLES

↑ - conductivity increased by dopant

↓ - conductivity decreased by dopant

= - conductivity unaffected by dopant

AUTHOR		REFERENCE NUMBER	MECHANISM PROPOSED
Mansfield	1953	(14)	'P' type electronic due to excess oxygen
Day	1953	(74)	'P' type electronic due to excess magnesium
Yamaka et al.	1955	(4)	'N' type electronic due to excess magnesium
Yamaka et al.	1956	(95)	'P' type electronic
Mitoff	1959	(5)	Extrinsic electronic conduction, perhaps due to iron.
Mitoff	1962	(6)	Low temperatures - ionic, high temperatures - electronic
Pal'guev et al.	1962	(27)	Predominantly ionic
Davies	1963	(18)	Magnesium ions and/or oxygen ions
Mitoff	1964	(28)	Magnesium ions
Zirkind et al.	1964	(7)	Electronic at low temperatures
Surplice et al.	1964	(20)	'N' type electronic
Budnikov et al.	1964	(21)	Magnesium ions and extrinsic'n' type electronic
Luzgin et al.	1965	(31)	Entirely ionic when sample is in molten iron
Lewis et al.	1968	(8)	Electron hopping
Lewis et al.	1970	(9)	Oxygen ion hopping
Afzal et al.	1974	(12)	'N' type electronic

TABLE 2 PROPOSED CONDUCTIVITY MECHANISMS

CRYSTAL NUMBER	CHROMIUM CONTENT	IRON CONTENT
1. (nominally pure)	<20	200
2. (chromium doped)	750	50
2. (chromium doped)	550	150
3. (nominally pure)	<20	80
3. (nominally pure)	<20	100
4. (iron doped)	150	1600
4. (iron doped)	<20	250

All results quoted in ppm $^{w}/_{w}$

Resolution ± 10 ppm $^{w}/_{w}$

TABLE 3 CHEMICAL ANALYSIS OF CRYSTALS

$10^3/T$ (K^{-1})	n_i (m^{-3})	n_e (m^{-3})							
		E_c-E_d = 2eV	E_c-E_d = 3eV	E_c-E_d = 3.5eV	E_c-E_d = 4eV	E_c-E_d = 4.5eV	E_c-E_d = 5eV	E_c-E_d = 6eV	E_c-E_d = 7eV
0.4	$9 . 10^{18}$	$5 . 10^{23}$	$5 . 10^{22}$	$2 . 10^{22}$	$5 . 10^{21}$	$2 . 10^{21}$	$5 . 10^{20}$	$5 . 10^{19}$	$5 . 10^{18}$
0.6	$6 . 10^{14}$	$4 . 10^{22}$	$1 . 10^{21}$	$2 . 10^{20}$	$4 . 10^{19}$	$6 . 10^{18}$	$1 . 10^{18}$	$3 . 10^{16}$	$1 . 10^{15}$
1.0	$4 . 10^{6}$	$3 . 10^{20}$	$8 . 10^{17}$	$4 . 10^{16}$	$2 . 10^{15}$	$1 . 10^{14}$	$7 . 10^{12}$	$3 . 10^{10}$	$6 . 10^{7}$
1.5	$4 . 10^{-4}$	$6 . 10^{17}$	$9 . 10^{13}$	$1 . 10^{12}$	$2 . 10^{10}$	$2 . 10^{8}$	$3 . 10^{6}$	$4 . 10^{2}$	$7 . 10^{-2}$
2.0	$4 . 10^{-14}$	$1 . 10^{15}$	$1 . 10^{10}$	$4 . 10^{7}$	$1 . 10^{5}$	$3 . 10^{2}$	$1 . 10^{0}$	$1 . 10^{-5}$	$9 . 10^{-11}$

$N_d = 5 . 10^{24}$ m^{-3}

TABLE 4 ELECTRONIC CARRIER CONCENTRATIONS AS A FUNCTION OF RECIPROCAL TEMPERATURE AND ENERGY LEVEL-BAND EDGE SEPARATION

$10^3/T$ (K^{-1})	n_e (m^{-3})			
	$N_d = 5 . 10^{20} m^{-3}$	$N_d = 5 . 10^{22} m^{-3}$	$N_d = 5 . 10^{24} m^{-3}$	$N_d = 5 . 10^{26} m^{-3}$
0.4	$5 . 10^{18}$	$5 . 10^{19}$	$5 . 10^{20}$	$5 . 10^{21}$
0.6	$1 . 10^{16}$	$1 . 10^{17}$	$1 . 10^{18}$	$1 . 10^{19}$
1.0	$7 . 10^{10}$	$7 . 10^{11}$	$7 . 10^{12}$	$7 . 10^{13}$
1.5	$3 . 10^{4}$	$3 . 10^{5}$	$3 . 10^{6}$	$3 . 10^{7}$
2.0	$1 . 10^{-2}$	$1 . 10^{-1}$	$1 . 10^{0}$	$1 . 10^{1}$

$E_c - E_d$ = 5eV

TABLE 5 ELECTRONIC CARRIER CONCENTRATION AS A FUNCTION OF RECIPROCAL TEMPERATURE AND ENERGY LEVEL CONCENTRATION